Atmospheric Physics

Adrian Tompkins, ICTP, Trieste, Italy

Email: tompkins@ictp.it

Version release date: July 1, 2019

These course notes and presentations have benefitted enormously from material taken (sometimes even with permission!) from Stephan de Roode, Keith Shine, John Chiang, Vince Larson, Bill Cotton, Ulrike Lohmann, Francesca Di Giuseppe, Denis Hartmann, Stephen Lower, in addition to figures and graphics from many other sources including the IPCC reports and Wikipedia. Apologies to authors of material that have still not been attributed. To my students, please note that brown links are citations, blue are cross-document links and red links are for external web resources. The index and contents page may also be useful. Please contact me for citation corrections, acknowledgments, suggestions and above, corrections to the numerous mistakes!

Contents

Chapter 1

Dry Thermodynamics

1.1 Kinetic theory of heat

Kinetic theory of heat
Let us consider a system at temperature T, consisting of N molecules. These move randomly in all directions in *Brownian motion*. This randomness implies the internal energies of the molecules are not equal, and they change in time. However, the mean internal energy of the molecules (i.e. of the system) is constant in time, and is proportional to the temperature of the system T.

A formal definition of a *mole* is the amount of a substance that has the same number of particles as there are in 12 grams of ^{12}C. This number $N = 6.022 \times 10^{23}$ is known as *Avoggadro's number*.

Avoggadro's hypothesis
In 1811, Avoggadro proposed that a volume of gas is directly proportional to the number of molecules of gas. Thus Avoggadro's hypothesis states that *a mole of any gas at constant temperature and pressure occupies the same volume*

1.2 Equation of state: The ideal gas law

Ideal Gas
The ideal gas model is a model of matter in which the molecules are treated as non-interacting point particles which are engaged in a random motion that obeys conservation of energy.

The model tends to fail at lower temperatures or higher pressures, when the molecules come close enough that they start interacting with each other, and not just with their surroundings. This is usually associated with a phase transition.

The *equation of state* for an ideal gas relates its pressure p, volume V and temperature T by

$$pV = NkT = \nu R^* T, \tag{1.1}$$

where

- N is the number of identical molecules
- ν is the number of moles of gas
- $k = 1.3806 \times 10^{-23}$ J K $^{-1}$ is Boltzmann's constant,
- $R^* \equiv N_a k = 8.341$ J mol^{-1} K^{-1} is the universal gas constant,
- with $N_a = 6.022 \times 10^{23}$ mol $^{-1}$ Avogadro's number.

As pointed out in the introduction, the Earth's atmosphere is a mixture of gases, mostly nitrogen, oxygen and argon, trace gases like carbon dioxide, ozone and methane, and variable amounts of water in its three physical phases (see Table 1).

Neglecting water vapour for the moment, the dry atmosphere can be taken to a very good approximation as an ideal gas.

In general, it is useful to formulate the thermodynamic relations in terms of *intensive* variables. An intensive variable is one whose value does not depend on the amount of matter in the system, like the temperature or pressure. In contrast, an *extensive variable*, depends on the size of the system. For instance, the internal energy of a gas is an extensive variable since if we double its size, all else being kept equal, its internal energy will double.

Given a system whose volume V contains an amount of mass M,

$$v = \frac{V}{M} \tag{1.2}$$

denotes the *specific volume* of the system. In principle, every extensive variable can be converted to its corresponding intensive form by normalizing it by the amount of matter it describes.

We will (generally, but not always!) use lower case letters to denote specific intensive quantities, as opposed to their non-intensive counterpart for which we will use capital letters, e.g. the specific volume v and the volume V.

We would like to write the gas law in terms of kilograms rather than moles and use the molecular weight of a species i, m_i (g/mol), which is the mass of 1 mole of identical molecules in grams.

If the total mass of the gas is M_i, we can express the gas law as,

$$pV = \frac{M_i}{m_i} R^* T. \tag{1.3}$$

The molecular weight can be substituted out by using the *specific gas constant* R_i for a species i, which is defined as

$$R_i \equiv R^*/m_i. \tag{1.4}$$

Partial Pressure

For a mixture of ideal gases the partial pressure p_i of the i^{th} gas is defined as the pressure p_i that it would have if the same mass (M_i) existed alone at the same temperature T and occupying the same volume V.

By eqn. (3) and eqn. (4) the partial pressure for an ideal gas can thus be expressed as

$$p_i = \frac{T}{V} M_i R_i. \tag{1.5}$$

Dalton's Law

According to *Dalton's law of partial pressures*, the total pressure p of a mixture of (ideal) gases is the sum of the pressures $\sum p_i$ of each species i as if it alone occupied a volume V,

$$p = \frac{T}{V} \sum_i (M_i R_i) = \rho R_m T. \tag{1.6}$$

If $M_{tot} = \sum_i M_i$ is the total mass, then $R_m = 1/M_{tot} \sum_i M_i R_i$ the specific gas constant for the mixture, and $\rho = M_{tot}/V$ is the density. Equation. eqn. (6) is the form of the gas law generally used in meteorology, although sometimes the specific volume is used instead of density ($v = 1/\rho$), thus

$$pv = R_m T. \tag{1.7}$$

Table 1 shows the value of the gas constant for dry air, $R_d = 287.05$ J kg^{-1} K^{-1}.

Reminders

1. What is the definition of a Ideal Gas?
2. Can dry air be considered an ideal gas?
3. What is Dalton's law?

Gas	Molecular weight m_i [g mol^{-1}]	Molar fraction	Mass fraction M_i/M_{tot}	Specific gas constant R_i [J kg^{-1} K^{-1}]	$(M_i/M_{tot})R_i$ [J kg^{-1} K^{-1}]
NO_2	28.013	0.7809	0.7552	296.80	224.15
O_2	31.999	0.2095	0.2315	259.83	60.15
Ar	39.948	0.0093	0.0128	208.13	2.66
CO_2	44.010	0.0003	0.0005	188.92	0.09
total		1.0000	1.0000		287.05

Table 1.1: Main components of dry atmospheric air (source Smithsonian Meteorological Tables).

1.3 The first law of thermodynamics

Heat and Temperature
Heat and temperature are not the same thing! The temperature of a body is a measure of the average thermal energy of the molecules in that body and does not depend on its mass. Heat is a form of energy that may be transferred from one body to another. The amount of heat required to raise 2kg of water by 1K is twice the amount required to raise 1kg.

Work
In thermodynamics, work performed by a system is the energy transferred by the system to/from its surroundings, for example through changes in the system volume/pressure. Work is measured in joules and the rate at which work is performed is power.

first law of thermodynamics
The *first law of thermodynamics* is a statement of two empirical facts:

1. Heat is a form of energy that can be transferred
2. Energy is conserved

Thus, the internal energy of a closed system (U) can change only if heat (Q) is added or if work (W) is done *on*[1] the system by its surroundings:

$$dU = dQ + dW \tag{1.8}$$

and for a unit mass of gas:

$$du = dq + dw \tag{1.9}$$

The rate of work (visualize a piston, as in Fig. 10) is given by

$$dw = -pdv, \tag{1.10}$$

such that eqn. (8) can be expressed as

$$du = dq - pdv. \tag{1.11}$$

1.4 Rules for differentiating

If the equation of state is governed by three state variables (p, v, T) then we can write

$$p = f_1(v, T) \quad , \quad v = f_2(p, T) \quad \text{or} \quad T = f_3(p, v). \tag{1.12}$$

In other words, there are only two independent state variables,

$$dp = \frac{\partial f_1}{\partial v}dv + \frac{\partial f_1}{\partial T}dT \ , \ dv = \frac{\partial f_2}{\partial p}dp + \frac{\partial f_2}{\partial T}dT \ , \ dT = \frac{\partial f_3}{\partial p}dp + \frac{\partial f_3}{\partial v}dv. \tag{1.13}$$

[1] Attention! Sometimes defined as work done *by* the gas thus changing the sign convention for dW

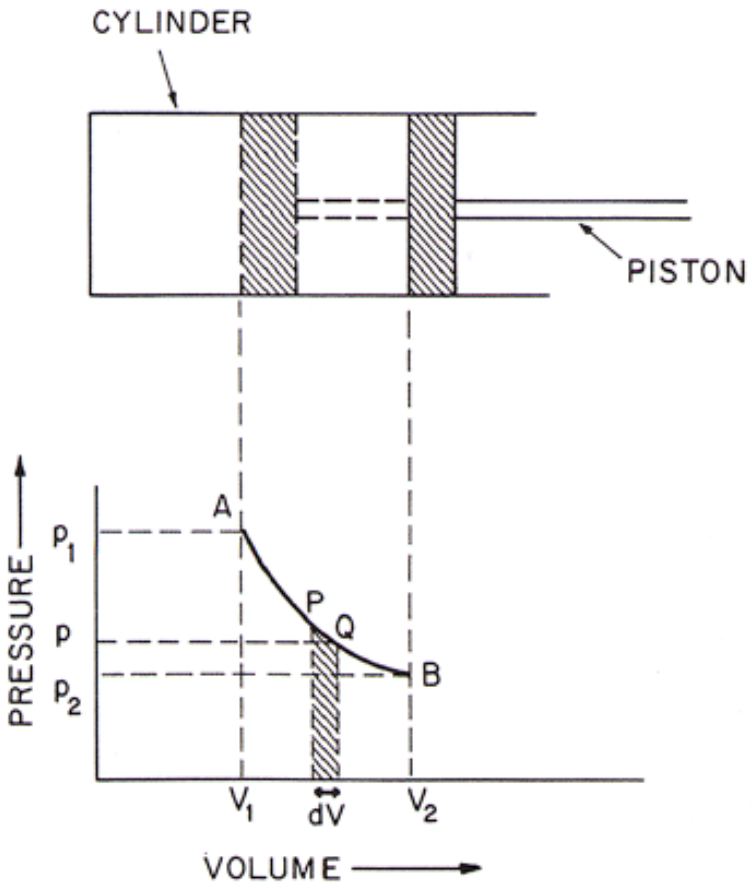

Figure 1.1: When heat is added to a gas, there will be an expansion of the gas (work is done) and an increase in its temperature (internal energy changes) - *Atmospheric Sciences: An Intro Survey.*

If we differentiate state variables other than p, v, or T, for instance, the specific internal energy u, we must specify which set of thermodynamics parameters we use. Otherwise $(\partial u/\partial p)$ is ambiguous and depends on the choice of thermodynamic coordinates, for example whether u is defined as a function of p and v or as a function of p and T.

Notation for differentiating
To express the rate of change of u as a result of an isothermal process, i.e. a change in the pressure p, we write

$$\frac{\partial u(p,T)}{\partial p} \equiv \left(\frac{\partial u}{\partial p}\right)_T \tag{1.14}$$

meaning that p and T are chosen as thermodynamical coordinates and that the the temperature is held constant for this process.

1.5 Enthalpy and specific heat

A measure of the quantity of heat needed to raise the temperature of a substance by 1 °C is called the heat capacity C, and is defined as:

$$C = dQ/dT. \tag{1.15}$$

But this definition is incomplete. There are many ways to add heat to a system. One could add heat to a system at *constant volume* or at *constant pressure*, or one could add heat as both the volume and pressure change.

We now define the specific heat capacity at constant pressure, c_p and the specific heat capacity

at constant volume, c_v. These are very different.

$$c_v = \left(\frac{\partial q}{\partial T}\right)_v. \tag{1.16}$$

$$c_p = \left(\frac{\partial q}{\partial T}\right)_p. \tag{1.17}$$

For dry air, $c_p = 1005$ J kg^{-1} K^{-1} and $c_v = 718$ J kg^{-1} K^{-1}. *Q: Why is c_p greater than c_v?*

If one *selects* the specific volume v and the temperature T as thermodynamic coordinates, then the specific internal energy u can be expressed as,

$$du = \left(\frac{\partial u}{\partial v}\right)_T dv + \left(\frac{\partial u}{\partial T}\right)_v dT = \left(\frac{\partial u}{\partial T}\right)_v dT. \tag{1.18}$$

where the last equality follows from the fact that the internal energy of an ideal gas does not depend on its volume,

$$\left(\frac{\partial u}{\partial v}\right)_T = 0. \tag{1.19}$$

eqn. (19) implicitly assumes that the intermolecular forces are negligibly small, and therefore is applicable only to an ideal gas. Equating eqn. (11) and eqn. (18) gives

$$dq = \left(\frac{\partial u}{\partial T}\right)_v dT + pdv, \tag{1.20}$$

where dq indicates the differential amount of heat added. For an *isometric* process $dv = 0$, which implies $\left(\frac{\partial u}{\partial T}\right)_v = \left(\frac{\partial q}{\partial T}\right)_v$ from (11), which equates to the definition of c_v giving:

$$dq = c_v dT + pdv, \tag{1.21}$$

Eqn. (21) is still not in a form useful in meteorology due to the difficulty of measuring volume of an air mass. We therefore use the chain-law on the ideal gas law to write *check!*

$$dq = c_v dT + RdT - vdp, \tag{1.22}$$

$$dq = (c_v + R)dT - vdp, \tag{1.23}$$

For an isobaric process (i.e. no pressure change, $dp = 0$), thus we see directly from Eqn. (23):

$$c_p = \left(\frac{\partial q}{\partial T}\right)_p = c_v + R. \tag{1.24}$$

which leads to the form of the first law commonly used in meteorology since it is formed in measurable quantities:

$$dq = c_p dT - vdp, \tag{1.25}$$

We now introduce another state variable that is often used in atmospheric thermodynamics is the *enthalpy* h

$$h = u + pv. \tag{1.26}$$

Given this definition, the first law can be expressed as

$$dq = du + pdv = dh - d(pv) + pdv = dh - vdp. \tag{1.27}$$

The enthalpy gives a measure of total potential energy of the atmosphere.

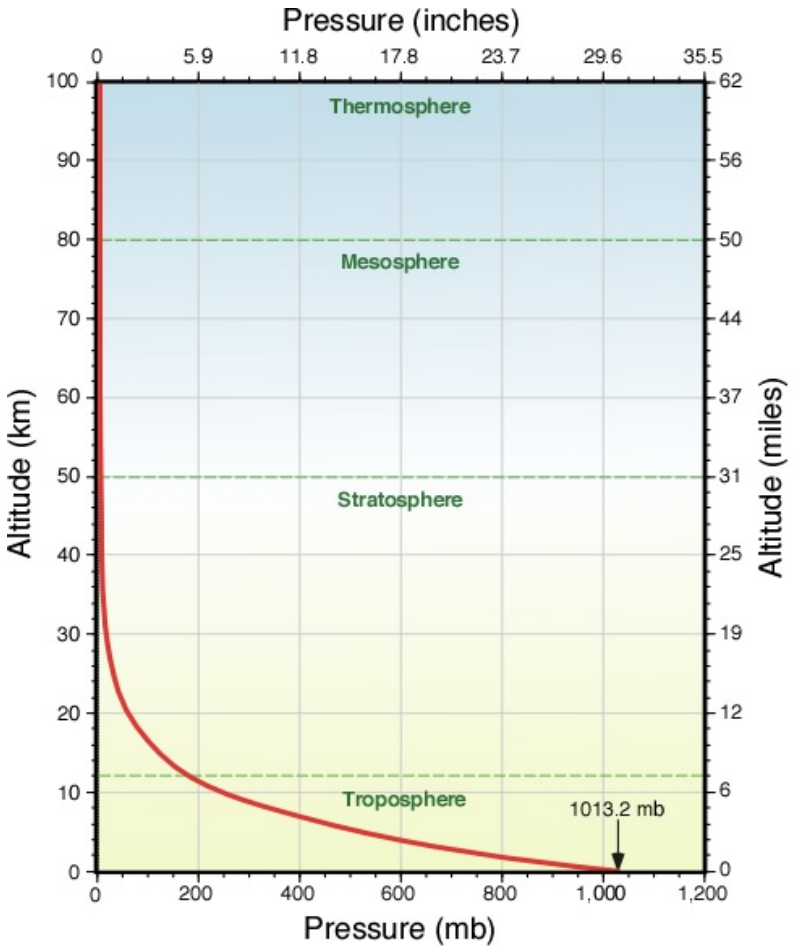

Figure 1.2: Pressure as a function of height force balances the upward acceleration due to the pressure gradient.

1.6 Hydrostatic balance

The atmospheric pressure is the force per unit area exerted on a surface by the weight of the air above. Thus it is clear that pressure will fall with height as shown in Fig. 11. We can derive how the pressure falls with height if we assume a state of equilibrium known as the hydrostatic balance.

Hydrostatic balance

Hydrostatic equilibrium exists if the force due to gravity is balanced by the vertical pressure gradient force. From Fig. 12 we see that

$$(p(z) - p(z + dz))A = \rho A dz g \tag{1.28}$$

giving

$$\frac{dp}{dz} = -\rho g \tag{1.29}$$

Hydrostatic equilibrium is widely satisfied over horizontal scales exceeding 10km, and thus the assumption is used to simplify the governing equations of numerical models of the atmosphere that use a grid-cell size exceeding this threshold.

Using the ideal gas law, we can write the hydrostatic relation as

$$\frac{dp}{dz} = -\frac{p}{RT} g, \tag{1.30}$$

which can be integrated to give

$$p = p_s exp(\frac{-gz}{RT}). \tag{1.31}$$

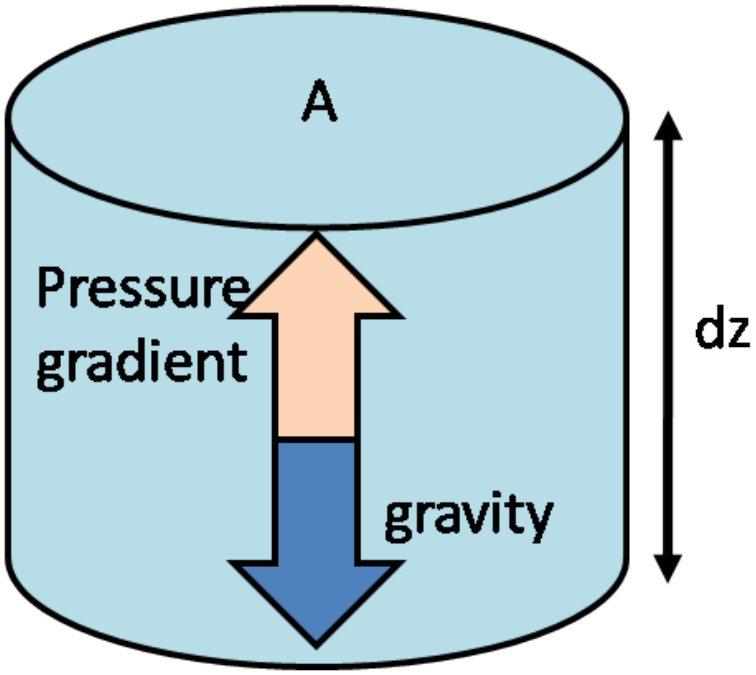

Figure 1.3: Schematic of a cylindric parcel of air of horizontal area A and height dz that is hydrostatic balance, i.e. the downward gravity force balances the upward acceleration due to the pressure gradient.

How do R and T affect the scale height?

Thus we see that the atmospheric pressure decreases exponentially with height with a scale height factor of RT/g (Fig. 13. Thus the rate at which pressure decreases with height depends on the gas constant, with heavier molecules leading to a smaller gas constant and a smaller scale height. On the other hand, higher temperatures result in the more energetic molecules and thus the scale height increases (Fig. 14.

1.7 Adiabatic Processes

Air parcel theory

We introduce the notion of a conceptual 'air parcel' at this point, which is a finite volume of air with uniform properties that may move through the atmosphere as a continuous entity. We may (sometimes) assume that some properties such as the parcel volume and pressure adjust quickly to stay in equilibrium with the parcel surroundings, but in general this is not the case (e.g. temperature).

For example, Fig. 15 shows a schematic of a balloon being released. We can imagine our air parcel to be represented by the balloon. If we assume the pressure of the balloon is always in equilibrium, then the balloon expands as it ascends.

What will happen to the temperature of the gas inside the balloon?

Before we answer this question, let us briefly consider which processes may alter the temperature of a gas in a particular location. Some of these are so-called *diabatic* processes, that involve the direct transfer of heat energy to/from an air parcel.

Conduction

The process of heat transfer from molecule to molecule, requiring contact. Heat can be transferred between (from/to) the ground and lowest layer of the atmosphere by conduction. Air is a poor conductor and conduction is not an efficient mechanism to transfer heat on large scales.

Convection (and advection)

The process of heat transfer by mass motions of a fluid (such as air or water). Heat can be transferred away from a heat source by the motion. Advection is a similar process but more

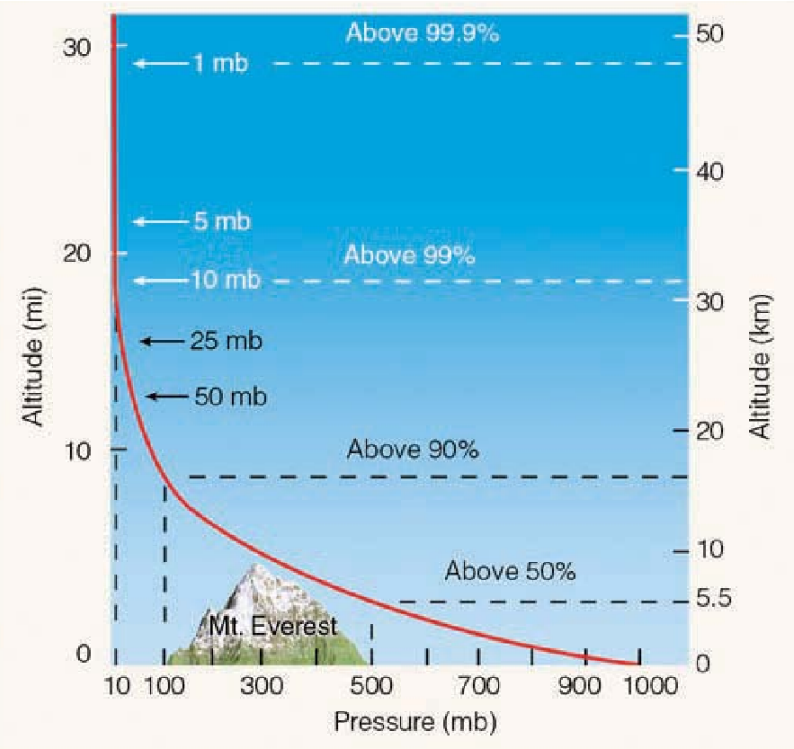

Figure 1.4: Graph showing how pressure decreases with height. Dash lines indicate percentage of atmosphere below the each level (source: Met Today)

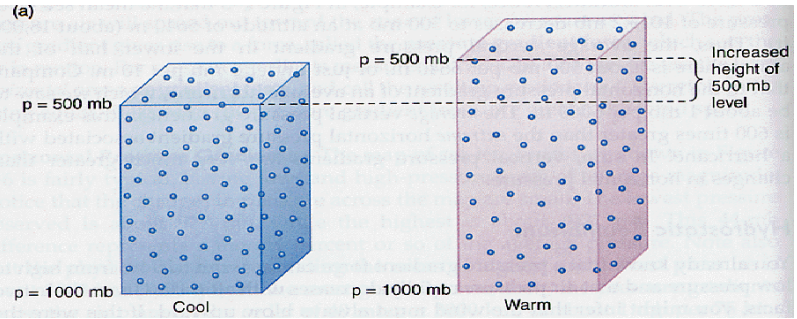

Figure 1.5: Graph showing how temperature affect the pressure scale height

commonly refers to heat transfer by horizontal motions. Convection/advection is an efficient mechanism to transfer heat in the atmosphere

Radiation
Heat transfer by the emission of electromagnetic waves which carry energy away from the emitting object

Latent heating
Latent heat is the heat released or absorbed when water changes phase, this will be discussed in more detail later.

A parcel of air can be subject to input of heat and changes in pressure. First we shall consider the case where no heat is input.

Adiabatic Process
An *adiabatic process* is one where there is no heat exchange, $dq = 0$, thus

$$c_p dT = v dp, \tag{1.32}$$

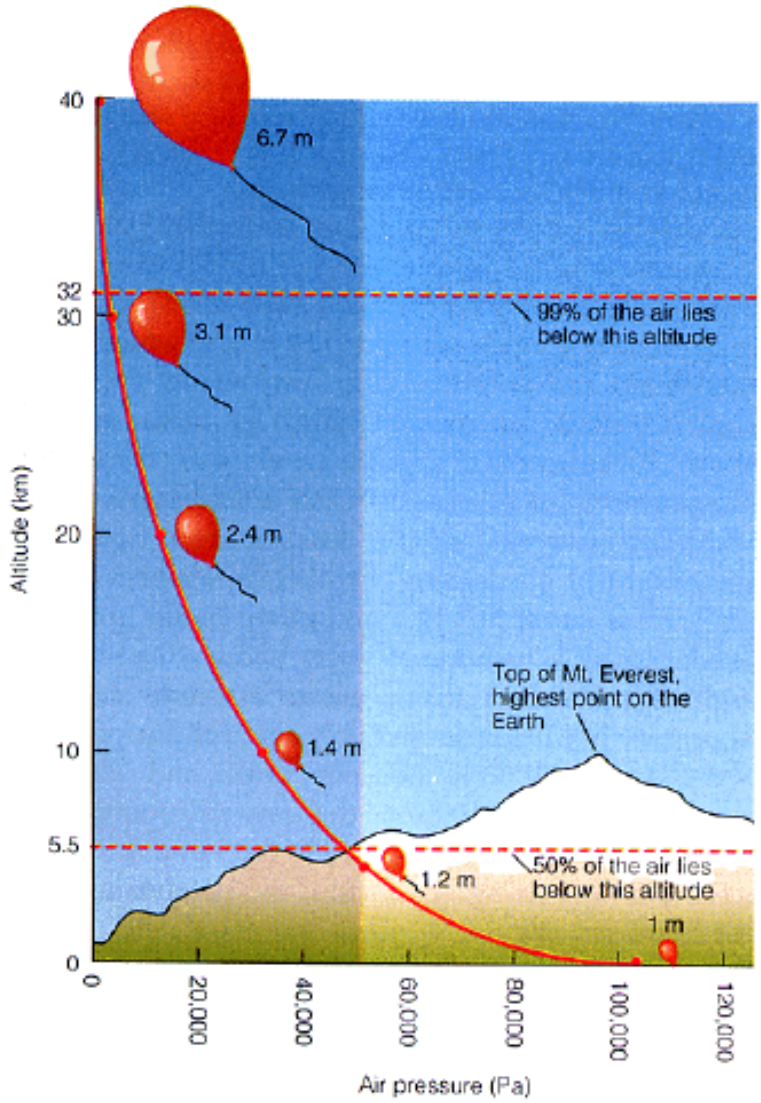

Figure 1.6: Graph showing how a balloon 'air parcel' expands during an ascent. A balloon that is 1m in diameter released at sea level will have a 6.7m diameter at 40km.

Thus if the pressure changes, a corresponding temperature change will result.

Adiabatic processes have special significance as many atmospheric motions can be approximated as adiabatic. Assuming that the atmosphere is in hydrostatic balance (eqn. (27), then eqn. (30) can be written

$$c_p dT = -v\rho g dz = -g dz, \tag{1.33}$$

This gives the adiabatic lapse rate as

$$\frac{dT}{dz} = -\frac{g}{c_p} \tag{1.34}$$

Thus if we lift a dry air parcel without heat exchange its temperature will fall by by 9.8 K km^{-1} as it expands to keep its pressure in equilibrium with its surroundings. (Fig. 16).

Q: Considering the atmospheric diabatic processes, what will determine how well a moving parcel's temperature changes is described by the adiabatic lapse rate?

Figure 17 shows the measured lapse rate on one particular day measured in Holland. The lapse rate is seen to be close to dry adiabatic .

Figure 17 shows observations made in a clear convective boundary layer (CBL). Because of solar radiative heating turbulent eddies are driven from ground surface. The thermals can penetrate into the thermal inversion, which for this case is located at about 380 m, above which they are damped by the stable stratification. The turbulent eddies warm the upper boundary layer thus bringing an unstable stratification profile back towards neutrality. The fact that the profile of temperature is

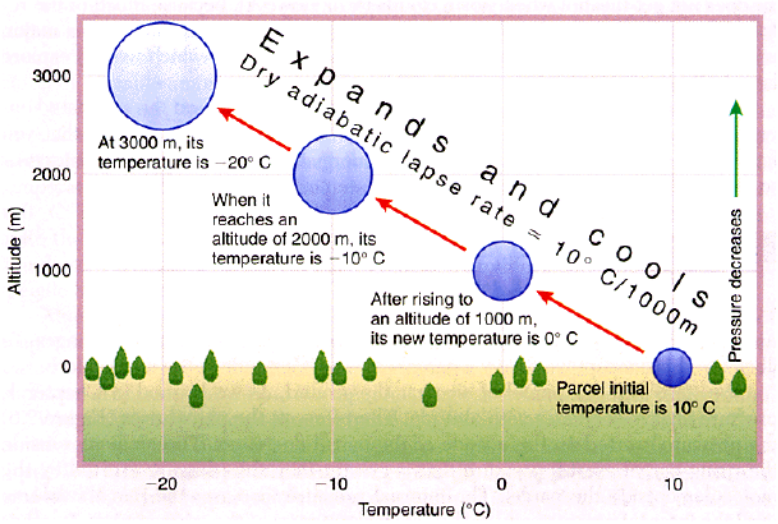

Figure 1.7: Graph showing how an air parcel expands and also cools during its ascent.

"well-mixed", with the temperature following approximately the dry-adiabatic lapse rate, implies that the warming timescale associated with the turbulent eddy mixing is fast compared to the processes that destabilize the profile (such as radiative cooling of the boundary layer). Were this not the case, super-adiabatic unstable layers could form, such as in the surface layer when strongly heated by the sun.

Conserved quantities

When we describe the atmosphere it is useful to be able to lable air parcels in terms of properties that are invarient under certain types of motion. In other words we wish to define Lagrangian *conserved quantities*.

Q: is temperature a conserved quantity? Now we will try to derive a quantity that is conserved in adiabatic motion. Using the equation of state we get

$$c_p dT = v dp = \frac{RT}{p} dp \tag{1.35}$$

$$\frac{dT}{T} = \frac{R}{c_p p} dp \tag{1.36}$$

Poisson's Equation

Eqn. (34) can be integrated to give *Poisson's Equation*:

$$\frac{T}{T_0} = \left(\frac{p}{p_0}\right)^{\frac{R_d}{c_p}} \tag{1.37}$$

where T_0 and p_0 are constants of integration.

Exercise: Derive this equation.

Note that we have reintroduced the subscript d on the gas constant to emphasize that this considers dry air.

1.8 Potential Temperature

Potential Temperature

If we set the reference pressure p_0 to 1000 hPa then T_0 is defined as the *potential temperature* (for dry air) which is commonly denoted θ:

$$\theta = T\left(\frac{p_0}{p}\right)^{\frac{R_d}{c_p}}. \tag{1.38}$$

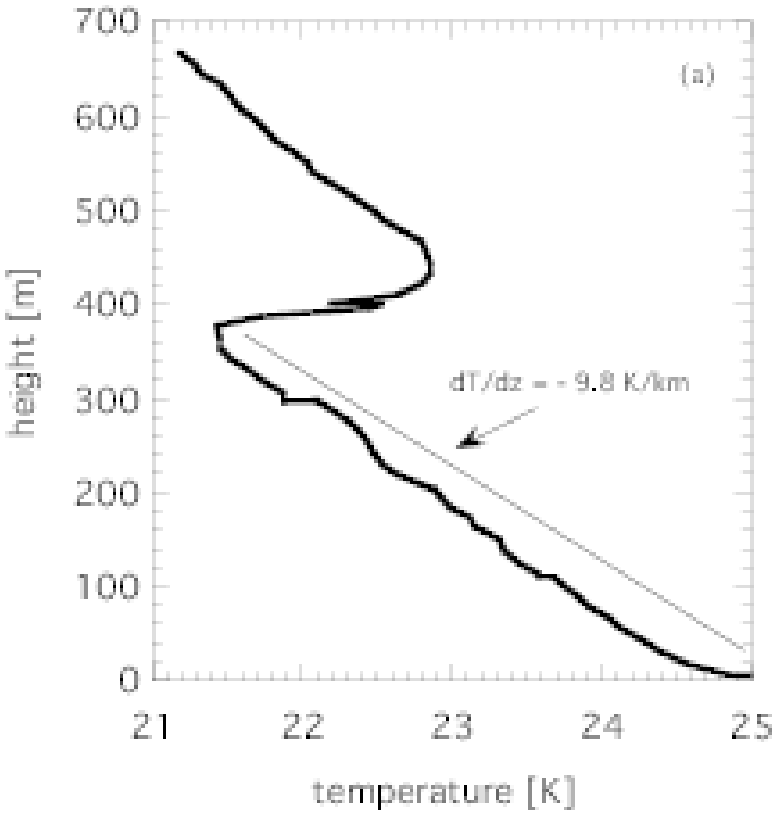

Figure 1.8: Vertical profile of the temperature T for a clear convective boundary layer as observed by a tethered balloon at Cabauw, Netherlands, around 10:00 h (local time), 23 Aug 2001.

The potential temperature θ can be interpreted as the temperature a parcel would have if it were displaced adiabatically to a reference height where the pressure is p_0, which is usually taken $p_0 =$ 1000 hPa. In other words, a parcel with temperature T at pressure level p will have a potential temperature θ, which value is equal to the temperature T_0 at the pressure level p_0.

The *lapse rate* of the potential temperature can be obtained by differentiating eqn. (36) with respect to height (*exercise*)

$$\frac{d\theta}{dz} = \frac{\theta}{T}\left(\frac{dT}{dz} - \frac{R_d T}{pc_p}\frac{dp}{dz}\right) \tag{1.39}$$

Assuming that the atmosphere is in a hydrostatic balance,

$$\frac{dp}{dz} = -\rho g \tag{1.40}$$

then with aid of the gas law eqn. (37) can be written as

$$\frac{d\theta}{dz} = \frac{\theta}{T}\left(\frac{dT}{dz} + \frac{g}{c_p}\right). \tag{1.41}$$

Since $-\frac{g}{c_p} = \Gamma_d$ is the *dry adiabatic lapse rate*, we conclude that if the temperature profile follows the dry adiabatic lapse rate, the potential temperature is constant with height.

Dry static energy

We can define an analogue to potential temperature in height coordinates. Integrating eqn. (31) (which we recall assumes hydrostatic balance) we get

$$c_p(T - T_0) = -g(z - z_0). \tag{1.42}$$

Analogously to the potential temperature, we see that the quantity

$$s = c_p T + gz \tag{1.43}$$

is conserved in dry adiabatic motion , and is referred to as the *dry static energy.*

1.9 Entropy

Another variable of relevance is the specific entropy ϕ which is measure of a system's energy per unit temperature available for doing useful work. It is defined as

$$d\phi \equiv \frac{dq}{T}. \tag{1.44}$$

The entropy is a state variable. Note that, with the temperature in the denominator of eqn. (43), heat and entropy are not linearly related. We will consider diabatic and adiabatic processes occuring to a parcel in a thermodynamic cycle. A thermodynamic cyclic process indicates a series processes transferring heat and work, while varying pressure, temperature, and other state variables, but that eventually return a system to its initial state. In the process of going through this cycle, the system may perform work on its surroundings. We use $\oint$ to indicate an integral over such a cycle. A *reversible* process is defined as

$$\oint d\phi = 0, \tag{1.45}$$

This integral is independent of the path. An isentropic process (iso = "equal" (Greek); entropy = "disorder") is one during which the entropy of the system remains constant; a reversible, adiabatic process is isentropic .

The second law of thermodynamics states that a process will tend to increase the entropy of a system, thus $Td\phi = du + pdv \geq 0$. The relevance of entropy to meteorologists is clear deriving the relationship between the potential temperature and entropy.

If we take logs of eqn. (36) we have

$$ln\theta = ln\left(T\left(\frac{p_0}{p}\right)^{\frac{R_d}{c_p}}\right) = lnT + \frac{R_d}{c_p}(lnp_0 - lnp). \tag{1.46}$$

Differentiating we obtain,

$$dln\theta = dlnT - \frac{R_d}{c_p}dlnp = \frac{dT}{T} - \frac{R_d dp}{c_p p}, \tag{1.47}$$

and multiplying through by c_p and using $pv = R_d T$ in term 2 we get

$$c_p dln\theta = \frac{c_p dT - vdp}{T} = \frac{dq}{T} = d\phi \tag{1.48}$$

1.10 Thermodynamic charts

The heat added in a cyclic process is[2]

$$\oint dq = \oint Td\phi = c_p \oint Td(ln\theta), \tag{1.49}$$

where the last equality follows from using eqn. (46). Thus it is clear that a chart that has perpendicular coordinates of temperature T and entropy ϕ, or equivalently T versus $ln\theta$ will have the properties of *equal areas=equal energy*; useful properties of a thermodynamic diagram.

Tephigrams

One thermodynamic chart is a *tephigram* . Using eqn. (36) one can plot p as a function of the two ordinates. Note that the lines of constant pressure, (isobars), are not exactly straight lines.

We are used to using orthogonal charts (left, Fig. 19), but no reason for orthogonality (right, Fig. 20).

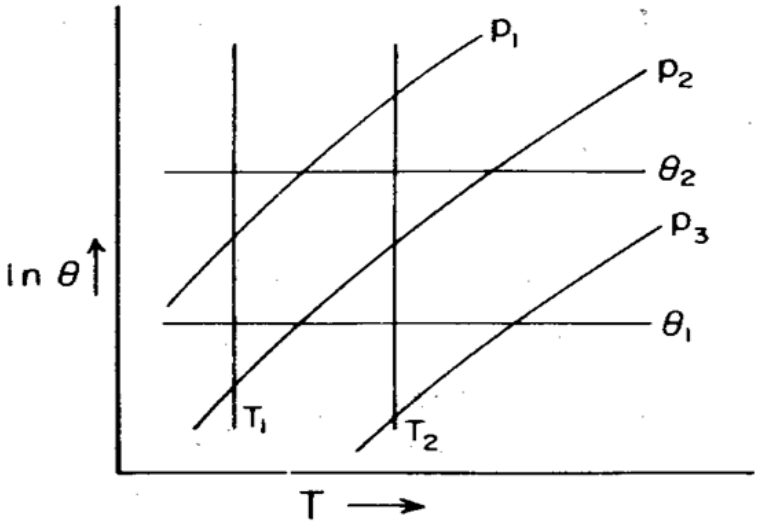

Figure 1.9: The tephigram basic structure

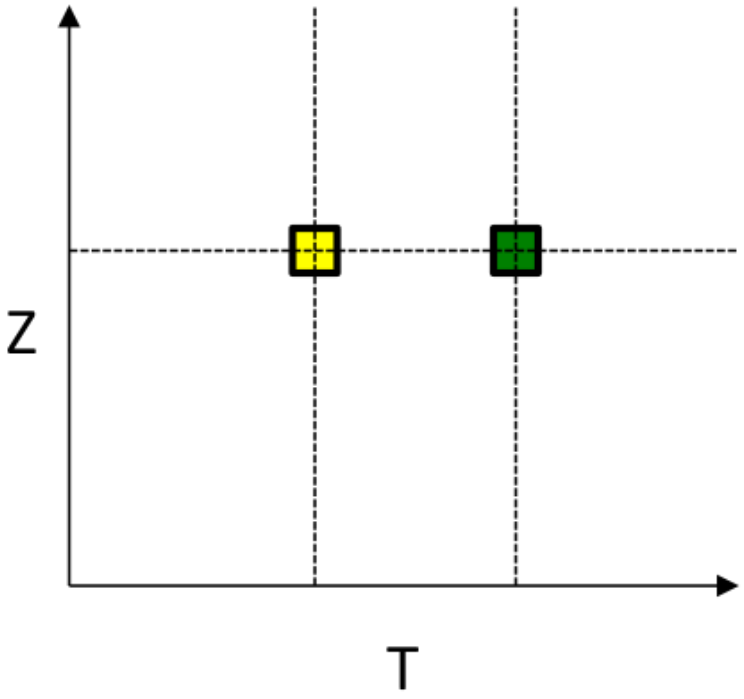

Figure 1.10: An orthogonal chart

Meteorologists are used to using pressure as a vertical height coordinate and thus rotate the chart to make the curved pressure lines almost horizontal, as shown in Figure 21.

Look at Fig. 22:

- Is the pressure of the green square greater or lower than the yellow one?
- Is it warmer or cooler?

Points that lie to the right (left) on a isobar are warmer (cooler).

[2]This can also be derived directly from the first law and the hydrostatic relation.

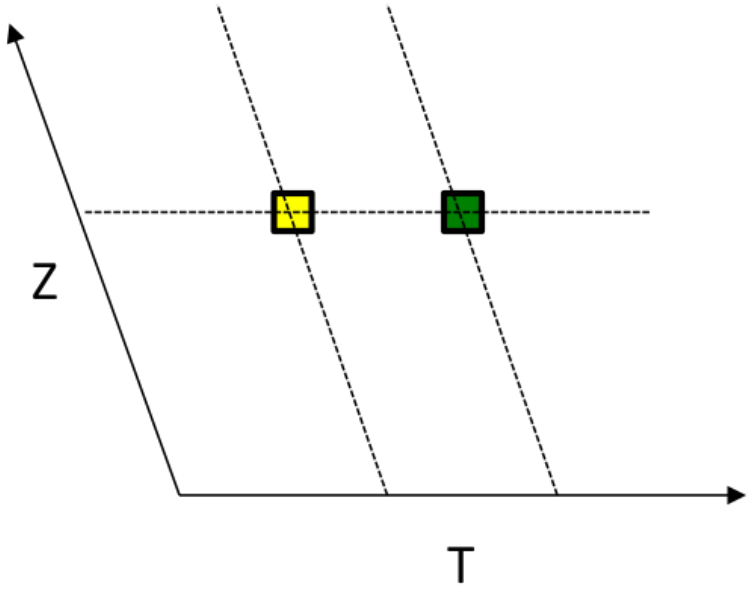

Figure 1.11: A non-orthogonal chart

1.11 Buoyancy force

1.11.1 Concept

A fixed body of fluid has a volume $V = \delta x \delta y \delta z$ and density ρ (Fig. 24). It displaces an equal volume of ambient fluid having density ρ_{env}. In the surrounging fluid we assume hydrostatic balance (Eqn. (38) and as density is everywhere constant $p = -\rho g z$.

The total force F on the box is thus the difference in pressure between the upper and lower faces scaled by the area of the face, and the gravitational force $\rho g V$:

$$F = \rho_{env} g \Delta z \Delta x \Delta y - \rho g V = g V (\rho_{env} - \rho) \tag{1.50}$$

In other words the buoyancy force is simply the difference between the weight of the body and the fluid it displaces.

If the body were released the buoyancy acceleration B would be

$$B = \frac{F}{M} = g \left(\frac{\rho_{env} - \rho}{\rho} \right) \tag{1.51}$$

1.11.2 Buoyancy of an air parcel

In the atmosphere[3] we are concerned with motions when gravity acts on variations of density in a fluid and in general the resulting motions will themselves alter the density anomalies through mixing and advection, which complicates matters and will be discussed later. For the moment, we consider the concept of buoyancy on a parcel of air and make the assumption that *local density and pressure variations in the parcel are small compared to their mean values in the ambient environment*

The buoyancy is derived from the vertical momentum equation for an ideal inviscid fluid

$$\frac{dw}{dt} = -\frac{1}{\rho} \frac{\partial p}{\partial z} - g \tag{1.52}$$

We now divide fields into the mean ambient values and the local perturbation values,

$$p = \overline{p} + p' \tag{1.53}$$

[3] this discussion is from Emanuel (1994)

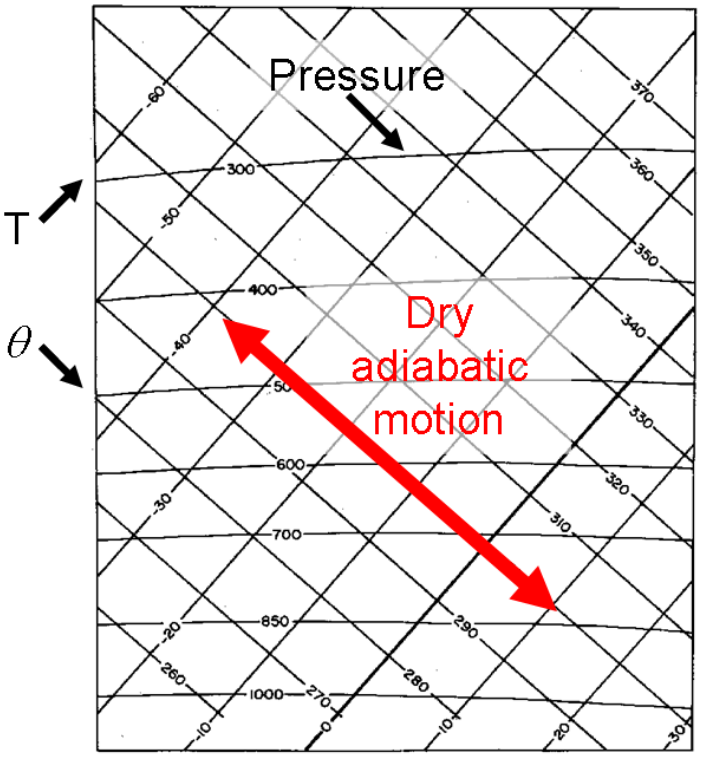

FIG. 1.7. Skeleton of a tephigram. Isobars are approximately horizontal, labeled in mb. Isotherms in deg C go upwards and to the right. Dry adiabats are normal to the isotherms and are labeled according to potential temperature (deg K).

Figure 1.12: A tephigram as they are usually used, with the chart rotated to make the pressure lines horizontal. Note that the lines of θ are not equally spaced - **Q: Why?**.

$$\rho = \overline{\rho} + \rho' \tag{1.54}$$

and again assuming the ambient fluid is in hydrostatic balance:

$$-\frac{1}{\overline{\rho}}\frac{\partial \overline{p}}{\partial z} - g = 0 \tag{1.55}$$

Equation (50) can be rewritten

$$\frac{dw}{dt} = -\frac{1}{(\overline{\rho}+\rho')}\frac{\partial}{\partial z}(\overline{p}+p') - g \tag{1.56}$$

The inverse density term can be expanded in an geometric series:

$$\frac{1}{\overline{\rho}+\rho'} = -\frac{1}{\overline{\rho}}\left(\frac{1}{1+\frac{\rho'}{\overline{\rho}}}\right) = -\frac{1}{\overline{\rho}}\left[1 - \frac{\rho'}{\overline{\rho}} + \left(\frac{\rho'}{\overline{\rho}}\right)^2 + \ldots\right] \tag{1.57}$$

Now since we assumed perturbation quantities are small, we can drop all terms of second order or higher, which gives (check)

$$\frac{dw}{dt} = -\frac{1}{\overline{\rho}}\frac{\partial \overline{p}}{\partial z} - g - \frac{1}{\overline{\rho}}\frac{\partial p'}{\partial z} + \frac{1}{\overline{\rho}}\frac{\partial \overline{p}}{\partial z}\left(\frac{\rho'}{\overline{\rho}}\right) \tag{1.58}$$

The first two terms on the RHS cancel due to the assumption of hydrostatic balance, which also allows us to substitute g in the final term on right, giving:

$$\frac{dw}{dt} = -\frac{1}{\overline{\rho}}\frac{\partial p'}{\partial z} - g\left(\frac{\rho'}{\overline{\rho}}\right). \tag{1.59}$$

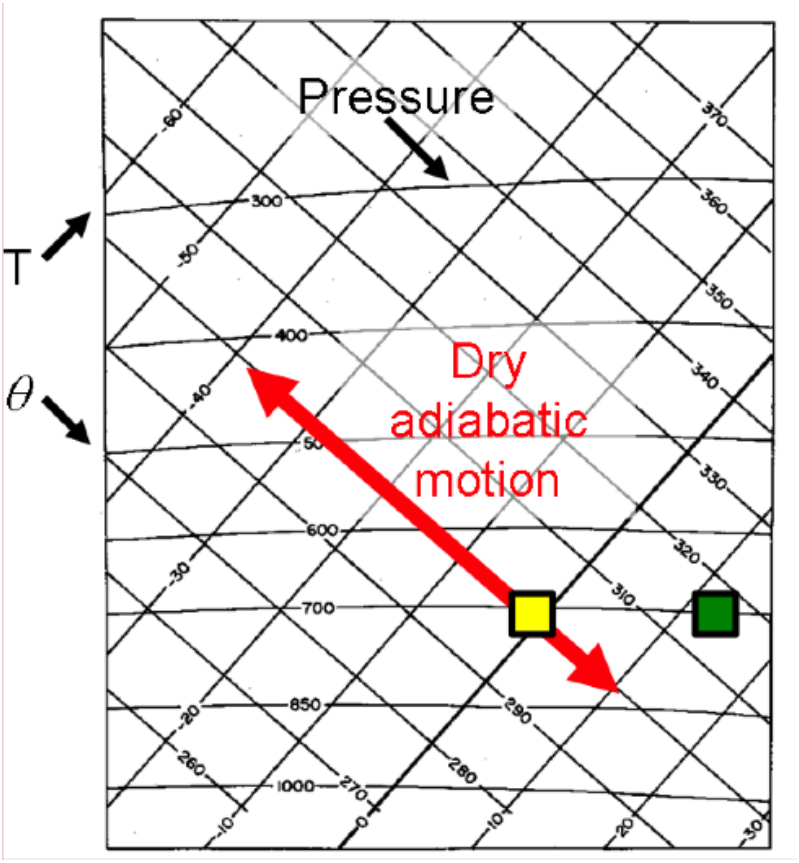

Figure 1.13: Reminder tephigram Questions

The first term in eqn. (57) is referred to as the *nonhydrostatic pressure gradient acceleration* which arises from dynamical effects of forced momentum changes [4] The second term on the RHS of eqn. (56) represents the action of gravity on density anomalies and is referred to as the *buoyancy acceleration*

$$B = -g\left(\frac{\rho'}{\overline{\rho}}\right) \tag{1.60}$$

Buoyancy is thus related to density anomalies, which is turn can be a result of temperature anomalies, pressure anomalies, or by the presence of dissolved solids in a fluid or suspensions of small particles.

However the contribution of pressure perturbations may usually be neglected for flows which are substantially subsonic, thus giving the approximate definition

$$B \approx g\left(\frac{T'}{\overline{T}}\right) \tag{1.61}$$

1.12 Introduction to convection

Convection

Convection is the name given to any motions that result from the action of the gravitional field on variations in density

Convection in the atmosphere can take a variety of forms, and often involves the complexity of phase changes of water vapour.

[4] When we discuss convection later, recall that in most atmospheric models this term is neglected.

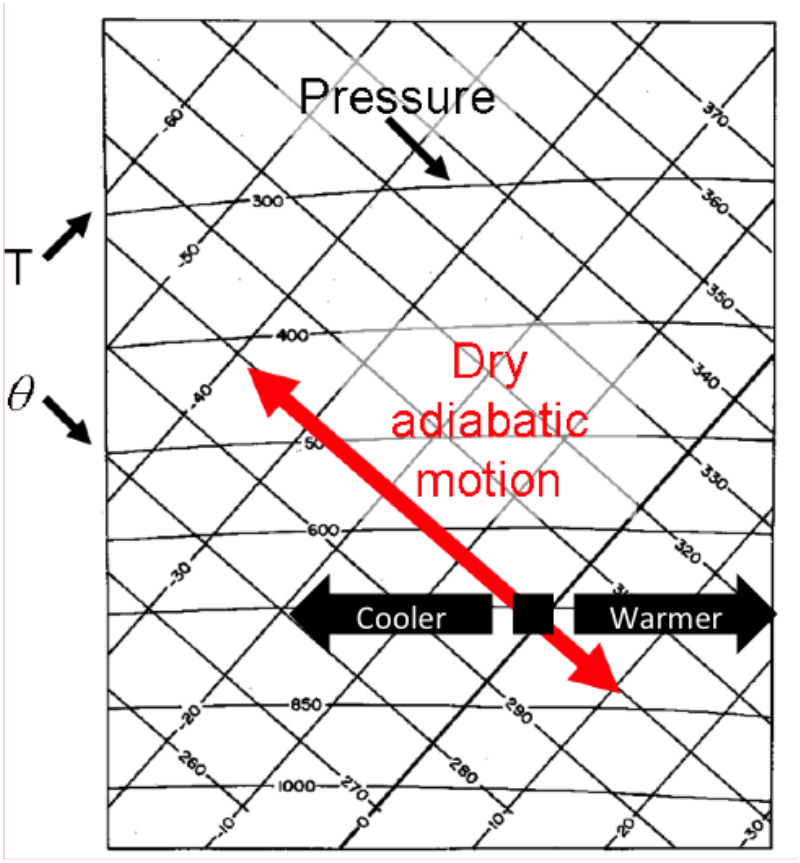

Figure 1.14: Reminder tephigram Questions

Neglecting these for the moment, we see from Eqn. (59) that convection can arise when temperature perturbations result in density anomalies and conseqently a buoyancy acceleration.

Many earlier studies of convection concerned motions arises from a point heat source. An example is the smoke rises from a lit cigarette (Fig. 25). In general, convection in geophysical flows almost always arises from bouyancy sources distributed over areas that are large relative to the depth of the convecting layer.

A classical example of this kind of convection was studied at the turn of the last century and is referred to as *Rayleigh Bénard* convection.

Rayleigh Bénard convection

If a fluid is placed between two plates of equal temperature, the fluid will remain at rest. If the temperature of the lower plate is increased with respect to the upper plate, heat transfer by molecular diffusion will occur. Increasing the temperature of the lower plate further, eventually a critical temperature difference is reached at which the unstable distribution of mass (density perturbations) is such that convective overturning commences. The convection takes the form of cells (Fig. 26

In 1916, Lord Rayleigh showed that the dimensionless parameter than determines the stability of this system is

$$R_a \equiv \frac{g\alpha\beta}{\nu\kappa} H^4 \tag{1.62}$$

where α is the fixed temperature gradient, H is the distance between the plates and β is the coefficient of thermal expansion of the fluid. ν is the kinematic viscosity and κ is the thermal diffusivity of the fluid.

Convection cells will thus occur if a fluid is heated from below. An obvious example of this in the atmosphere is when the ground is heated by solar radiation, which subsequently is warmer than the overlying atmosphere.

The surface will heat the lowest layer of the atmosphere in contact with the ground, and this will induce a similar unstable vertical profile of mass, with convection ensuing (Fig. 27) .

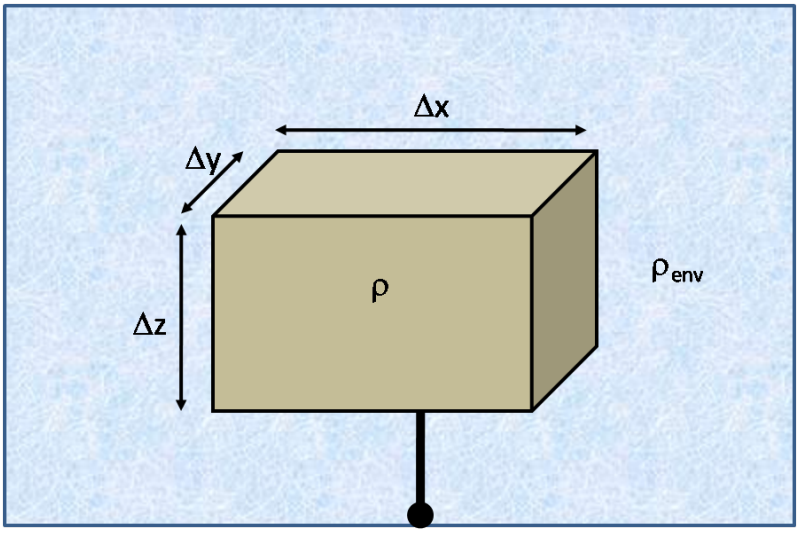

Figure 1.15: Schematic: parcel of fluid/air "tied" to the bottom in a fluid/gas of density ρ_{env}.

These convective cells are usually restricted to the lowest few hundred metres of the atmosphere for reason we will see later, and thus this layer, subjected to the strong vertical mixing of convection is referred to commonly as the *boundary layer* . Above the boundary layer the effect of earth surface on winds is minimal.

1.13 Atmospheric Stability

We now introduce the concept of stability in the atmosphere. What do we mean by stability? We refer to an unstable situation as one where a small initial perturbation will grow rapidly in time 28.

If a parcel of air is warmer(cooler) than its environment it will be subject to a net upwards (downwards) buoyancy force and will accelerate upwards (downwards), and is usually referred to as *positively (negatively) buoyant*. Equal temperatures are referred to as *neutral buoyancy*.

A parcel of air that is neutrally buoyant and subjected to a small vertical displacement may become positively or negatively buoyant, depending on whether the parcel's temperature changes changes more or less rapidly than the environmental lapse rate.

The environmental θ lapse rate is $\frac{d\theta_{env}}{dz}$ and we will assume the lifted parcel cool adiabatically (reminder: what does this mean?) and thus θ of the parcel is invariant.

We can thus define three situations:

$\frac{d\theta_{env}}{dz} < 0$: **Unstable**

$\frac{d\theta_{env}}{dz} = 0$: **Neutral**

$\frac{d\theta_{env}}{dz} > 0$: **Stable**

With the example stable and unstable profiles shown in Fig. 29 This is illustrated schematically in Fig. 30

Figure 1.16: Cigarette smoke acts as a conventient marker for the convective motions arises from the point heat source

Without instrumentation to measure the profile of temperature one can not say whether a boundary layer is well mixed, however one clue is the presence of a gusty intermittent wind associated with the turbulent eddies, while if the layer is deep enough such that the top of the boundary layer becomes saturated and forms "fair weather cumulus" cloud (see next section) then this is a sure sign that the boundary layer is well mixed and close to neutral stability.

Thus *unstable* layers are quite uncommon except in the lowest few metres of the atmosphere, *neutral* layers are quite common and result from the convective/turbulent reaction to processes that produce instability, and *stable* layers are also common. In this case displaced parcels of air

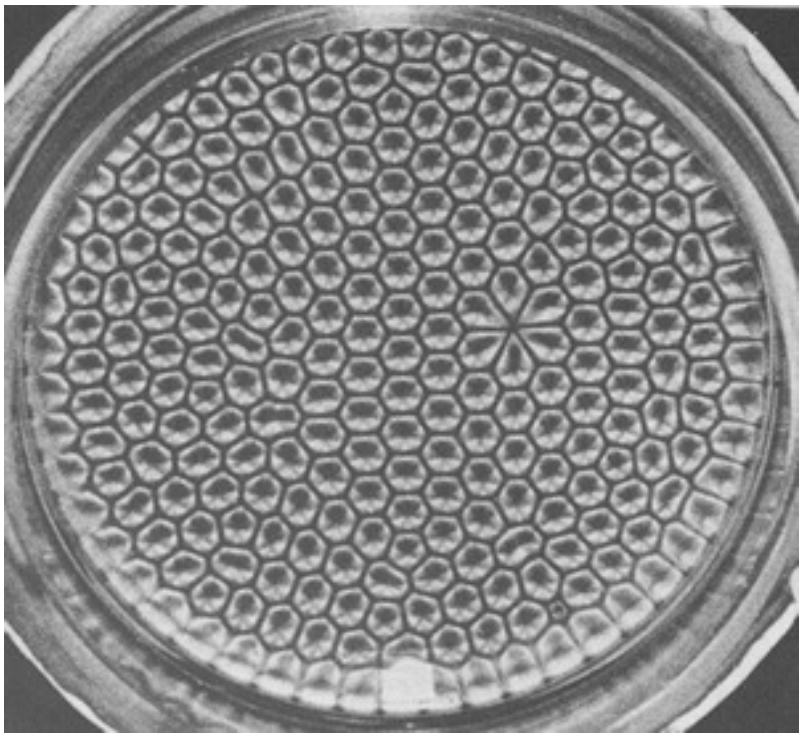

Figure 1.17: Examples of bénard cells (http://www.catea.gatech.edu)

will undergo simple harmonic motion.

Reminders:

- If we express the gas law in terms of mass instead of moles, we switch from using the universal gas constants to a specific gas constant whose value depends on the molecular weight.
- The dry atmosphere and water vapor can be taken to a good approximation as ideal gases.
- The state of the atmosphere can be expressed by three state variables, p, v and T, of which two are independent.
- The first law of thermodynamics dictates that energy is conserved.

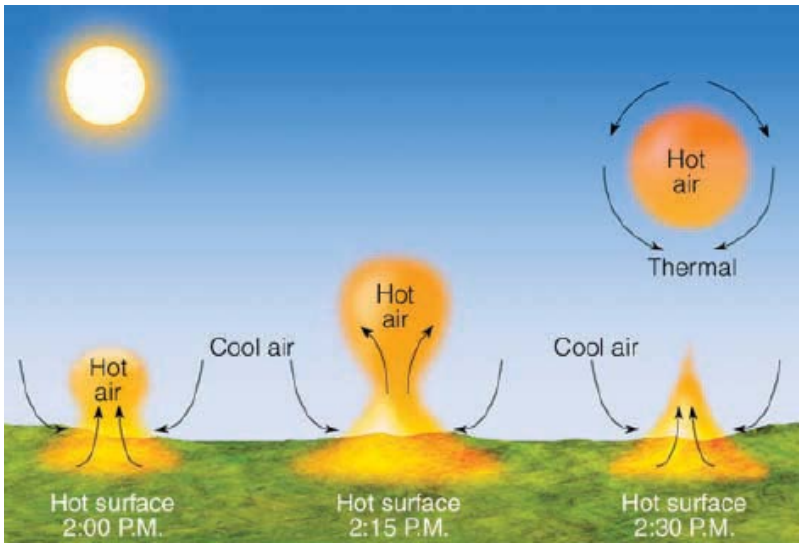

Figure 1.18: The development of a thermal. A thermal is a rising bubble of air that carries heat energy upward by convection (source Meteorology today)

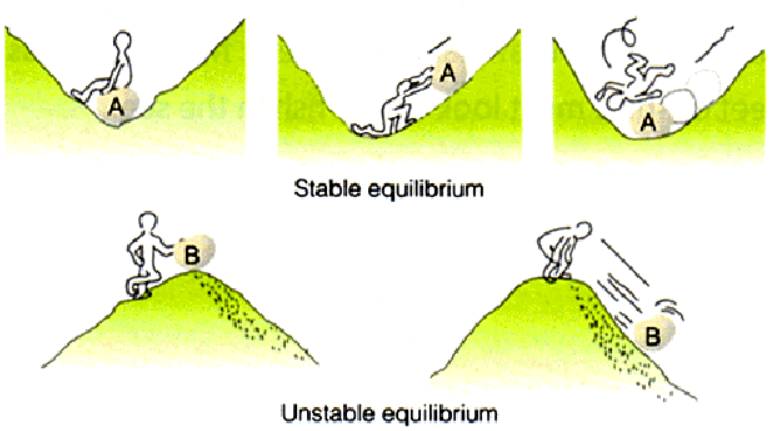

Figure 1.19: Cartoon illustrating stable and unstable situations (from Meteorology today)

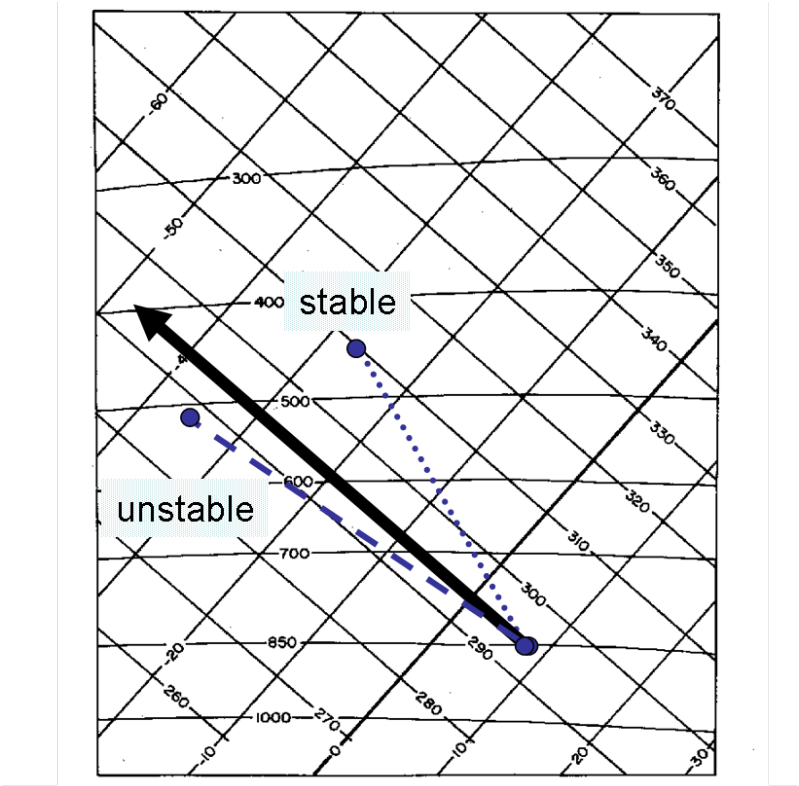

Figure 1.20: Two idealized profiles showing (dotted/dashed) stable/unstable environmental temperature profiles

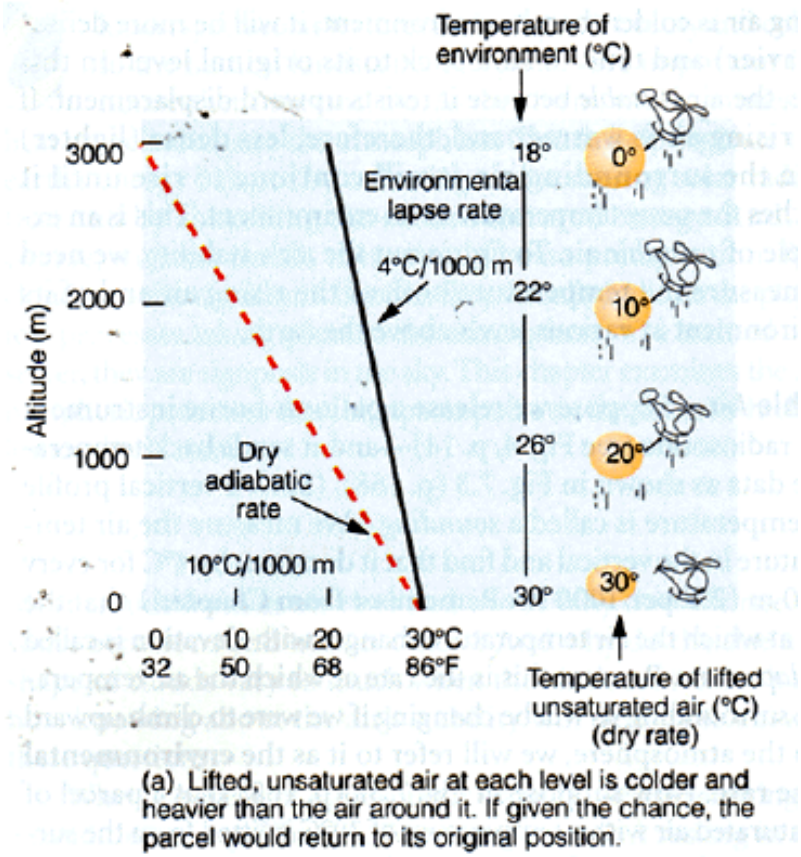

Figure 1.21: Cartoon illustrating dry stable situations (from Meteorology today)

Figure 1.22: Lenticular or lee-wave cloud indicating atmospheric stable layer. Courtesy UCAR

Chapter 2

Moist Thermodynamics

Moist thermodynamics
In the previous section we restricted our analysis to dry air, *we now extend this to include water*, which unlike other atmospheric constituents, can appear in all its three phases: solid, liquid and vapour (Fig. 32).

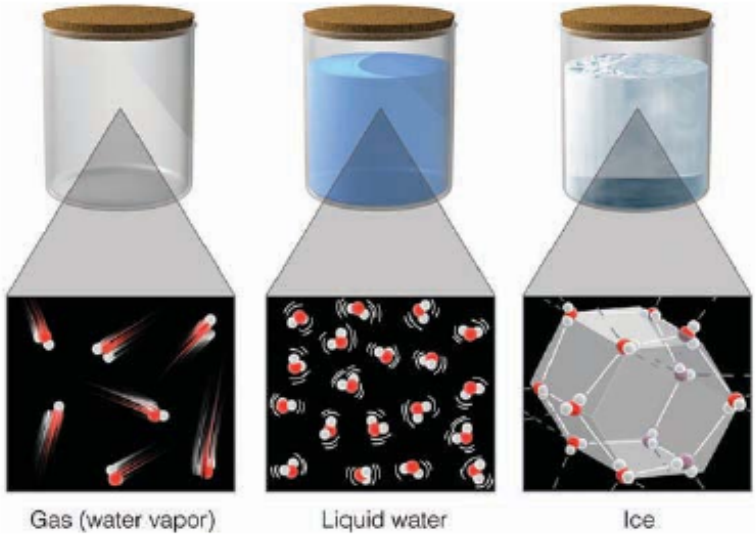

Figure 2.1: The structure of the three states of water (from Meteorology Today)

In water[1], each hydrogen nucleus is bound to the central oxygen atom by a pair of electrons that are shared between them (Fig. 33). In H2O, only two of the six outer-shell electrons of oxygen are used for this purpose, leaving four electrons which are organized into two non-bonding pairs. The repulsions of the electrons lead to the assymetry of the molecule giving it a charge dipole.

The four electron pairs surrounding the oxygen tend to arrange themselves as far from each other as possible in order to minimize repulsions between these clouds of negative charge. This would ordinarly result in a tetrahedral geometry in which the angle between electron pairs (and therefore the H-O-H bond angle) is 109.5^o. However, because the two non-bonding pairs remain closer to the oxygen atom, these exert a stronger repulsion against the two covalent (i.e. bonds that share electrons) bonding pairs, effectively pushing the two hydrogen atoms closer together. The result is a distorted tetrahedral arrangement in which the H-O-H angle is 104.5^o. The H2O molecule is electrically neutral, but the positive and negative charges are *not distributed uniformly* (Fig. 34). The electronic (negative) charge is concentrated at the oxygen end of the molecule, owing partly to the nonbonding electrons (solid blue circles), and to oxygen's high nuclear charge

[1]the following discussion is adapted with permission from the from the excellent Chem1 Virtual Textbook by Stephen Lower. The full link is http://www.chem1.com/acad/webtext/virtualtextbook.html with an abbreviated link given in figure sources

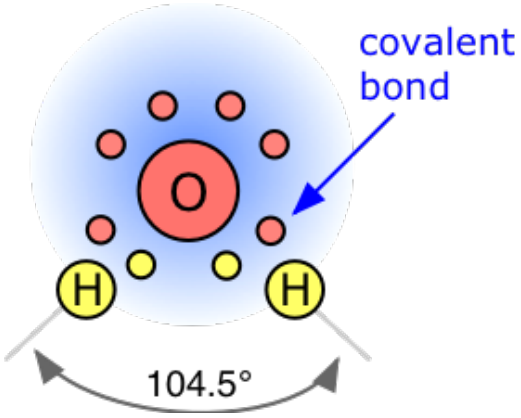

Figure 2.2: The structure of the water vapour molecule(www.chem1.com)

which exerts stronger attractions on the electrons. This charge displacement constitutes an electric dipole, represented by the arrow at the bottom. Opposite charges attract, so it is not surprising that the negative end of one water molecule will tend to orient itself so as to be close to the positive end of another molecule that happens to be nearby (Fig. 35). The strength of this dipole-dipole attraction is less than that of a normal chemical bond, and so it is completely overwhelmed by ordinary thermal motions in the gas phase.

When the H2O molecules are crowded together in the liquid, these attractive forces exert a very noticeable effect, which is referred to as hydrogen bonding.

- The hydrogen bond is somewhat longer than the covalent (a chemical bond involving the sharing of electrons) O-H bond, and is also weaker; about 23 kJ mol^{-1} compared to the O-H covalent bond strength of 492 kJ mol^{-1}
- Owing to disruptions of these weak attractions by thermal motions, the lifetime of any single hydrogen bond is very short

Equation of state for water vapour
Water vapour can be treated as an ideal gas to a good approximation and thus from the gas law it follows that

$$e = \rho_v R_v T, \tag{2.1}$$

where ρ_v is the density of water vapor, and R_v is the specific gas constant for water vapour which is equal to 461.5 J kg^{-1} K^{-1}.

In the literature the ratio between the gas constants for dry air and water vapour is used:

$$\epsilon = \frac{R_d}{R_v} = \frac{m_v}{m_d} \tag{2.2}$$

where $\epsilon = 0.622$ from the values of the gas constants.

Atmospheric air is a mixture of the ideal gases of dry air and water vapour (Fig. 37). From Dalton's law, the total pressure of moist air is the sum of the partial pressures of the dry air and the vapour

$$p = p_d + e. \tag{2.3}$$

2.1 Saturation

Evaporation
Imagine a closed system consisting of a water body and a vacuum above. The water molecules in the water body are in a state of thermal agitation and the most energetic ones will overcome the inter-molecular hygrogen bond attraction and break free of the water body surface. The rate at which vapor molecules leave the surface depends upon the characteristics of the surface.

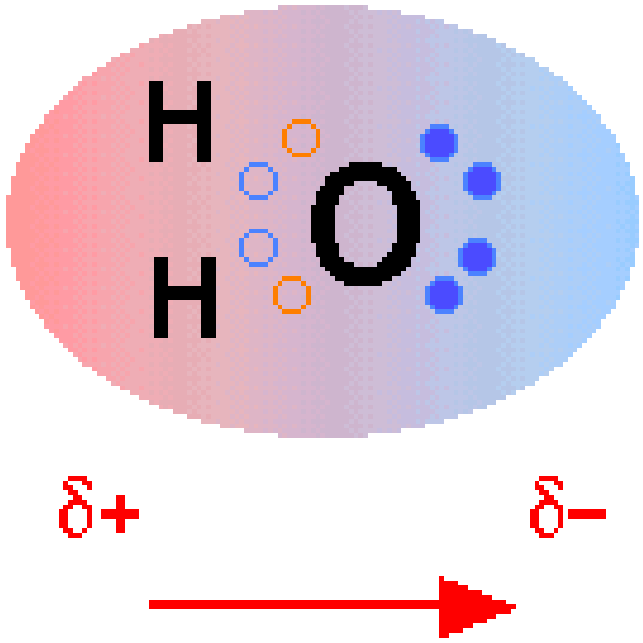

Figure 2.3: The charge dipole (www.chem1.com)

The process is known as *evaporation*.

The vapour vapour pressure increases as a result, which will be denoted e.

Some of the water molecules will subsequently collide with the water surface and stick to the surface. This process is known as *condensation*, and decreases the vapour pressure. The rate at which vapor molecules arrive at a surface of liquid (cloud drop) or solid (ice crystal) depends upon the *vapor pressure*. Since the condensation depends on the vapour pressure, it is apparent that in the absence of external perturbations a state of dynamic equilibrium will eventually be reached in which the rates of *condensation* and *evaporation* equal each other (considering only liquid for now). The vapour is said to be *saturated* in this case, and the vapour pressure e is equal to the so-called *saturation vapour pressure e_s with respect to water.*

As the evaporation rate is only dependent on temperature, and the condensation rate on the vapour pressure, there are two important consequences to note concerning e_s:

1. e_s depends on T and T *only.*

2. Saturation is *independent* of the pressure of other gases

Supersaturation

If the saturation vapour pressure exceed the saturation value $e > e_s$ then the air is said to be *supersaturated* with respect to liquid water. We shall see that greatly supersaturated states *with respect to liquid water* in the atmosphere are not observed, as the excess water vapour quickly condenses to form liquid cloud droplets. The phrase *liquid water* is emphasized as the situation is not the same when it comes to cloud ice crystals as we shall see.

We now derive the dependence of e_s on T. Heat must be supplied to change a unit mass of liquid to vapour at a constant temperature; this is known as the *Latent Heat of Vaporization*, denoted L_v. Throughout the process of evaporation the e_s remains constant as it is a function of T only. For the transition from liquid phase q_1 to vapour phase q_2,

$$L_v = \int_{q_1}^{q_2} dq = \int_{u_1}^{u_2} du + \int_{v_1}^{v_2} pdv = u_2 - u_1 + e_s(v_2 - v_1). \tag{2.4}$$

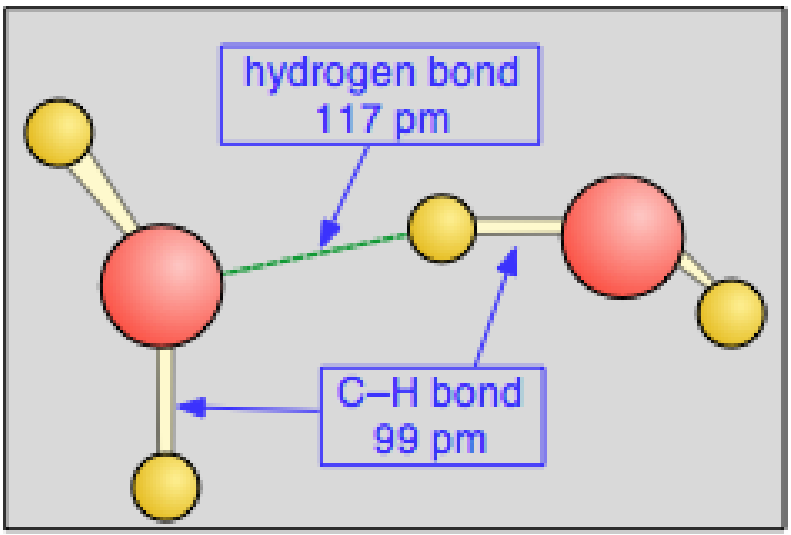

Figure 2.4: The Hydrogen bond between two water vapour molecules. (www.chem1.com)

However, since temperature is also constant we can write

$$L_v = T \int_{q_1}^{q_2} \frac{dq}{T} = T(\phi_2 - \phi_1) \tag{2.5}$$

Equating eqn. (64) and eqn. (65) shows

$$u_1 + e_s v_1 - T\phi_1 = u_2 + e_s v_2 - T\phi_2. \tag{2.6}$$

Gibbs Energy or Gibbs Function
This implies that the so-called *Gibbs Function/Energy*

$$G = u + e_s v - T\phi \tag{2.7}$$

of a system is constant during isothermal, isobaric changes of phase.

The Gibbs function is a measure of the maximum obtainable work from a system at constant temperature and pressure.The Gibbs function does vary however as a function of temperature and pressure, and differentiating eqn. (67) gives:

$$dG = du + v de_s + e_s dv - T d\phi - \phi dT. \tag{2.8}$$

But $Td\phi = dq = du + e_s dv$ giving

$$dG = v de_s - \phi dT. \tag{2.9}$$

The Gibbs function is independent of phase, such that $dG_1 = dG_2$:

$$v_1 de_s - \phi_1 dT = v_2 de_s - \phi_2 dT. \tag{2.10}$$

Clausius Clapeyron Equation
We can now rearrange eqn. (70) to derive the *Clausius Clapeyron Equation*:

$$\frac{de_s}{dT} = \frac{\phi_2 - \phi_1}{v_2 - v_1} = \frac{L_v}{T(v_2 - v_1)}, \tag{2.11}$$

where the last relationship uses eqn. (65). Under ordinary conditions the specific volume for water vapour is much greater than that of liquid, $v_2 \gg v_1$, allowing the Clausius Clapeyron equation to be approximated as

$$\frac{de_s}{dT} \approx \frac{L_v}{T v_2} = \frac{L_v e_s}{R_v T^2}, \tag{2.12}$$

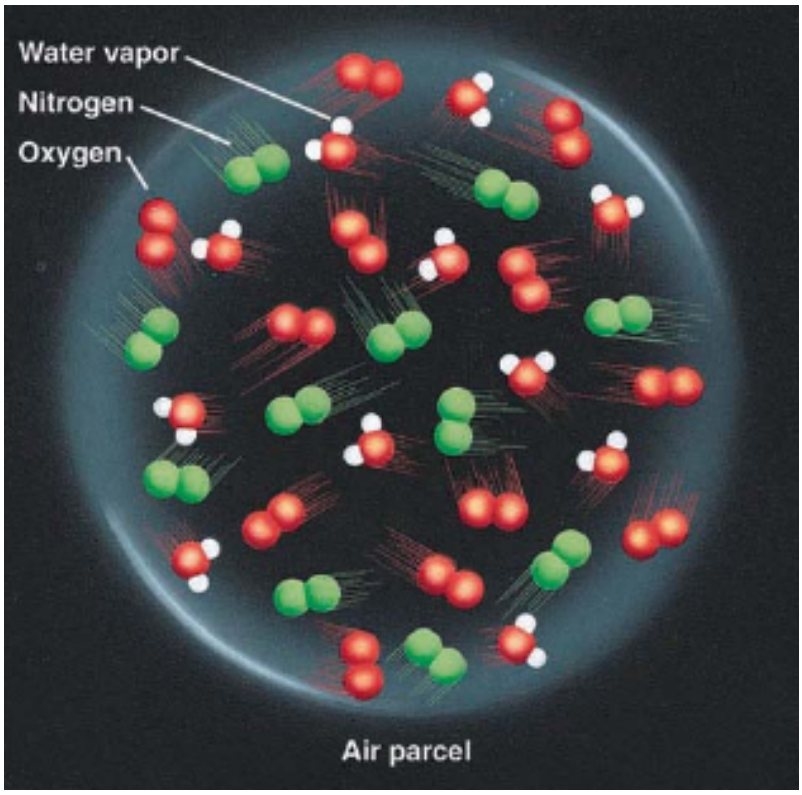

Figure 2.5: Schematic of molecules in moist air (Meteorology today)

where the final relationship uses the Gas Law once again.

At first sight it would appear to be straightforward to integrate eqn. (72) to give e_s as a function of T, but this is complicated by the fact that the Latent heat of vaporization L_v is itself a function of temperature. Fortunately this dependence is weak, with L_v varying by 6% from -30°C to +30°C. Neglecting this dependence as a first approximation, integrating eqn. (72) gives

$$e_s = e_{s0}\exp\left[\frac{L_v}{R_v}\left(\frac{1}{T_0}-\frac{1}{T}\right)\right]. \tag{2.13}$$

e_{s0} is the vapour pressure at temperature T_0, and at $T = 0$°C we have e_{s0} =6.11 hPa, and a value of 2.50×10^6 J kg^{-1} can be assumed for L_v. Substituting these values gives an approximate for for e_s as

$$e_s(T) = Ae^{\frac{-B}{T}} \tag{2.14}$$

where the constants are $A = 2.53 \times 10^8$ kPa and $B = 5.42 \times 10^3$ K. A more accurate empirical form is given by Bolton's formula for the saturation vapour pressure as a function of T in ^{o}C:

$$e_s(T) = 611.2exp\left(\frac{17.67T}{T+243.5}\right) \tag{2.15}$$

e_s doubles for every 10°C increase in temperature. Note that the nonlinearity of the saturation vapour pressure has important consequences for mixing of air parcels as is thus relevant for processes such as atmospheric convection. Below the freezing point at $T = 0$°C the Clausius Clapeyron equation describes the saturation pressure of *supercooled* liquid water (liquid water at temperatures below 0°C), and this is still relevant as we will see later that ice crystals do not form at $T = 0$°C and supercooled liquid cloud droplets are common. Of course at temperatures below freezing ice crystals may be present, and the saturation vapour pressure of ice, denoted e_i is also described by eqn. (72) but with L_v replaced by L_s, which is the *Latent heat of Sublimation*, for which a value of 2.83×10^6 J kg^{-1} can be used. The ratio between the two at subfreezing temperatures is

$$\frac{e_s(T)}{e_i(T)} = \exp\left[\frac{L_f}{R_v T_0}\left(\frac{T_0}{T}-1\right)\right], \tag{2.16}$$

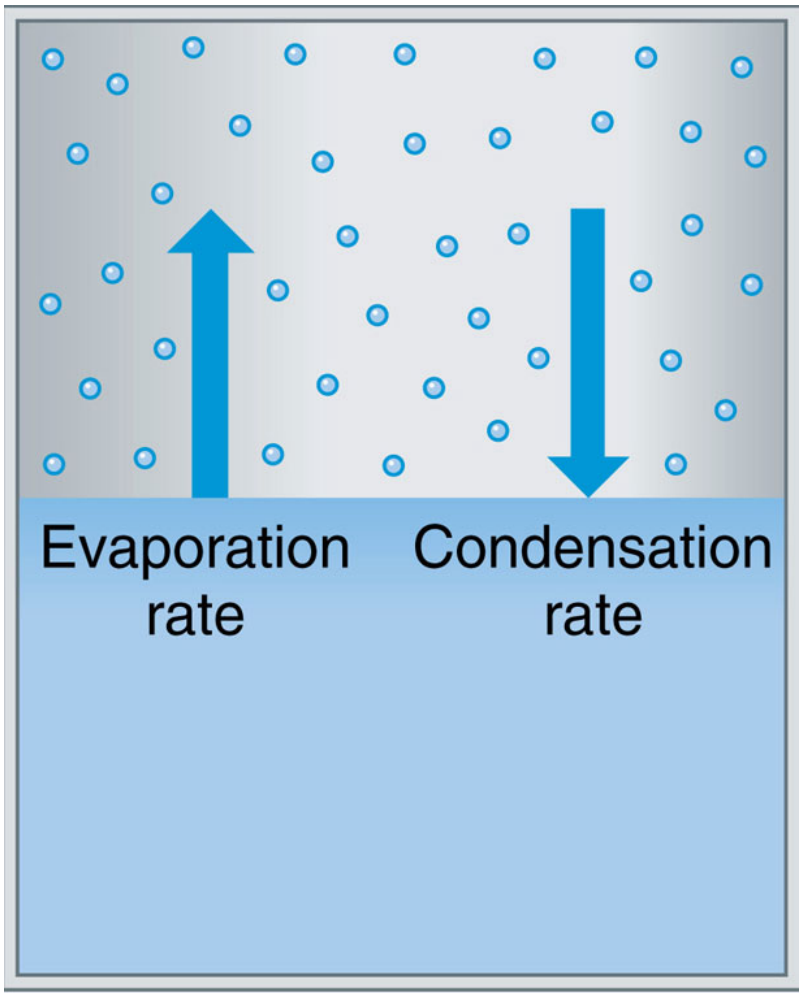

Figure 2.6: Schematic of the evaporation and condensation processes.

where L_f is the *Latent Heat of Fusion* and is equal to $L_s - L_v$. Thus the saturation *with respect to ice* is lower than that *with respect to (supercooled) liquid water* (Fig. 39). Note that while the ratio of e_i and e_s increases as temperature decreases, the *difference* maximizes at around -12C (Fig. 40).

The dependency of the latent heat of vaporization on the temperature
To calculate the dependency of L_v on T we use eqn. (64) and note again that $v_2 \gg v_1$ and that $e_s v_2 = R_v T$. Then differentiating we get

$$\frac{dL_v}{dT} = \frac{du_2}{dT} - \frac{du_1}{dT} + R_v \tag{2.17}$$

Now $\frac{du_2}{dT} = c_{vv}$ which is the *specific heat capacity of water vapour at constant volume* and $\frac{du_1}{dT} = c_{vl}$ is the *specific heat capacity of liquid water at constant volume.*

We again note the relationship that the *specific heat of water vapour at constant pressure* $c_{pv} = c_{vv} + R_v$, and then integrate to get

$$L_v(T) = L_0 - (c_{vl} - c_{pv})(T - T_0), \tag{2.18}$$

where $L_0 = L(T_0)$ is the constant of integration. Both c_{vl} and c_{pv} vary as a function of temperature and pressure, but this variation is weak amounting to less than 3% over the full range of tropospheric conditions, and the constant values of c_{pv} =1870 J kg^{-1} K^{-1} and c_{vl} =4187J kg^{-1} K^{-1} will be assumed here, while c_{vv} ≃1410 J kg^{-1}K^{-1}. For a complete list of gas constants and specific heat values refer to Appendix 2 of Emanuel (1994).

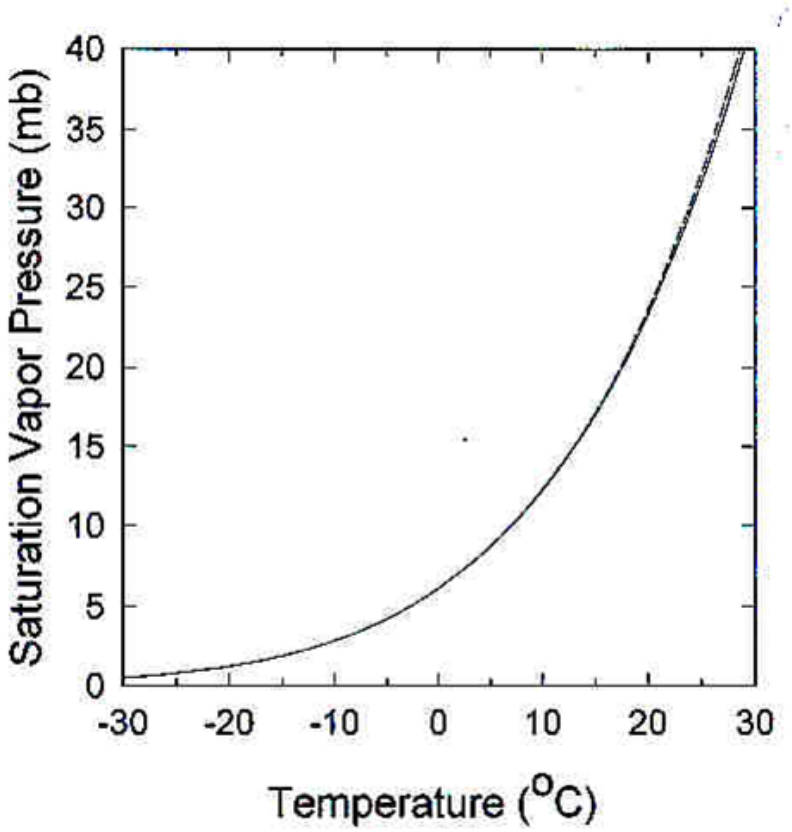

Figure 2.7: The saturation vapour pressure as a function of temperature

2.2 Other measures of water vapour

In addition to the *vapour pressure* e and the *vapour density* ρ_v, there are alternative ways to describe the water vapour content of air that are more commonly used in meteorology.

Mixing Ratio r_v
This is defined as the mass of water vapour per unit mass of *dry* air

$$r_v = \frac{M_v}{M_d} = \frac{\rho_v}{\rho_d}. \tag{2.19}$$

From the equation of state, $\rho_d = \frac{p-e}{R_d T}$, so that

$$r_v = \frac{\rho_v R_d T}{p-e} = \frac{\rho_v R_v T \frac{R_d}{R_v}}{p-e} = \frac{\epsilon e}{p-e} \tag{2.20}$$

The saturation mixing ratio r_s, *with respect to liquid water*, is defined by replacing e with e_s, and *is a function of both pressure and temperature.*

The more accurate Teten's empirical formula for the saturation mixing ratio r_s as a function of pressure p and temperature T is:

$$r_s(T) = \frac{380}{p} exp\left(17.5\frac{(T-273.16)}{(T-32.19)}\right) \tag{2.21}$$

which, neglecting variations of temperature with height, can be differentiated to give:

$$\frac{dr_s(T)}{dT} = r_s \frac{4217}{(T-32.19)^2} \tag{2.22}$$

where p_s is the surface (z=0) pressure.

Specific Humidity q_v

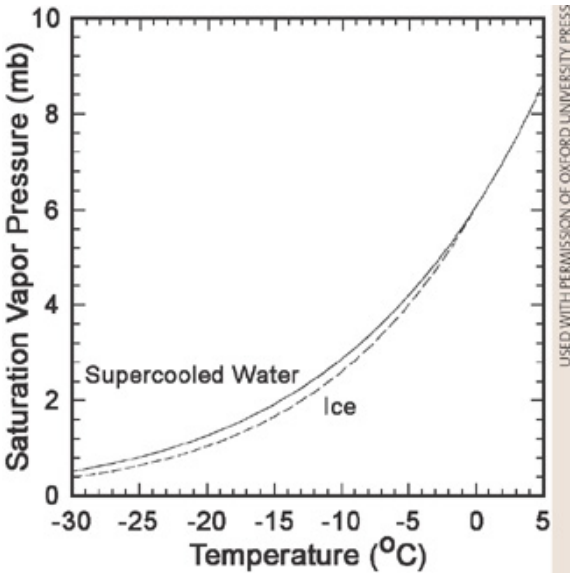

Figure 2.8: The saturation vapour pressure as a function of temperature with respect to ice and liquid (source Atmospheric Thermodynamics by Craig F. Bohren and Bruce A. Albrecht)

The specific humidity is defined as the mass of water vapour per unit mass of *moist* air

$$q_v = \frac{\rho_v}{\rho} = \frac{\rho_v}{\rho_d + \rho_v}, \tag{2.23}$$

and using the same substitution as above (exercise: show)

$$q_v = \frac{\epsilon e}{p - (1-\epsilon)e} \tag{2.24}$$

The saturation specific humidity is defined by replacing e with e_s. At all normal atmospheric conditions $e \ll p$, implying that in practice

$$q_v \approx r_v \approx \frac{\epsilon e}{p}, \tag{2.25}$$

The difference between r_v and q_v is greatest at the surface in the tropics and roughly 2% there[2].

Relative Humidity *RH*
The ratio of the vapour pressure to its saturated value:

$$RH = \frac{e}{e_s}. \tag{2.26}$$

Note that the relative humidity can be approximated as

$$RH \approx \frac{r}{r_s}, \tag{2.27}$$

however often this is used as an exact relationship in the literature. Some texts such as Rogers and Yau (1989) break this convention altogether and define RH in terms of mixing ratio and state eqn. (86) as an approximate relationship Adding water vapour to dry air changes its density. *Q: in which direction?* The molecular weight of water is 18.02 g mol^{-1}, less than that of dry air at 28.97 g mol^{-1}. Therefore the density of water vapour at standard temperature and pressure (1000 hPa and 0^{o}C) is lower than that of dry air *Exercise: calculate these densities.* So a sample of moist air will be less dense than the equivalent dry sample.

Virtual Temperature T_v

[2]This similarity leads to the two terms being used almost interchangeably in meteorology, not good practice, and one that is not helped by the fact that the notation for the specific humidity and mixing ratio are not standard, with q_v often used for mixing ratio in the literature. Note also that the subscript v is not always used.

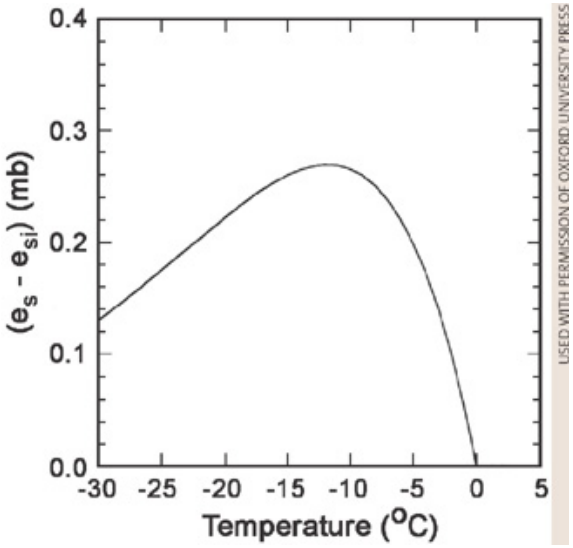

Figure 2.9: The difference in saturation vapour pressure as a function of temperature with respect to ice and liquid (source Atmospheric Thermodynamics by Craig F. Bohren and Bruce A. Albrecht)

A *hypothetical temperature*, the virtual temperature is the temperature a sample of dry air would have to have in order to have the same density an identical volume of the moist air in question, at the same pressure.

To derive T_v we recall:

$$p = p_d + e = \rho_d R_d T + \rho_v R_v T = \rho_d R_d T + \rho_d \frac{\rho_v}{\rho_d} R_d \frac{R_v}{R_d} T \tag{2.28}$$

Recalling the definitions of $\epsilon = R_d/R_v$ and $r_v = \rho_v/\rho_d$, eqn. (88) can be simplified to

$$p = \rho_d R_d T \left(1 + \frac{r_v}{\epsilon}\right) \tag{2.29}$$

and then using the relation $\rho_d = \frac{\rho}{1+r_v}$ (*Exercise: show*)

$$p = \rho R_d T \left(\frac{1 + \frac{r_v}{\epsilon}}{1 + r_v}\right) \tag{2.30}$$

Thus the equation of state for moist air can be written as the equation of state for dry air, but using the adjustment factor in brackets. We thus define the virtual temperature as

$$T_v \equiv T \left(\frac{1 + \frac{r_v}{\epsilon}}{1 + r_v}\right) \tag{2.31}$$

Allowing us to write the equation of state for moist air as

$$p = \rho R_d T_v. \tag{2.32}$$

Since $r_v \ll 1$, by ignoring second order terms the definition of T_v can be simplified to *Exercise: show*

$$T_v = T(1 + \frac{1 - \epsilon}{\epsilon} r_v) \tag{2.33}$$

We can see that for moist air $T_v > T$ always since a unit volume of moist air is less dense than a unit volume of dry air. Thus for moist air it is T_v that should be used in the definition of buoyancy to account for this effect. We define the *virtual* potential temperature in terms of T_v

$$\theta_v \equiv T_v \left(\frac{p_0}{p}\right)^{\frac{R_d}{c_p}}. \tag{2.34}$$

and this quantity is conserved in adiabatic motion of moist air. We can apply the equation of state to moist air by replacing T with T_v, or we can alternatively use the gas constant for moist air R_m:

$$pv = R_d T_v = R_m T \tag{2.35}$$

Thus we can see that R_m is related to R_d by

$$R_m = R_d \left(\frac{1 + \frac{r_v}{\epsilon}}{1 + r_v} \right). \tag{2.36}$$

Take care not to confuse R_m with R_v.

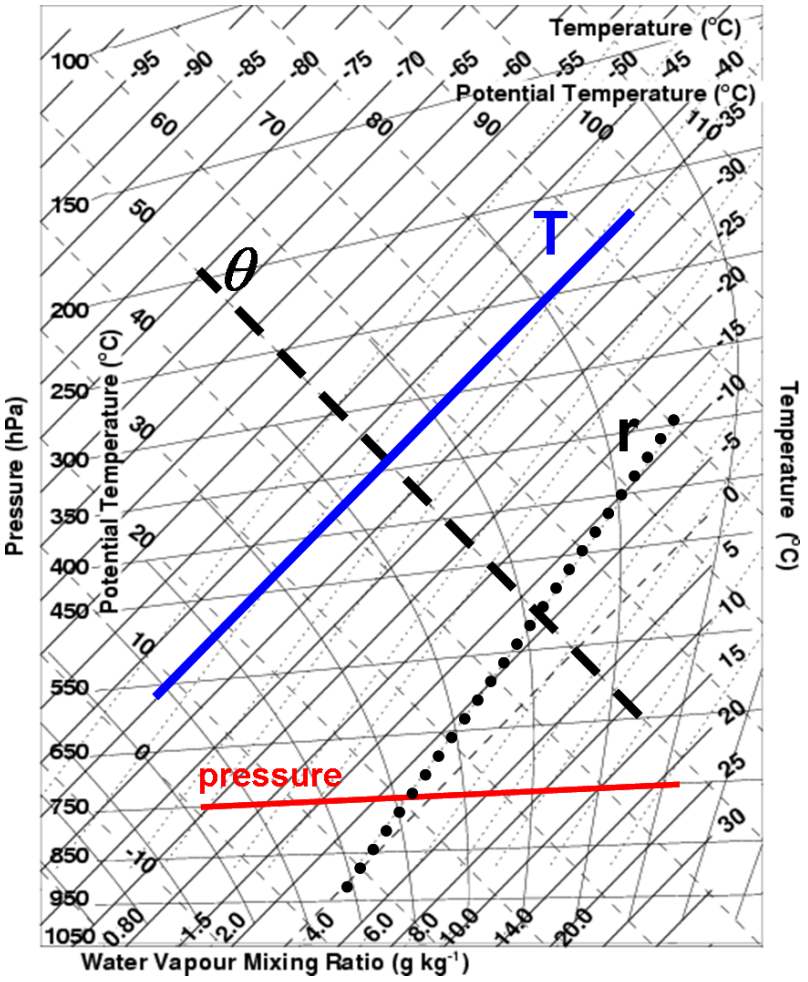

Figure 2.10: A blank tephigram with isopleths of r_s highlighted.

Water Vapour in Tephigrams

We now return to the tephigram introduced in the previous section and add lines of constant (isopleths of) saturation mixing ratio to the tephigram, recalling from eqn. (80) that r_s is a function of pressure and temperature (Fig.41). *Q: This tephigram has an error, such that it is not a true thermodynamic chart. What is it?*

As an aside we reproduce a scanned correct tephigram in Fig. 42, as used and produced by the UK Meteorological Office, unfortunately only for the lower half of the troposphere to 500 hPa. Thus if at a pressure of 950 hPa we measure a temperature of 20°C, we can plot this on the tephigram, marked as a cyan star in Fig. (43. Likewise if we measure a mixing ratio of $r = 10gkg^{-1}$ we can also plot this using the mixing ratio isopleths, marked as an orange star. Making measurements through out the atmosphere (e.g. by a balloon) we can plot a sounding of temperature and humidity, as show by the yellow and blue stars.)

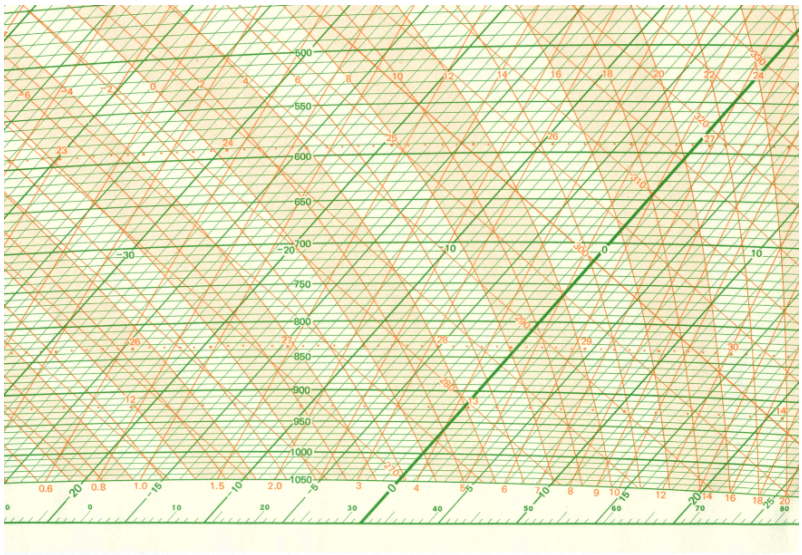

Figure 2.11: A *correct* tephigram. Courtesy EWG at McGill.

attempt tephigram exercise I

We will now return to the Cabauw profiles (Fig. 17) and examine the humidity measurements taken during the balloon ascent, which are shown in Fig. 44. These show the sharp drop in humidity at the boundary layer top at 400m and that the humidity is roughly constant through the boundary layer. From the RH profile, we can see relative humidity increasing through the boundary layer and that the top of the boundary layer is almost saturated.

2.3 Water variables in the liquid and ice state

Analogous to the water vapour variables described above we can define similar variables that describe the quantity of liquid water or ice in air

- Absolute liquid (ice) water ice density[3] : ρ_l or L kg m^{-3} (or ρ_i)
- Liquid (ice) water mixing ratio: $r_l = \frac{\rho_l}{\rho_d}$ kg kg^{-1} (or r_i)
- Specific liquid (ice) water content: $q_l = \frac{\rho_l}{\rho}$ kg kg^{-1} (or q_i)

The total water mixing ratio is the sum of the three phases $r_t = r_v + r_l + r_i$. Additionally, analogous to the T_v we can define the density temperature[4] T_ρ which is the temperature dry air would have to have equal density to moist cloud air (*exercise: show*):

$$T_\rho \equiv T\left(\frac{1+\frac{r_v}{\epsilon}}{1+r_t}\right) \tag{2.37}$$

Similarly to T_v, if we assume $r_l \ll 1$ and $r_i \ll 1$ and ignore second order terms we get

$$T_\rho \simeq T(1+\frac{1-\epsilon}{\epsilon}r_v - r_l - r_i) \tag{2.38}$$

The last two terms show how liquid and ice make a parcel more dense, and this effect is referred to as the *water loading effect*.

[3] Attention! The absolute liquid water density here is the total mass of liquid water droplets divided by a unit volume of cloudy air - this is not to be confused with the density of liquid water which will denoted ρ_L. To avoid confusion, the rest of this course always uses liquid water mixing ratio or specific water content, or we will use the notation L instead of ρ_l

[4] Again, there is not agreement in the literature concerning the virtual temperature T_v which is sometimes defined to include liquid and ice. Here we follow the notation of Emanuel (1994)

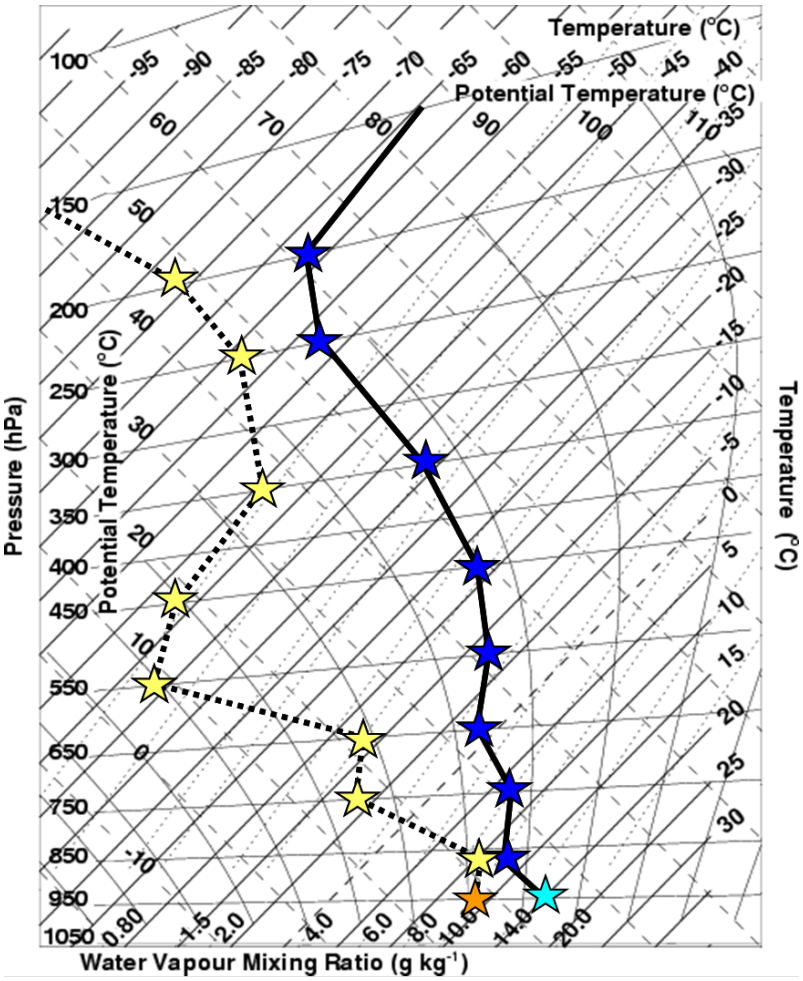

Figure 2.12: tephigram with T and r soundings plotted

2.4 Specific heat of moist air

Specific heat of moist air c_{vm} and c_{pm}
The presence of moisture alters the specific heat capacity of air. We add heat to a sample of air consisting of a unit mass (1kg) of dry air and r kilograms of water vapour

$$(1+r)dq = c_v dT + r c_{vv} dT \tag{2.39}$$

this gives

$$c_{vm} = \frac{dq}{dT} = c_v \left(\frac{1 + \frac{c_{vv}}{c_v} r}{1+r} \right) \tag{2.40}$$

As $c_{vv}/c_v = 1.96 \approx 2$ then ignoring second order terms,

$$c_{vm} \approx c_v(1+r) \tag{2.41}$$

Likewise the *specific heat of moist air at constant pressure* can be approximated

$$c_{pm} \approx c_p(1+0.9r) \tag{2.42}$$

As $r < 10^{-2}$ these correction factors can generally be neglected.

Reminders:

- What does it mean for air to be saturated?
- What is e_s a function of?

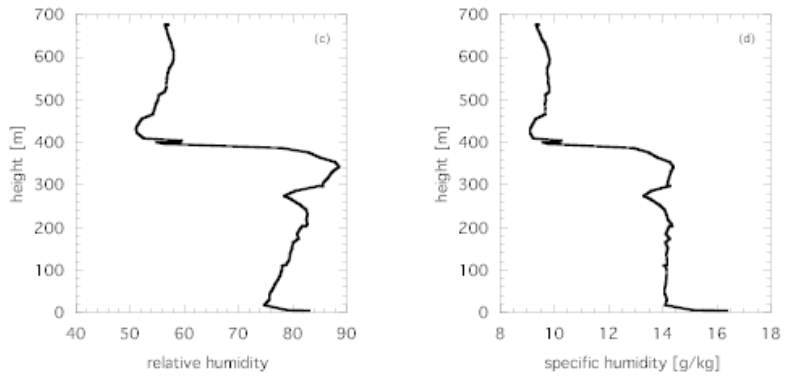

Figure 2.13: Vertical profile of RH and θ for the Cabauw profile in Fig. 17.

- What was one of the problems to get an expression $e_s = F(T)$?
- *Q: Can you think of some processes by which air can become saturated?*

2.5 Ways of reaching saturation

Figure 2.14: We will now start to consider processes relevant to deep moist convection so here is a superfluous photo to motivate you (source unknown)

Ways of reaching saturation
There are several processes by which a parcel of air may become saturated which are all relevant to cloud physics:

- Diabatic cooling (e.g. radiation)
- Adiabatic cooling (e.g. ascent)
- Evaporation (e.g. of precipitation falling through parcel)

Diabatic Cooling: Dew Point Temperature T_d
As air is cooled isobarically, r is conserved, and the air will reach saturation when T is such that

$$r_s(T) = r. \tag{2.43}$$

This temperature is known as the *Dew Point Temperature* T_d. One can write equivalently $e(T) = e_s(T_d)$.

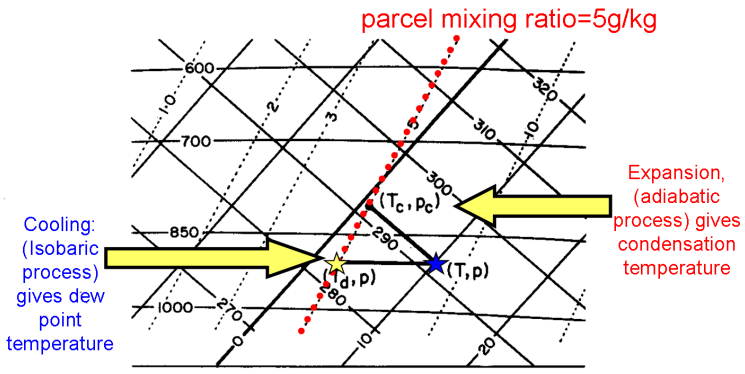

FIG. 2.2. Temperature, dew point, and isentropic condensation temperature, indicated on a tephigram. In the example shown the sample of air at 10°C, 900 mb, is assumed to have a mixing ratio of 5 g/kg. Its dew point, found from the intersection of the 900 mb isobar and the 5 g/kg vapor line, is 2.2°C. Its isentropic condensation point, found from the intersection of the adiabat through (T, p) with the 5 g/kg vapor line, is at 0.7°C and approximately 800 mb.

Figure 2.15: Figure from Rogers and Yau (1989) showing the dew-point and condensation temperatures. See text for details

Adiabatic Cooling: Condensation Temperature T_c

As air is cooled adiabatically, θ_v is conserved, and the air will reach saturation at the *isentropic condensation temperature and pressure*. This pressure level is sometimes referred to as the *lifting condensation level* or LCL.

If ascent and expansion continues condensation will occur (we will see why air does not become supersaturated with respect to liquid later), *thus the temperature will decrease at a slower rate.* Now in this conceptional model of a parcel of air undergoing ascent in a cumulus cloud, we need to decide what happens to the condensed water: Does it remain in the parcel or will it fall out? *Q: If the droplets remain in the parcel what do we need to consider?*

Pseudo-adiabatic process

If it is assumed that the condensed water remains in the parcel of air then we would need to account for its *water loading* effect and its modification of the *heat capacity*. Moreover when the freezing point is reached we need to consider if and how some of the liquid droplets will freeze, invoking ice processes which are complex, as we shall see. These are issues concerning *microphysics* and *cloud dynamics*, thus involving a *cloud model*.

For now we take the simplest case and assume that all condensate is immediately lost as precipitation, known as the *pseudo-adiabatic* assumption (Fig. 47).

For moist saturated ascent and neglecting the correction factor for the specific heat (so we can use c_p),

$$c_p dT - v dp + L_v dr_s \simeq 0 \tag{2.44}$$

Thus the saturated moist adiabatic lapse rate Γ_s is

$$\Gamma_s = \frac{dT}{dz} = \frac{v}{c_p}\frac{dp}{dz} - \frac{L_v}{c_p}\frac{dr_s}{dz} = \Gamma_d - \frac{L_v}{c_p}\frac{dr_s}{dz} \tag{2.45}$$

(*Exercise: show* $\Gamma_d = \frac{v}{c_p}\frac{dp}{dz}$).

As temperature falls with height, $\frac{dr_s}{dz}$ is negative implying that $\Gamma_s > \Gamma_d$. Recalling that Γ_d = -9.8 K km^{-1}, Γ_s is generally between -3 to -4 K km^{-1} in the lower troposphere. *Q: In the upper troposphere* $\Gamma_s \sim \Gamma_d$*, why is this the case?*

Isobaric Equivalent temperature T_{ie}

Let us take two parcels of air at the same pressure, but that differ in both their temperatures and humidity contents; how can we compare them energetically? One measure is the *isobaric*

Figure 2.16: Schematic of parcel ascending and reaching saturation, with condensed water falling out instantaneously in the so-called *pseudo-adiabatic* assumption.

equivalent temperature, T_{ie}. T_{ie} is the temperature that a parcel would have if all of the humidity would condense isobarically.

As this is an isobaric process then $dp = 0$ and integrating eqn. (104):

$$T_{ie} = T + \frac{L_v}{c_p} r_v \tag{2.46}$$

neglecting the temperature dependence of L_v as always.

Adiabatic Equivalent temperature T_e

As this isobaric process of T_{ie} can not occur in the atmosphere, we can instead define the tephigram related *adiabatic equivalent temperature* T_e, by raising the parcel to the upper troposphere, condensing the water and then descending to the original pressure.

From eqn. (104), we divide by $c_p T$, use the first law in the pressure term to get,

$$\int_T^{T_e} \frac{dT}{T} - \int_p^p \frac{Rdp}{C_p p} + \int_{r_v}^0 \frac{L dr_s}{C_p T} = 0, \tag{2.47}$$

and then assume T is a constant in the humidity term (a fairly reasonable approximation as T varies by at most 30%) to permit the integration and get

$$T_e = T \exp\left(\frac{L_v r_v}{c_p T}\right). \tag{2.48}$$

Sometimes you will see T set to T_c in the humidity term (why?), giving T_c in the exponential term on the RHS.

Equivalent potential temperature θ_e

We found it useful to derive θ_v which was conserved in dry adiabatic motions. An analogous quantity (approximately) conserved in moist adiabatic motions is the *equivalent potential temperature* θ_e.

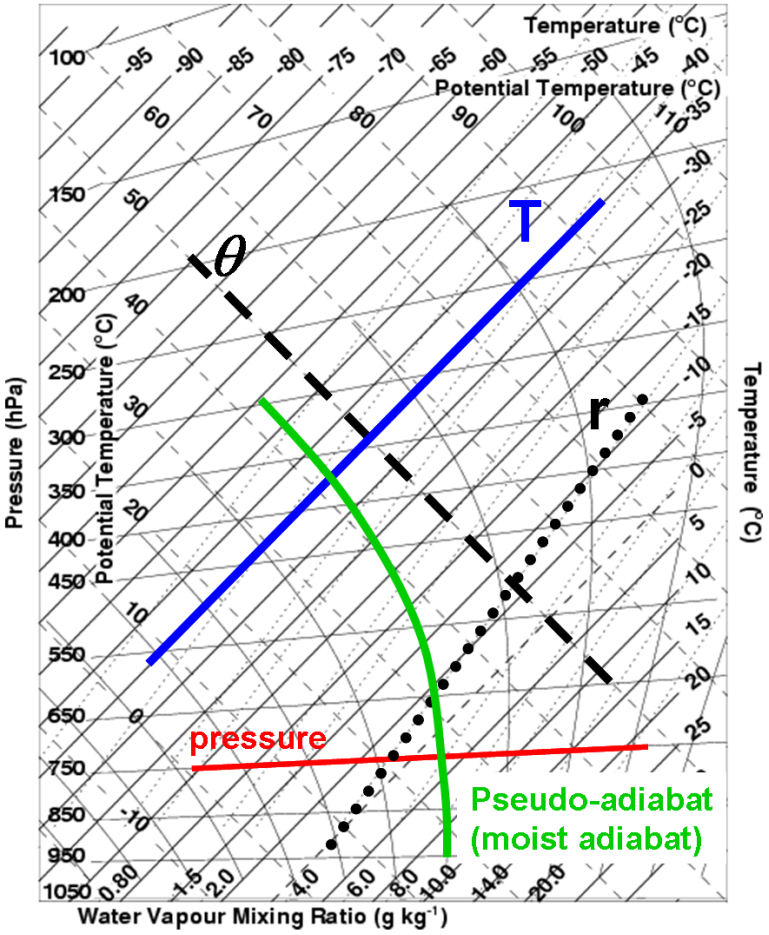

Figure 2.17: A blank tephigram with moist adiabats highlighted.

We will see that each moist adiabat is uniquely labelled by one value of θ_e. The graphical determination of this is given in Fig. 49: after condensation the parcel follows a moist adiabat until all moisture is condensed, and then descends dry adiabatically to the reference pressure. θ_e can be approximated by

$$\theta_e = \theta \exp\left(\frac{L_v r_v}{c_p T}\right) \tag{2.49}$$

Evaporation: Wet Bulb Temperature T_w
In a Stevenson screen there is usually a wet bulb thermometer to measure the wet bulb temperature T_w, and determine the atmospheric water vapour content. The thermometer bulb is wrapped in a muslin cloth kept damp by a wick to a liquid reservoir, and the bulb is thus cooled by the evaporation process (Fig. 50). T_w is the temperature reached if water vapour is evaporated into it until it becomes saturated, with the latent heat provided by the air. Note that $T_d \leq T_w \leq T$, and that the difference between T_w and T_d provides a measure of the saturation of the atmosphere

To calculate the wet-bulb temperature we consider an air parcel consisting of unit mass of dry air with mixing ratio r_v of water vapour. The heat associated with the evaporation of dr_v is $-L_v dr_v$. Thus

$$(1 + r_v) C_{pm} dT = -L_v dr_v \tag{2.50}$$

Using the definition of C_{pm} we get

$$C_p dT \simeq \frac{-L_v dr_v}{(1 + r_v)(1 + 0.9r)} \tag{2.51}$$

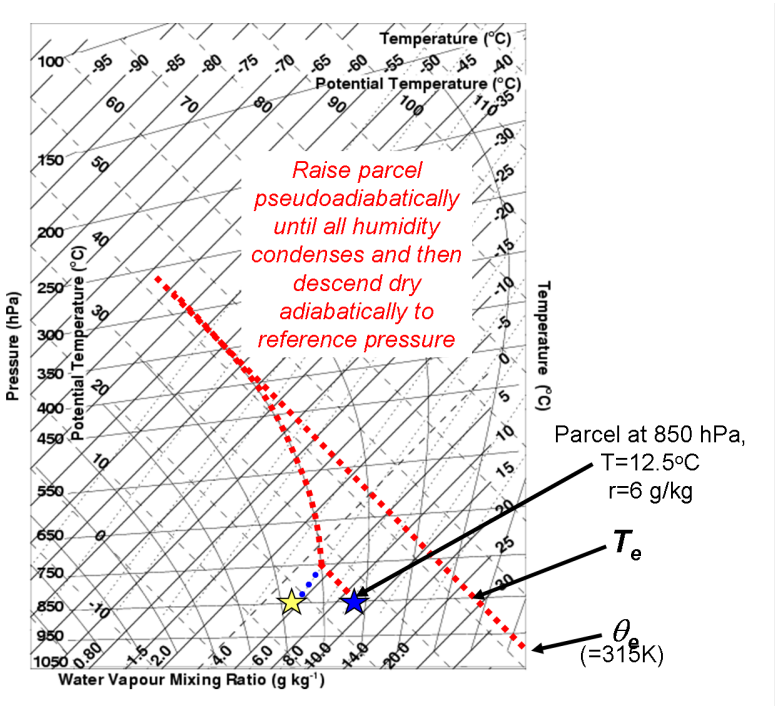

Figure 2.18: A blank tephigram showing the definition of T_e and θ_e.

For most purposes, we can neglect the correction factors and assume

$$C_p dT \approx -L_v dr_v \tag{2.52}$$

Treating L_v as constant we can integrate to get

$$T_w = T - \frac{L_v}{C_p}(r_s(p, T_w) - r_v) \tag{2.53}$$

Q: what is the problem to solve this equation for T_w? To get T_w we substitute eqn. (74) to give a form that can be solved by iteration:

$$T_w = T - \frac{L_v}{C_p}(Ae^{\frac{-B}{T_w}} - r_v) \tag{2.54}$$

However we can estimate T_w directly from the tephigram as we shall see now. Figure 51 shows the construction to derive the wet bulb temperature T_w from a tephigram by lifting a parcel adiabatic to reach saturation and then following a moist adiabat back down to the original pressure. If the moist adiabat is followed to a reference pressure P_0 =1000 hPa, then the resulting temperature is known as the *wet bulb potential temperature* θ_w. Note that there is a one-to-one unique mapping between θ_w and $theta_e$. With each referring to a unique moist adiabat.

Exercise: attempt tephigram exercise II

Summary

We have introduced variables that described the thermodynamic state of air and allow us to compare the energetics of two air masses equivalently that may have differing properties of temperature and humidity. We discussed a number of conserved variables, that act as "markers of air" and are conserved under adiabatic motion. θ was conserved in dry adiabatic ascent of a dry air parcel, and for a moist air parcel undergoing unsaturated ascent θ_v and r_v were conserved. For an air-mass undergoing moist saturated ascent θ_e or equivalently θ_w are (approximately) conserved. If the condensed water falls out of the air parcel instantaneous the process is called pseudo-adiabatic. If the condensed water remains in the parcel, r_t is conserved, and the water loading and condensate heat capacity must be accounted for. The vertical gradients of θ and θ_e indicate the likelihood of convection.

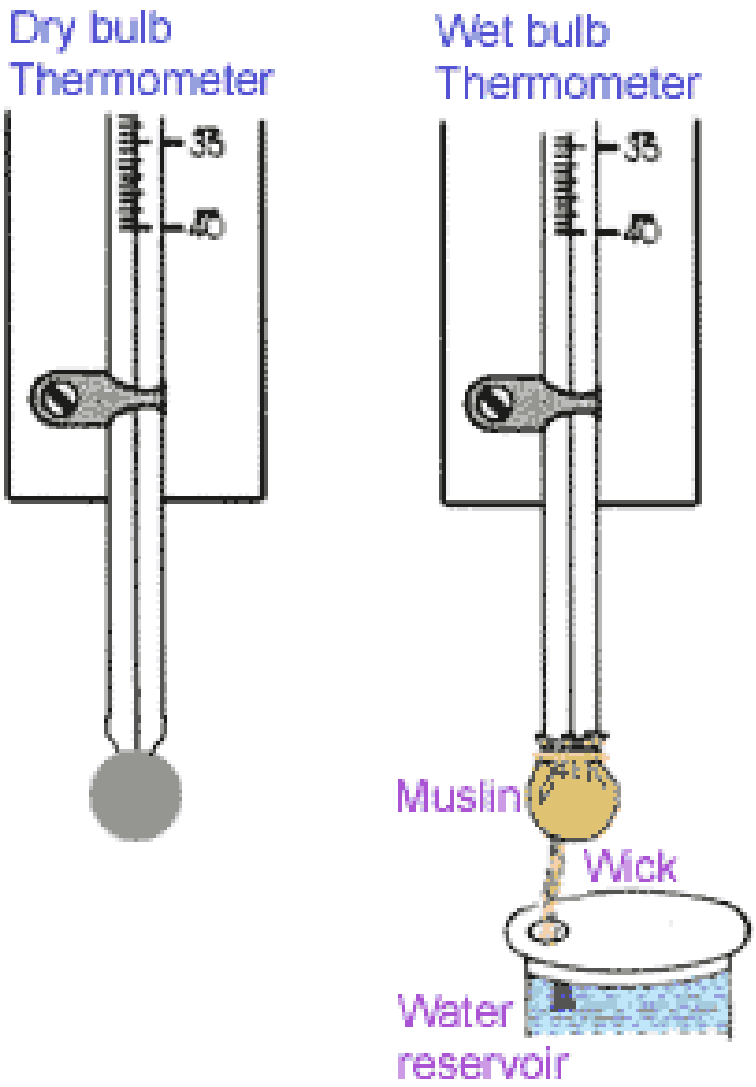

Figure 2.19: Method of measuring the wet-bulb temperature

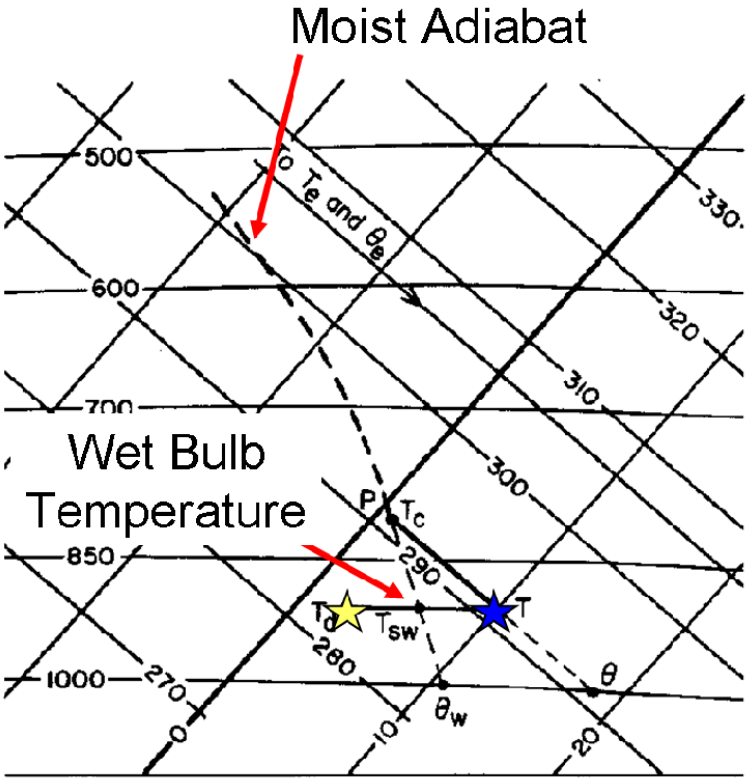

Figure 2.20: Figure from Rogers and Yau (1989) showing the calculation of wet-bulb temperature from a tephigram. This is known as **Normand's Construction**.

Chapter 3

Atmospheric Convection

3.1 Overview

In this section we will briefly introduce various types of convection that can occur. The detailed study of the dynamical equations concerning the each regime type is beyond the scope of this introductory course, however it is important to be able to place the convection regime types into context, which are given in Fig. 52.

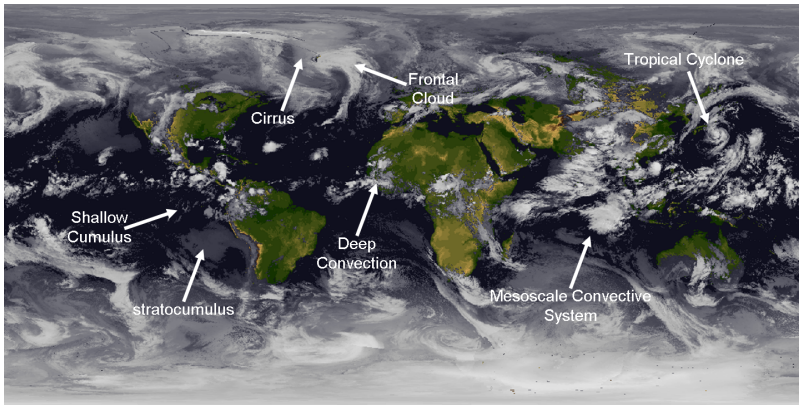

Figure 3.1: A composite infra-red cloud image where bright white indicates cold cloud tops. Some example convective cloud regimes/types are highlighted

The chart of vertical cloud types (Fig. 53) illustrates common cloud types as a function of height. It is seen that many of these are of type "cumulus" which are associated with vertical atmospheric instability and thus are vertically extended.

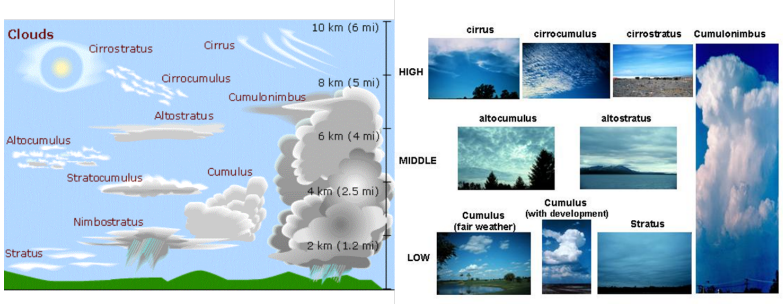

Figure 3.2: Chart of cloud types as a function of height (left) schematic chart with height scale and (right) photos (source unknown)

Photos of tropical convective clouds are given in Fig. 54.

Convection

Figure 3.3: Tropical convective cloud types (source UCAR)

Convection is the name given to any motions that result from the action of the gravitional field on variations in density

Convection in the atmosphere can take a variety of forms, and often involves the complexity of phase changes of water vapour.

3.2 Convection in the atmospheric boundary Layer

The lower boundary of the atmosphere is the solid or liquid surface of the Earth.

The planetary boundary layer
The part of the atmosphere that is directly influenced by the presence of this surface and responds to the presence of this surface on *timescales shorter than one hour* is generally referred to as the atmospheric or planetary *boundary layer*, which we will refer to as the *PBL*.

SKIP to PBL

3.2.1 Heat capacity of the surface

The sea surface in low wind conditions is relatively simple in its interaction with the atmosphere, while land surfaces, with complicated topography and varying land surface properties is more complex. One major difference between the two is the effective heat capacity which governs the daily (diurnal) and seasonal cycles of temperature.

Heat Capacity of water
Water is very transparent to solar radiation, especially in the visible range of wavelengths. sunlight is attentuated as it travels downwards from the surface, with a small fraction reaching depths of tens of metres, depending on the turbidity (cloudiness) of the water.

Turbulent mixing can spread the heating deeper, especially over longer (seasonal timescales), implying daily and seasonal equivalent depths of the absorbing layer of 10 and 50m. The resulting heat capacity of this layer, and the difference in net heat loss/gain of the diurnal and seasonal cycles of radiation input, imply a diurnal temperature range of about 0.1K and seasonal range of approximately 2.5 K.

In the absence of vegetation the surface heat balance is relatively straightforward:

$$R_n - G = H + LE \tag{3.1}$$

where R_n is the net radiative flux density, G is the heat flux into the soil, and H and LE are the sensible and latent heat fluxes, respectively (Noilhan and Planton, 1989).

Bowen Ratio
The ratio of the sensible to latent surface heat fluxes is known as the Bowen ratio: $\frac{H}{LE}$

The land surface is complex, with a highly varying surface characteristics. The albedo (reflectivity) of the surface, for example, can change dramatically from low values over forest or swamp to very highly reflective snow or ice covered surfaces. We do not cover the details here, but the depth of the layer heated by the daily and seasonal cycles is determined by the thermal diffusivity of the surface material. Even a relatively conductive wet soil is effected by the annual cycle to a depth of no more than a few metres, the daily cycle affects a much thinner layer, and thus the daily cycle of surface temperature over land is far greater than that over ocean.

This is seen in Fig. 55. A worm living at a depth of 6m only experiences at most 10% of the annual temperature cycle of the surface, and usually a lot less! the daily temperature cycle only affects a depth of tens of centimetres.

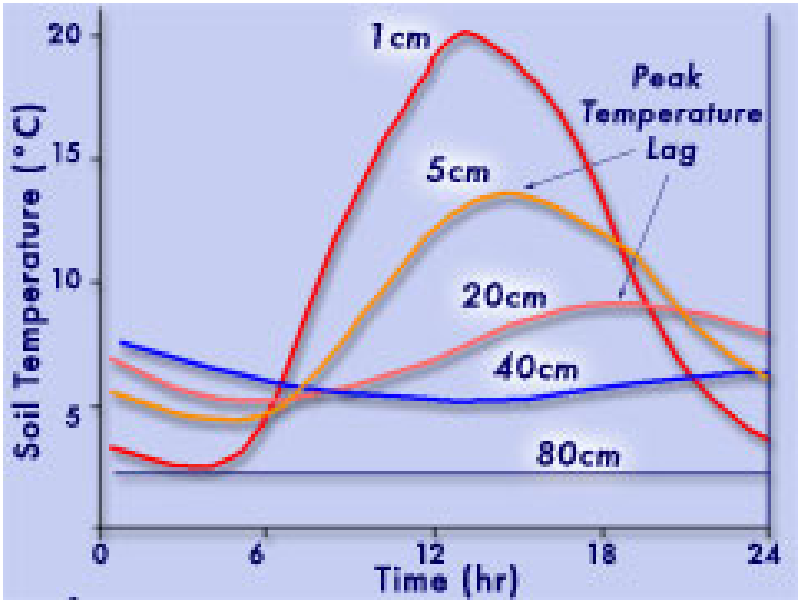

Figure 3.4: The reduction in temperature cycle as a function of depth, note how the temperature wave phase changes as a function of depth.

This difference in thermal capacity is summarized in table 2.

material	dry peat	wet sand	water	air	units
density	300	2000	1000	1.2	kg m^{-3}
specific heat capacity	1910	1480	4180	1000	J kg^{-1} K^{-1}
thermal conductivity	0.06	2.2	0.57	0.025	W m^{-1} K^{-1}
damping depth					
diurnal	5.2	14	500^A	30000^A	cm
annual	1.0	2.7	100^A	7000^A	m
heat capacity					
diurnal	0.04	0.6	31^A	0.63^A	M J K^{-1} m^{-2}
annual	0.81	11.4	590^A	12^A	M J K^{-1} m^{-2}

Table 3.1: Thermal properties of surface materials taken from McIlveen (1991). ^{A} marks turbulent eddy values.

3.2.2 Structure of the PBL

The boundary layer can be divided into the interfacial layer, the surface layer and the turbulent layer above (Fig. 56)

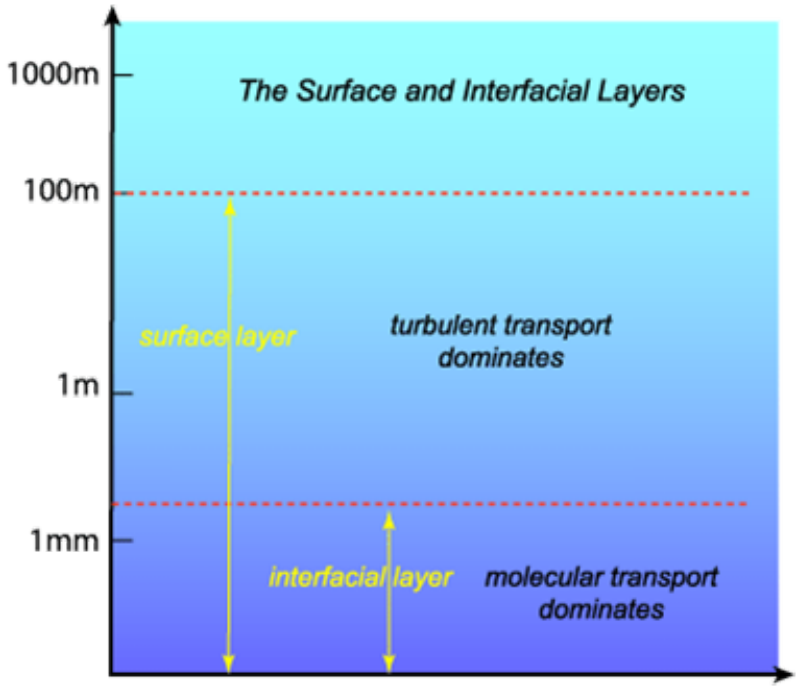

Figure 3.5: A sketch of the layers that make up the boundary layer.

3.2.3 The laminar layer

Laminar Layer
Air molecules in contact with a liquid or solid surface are at rest, due to the forces of intermolecular attraction. At a short distance from the surface, air can move, but the flow is orderly and laminar due to the viscous friction, hence the name *laminar layer*.

The depth of the laminar layer is extremely thin, on the order of 1mm and the viscosity implies gradients of meteorological quantities are very high in this layer. For example over a strongly heated land surface, temperature can drop by 2K over the laminar layer.

Further from the surface, flow speeds increase and the impact of the surface roughness leads to non-laminar or *turbulent* flow. In the lowest tens of metres, the turbulence energy transport can not remove the instability that results from the strong surface heating, and the temperature profile is super-adiabatic, in this *surface layer*.

Further from the surface the impact of the heating reduces, and the turbulence results in a *well mixed layer* that is close to neutral.Thus the turbulent boundary has a structure along the lines of Fig. 57, which also shows the *entrainment zone* at the boundary layer top where turbulent eddies encounter the temperature inversion.

Their upward momentum can carry them through the inversion where they mix with air above and within the inversion layer and then sink to their level of neutral buoyancy. This mixing process is important and weakens the inversion strength, while also bringing more mass into the boundary layer, causing it to deepen.

3.2.4 Diurnal cycle of the PBL

The diurnal cycle of the PBL is thus depicted in fig. 58. Note how the stable noctural layer leaves evidence of a residual inversion from the day before.

Note that the boundary layer is highly turbulent during the day as alternatively emphasized in Fig. 59.

If the turbulent boundary layer becomes deep enough to cause saturation then cloud will form. We saw an example of this fair-weather cumulus earlier in the course. If the well mixed layer is capped by a strong stable temperature inversion then the buoyant turbulent updraughts will be stunted quickly when rising into the base of the stable layer. Thus strong temperature inversions

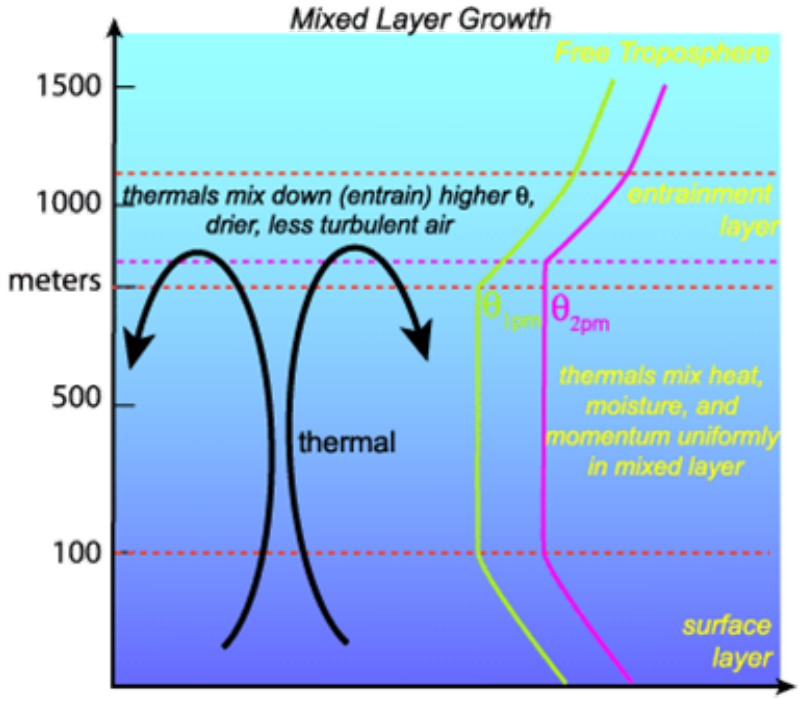

Figure 3.6: A sketch of the deeper layers that make up the boundary layer, also showing the entrainment zone at the boundary layer top.

Figure 3.7: A smoke plume in the PBL showing the nature of turbulence

forming under regions of subsidence (such as associated with anti-cyclone or over the Eastern Pacific) lead to stratocumulus with a high cloud cover

In the literature we talk of stratus or stratocumulus; the accepted division being based on the optical thickness (i.e. thickness measured in radiative terms) being greater (less) than 23. However the terms are used interchangeably in reality.

This schematic in Fig. 60 illustrates the main features of Marine stratocumulus (source Bjorn

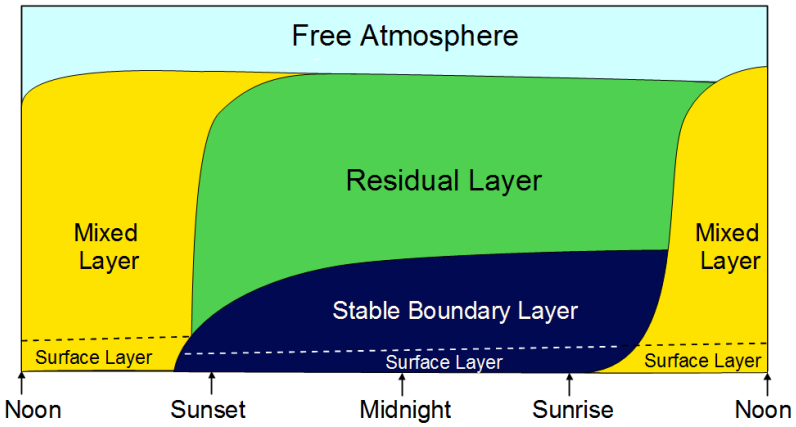

Figure 3.8: A sketch of the diurnal evolution of the PBL, also showing the entrainment zone at the boundary layer top.

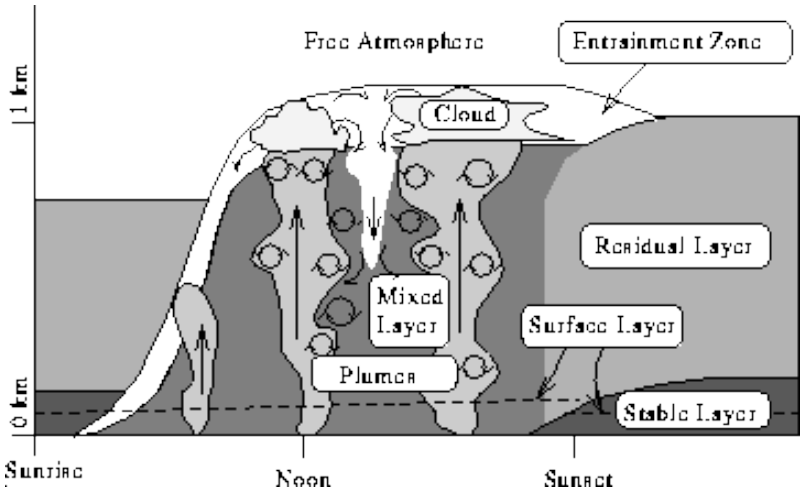

Figure 3.9: A second sketch of the diurnal evolution of the PBL, also showing the entrainment zone at the boundary layer top. Source: Antti Piironen, http://lidar.ssec.wisc.edu/

Figure 3.10: Example stratocumulus

Stevens). We remind ourselves that θ and q_v are near constant in the well mixed sub-cloud layer.

Part of the entrainment is radiatively driven by cloud top cooling (see radiation component of PA).

The strong temperature inversion acts as a cap to parcel ascent. But what happens if the inversion reduces or a parcel is particularly energetic?

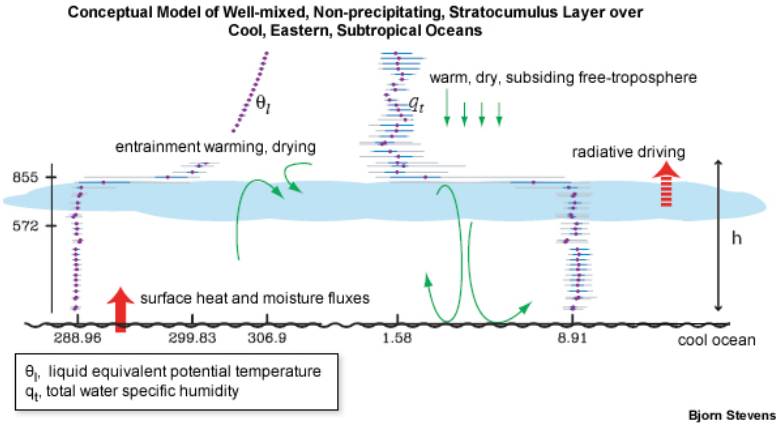

Figure 3.11: Example stratocumulus (source Bjorn Stevens)

3.3 Single cell deep convection

Deep convection involves parcel ascent from the boundary layer to the tropopause. We introduce the concepts of stability measures relevant for deep convection.

If the strength of the inversion erodes, some energetic parcels of air may penetrate the inversion, and then undergo moist saturated ascent to the tropopause, forming thunderstorms, or *deep moist convection*. These have three distinct development stages (ca. 1 hour lifetime). (Fig. 62)

- Cumulus growth stage: successive moistening of environment
- Mature stage: droplets suspended by updraughts, precipitation formation, drop evaporation and rainfall drags forms downdraughts.
- Dissipation stage: intense precipitation, downdraughts dominate updraughts, updraughts cease (low shear), storm dissipation.

Note: The following more detailed description of thunderstorm development is taken from *Meteorology Today* **by C. D. Ahrens.** Ordinary cell (air mass) thunderstorms or, simply, ordinary thunderstorms, tend to form in a region where there is limited wind shear - that

Figure 3.12: Photo of deep cumulus cloud (source ?)

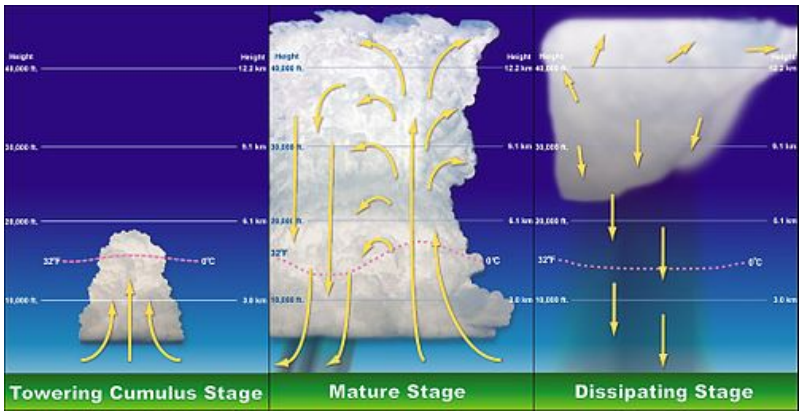

Figure 3.13: Schematic of the development and dissipation of a single-cell thunderstorm convective event (Doswell)

.

is, where the wind speed and wind direction do not abruptly change with increasing height above the surface. Many ordinary thunderstorms appear to form as parcels of air are lifted from the surface by turbulent overturning in the presence of wind. Moreover, ordinary storms often form along shallow zones where surface winds converge. Such zones may be due to any number of things, such as topographic irregularities, sea-breeze fronts, or the cold outflow of air from inside a thunderstorm that reaches the ground and spreads horizontally. These converging wind boundaries are normally zones of contrasting air temperature and humidity and, hence, air density.

Extensive studies indicate that ordinary thunderstorms go through a cycle of development from birth to maturity to decay. The first stage is known as the cumulus stage, or growth stage. As a parcel of warm, humid air rises, it cools and condenses into a single cumulus cloud or a cluster of clouds (Fig. 62a). If you have ever watched a thunderstorm develop, you may have noticed that at first the cumulus cloud grows upward only a short distance, then it dissipates. The top of the cloud dissipates because the cloud droplets evapo- rate as the drier air surrounding the cloud mixes with it. However, after the water drops evaporate, the air is more moist than before. So, the rising air is now able to condense at successively higher levels, and the cumulus cloud grows taller, often appearing as a rising dome or tower. As the cloud builds, the transformation of water vapor into liquid or solid cloud particles releases large quantities of latent heat, a process that keeps the rising air inside the cloud warmer (less dense) than the air surrounding it. The cloud continues to grow in the unstable atmosphere as long as it is constantly fed by rising air from below. In this manner, a cumulus cloud may show extensive vertical development and grow into a towering cumulus cloud (cumulus congestus) in just a few minutes.

During the cumulus stage, there normally is insufficient time for precipitation to form, and the updraughts keep water droplets and ice crystals suspended within the cloud. Also, there is no lightning or thunder during this stage. As the cloud builds well above the freezing level, the cloud particles grow larger. They also become heavier. Eventually, the rising air is no longer able to keep them suspended, and they begin to fall. While this phenomenon is taking place, drier air from around the cloud is being drawn into it in a process called entrainment. The entrainment of drier air causes some of the raindrops to evaporate, which chills the air. The air, now colder and heavier than the air around it, begins to descend as a downdraught. The downdraught may be enhanced as falling precipi- tation drags some of the air along with it. The appearance of the downdraught marks the beginning of the mature stage. The downdraught and updraught within the mature thunderstorm now constitute the cell. In some storms, there are several cells, each of which may last for less than 30 minutes. During its mature stage, the thunderstorm is most intense. The top of the cloud, having reached a stable region of the atmosphere (which may be the stratosphere), begins to take on the familiar anvil shape, as upper-level winds spread the cloud's ice crystals horizontally (see Fig. 62b).

The cloud itself may extend upward to an altitude of over 12 km and be several kilometers in diameter near its base. Updraughts and downdraughts reach their greatest strength in the middle of the cloud, creating severe turbulence. Lightning and thunder are also present in the mature stage. Heavy rain (and occasionally small hail) falls from the cloud. And, at the surface,

there is often a downrush of cold air with the onset of precipitation. Where the cold downdraught reaches the surface, the air spreads out horizontally in all directions. The surface boundary that separates the advancing cooler air from the surrounding warmer air is called a gust front. Along the gust front, winds rapidly change both direction and speed. Look at Fig. 62b and notice that the gust front forces warm, humid air up into the storm, which enhances the cloud's updraught. In the region of the downdraught, rainfall may or may not reach the surface, depending on the relative humidity beneath the storm. In the dry air of the desert Southwest, for example, a mature thunderstorm may look ominous and contain all of the ingredients of any other storm, except that the raindrops evaporate before reaching the ground. However, intense downdraughts from the storm may reach the surface, producing strong, gusty winds and a gust front.

After the storm enters the mature stage, it begins to dissipate in about 15 to 30 minutes. The dissipating stage occurs when the updraughts weaken as the gust front moves away from the storm and no longer enhances the updraughts. At this stage, as illustrated in Fig. 62c, downdraughts tend to dominate throughout much of the cloud. The reason the storm does not normally last very long is that the downdraughts inside the cloud tend to cut off the storm's fuel supply by destroying the humid updraughts. Deprived of the rich supply of warm, humid air, cloud droplets no longer form. Light precipitation now falls from the cloud, accompanied by only weak downdraughts. As the storm dies, the lower-level cloud particles evaporate rapidly, some- times leaving only the cirrus anvil as the reminder of the once mighty presence. A single ordinary cell thunderstorm may go through its three stages in one hour or less. **End of book quote**.

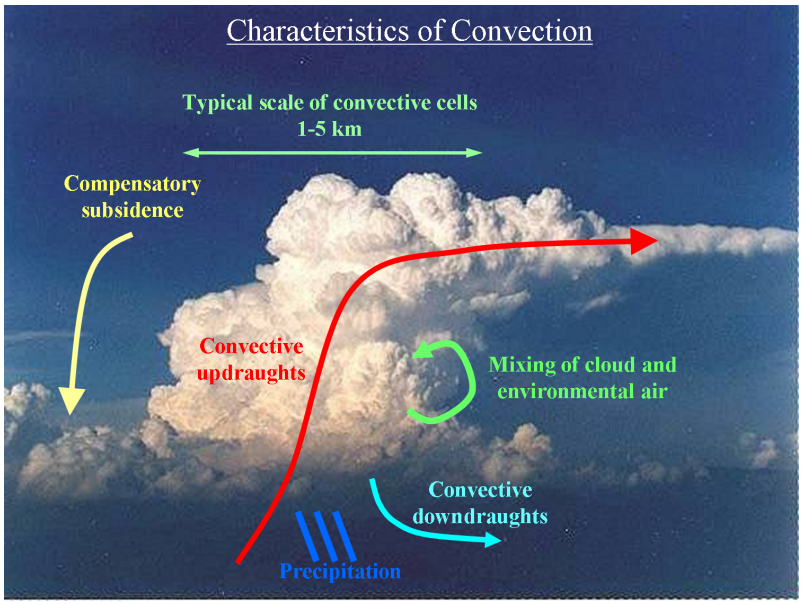

Figure 3.14: Schematic of other processes to consider in deep convection

Processes in deep convection

There are several factors to consider in a model of deep convection (Fig. 63):

- Mixing between convection and its environment
- Ultimate depth of the cloud
- Precipitation and convective moisture transport
- Convective heating rates
- Downdraught formation
- Convective 'triggering'

3.3.1 Key convective parameters

The presence of instability is of great importance in weather forecasting and to understand the various climatic regimes. Earlier we classified three stability states in a dry environment. For a moist environment there are five stability categories.

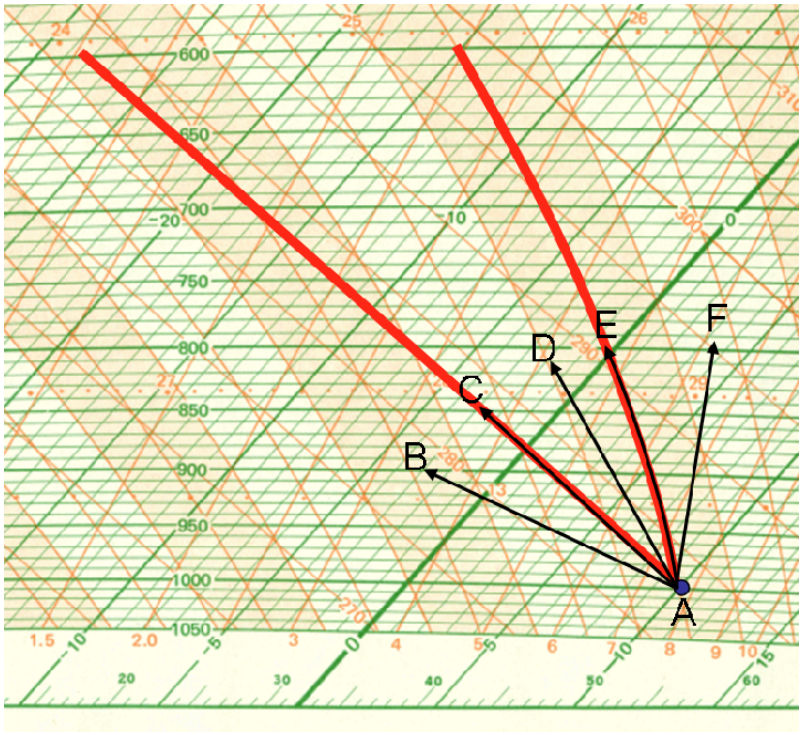

Figure 3.15: Tephigram showing 5 possible stability categories for environmental lapse rate. The red lines highlight the parcel dry and moist adiabats.

.

- AB: Absolutely unstable (even if unsaturated, parcel is warmer),
- AC: Dry Neutral (parcel is neutral to dry ascent),
- AD: Conditionally unstable (for unsaturated ascent profile is stable, while it is unstable for saturated ascent),
- AE: Saturated Neutral (for saturated ascent parcel neutral),
- AF: Absolutely stable

Key convective parameters
We now examine the case of conditional instability further to define a range of parameters that are important for describing the potential for, and characteristics of, convection

. Let us examine the case of the surface parcel in the blown up tephigram in Fig. 65. The parcel is unsaturated and thus if lifted follows a dry adiabat. The profile is stable to dry adiabatic ascent, but let us assume that the mechanical lifting and/or the parcel initial momentum is sufficient such that ascent can continue. The parcel continues until it reaches the condensation temperature and pressure that we defined earlier. This pressure level is called the *lifting condensation level*, or LCL.

If ascent continues, after the LCL the parcel follows a moist adiabat. Since the profile is conditionally unstable, the moist adiabat must eventual cross the environmental temperature profile, implying that the parcel becomes warmer than the environment. After this point the saturated parcel accelerates upwards, undergoing *free convection* in meteorology terminology. Thus the level at which the parcel becomes positively buoyant is called the *level of free convection* or LFC.

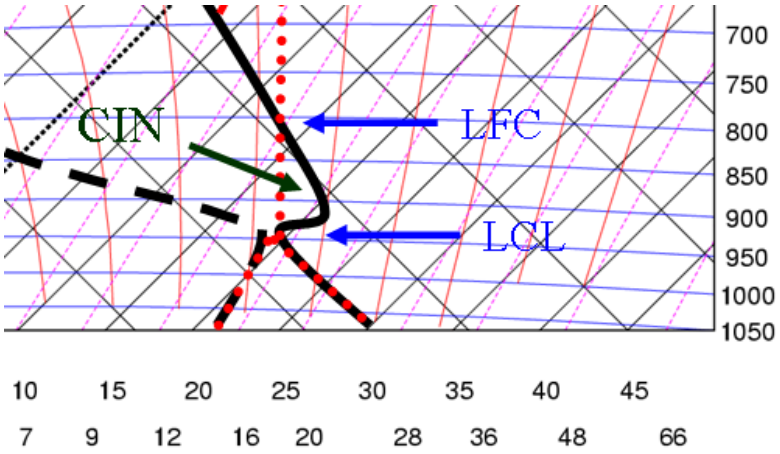

Figure 3.16: Tephigram showing the boundary layer profiles of temperature and humidity and the pseudo-adiabatic ascent of the surface parcel. See text for details of definitions.

.

Convective inhibition, CIN

The area enclosed on the tephigram between the parcel trajectory and the environmental profile when the parcel is negatively buoyant (i.e. colder than the environmental) is proportional to the energy that the parcel must be supplied to overcome this inhibition barrier to undergo free convection. This area is thus called the *convective inhibition*, more commonly abbreviated to *CIN*.

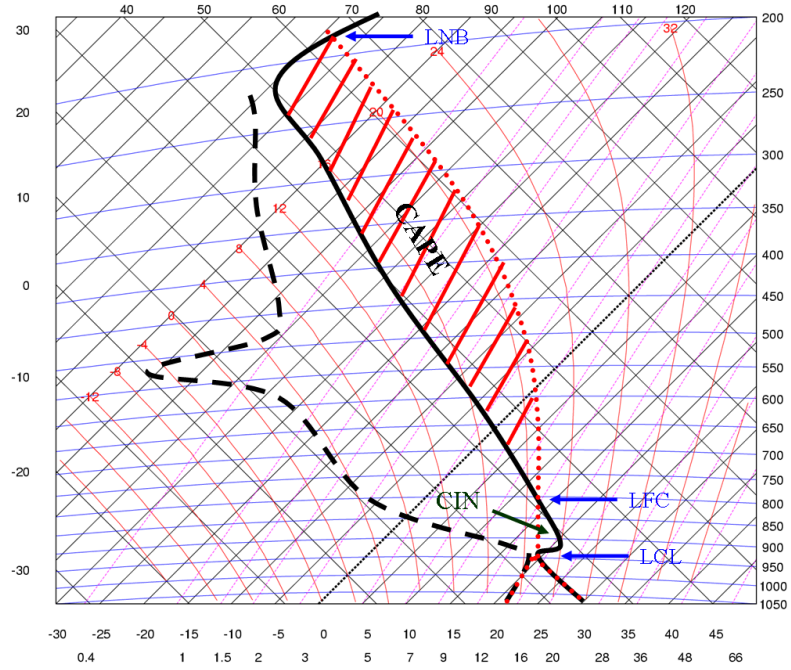

Figure 3.17: Full tephigram from Fig. 65 additionally showing the full parcel ascent and the positive energy area of CAPE.

.

After the LFC, the parcel accelerates upwards following a moist adiabat. *Reminders: What assumptions does this make concerning the parcel?* The ascent may continue to the upper troposphere where it recrosses the environmental temperature line. This level is called the *level of neutral buoyancy* or LNB . The parcel will overshoot and undergo oscillatory motion, but the LNB marks the cloud top approximately.

CAPE

The positive area demarked is proportional to the energy that can be potentially gained by the parcel. We will call the *total*[1] energy available to a parcel starting from level i the *convective available potential energy* or CAPE.

If we concern ourselves only with the motions in the vertical then CAPE calculated for a parcel starting from pressure level p is thus the integral of the buoyancy acceleration

$$CAPE_p = \int_i^{LNB} B dz, \tag{3.2}$$

and substituting the approximation of buoyancy using the virtual temperature ($B = g(T_{v,u} - T_{v,env})/T_{v,env}$), we get

$$CAPE_p = g \int_i^{LNB} \left(\frac{T_{v,u} - T_{v,env}}{T_{v,env}} \right) dz, \tag{3.3}$$

where $T_{v,u}$ and $T_{v,env}$ are the updraught/environment parcel virtual temperatures. We recall that equall areas are proportional to equal energies on a thermodynamic chart. If we follow a parcel through its moist adiabatic ascent and then then trace the environmental temperature profile back down to the original pressure, the area enclosed by this trajectory, the $CAPE$, is equivalent to the energy available to do work on the parcel. If we assume that all of the potential energy represented by the $CAPE$ is converted to the parcel kinetic energy, we can estimate the peak updraught velocity as

$$w_{max} = \sqrt{2CAPE_{p_s}}, \tag{3.4}$$

where we are assuming a parcel starting from the surface (p_s is the surface pressure). In reality frictional forces and updraught mixing greatly reduce the actual velocities achieved in convective clouds.

Q: updraught velocities tend to be higher in convection over land than oceans, why do you think this is?

To summarize this, we have defined

- LCL: Lifting Condensation Level
- LFC: Level of Free Convection
- CIN: Convective Inhibition
- LNB: Level of neutral buoyancy
- CAPE: Convective available potential energy

Figure 67 shows the anvil cloud spreading out from a thunderstorm over Mali in West Africa. Notice how flat the anvil top is, marking the LNB. Over the convective updraught region, the cloud top is undulating and higher, revealing the over-shooting updraughts.

3.3.2 Convective triggering

We can see from the tephigram in Fig. 66 that surface parcels are stable to small displacements, but unstable for large displacements. This is why the profile is termed *conditionally unstable* when $\Gamma_d < \Gamma_{env} < \Gamma$. The triggering of deep convection is a rather discrete occurrence. If the atmospheric profile has positive CAPE, then if a boundary layer parcel can overcome CIN, it will then often proceed to form deep convection, which will reach teh LNB near the radiative troposphere.

This is apparent when examining the PDF of cloud top heights which lead to this picture of trimodal convection in Johnson et al. (1999) (Fig. 68). There are a number of mechanisms by which the CIN can be overcome:

- Mechanical lifting
  - Flow over orography
  - Air rising over colder, denser air masses at fronts

[1] i.e. including CIN. Often the literature refers to the CAPE of a sounding as *only* the positive area, as marked in Fig. 66, but here we follow Emanuel (1994).

Figure 3.18: View from space of a convective even over Mali (image courtesy of NASA)

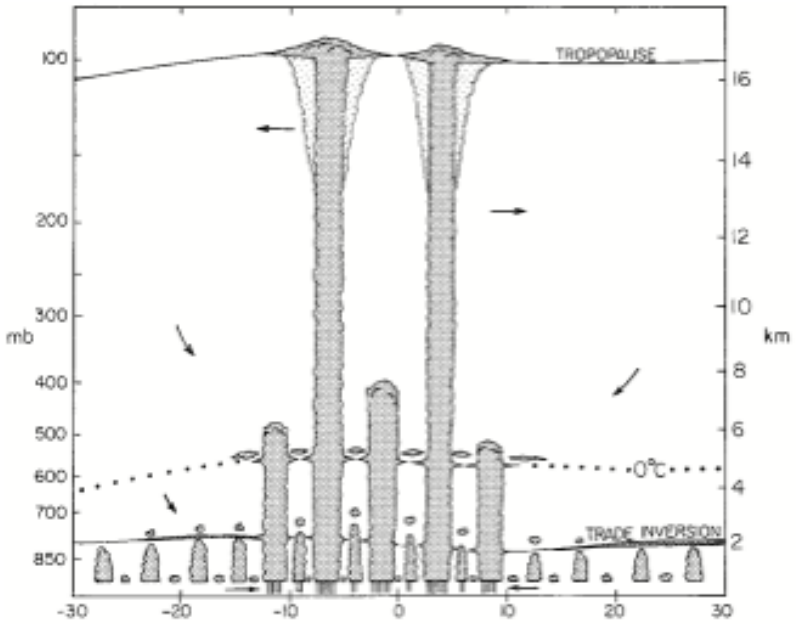

Figure 3.19: Schematic of convection structure in the Tropics (from Johnson et al., 1999)

  - Air rising over denser cold-pools from other convective events.

- Surface convergence due to low pressure perturbation
  - land-sea breeze
  - elevated heat low
  - meso-scale pressure perturbations
- Increasing boundary layer h (moist static energy)
  - Surface heating
  - or moistening

Triggering: Flow over orography
A schematic of flow-induced orographic triggering is given in 69 from Banta and Barker Schaaf (1987). They use radar and satellite imagery to locate common triggering locations of convection over the Rocky Mountains.

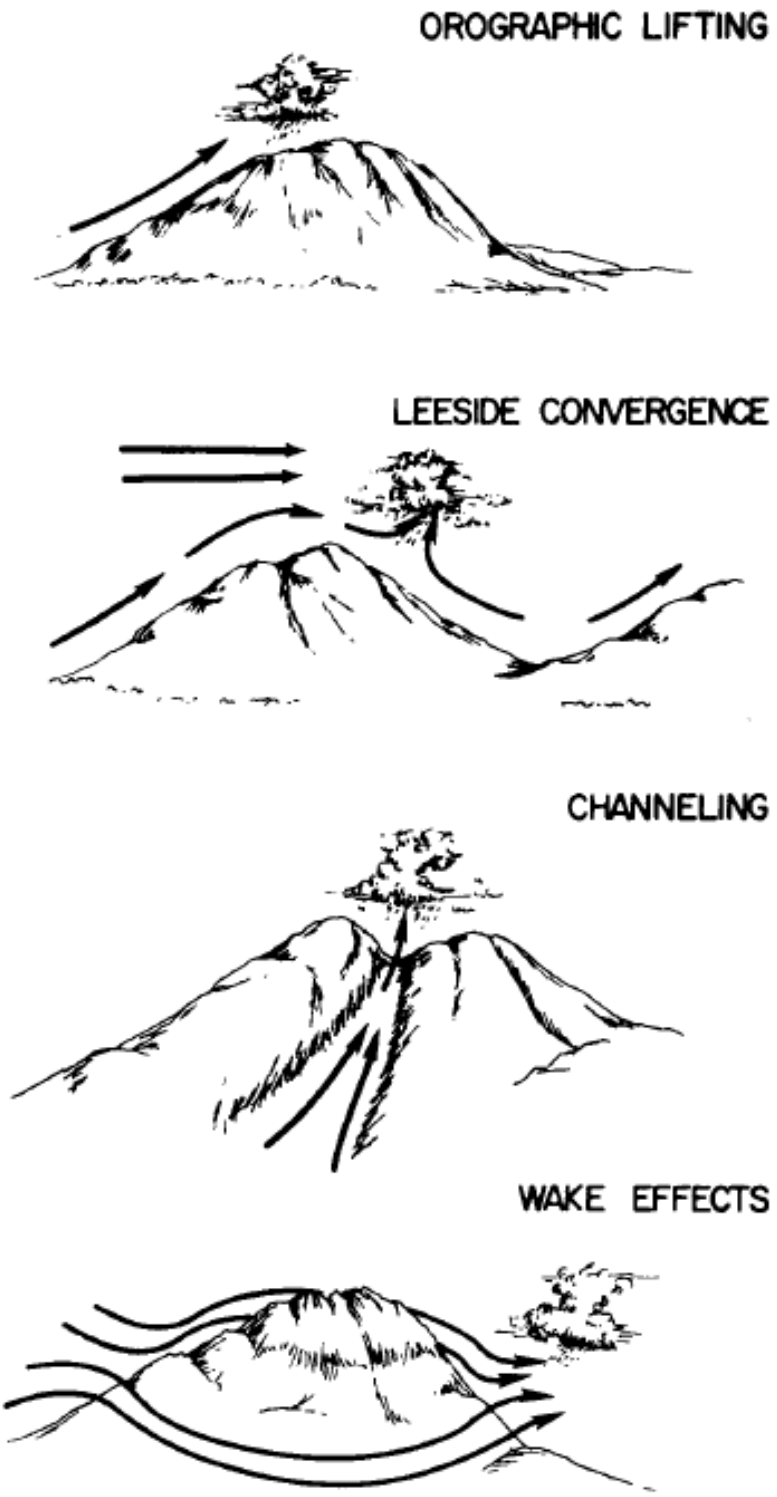

Figure 3.20: Schematic of orographically-forced mechanical triggering mechanisms (from Banta and Barker Schaaf, 1987)

Triggering: Elevated heat low

However, triggering over orography can also be due to their creation of elevated heat lows, as the mountain top warms more than the surrounding air.

An example of this during summer 2015 observed with a precipitation radar is shown in Fig.

Figure 3.21: Series of radar images taken between 1310 and 1410 CEST over the Carnic alps (courtesy of Osmer)

70 from the Carnic Alps.

Triggering: Coldpool dynamics
Downdraughts and their associated coldpools are an important component of convective systems since the spreading coldpools can lift environmental air and trigger new convective events.

This is shown in the schematic of Fig. 71 The strength of the wind shear in the boundary layer is key to this role, as it determines whether the coldpool-induced vorticity is enhanced or offset.

The impact of coldpools on convective triggering can be clearly seen in the visable satellite imagery (Fig.72). Note the small cumulus at the leading edges and that some of these are able to overcome CIN and trigger new events. .

3.3.3 Mid-tropospheric convection

The lifting of convectively unstable layers can lead to the commonly observed cloud types of altocumulus (mid tropospheric, up to around 6000m) and cirrocumulus (upper tropospheric). The vertical division between the two cloud types is not purely taxonomic as cirrocumulus are cloud consisting purely of ice crystals while altocumulus are generally mixed phase clouds (consisting of both liquid and ice). Altocumulus normally occurs when a large air mass is lifted to middle levels by a landmass or an incoming frontal system.

Layer Convective Instability
If a layer of the atmosphere is lifted that is absolutely stable, but which becomes conditionally (or absolutely) unstable through lifting then the *layer* is termed *convectively unstable*

Examining the tephigram it is clear that a criterion for convective instability can be understood in terms of θ_e (or equivalently θ_w).

Three criteria for convective Instability:
$\frac{d\theta_e}{dz} < 0$: *Convectively Unstable*
$\frac{d\theta_e}{dz} = 0$: *Convectively Neutral*

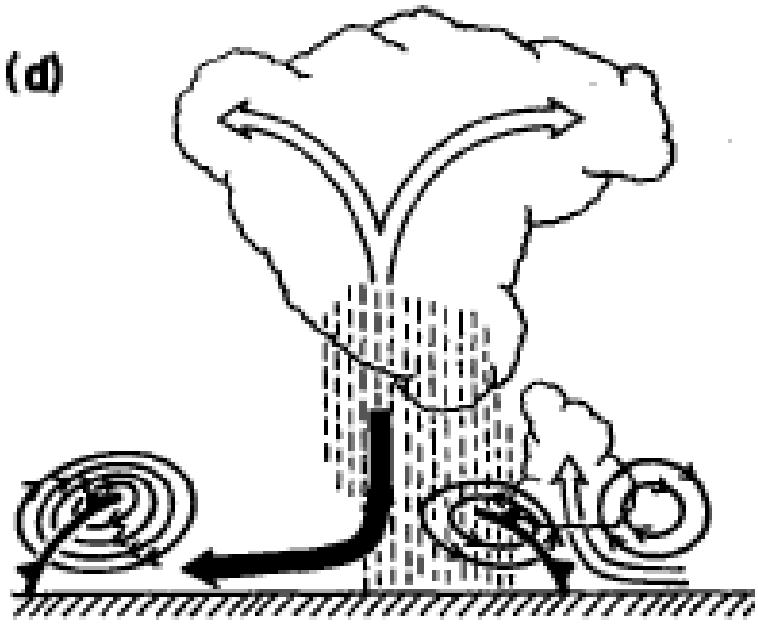

Figure 3.22: Schematic from Rotunno et al. (1988) showing how air lifted by spreading coldpools can lead to new convective cells being formed

.

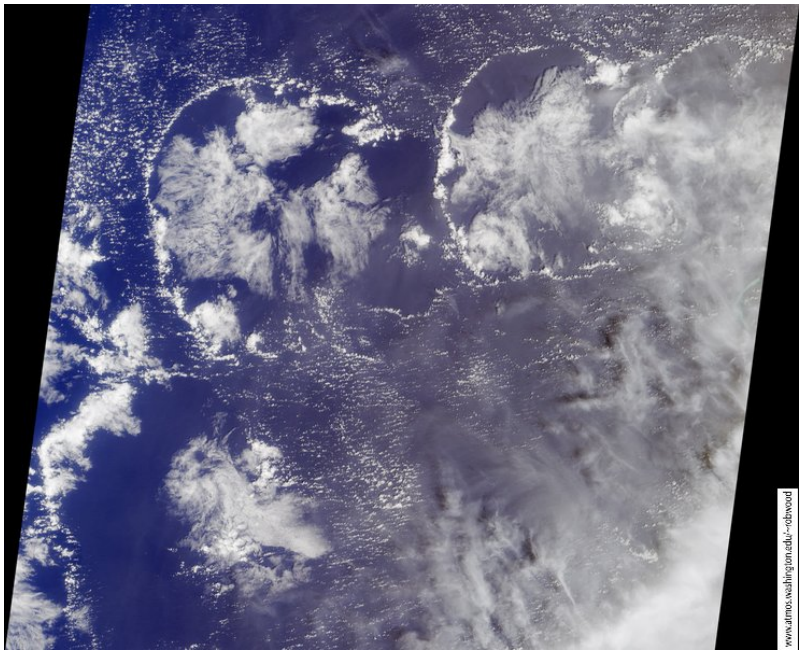

Figure 3.23: Visible satellite image clearly showing the inhibition of all convection within the wake itself but highlighting new convection at the wake boundaries. (source isites.harvard.edu)

$\frac{d\theta_e}{dz} > 0$: *Convectively Stable*

This kind of layer instability can lead to altocumulus or cirrocumulus clouds, which can be signs of impending arrival of a front, and are illustrated in Fig. 73. This layer instability can be best understood using the tephigram, which show a case where $\frac{d\theta_e}{dz} < 0$. Lifting the layer through a sufficient distance to result in saturation leads to absolute instability within the layer. (fig. 74

Deep convection triggering at fronts
The lifting of air at cold fronts can triggering convection, as shown by the embedded cumulus towers in the schematic (Fig. 75).

Figure 3.24: Examples of clouds formed by convectively unstable layers. (a) Altocumulus (b) Altocumulus undulus, resulting from vertical wind shear (c) cirrocumulus (source: theairlinepilots.com)

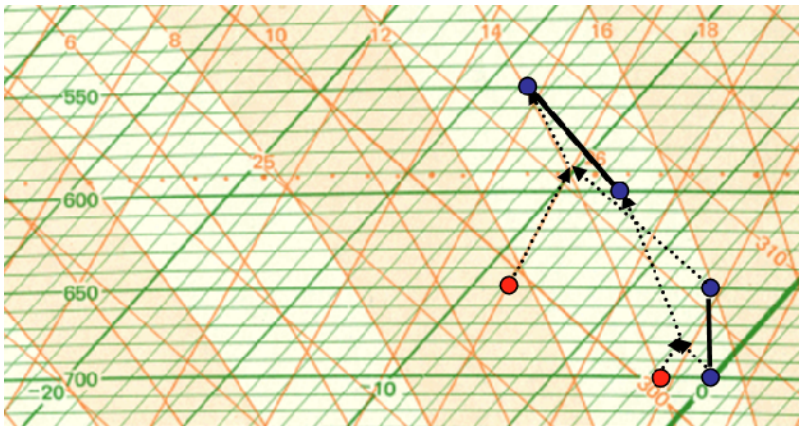

Figure 3.25: Illustration of layer instability

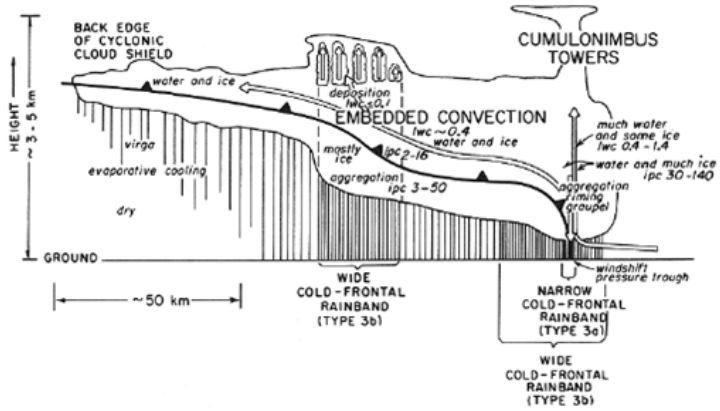

Figure 3.26: Schematic cross section of convection embedded in a front (source).

3.3.4 Trigger Temperature

Convective Trigger Temperature
Concerning thermodynamic triggering mechanisms, the convective trigger temperature is the temperature the surface layer would have to be heated to in order to remove all CIN, assuming no change in boundary layer mixing ratio during this heating process.

Q: is this a good assumption and when is the trigger T relevant? . The convective trigger temperature is found by tracing a humidity isopleth of the surface layer mixing ratio to the environmental temperature curve and then following a dry adiabat back to the surface pressure (Fig. 76). For this particular example the trigger temperature is 35°C, requiring a warming of roughly 5°C. The convective trigger temperature is more relevant for cases where convection is not mechanically forced, for example whether convection will occur in undisturbed conditions as a result of the diurnal heating, particularly over land in the tropics over mid-latitude summers.

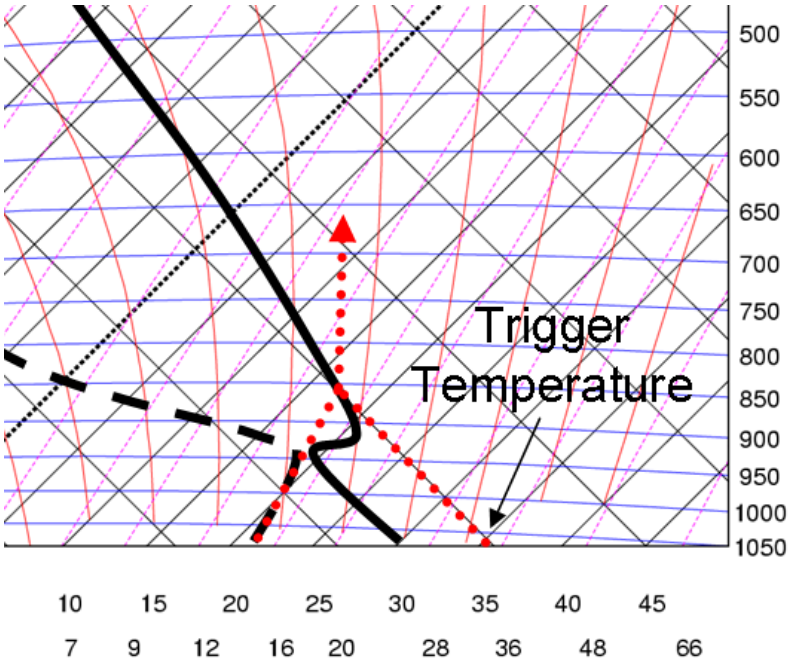

Figure 3.27: Tephigram showing the derivation of the convective trigger temperature

If the soil conditions are wet then the surface heating can also lead to a significant latent heat (humidity) flux, which will lower the trigger temperature. ENTRAINMENT MCS It is thus clear to see why dry situations over land can become "locked-in" through a positive feedback. If a blocking high causes persistent dry conditions, the soil will dry out and the trigger temperature will be higher, making future convective storms less likely. Such a feedback has been shown to be relevant in Africa (Taylor et al., 1997) and has been also highlighted as playing a role in increasing the severity of the 2003 summer heatwave over Europe (Fischer et al., 2007).

Q: attempt tephigram exercise III and IV

3.3.5 Updraught structure and entrainment

Entrainment

In deep convection, updraught air may ascent to close to the tropopause without mixing with the environment. However, much of the air at the cloud boundaries undergoes turbulent mixing events with environmental air, a process known as *entrainment*.

The process of mixing was proven in early laboratory studies using buoyant plumes of dyed liquids mixing, however these studies were unable to adequate represent the effect of latent heating. The understanding and representation of mixing in convection is a long-standing problem. The highly turbulent nature of clouds was evidenced in the first aircraft measurement that were taken after the second world war, such as by (Byers and Braham Jr., 1948; Warner and Newnham, 1952; Warner, 1955), with example aircraft and instruments of this period shown in (Fig. 78).

Examples of in-cloud measurements from Telford and Warner (1962) (Fig. 79), show the *highly turbulent nature of the cloud* and reveal the differences between updraught and downdraught regions. SKIP MATHS If the figure is closely examined, it is seen that the main updraught is towards the centre of the cloud region while the main (saturated) downdraught areas are at the edges of the cloudy region. The value of the liquid cloud water content is fairly similar in much of the central area of the cloud, indicating that this air ascended to this level from the boundary layer with little mixing occuring with the environment. The liquid cloud water is said to be close to its adiabatic value. Close to the cloud edges however, the values are much smaller, indicating turbulent mixing which results in evaporative cooling. This can lead to negatively buoyant downdraughts (especially in the presence of precipitation) which are discussed in the following section.

Mixing in Cumulus clouds

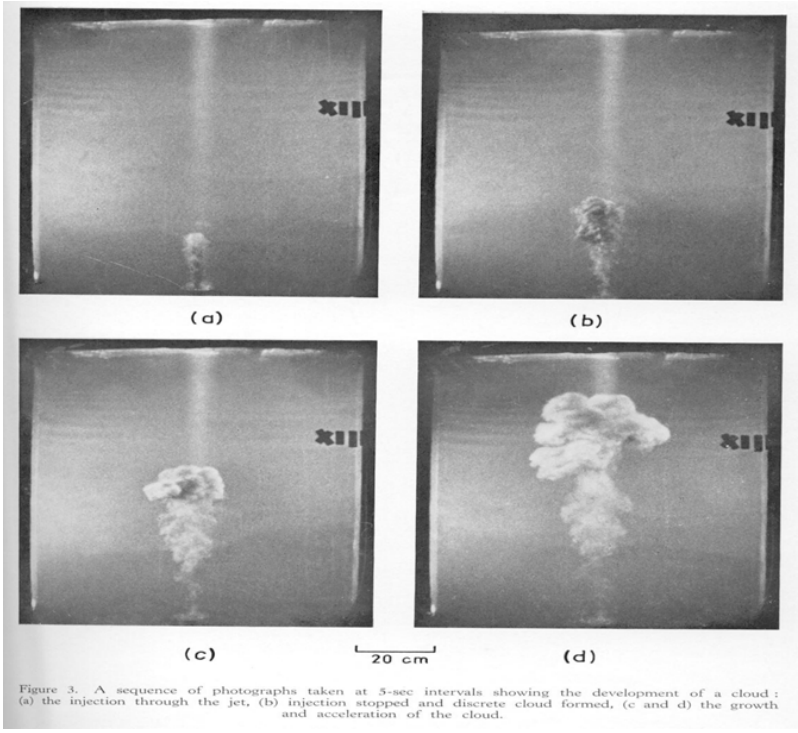

Figure 3.28: Example of a laboratory experiment of buoyant plumes in a tank experiment of Turner (1963)

Consider two masses of moist air at pressure p with diverse properties (we use subscripts 1 and 2) of temperature and humidity and are subsequently thoroughly mixed isobarically.

The specific humidity of the mixture is

$$q_v = \frac{M_1}{M_1 + M_2} q_{v1} + \frac{M_2}{M_1 + M_2} q_{v2} \tag{3.5}$$

We can write this relationship approximately using mixing ratios and vapour pressure

$$r_v \approx \frac{M_1}{M_1 + M_2} r_{v1} + \frac{M_2}{M_1 + M_2} r_{v2} \tag{3.6}$$

$$e \approx \frac{M_1}{M_1 + M_2} e_1 + \frac{M_2}{M_1 + M_2} e_2 \tag{3.7}$$

We will assume that there is no net loss of gain of heat during mixing so that the change in heat of the two parcels is equal

$$M_1(c_p + c_{pv} r_{v1})(T - T_1) + M_2(c_p + c_{pv} r_{v2})(T - T_2) = 0. \tag{3.8}$$

If we neglect the contribution of water vapour in the heat capacities then we can see that temperature also approximately is linearly mixed:

$$T \approx \frac{M_1}{M_1 + M_2} T_1 + \frac{M_2}{M_1 + M_2} T_2 \tag{3.9}$$

As the saturation vapour pressure is a nonlinear function of temperature, then the approximate linear mixing property of vapour pressure and temperature imply that the mixing of two unsaturated parcels of air can result in a mixed parcel that is saturated (draw sketch). This phenomenon is commonly seen when your breath is visible on a winter's day. In fact it was from this observation that James Hutton deduced in 1784 the concave shape of the Clausius Clapeyron curve a century before it was derived.

The degree of mixing impacts the eventual cloud top height (Fig. 80). Note the strongly nonlinear vapour mixing ratio. Paluch (1979) showed strong evidence that most air in clouds had undergone one or two mixing "events", suggesting an *episodic* mixing model as a result (Fig. 81).

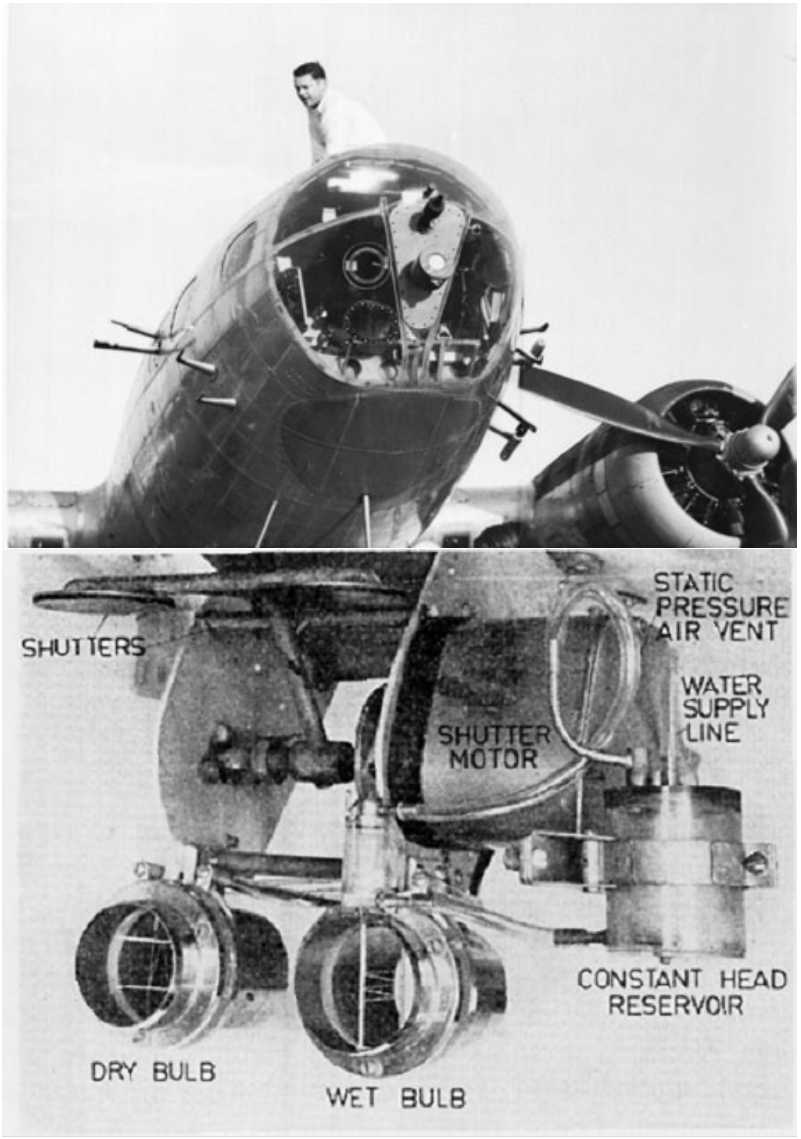

Figure 3.29: Early post-war aircraft fitted out with cloud observation instrumentation (source www.egoaltar.com), and example of the instrumentation (Telford and Warner, 1962)

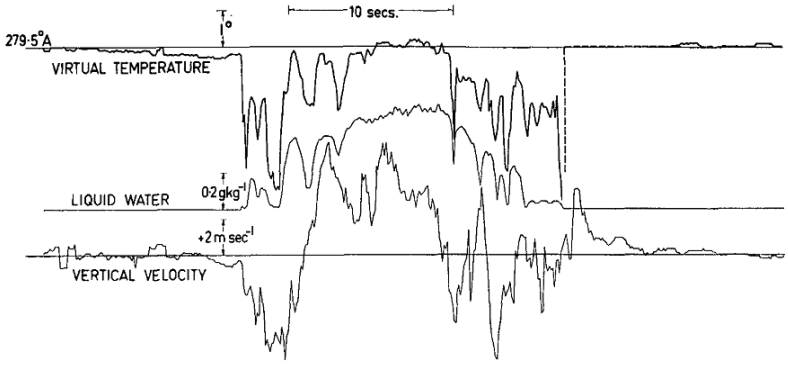

Figure 3.30: Some of the instrumentation and an example transect through a fair weather cumulus cloud from Telford and Warner (1962).

- e_s doubles for every 10°C increase in temperature.
- All vapour in excess of saturation condenses (ice more complex)

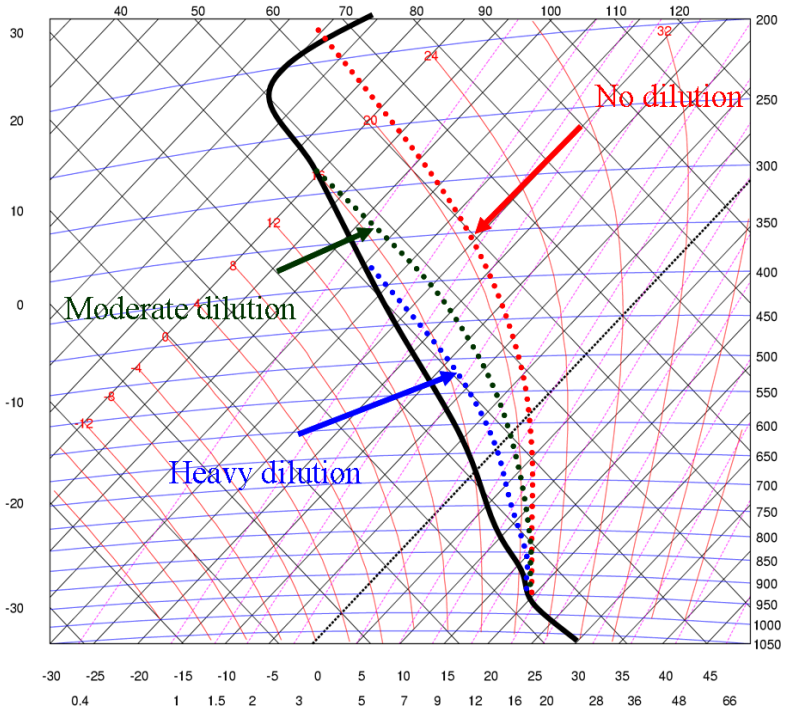

Figure 3.31: Mixing in deep convection

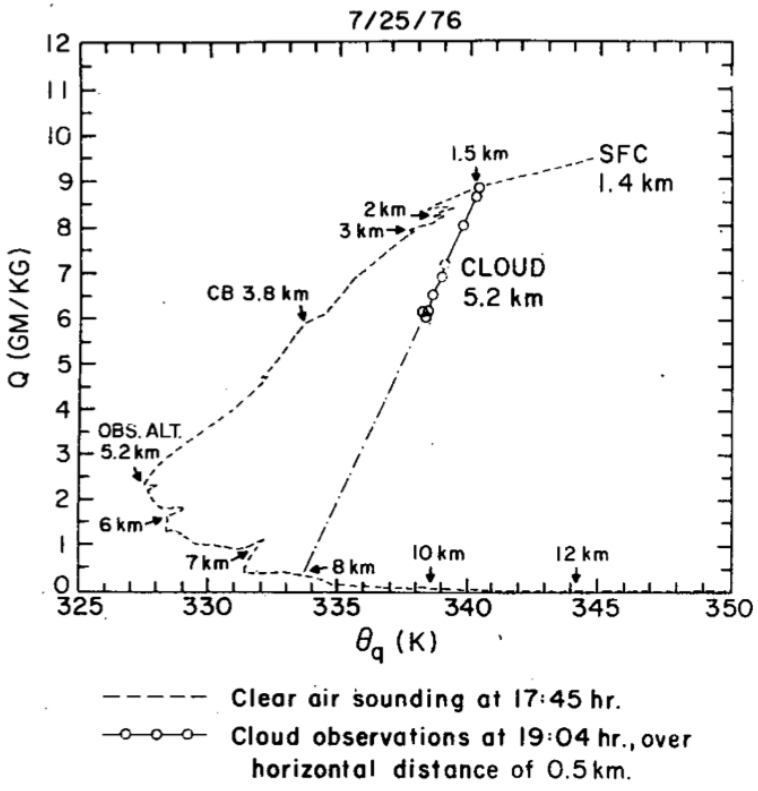

Figure 3.32: Comparison of the total mixing ratio and the wet equivalent potential temperature computing from data collected inside a growing cumulus, taken from Paluch (1979)

- Formation of precipitation efficient in fast updraughts (ice)
- precipitation efficiencies high (60-80%)

What does this mean?

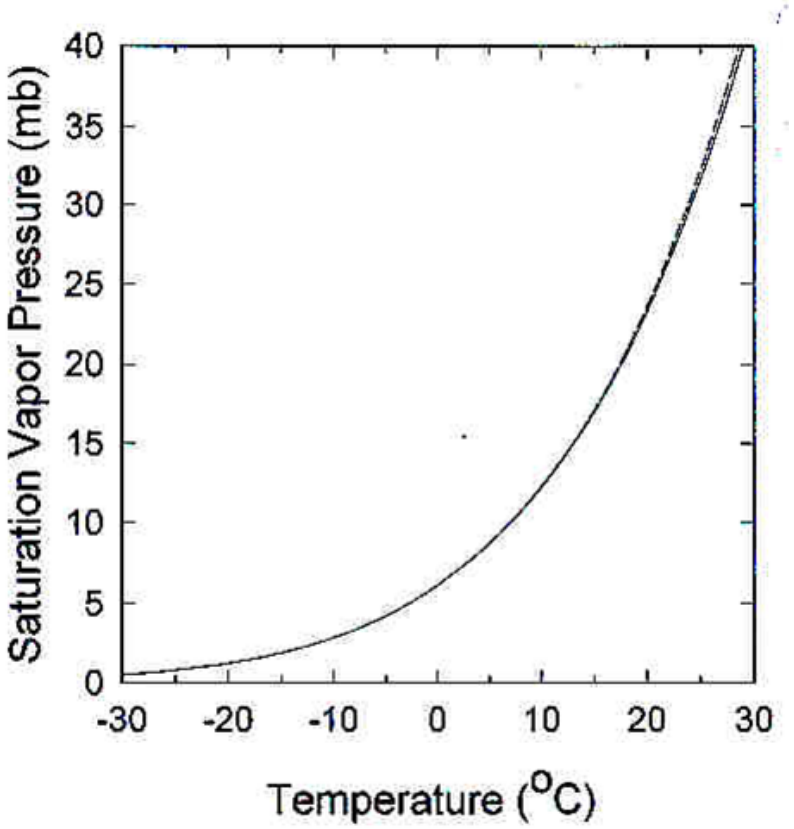

Figure 3.33: The saturation vapour pressure as a function of temperature

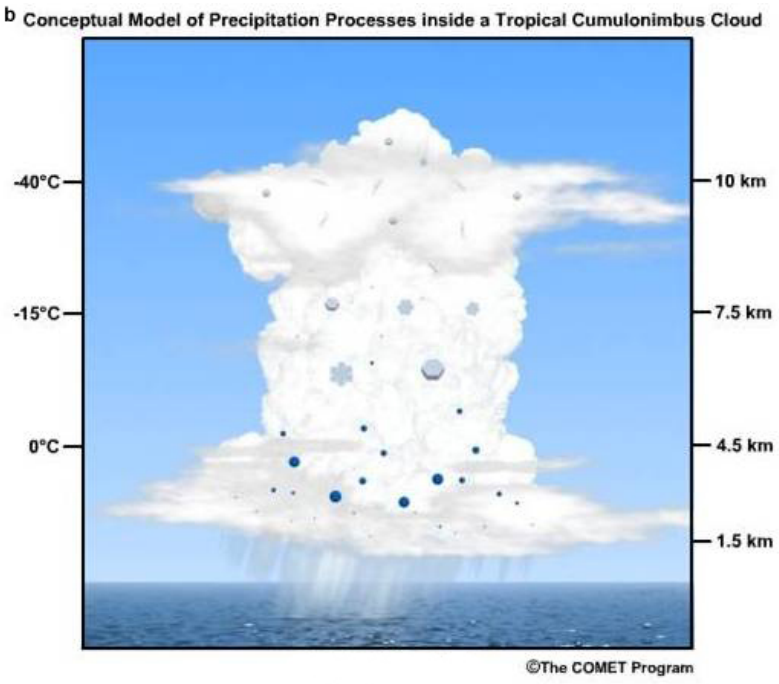

Figure 3.34: Schematic of precipitation formation in deep convection (source COMET goes-r.gov)

- Essentially 60 to 80% of the water vapour in the parcels of the boundary layer that undergo ascent in deep convective clouds, falls back to the surface as precipitation.

- The number is much higher for the parcels that rise undilute to the LNB.

3.3.6 Downdraughts

From the transect through a fair weather cumulus cloud it was seen that clouds consist of both updraught and also *downdraught* components.

Coldpools
In deep convective systems these saturated downdraughts form at mid-tropospheric levels and can penetrate all the way to the surface, spreading out to form a convective *Coldpool* , sometimes referred to as a *convective wake*.

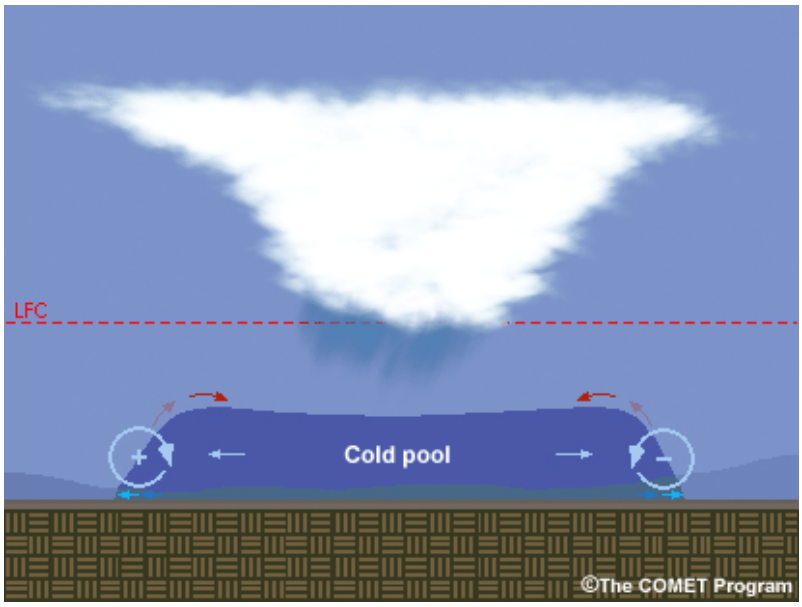

Figure 3.35: Schematic of a coldpool (source: meted.ucar.edu)

Coldpools are most visible in dusty environments as seen in this example from NOAA of a dust storm in Iraq (Fig. 85). See also (Seigel and van den Heever, 2012) for high resolution simulations

Figure 3.36: Photo of dust lifted in a coldpool outflow in Iraq (source: www.see.leeds.ac.uk)

of dust lofting in coldpool structures, and also further details available by clicking here.

- Downdraughts are formed both by the frictional drag of falling precipitation and are also buoyancy driven.

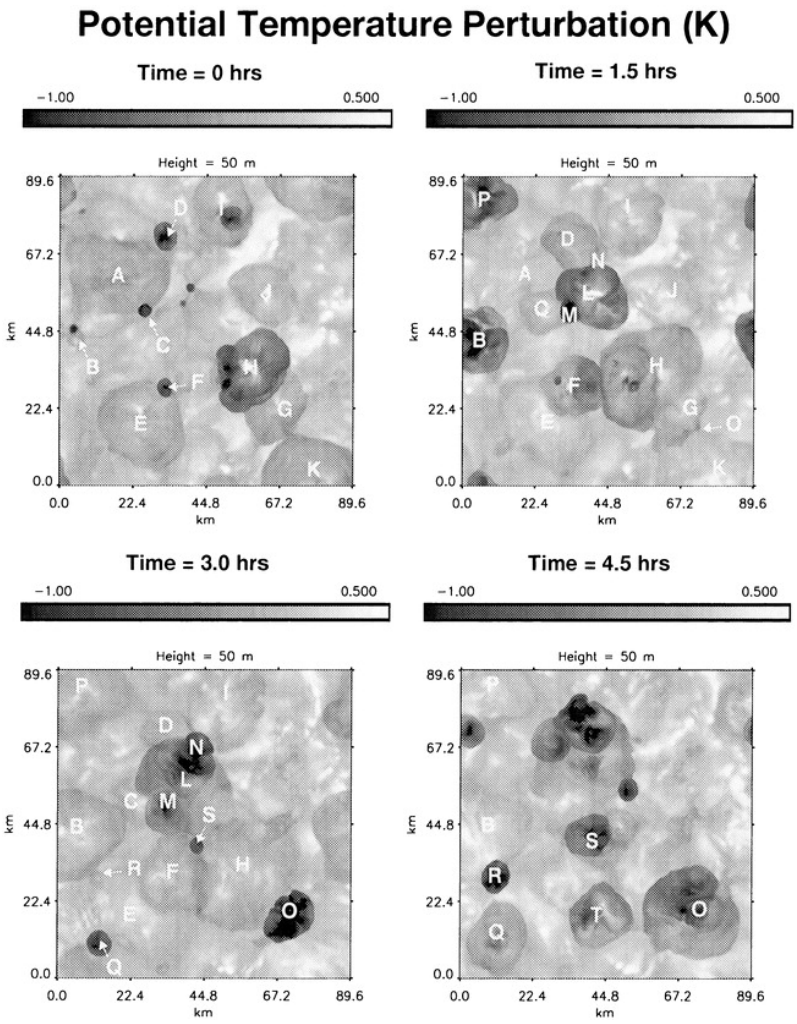

Figure 3.37: Four time slices of a coldpool evolution from (taken from Tompkins, 2001).

- The buoyancy effect derives from the nonlinearity of the saturation vapour pressure curve and the fact that temperature and mixing ratio are approximately *linearly mixing*.
- This means that a mixture of updraught cloudy air and its environment air, subsequently brought to saturation by evaporation of precipitation, can be *negatively bouyant* with respect to the surrounding environment (see tephigram exercise sheet).

Fig. 86 shows coldpool development in a domain of 90 by 90km, using a horizontal resolution of 350m. Note the structure of the coldpools with temperature depressions ranging up to 1-2K. Click for movie.

The tephigram exercises show how important the mixing and precipitation evaporation (wet bulb) processes are to forming convective downdraughts. Downdraughts and coldpools can be dangerous for aircraft landings (Fig. 87) and thus their short-term prediction is a crucial task of short-term aviation *nowcasting* in potentially convective situations. Severe events are sometimes referred to as microbursts.

3.4 Organised deep convection

3.4.1 Mesoscale Convective systems

Mesoscale convective systems
If convection becomes self-propagating and one can speak of organised *mesoscale convective systems* (or MCS) consisting of numerous convective cells. Such systems can have a life time that

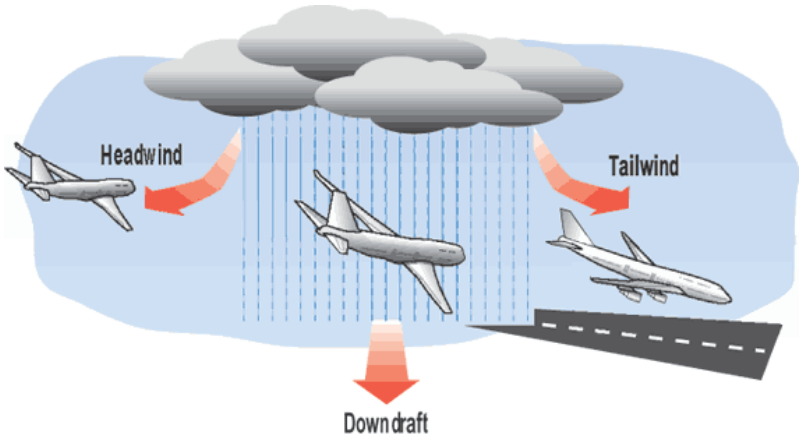

Figure 3.38: Schematic showing how a downdraught or severe microburst can cause an aircraft stall on approach (source: electronicdesign.com)

.

greatly exceeds the life-span of an individual convective events.

Examples of organised convective in mesoscale systems are

- Multi-celluar systems
- Squall-lines
- Madden Julian Oscillation
- Convectively-coupled waves

In the presence of wind shear the convective can become linearly organised and is referred to as a *squall line*, with examples shown in Fig. 88. In addition to the saturated convective downdraughts, larger mesoscale downdraught also play a thermodynamical and dynamical role in squall line evolution. Note that impact convection *organisation* is rarely represented in the

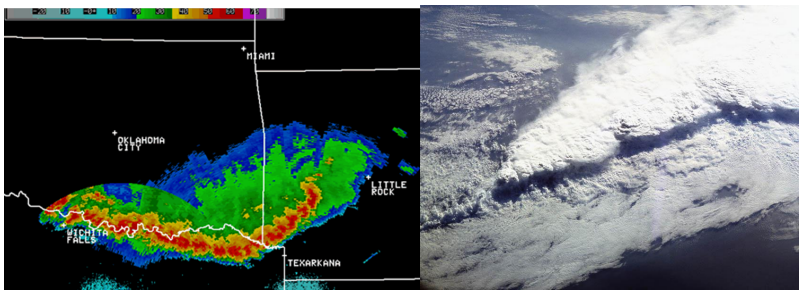

Figure 3.39: Left: Radar image of a squall line over the United States (source: NOAA). Right: Photo of a squall line over Mexico taken from the Space Shuttle (source: NASA)

.

representation of convection in numerical weather prediction or climate models. Conclusions

An example of a squall feature during summer 2015 observed with a precipitation radar is shown in Fig. 89 from the Carnic Alps.

3.4.2 Madden Julian Oscillation

In the tropics, convection sometimes organises into Eastward propagating wave, known as the Madden Julian Oscillation after the scientists who discovered the phenomenom in the 1970s.

Figure 3.40: Series of radar images taken between 1310 and 1410 CEST over the Carnic alps (courtesy of Osmer)

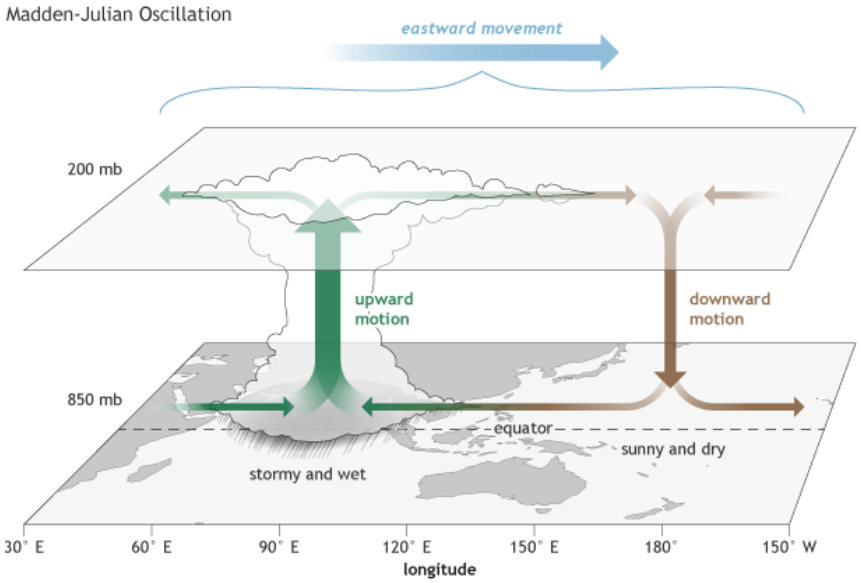

Figure 3.41: Schematic of MJO (source, Met Office and NOAA)

3.4.3 Convection and large-scale circulation

Warmer sea surface temperatures (SSTs) increase lead to higher moist static energy values in the boundary layer. It is reasonable thus to expect the convection to occur over the warmest SSTs.

In the tropics in the present day climate there is an apparent approximate threshold of around 27^{o}C that demarks convective areas (Fig. 94). *Q: what sets this threshold?*

There is nothing special about this threshold, it is merely a boundary between cooler and warmer regions, and one would expect this threshold to increase with future increases in global mean temperature.

The mean SST for Aug 2018 (Fig. 95) highlights the warmpools of the western Pacific and Indian/Atlantic tropical Oceans, which relates closely to near surface temperature of the atmosphere (Fig.)

The following schematic shows the large scale circulation associated with the Hadley cell. *Q: why does subsidence lead to a temperature inversion?*

To answer this question we return to the tephigram again and plot the imaginary trajectory of a parcel of air starting in the boundary layer over the Western Pacific (which we will assume is on the left side of the schematic in Fig. 96). The boundary layer parcel has $T = 25°$C and a RH equal to 85%. The parcel undergoes deep pseudo-adiabatic convective ascent until it reaches the upper troposphere, and we shall assume it leaves the deep convective cloud (this process is

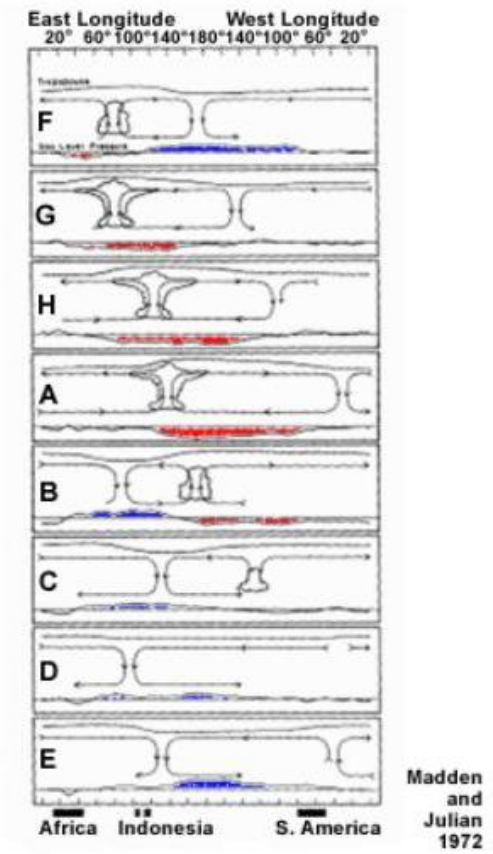

Figure 3.42: Schematic of MJO (source, Met Office and NOAA)

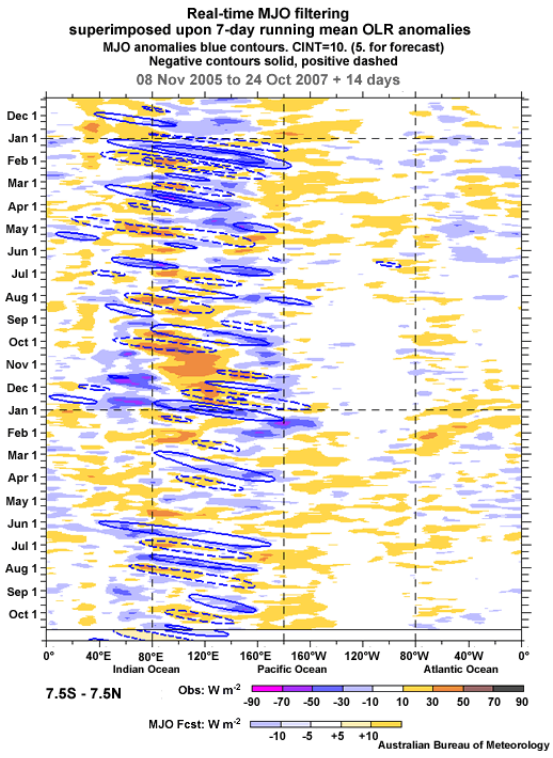

Figure 3.43: Filtering OLR to highlight MJO

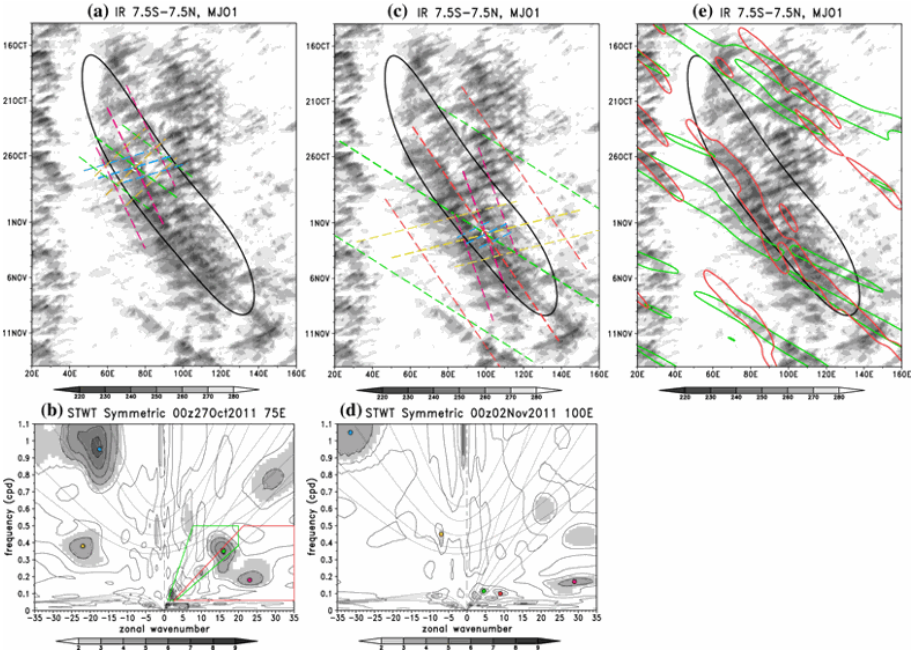

Figure 3.44: Filtering OLR to highlight MJO (Kikuchi et al. (2018))

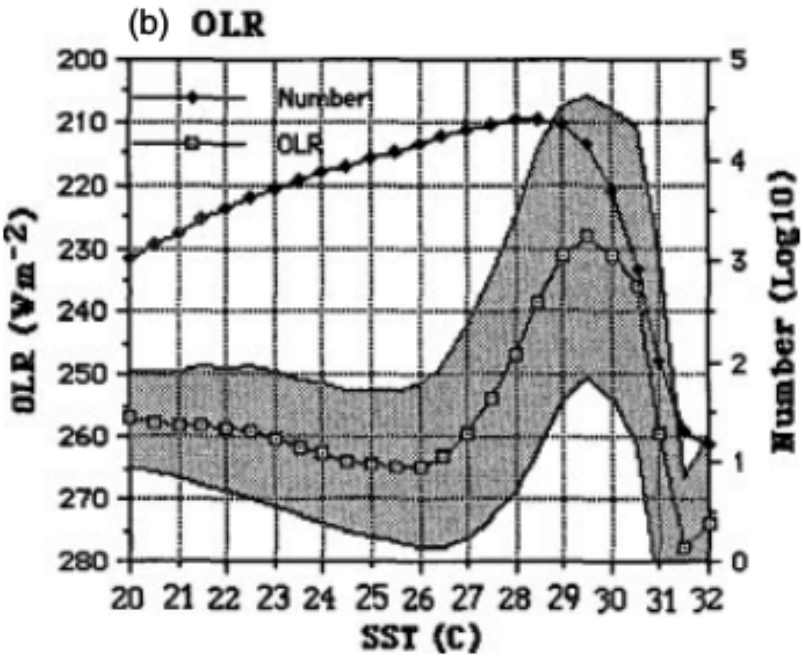

Figure 3.45: Outgoing longwave radiation (proxy for convection) as a function of local SST (source Waliser and Graham (1993) adapted by Sabin et al. (2013))

call *detrainment*) at 200hPa. As the parcel is advected across the Pacific it is also descending[2] *Q: Neglecting other processes what would be its temperature and RH when it arrives at p=900 hPa?*

We can see that the parcel arrives at the top of the boundary layer extremely dry, and also much warmer than the typical surface temperature in the Eastern Pacific. However, this simple trajectory model massively exaggerates this, since in reality the air detrained from convection is not 'just' saturated as in the pseudo-adiabatic model, but also contains cloud ice, increasing the total water r_t, and the air will be subject from moistening by nearby deep convection during its

[2]hence the schematic in Fig 96 is a poor one since the arrow is horizontal indicating no subsidence.

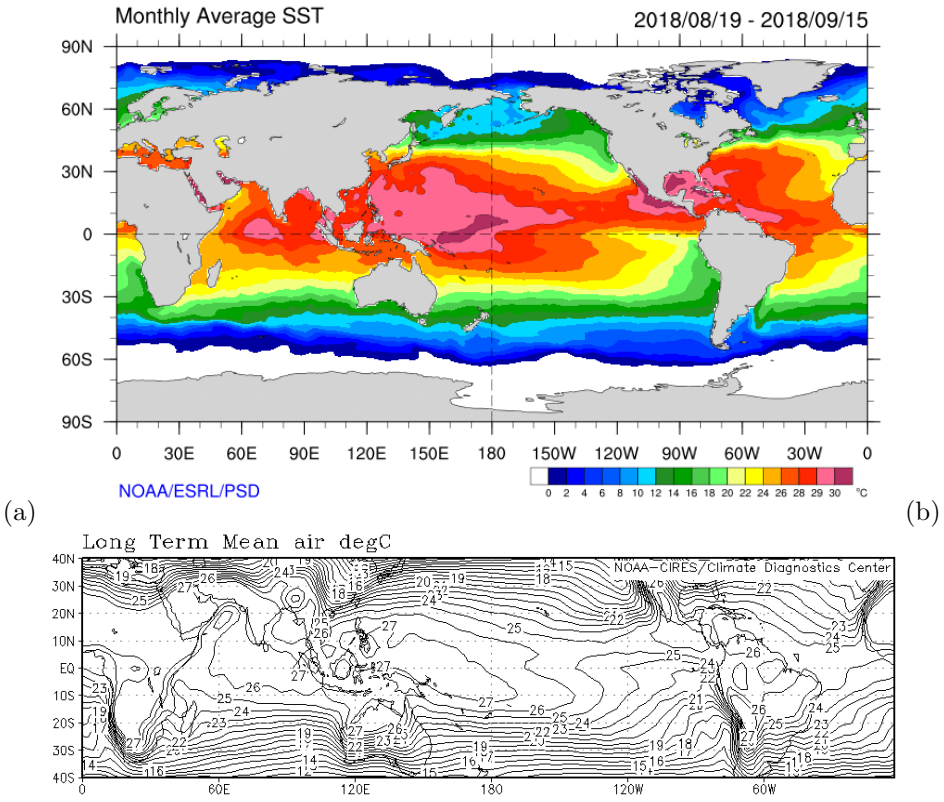

Figure 3.46: (a)Average sea surface temperature for Aug-Sept 2018 (source: www.esrl.noaa.gov), (b) long term average T2m, period is not the same but the relationship with the warm pools is nevertheless clear (source NCEP/Rogers Smith lecture LMU)

descent.

Moreover we know that the warming must be approximately balanced by radiative cooling during its journey across the Pacific. The trajectory plot is also a vast over simplification itself of course, since air will get recirculated in other convective events and so on. The trajectory pattern in the schematic crudely represents an averaged mean flow.

3.5 Summary of convection

- Convection is the name given to any motions that result from variations in density.
- Convection in the atmosphere can be considered as three *modes*:
  - turbulence in the boundary layer (dry and moist) capped by an inversion
  - deep moist convection penetrating to the tropopause
  - mid level convection arising from frontal lifting
- Convection components:
  - turbulent updraughts
  - entrainment and detrainment
  - condensation and formation of precipitation
  - downdraughts and coldpools
- While the "parcel" view of convection is very informative, it neglects the complexities of convective *organisation*.

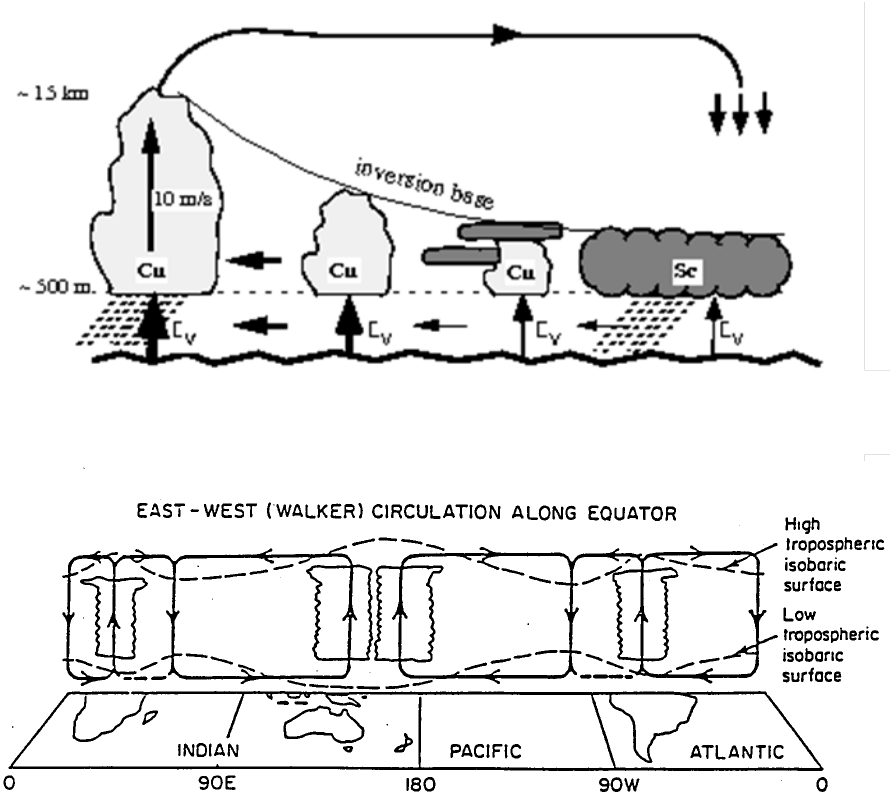

Figure 3.47: Schematic of the Walker/Hadley circulations, showing Stratocumulus forming under the strong capping inversions associated with the subsidence that balances deep convection. (source: S. De Roode cloud lecture notes)

Chapter 4

Cloud Physics

4.1 Introduction

Competition between homogeneous and heterogeneous ice mechanisms
LET'S START

Introduction to cloud physics
In all our discussions so far of convection, we have readily assumed that in updraught motions, once saturation is reached cloud drops readily form. However it is not obvious that this is the case. Indeed, we shall see that this is not the case for the formation of ice crystals.

In this part of the course we move to the small scale physics that occurs on the *microscale* of droplets within clouds, known as *cloud microphysics*. What are the processes that we need to consider in clouds therefore?

Cloud processes
We will consider the

- change of phase from water vapour to liquid droplets or ice crystals
- transformation of small cloud droplets to larger rain drops
- freezing of cloud droplets
- formation of ice crystals from water vapour
- advection/falling of the larger sized droplets (precipitation)
- evaporation/sublimation of precipitation and cloud

Cloud particle modes
Condensed droplets of water can obviously have a range of sizes, or droplet radius. However the probability density function describing the droplet sizes is not a smooth function from the very small to the very large (large being a relative term!), but instead we shall see that diverse and discrete cloud processes contrive to produce distinct peaks in the droplets size spectra, termed *modes*. We shall follow the convention of considering each mode as a *bulk quantity*.

For example, Fig. 97 shows typical drop size spectra for a range of cloud types (Quante, 2004). We will consider modes of

- cloud drops
- rain drops
- ice crystals
- snow flakes

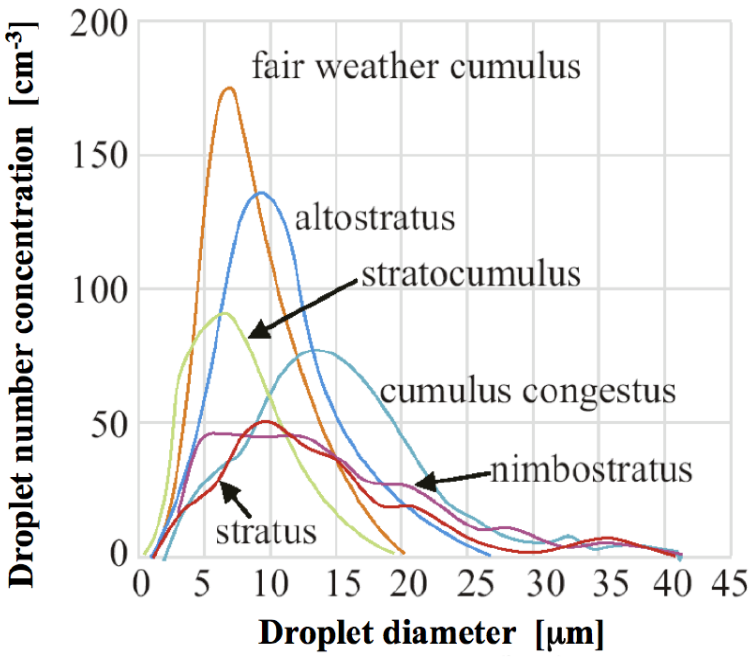

Figure 4.1: Measured drop sizes from various types of clouds, from Quante (2004).

For ice processes the division is less obvious since ice crystals can form many different shapes or *habits*, with differing radiative and microphysical (e.g. fall-speed) properties despite similar particle sizes which may be treated as a separate category. It is always possible to divide each mode into finer size categories of course, for instance considering small and large cloud ice particles separately.

Figure 98 shows a schematic of the typical sizes of cloud particles in *warm phase* (i.e. no ice processes involved) clouds. The cloud droplet has a typical radius of 10μm, (a micron=1 μm), 100 times smaller than a typical raindrop. In general we will consider cloud microphysical processes as pathways that can either convert particles from one or more discrete modes to a different particle mode, or can change the mass or size distribution within one particular mode. Figure 99 reveals a bewildering array of such processes. A full description of clouds at this level of complexity is beyond the scope of this course, but the diagram reemphasizes the complexity of the task to represent such small-scale complex processes in global climate models with 100km size grid-boxes.

4.2 Cloud drop formation

In our earlier lecture we assumed that supersaturated states could not exist and water vapour in excess of the saturation mixing ratio was immediately condensed into cloud droplets. It is not obvious that this should be the case. We will now consider the effects imports for cloud particle activation.

Water molecules exhibit two types of interactions in the liquid and solid phases: strong covalent bonds within the molecule (O-H bonds, with energy 492 kJ mol^{-1}) and relatively weak hydrogen bonds between them (Fig. 100). Hydrogen bonds have approximately 1/20th (23 kJ mol^{-1}) of the strength of O-H bonds and extremely short lifetimes of $\approx 1ps$ (picosecond=10^{-12}s).

Surface tension

A molecule within the bulk of a liquid experiences attractions to neighboring molecules in all directions, but since these average out to zero, there is no net force on the molecule (Fig.101). Instead a molecule at the surface experiences forces only sideways and downward. As a consequence, a molecule at the surface will tend to be drawn into the bulk of the liquid. But since there must always be some surface, the overall effect is to minimize the surface area of a liquid. This is what creates the stretched-membrane effect known as *surface tension*, $\sigma_{l,v}$.

The surface tension is the free energy per unit surface area of the liquid and can be viewed as the work per unit area required to extend the surface of liquid at constant temperature. The

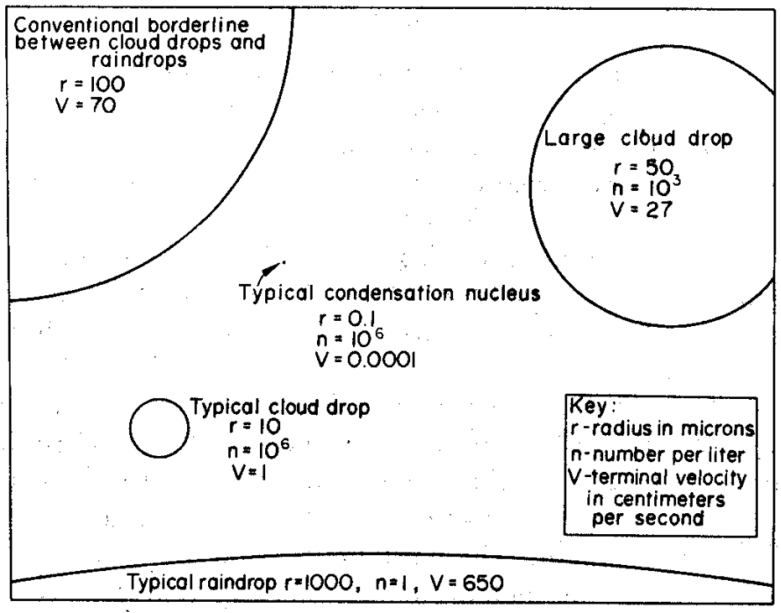

Figure 4.2: Typical drop sizes, from Mcdonald 1958 McDonald (1958), reproduced from Rogers and Yau (1989).

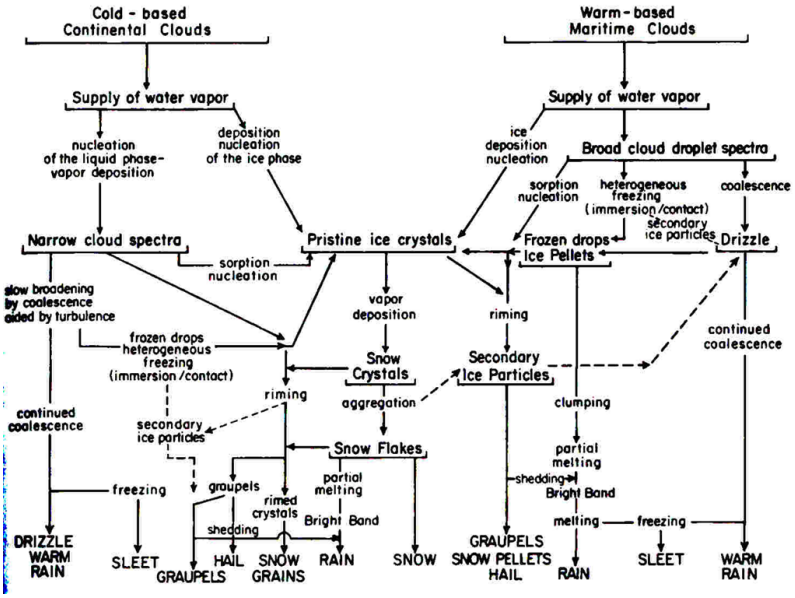

Figure 4.3: Schematic of cloud process pathways between various cloud particle modes (source unknown)

formation of a liquid drop needs an energy:

$$\Delta E = 4\pi r^2 \sigma_{l,v} \tag{4.1}$$

r is the drop radius. $\sigma_{l,v} \approx 7.5 \times 10^{-2} Nm^{-1}$ for usual conditions. The distinction between molecules located at the surface and those deep inside is especially prominent in water, owing to the strong hydrogen-bonding forces. Thus, compared to most other liquids, water also has a high surface tension. The geometric shape that has the smallest ratio of surface area to volume is the sphere, so very small quantities of liquids tend to form *spherical drops*. The fact that energy is required to form the drop interface implies an energy barrier. The implication is that phase transitions are *not* spontaneous, even if the Gibbs free energy would be lower as a result.This is illustrated in Fig. 102. Even if $e > e_s$ and thus liquid is the "preferred" phase, exhibiting a Gibbs energy minimum, phase transition requires an energy barrier to be overcome. There

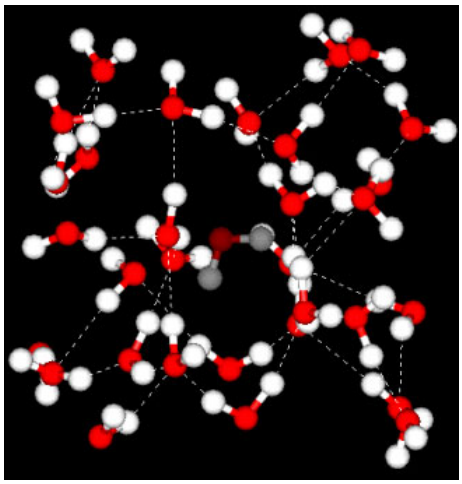

Figure 4.4: Schematic of liquid water structure

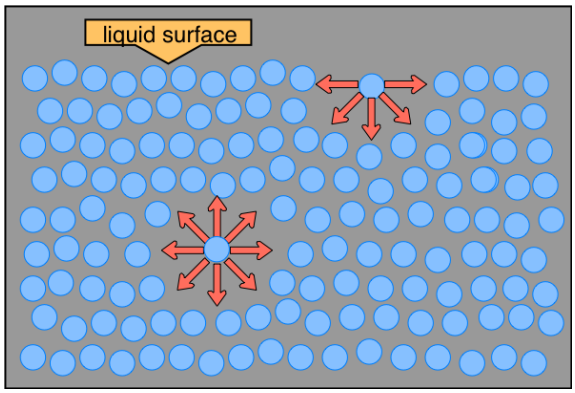

Figure 4.5: Schematic of the surface tension effect (source: www.chem1.com)

is no thermodynamical reason why a system in a local stable state may increase its Gibbs free energy and cross the barrier to change phase. Thus processes of phase transition require concepts from statistical mechanics that describe molecular-scale fluctuations of the system, in addition to thermodynamics. Random fluctuations may lead to some molecules overcoming the Gibbs energy barrier. The size of the barrier depends on the path. For example, in Fig. 102 we can view the path along the line $p = p_s$ as the result of all molecules changing phase from gas to liquid, which would involve a high energy barrier. Instead, the barrier energy is much lower if the new phase occurs as the result of the formation of a small stable nucleus, involving a subset of n molecules (Fig. 103). Hence phase transition in this way is referred to as a *nucleation event* . The nucleation event in this example is referred to as *homogeneous*, since no foreign surface is present to lower the energy barrier.

4.2.1 The energy barrier and Kelvin's equation

We now examine the energy barrier associated with the formation of a nucleus of n molecules in the new liquid phase formed from a parent phase of N molecules as illustrated in Fig. 103. The Gibbs State 1 has a Gibbs free energy of $G_1 = Ng_v$, where g_v is the Gibbs free energy per molecule in the vapour phase. $G_2 = (N - n)g_v + G(n)$, where $G(n)$ is the Gibbs free energy of the liquid phase nucleus, and has two contributions: $G(n) = ng_l + G_{surf}(n)$. The first term is the Gibbs free energy associated with the molecules in the liquid phase, while $G_{surf}(n)$ represents the work that has to be done to form a surface around a volume containing n molecules. The work needed to form the cluster is therefore

$$G_2 - G_1 = \Delta G = n(g_l - g_v) + G_{surf}(n) \tag{4.2}$$

To calculate the first term, we integrate dg from e_s for liquid to e the vapour pressure of the

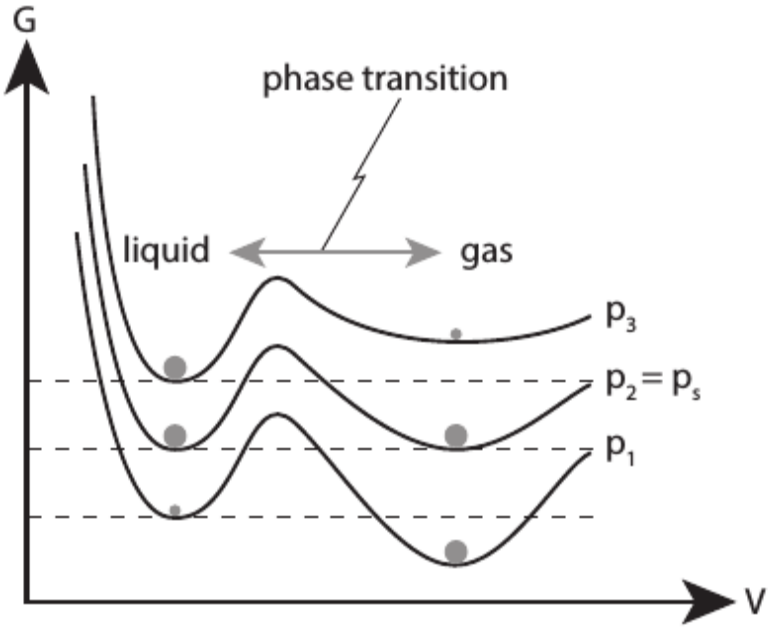

Figure 4.6: Schematic of Gibbs free energy as a function of the substance volume at three different pressures that are respectively less than, equal, or exceed the saturation pressure p_s. Local equilibria (energy minima) are shown with circle, with the larger circles indicating absolute minima. From Kashchiev (2000)

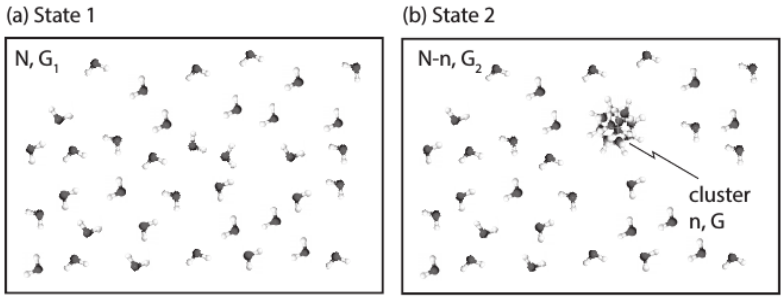

Figure 4.7: Schematic of the a nucleation event (source: Lohmann U, ETH)

surroundings at constant temperature:

$$g_v - g_l = \int_{e_s}^{e} dg = \int_{e_s}^{e} v dp = \int_{e_s}^{e} \frac{kT}{p} dp \tag{4.3}$$

where we use $pv = kT$ for a single molecule to derive the final term. Integration of this gives $g_v - g_l = kTln(e/e_s)$ (refer to derivation of Clausius Clapeyron in the thermodynamics notes). This is per molecule, thus for n molecules we can write

$$n(g_l - g_v) = nkTln(S), \tag{4.4}$$

where S is the saturation ratio, $S = \frac{e}{e_s}$. Using $k = R^*/N_a$

$$n(g_l - g_v) = nkTln(S) = \frac{nR^*Tln(S)}{N_a} = nR_vTln(S)\frac{m_v}{N_a}. \tag{4.5}$$

But the ratio $\frac{m_v}{N_a}$ is the mass per molecule, thus $n\frac{m_v}{N_a}$ is the mass of the drop that is nucleated, which can also be written as $\frac{4\pi r^3}{3v_l}$, where v_l is the specific volume of liquid water and r is the nucleus radius.

Thus we can write:

$$n(g_l - g_v) = \frac{R_vT}{v_l}\frac{4}{3}\pi r^3 ln(S) \tag{4.6}$$

The second term of eqn. 125 should account for the pressure difference within the droplet, but liquid droplets are approximately incompressible, and thus the energy is given by Eqn 124

$$G_{surf} = 4\pi r^2 \sigma_{l,v} \tag{4.7}$$

Combining eqns 128 and 129, we obtain the equation for Gibbs free energy for a cluster formation in a parent phase.

$$\Delta G = \underbrace{4\pi r^2 \sigma_{l,v}}_{\text{surface term}} - \underbrace{\frac{4R_v T}{3v_l}\pi r^3 ln(S)}_{\text{volume term}} \tag{4.8}$$

The first term on the right is referred to as the *surface term* and the second is the *volume term*. Note the different r dependency. We assumed a constant temperature in this derivation and thus latent heating is neglected.

Equation 130 is illustrated in Fig. 104. If $S < 1$ then the volume and surface terms are

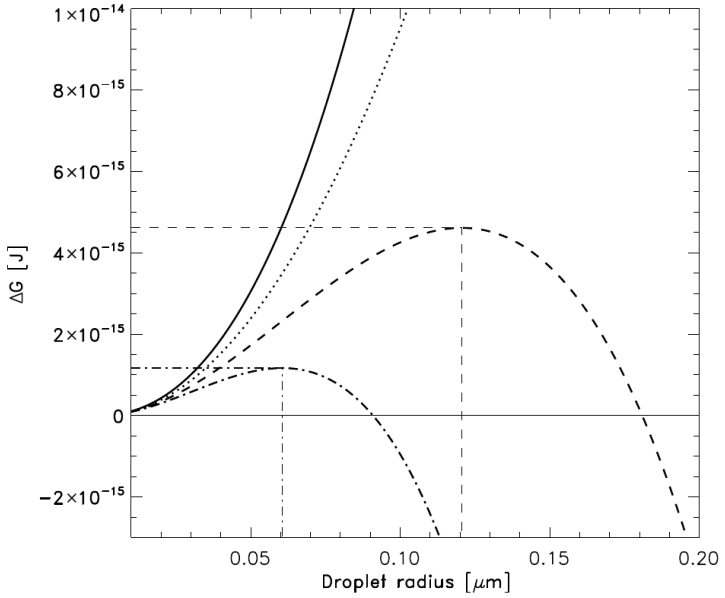

Figure 4.8: Gibbs free energy for homogeneous water droplet formation of radius r at T=273.15K for saturation ratios of S= 0.99 (solid), 1 (dotted), 1.01 (dashed) and 1.02 (dot-dash). The critical radii of 0.06 and 0.12 μm are shown for the latter two saturation values (source U. Lohmann).

both positive, and ΔG increases monotonically with r. If $S = 1$ the volume term is zero, but ΔG increases due to the surface term. For $S > 1$, there is a peak value of ΔG occuring at a critical radius, which is an unstable equilbrium and marks the magnitude of the energy barrier. If the drop radius is smaller than the critical radius the drop will tend to dissipate, while for a radius exceeding this critical threshold the drop should grow (in theory infinitely).

To calculate the critical radius, we can differentiate eqn. 130 to get $\frac{dG}{dr}$ (*exercise!*) and then set $\frac{dG}{dr} = 0$. The critical radius r_c is then

$$r_c = \frac{2\sigma_{l,v} v_l}{R_v T ln(e/e_s)} \tag{4.9}$$

Thus we have seen that there is an energy barrier resulting from the surface tension of a droplet, which was defined as the work per unit area required to extend the surface of a drop. A more physical interpretation for this is as follows. We saw that surface tension resulted from the asymmetry of the forces of attraction at the drop surface. Work is thus required to bring a molecule from the interior of a drop to its surface, as it requires bonds to be broken. A molecule on the surface will then require less energy to overcome the remainding binding H-bonds and be released in the gas phase. The smaller the droplet, the more curved the surface and the stronger this effect becomes.

Saturation over a curved surface

The relationship given earlier in the thermodynamics course for the saturation vapour pressure was for a *planar water surface*. We have seen that on the scale of a cloud droplet the curvature of the surface is sufficient to reduce the number of (attracting) neighbouring molecules.

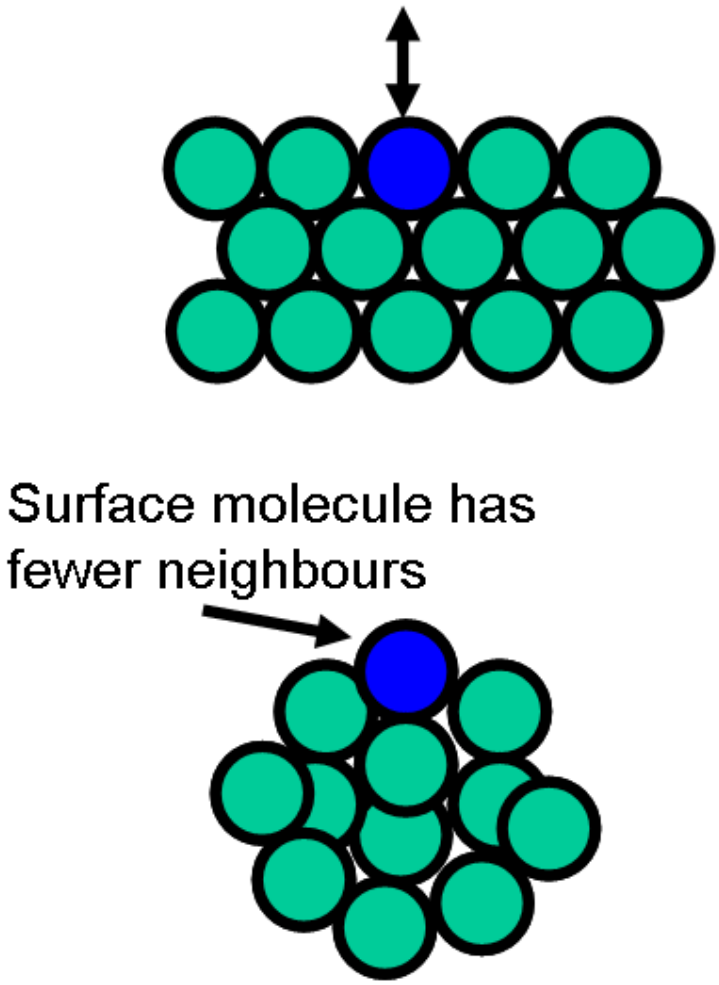

Figure 4.9: Schematic of evaporation process showing how water molecules have fewer neighbours in a curved drop relative to a planar surface.

The saturation vapour pressure is thus higher over a *curved surface*. The saturation vapour pressure of a liquid droplet of radius r given by inverting Eqn. 131, thus giving the minimum supersaturation $S = e/e_s$ that is required for a droplet of radius r to exist. :

$$\frac{e_s(r)}{e_s(\infty)} = \exp\left(\frac{2\sigma_{l,v}}{r\rho_l R_v T}\right), \tag{4.10}$$

[1]. This is known as the *Thomson* or *Kelvin* effect. Although T is in the denominator on the RHS, e_s is also a function of T and the temperature dependence is in fact weak. Note that the surface tension in the above equation refers to the surface tension of a pure liquid water droplet in water vapour. Presence of aerosols will change this value. Moreover, the above formulations are also valid for other phase changes, e.g. ice germ formation in a liquid, but the surface tension value are less well defined from experimentation. We can simplify eqn. 132 to

$$\frac{e_s(r)}{e_s(\infty)} = \exp\left(\frac{a}{rT}\right), \tag{4.11}$$

[1] We will use notation $e_s(r) = e_s^r$ interchangeably.

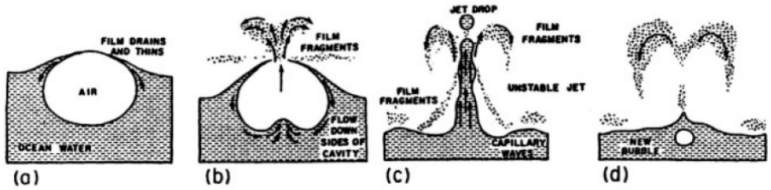

Figure 4.10: Formation of sea salt aerosol, from Pruppacher and Klett (1997).

where $a = 2\sigma_{l,v}/R_v\rho_L$ which is (almost) constant at 3.3×10^{-7} m K.

The right hand side of the expression can be usefully approximated to

$$\frac{e_s(r)}{e_s(\infty)} \approx 1 + \frac{a}{rT}, \tag{4.12}$$

Homogeneous nucleation of liquid droplets

A chance collision of molecules to form a droplet is called *homogeneous nucleation.*

Let us consider such an event involving a relatively rare event: the chance collision contemporaneously of N =183 molecules of water vapour.

To calculate the radius of this newly formed droplet we note that the droplet volume is given by

$$V = \frac{4}{3}\pi r^3 = \frac{m_v N}{N_a \rho_L}. \tag{4.13}$$

Recall that the molecular weight m_v is the mass per mole, while N_a is the number of molecules per mole, thus $\frac{m_v}{N_a}$ is the mass per molecule.

Solving eqn. 135 for r (*exercise*), tells us that the droplet of N=183 molecules has a radius of approximately 10^{-3} μm. At a temperature of 273K, the ratio of the equilibrium vapour pressure $e_s(r)$ is three times greater than the value over a planer surface $e_s(\infty)$. The rate of growth of the droplet is proportional to the difference $e - e_s(r)$. If $e < e_s(r)$ then the droplet will evaporate, while it will grow if $e > e_s(r)$. If we define the saturation ratio S as

$$S = \frac{e}{e_s(\infty)} \tag{4.14}$$

so that S =3 equates to a relative humidity of 300%, then for the nascent droplet to grow would require a saturation ratio of S >3. *Q: Do we observe such values of relative humidity?*. In fact, such high values are never measured in the atmosphere, thus homogeneous nucleation is not a relevant mechanism for cloud formation. So what is it?

Aerosols

Aerosols in the atmosphere can range in size from 10^{-4} to 10 μm radius with particle concentrations also widely varying from 10^3 cm^{-3} in a remote location to $> 10^5$ cm^{-3} in an urban environment such as London.

There are a number of *natural and anthropogenic* sources for aerosols:

- mineral soil dust
- sea salt (e.g. Fig. 106)
- gas to particle conversion SO_2 →sulphate aerosols
- combustion of fossil fuels / biomass burning

Small aerosols with radii < 0.2 μm are referred to as *Aitken particles*, 0.2 < r < 2 μm are *large aerosols*, and r > 2 μm are *giant aerosols*. Both *dry deposition* (sedimentation) and *wet deposition* (removal by precipitation) are the sinks of aerosols, with a typical aerosol lifetime being around 1 week.

Heterogeneous nucleation of liquid droplets

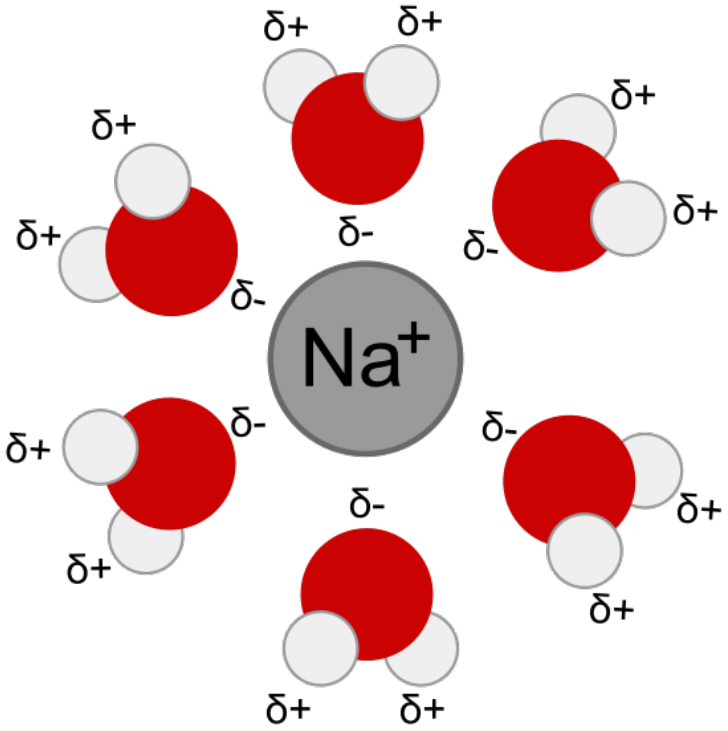

Figure 4.11: Schematic showing dissolution of sodium ion in water (wikipedia)

Many aerosols in the atmosphere are hydrophilic (A hydrophilic molecule is one that has a tendency to interact with or be dissolved by water) and thus water molecules can collect on their surface. Clouds can thus form by a process known as *heterogeneous nucleation*, where water molecules collect on a foreign substance. These hydrophilic aerosols are called *Cloud Condensation Nuclei* or CCN. These CCN are always present in sufficient numbers in the lower and middle troposphere to initiate cloud growth.

CCN aerosols can be insoluble but *wettable*, which means that the surface tension between their nucleating surface and water is sufficiently low and water can form a spherical cap completely surrounding the aerosol. Thus the physics of drop nucleation is the same as for pure water. Only large or giant aerosols ($r > 0.2$ μm) generally have a low enough curvature to form cloud droplets at observed supersaturations. However, aerosols can instead be *soluble*, in which case aerosols with much smaller radii can act as CCN. *Solvation*, also sometimes called *dissolution*, is the process of attraction and association of molecules of a solvent with molecules or ions of a solute.As ions dissolve in a solvent they spread out and become surrounded by solvent molecules (Fig. 107).

The solution term

The presence of dissolved substances implies that the some water molecules are replaced from the droplet surface (Fig. 108). Thus the saturation vapour pressure is reduced for a *solute*.

If $e_s(sol)$ is the saturation vapour pressure over a solute and n_w and n_s are the number of water and solute molecules, respectively, then the fraction of surface which is occupied by water molecules is simply:

$$\frac{e_s(sol)}{e_s^\infty} = \frac{n_w}{n_w + n_s} = \left(1 + \frac{n_s}{n_w}\right)^{-1} \simeq 1 - \frac{n_s}{n_w}, \tag{4.15}$$

where the final approximation assumes $n_s \ll n_w$. In a droplet the number of water molecules is proportional to r^3, thus for a fixed mass of aerosol this effect adjust the saturation vapour pressure by a factor

$$\frac{e_s(sol)}{e_s^\infty} = 1 - \frac{b}{r^3} \tag{4.16}$$

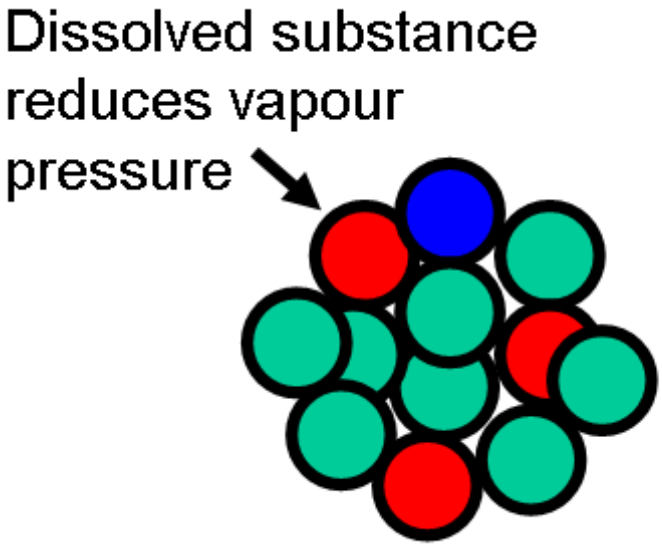

Figure 4.12: Schematic showing how saturation vapour is instead reduced when there are molecules of dissolved substance (red) present in the droplet.

where b is a constant that depends on the aerosol mass and type. The curvature (134) and solute (138) effects can be combined to give the resultant equilibrium curve referred to as the *Köhler curve* given by:

$$\frac{e_s^r(sol)}{e_s^\infty} = \left(1 - \frac{b}{r^3}\right) \exp\left(\frac{a}{rT}\right) \approx \left(1 + \underbrace{\frac{a}{rT}}_{\text{curvature term}} - \underbrace{\frac{b}{r^3}}_{\text{solute term}}\right) \tag{4.17}$$

Figure 109 shows a normalized curve, and the actual shape depends on the mass and type of solute. For a solute formed with 10^{-16} g of ammonium sulphate the solution term is ineffective for radii above 0.3 μm. Due to the r^3 factor the solute term dominates at small droplet radii.

If RH increases starting from a low value, water vapour start to condense on aerosol parcels as RH reaches about 80% (S =0.8), referred to as *haze* particles. At these small radii the droplet is stable as an increase in RH will cause the haze particle to grow until a new equilibrium radius is reached. However, if the RH continues to increase a critical radius R^* is reached at the critical supersaturation S^* value at which the droplet becomes unstable, and grows rapidly by diffusion. The droplet is said to be *activated*. The impact of the mass and type of aersol is more clear in Figure 110 (note the discontinuous y-axis). At a super saturation of 0.4%, a solute particle containing 10^{-18} kg of Ammonium Sulphate is *stable* with a radius of approximately 0.1 μm, while a solute droplet with 10^{-18} kg of Sodium Chloride (NaCl) is *activated* and will grow rapidly by diffusion. It is the haze particles that are responsible for reducing visibility on a sunny (humid) day.

In summary, about 10 to 20% of aerosols over oceans can act as CCN, while over land only about 1% can act as CCN. Nevertheless, the total concentration of CCN is still higher over land with a typical value of 500 cm^{-3} compared to 100 cm^{-3} over oceans, but these numbers are highly temporarily and spatially variable. Therefore a cloud air parcel brought to saturation over ocean shares the available water between fewer CCN, so we would expect fewer but larger cloud droplets. The consequence of this is that maritime clouds are more likely to rain. We will see that with larger droplets it is easier to grow raindrops.

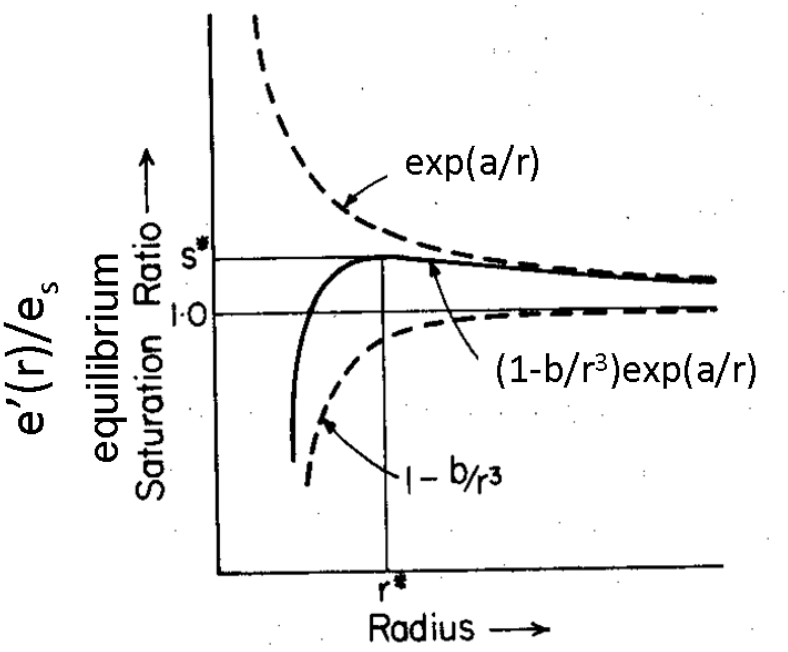

Figure 4.13: Köhler curve for the equilibrium saturation vapour pressure for a liquid solute droplet.

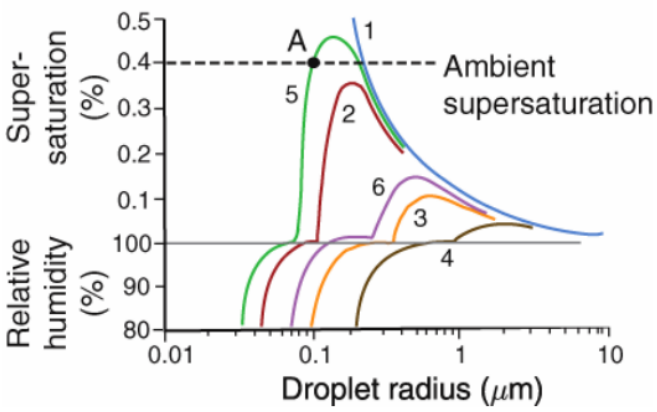

Figure 4.14: Variations of the relative humidity and supersaturation adjacent to droplets of (1) pure water (blue), and adjacent to solution droplets containing the following fixed masses of salt: (2) 10-19 kg of NaCl (red), (3) 10-18 kg of NaCl (orange), (4) 10-17 kg of NaCl (brown), (5) 10-19 kg of (NH4)2SO4 (green), and (6) 10-18 kg of (NH4)2SO4 (violet). Note the discontinuity in the ordinate at 100% relative humidity. From Rasool (1973) and lecture notes of Cotton and Yuter.

4.3 Diffusional growth

Diffusional Growth of droplet

Once a cloud particle is activated it grows rapidly by diffusion of water vapour. As is usual, the local diffusive flux is assumed proportional to the vapour gradient. Integrated over a sphere of radius n (Fig 111) the total diffusive flux F (kg s^{-1}) is:

$$F = 4\pi n^2 D \frac{d\rho_v}{dn}, \tag{4.18}$$

where D is the diffusion coefficient ($\approx 2.2 \times 10^{-5}\mathrm{m}^2 s^{-1}$ at 273K) and ρ_v is the vapour density.

In a steady state the diffusion rate is balanced by rate of increase of mass of droplet M:

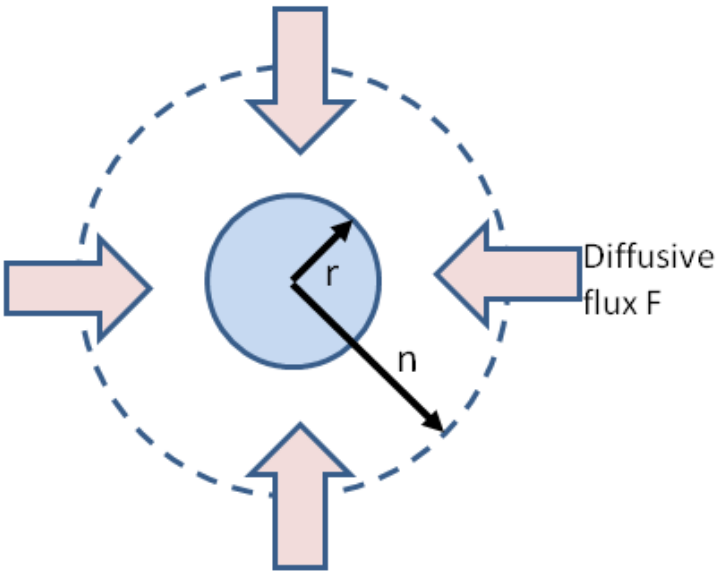

Figure 4.15: Sketch of diffusion growth of a cloud drop.

$$\frac{dM}{dt} = 4\pi n^2 D \frac{d\rho_v}{dn}. \tag{4.19}$$

We will assume that the growth is constant. Thus

$$\frac{dM}{dt}\int_r^\infty \frac{dn}{n^2} = 4\pi D \int_{\rho_v(r)}^{\rho_v(\infty)} d\rho_v. \tag{4.20}$$

giving

$$\frac{dM}{dt} = 4\pi D r(\rho_v(\infty) - \rho_v(r)) \tag{4.21}$$

We want the rate of change of radius, so we need the expression

$$M = \frac{4}{3}\pi r^3 \rho_L, \tag{4.22}$$

which we differentiate to give

$$\frac{dM}{dt} = 4\pi r^2 \rho_L \frac{dr}{dt}. \tag{4.23}$$

Substituting (145) into (143) gives

$$\frac{dr}{dt} = \frac{D}{\rho_L r}(\rho_v(\infty) - \rho_v(r)). \tag{4.24}$$

We now use the ideal gas law ($e = \rho_v(\infty)R_v T$) to change the density to vapour pressure, noting that at the droplet surface the air is exactly saturated:

$$\frac{dr}{dt} = \frac{D}{\rho_L r R_v T}(S e_s^\infty - e_s^r(sol)) \tag{4.25}$$

Now we use our earlier approximate expression for the Köhler curve given in (139):

$$\frac{dr}{dt} = \frac{D e_s^\infty}{\rho_L r R_v T}(S - 1 - \frac{a}{rT} + \frac{b}{r^3}) \tag{4.26}$$

This equation is not tractable, but we can solve for $r > 1\mu$m, with the subsequent simplification:

$$\frac{dr}{dt} \simeq \frac{D e_s^\infty}{\rho_L r R_v T}(S - 1) \tag{4.27}$$

This expression is approximate and ignores an important effect. We have neglected the fact that *latent heat is warming the droplet*, and to be strict the expression should account for the diffusion of heat *away* from the droplet. This "complication" reduces the droplet growth rate very roughly by a factor of 2.

Availability of water vapour
For a hypothetical cloud parcel there are two main terms that affect the supersaturation (or equivalently relative humidity):

- increase due to the parcel cooling: rate proportional to the parcel velocity
- decrease due to the diffusion process

The evolution of an air parcel containing a spectra of diverse CCN can be calculated numerically using a Lagrangian *parcel model* (see Ren and Mackenzie, 2005, for an example in ice clouds).

Time taken for diffusional growth
We have an expression for the rate of change of r as a function of time and supersaturation. If we assume S is time-independent we can find out how long it takes to grow cloud droplets of a certain size by the diffusion process by integrating (149).

This gives (*exercise: check!*)

$$t = \frac{\rho_L R_v T}{2De_s^{\infty}(S-1)}(r^2(t) - r^2(0)). \tag{4.28}$$

If we take an example of T=284K and $r(0)$=0.5 μm and $S-1$ =0.002 (a *supersaturation* of 0.2%) then table 3 gives the time taken to grow a cloud droplet of the given sizes *Which size is a cloud*

r (μm)	1	5	10	100
t (seconds)	1	36	150	15000

Table 4.1: Time taken to grow a cloud drop of given radius by diffusion.

droplet? Can drops grow by diffusion? The nonlinearity of the diffusional growth is emphasized in Fig. 112. We recall that 10 μm was a typical cloud radius and thus growth by diffusion *is* fast enough to produce such droplets. However 100 μm is a small raindrop size, and it is seen that over 4 hours are required to achieve this initial raindrop, far longer than the observed life-cycles of precipitating clouds.

We will consider the hypothetical evolution of the parcel:

1. All CCN start to form haze particles at $RH \approx 80\%$,
2. the larger droplets formed on giant CCN (and thus have lower activation S) become activated first.
3. These giant nuclei are few, thus have limited effect on the water availability, RH continues to increase,
4. and we start to activate drops with higher activation S^*. There are many of these and thus water vapour is consumed, eventually balance is reached where S is at a maximum.
5. After this point particles with lower S^* will continue to grow, while those with higher S^* will decay as S decreases.

The final points to note are that

- The maximum supersaturation between (0.1 to 0.5%) occurs within 10 to 100 metres of cloud base,
- S_{max} defines the number concentration of cloud droplets, and is thus also determined close to cloud base,
- higher updraught speeds give higher S_{max}, thus higher number of activated droplets leading to a higher number of final cloud droplets,

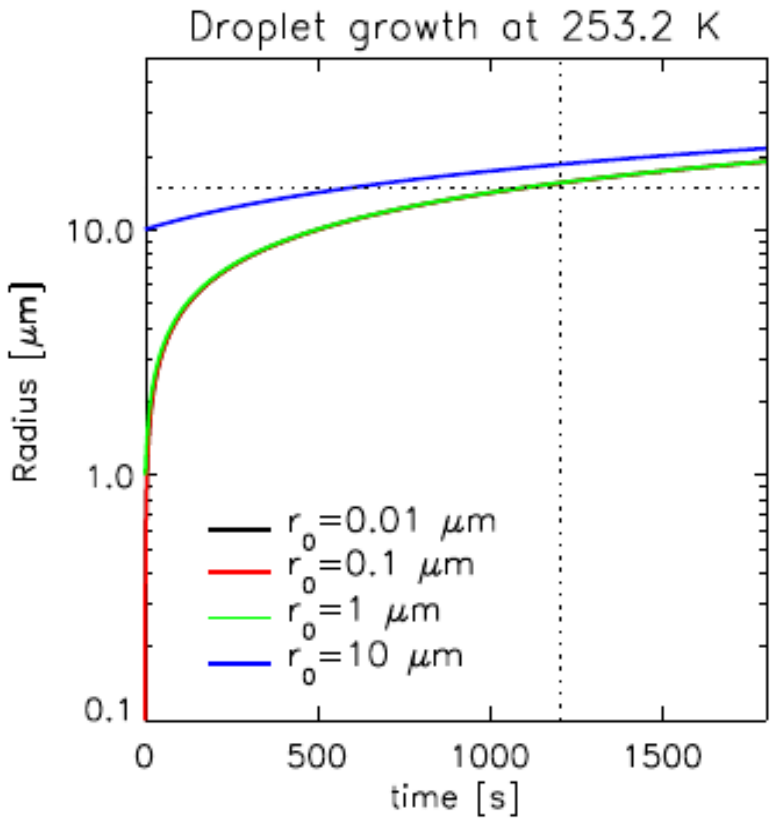

Figure 4.16: Diffusion growth curves, from Lohmann U.

- Growth of cloud droplets from an initial aerosol of 0.5 μm takes only a few seconds explaining why the cloud base is *well defined*,
- Calculated drop size spectra from modelling this process are *narrower* than observed (i.e. less size variability). This is because we have neglected the processes of cloud mixing and coalescence of droplets.

4.4 Terminal velocity of particles

Terminal velocity

We now introduce the concept of the terminal fallspeed of particles in a simplified way. The terminal velocity is achieved when the force due to gravity $F = \frac{4}{3}\pi r^3 g(\rho_L - \rho)$ is balanced by the drag on the droplet.

The drag strongly depends on the drop size, as seen in Fig. 113. The drag on a droplet is related to the particle velocity V and the radius r and can be divided into three regimes, leading to three distinct terminal fall speed V_t relationships:

- $r < 30\mu$m: Drag $\propto Vr$ giving $V_t = X_1 r^2$ where $X_1 \sim 1.2 \times 10^8 \mathrm{s}^{-1}$ m^{-1}.
- $30 < r < 1000\mu$m: Drag $\propto Vr^2$ giving $V_t = X_2 r$ where $X_2 \sim 8 \times 10^3 \mathrm{s}^{-1}$.
- $r > 1000\mu$m: Drag $\propto V^2 r^2$ giving $V_t = X_3\sqrt{r}$ where $X_3 \sim 250 \mathrm{s}^{-1}$ $\mathrm{m}^{0.5}$.

Table 4 gives typical fallspeeds as a function of radius. From these fallspeeds we notice two facts:

- The fallspeed of typical cloud droplets (2 to 20 μm) is negligibly small compared to typical updraught and downdraught velocities, with a 10 micron droplet requiring a day to fall 1km. This means that to a good approximation we can assume that cloud droplets are in suspension in the air.

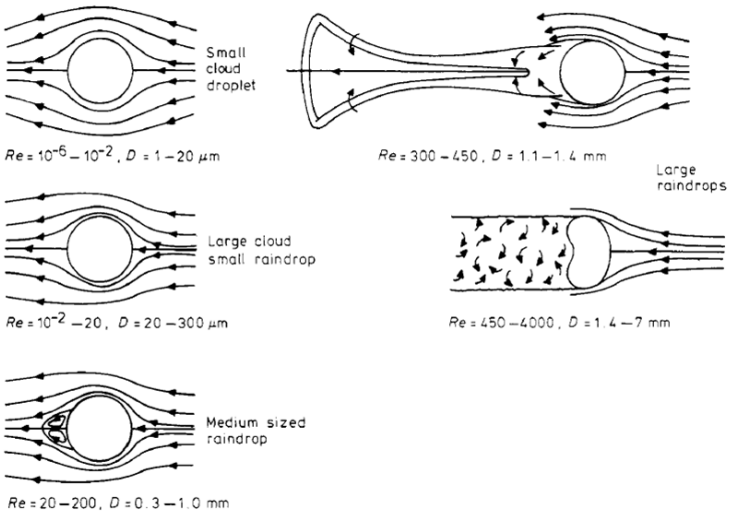

Figure 4.17: Changes in the air flow patterns round falling water drops as the Reynolds number increases (source: Mason, 1978)

r (μm)	1	10	20	100	1000
V_t (m s^{-1})	1.2×10^{-4}	0.012	0.048	0.8	8

Table 4.2: Time taken to grow a cloud drop of given radius by diffusion.

- The differential terminal fallspeeds also implies that larger droplets falling faster than smaller ones may collide and collect smaller droplets during their descent (see schematic in Figs. 114)

The sequence of laboratory photos shown in Fig. 115 show a droplet collision and cohesion event.

4.5 Collision and coalescence

We consider a large drop of radius R is falling through a cloud of smaller droplets radius r. If we take a simple view and assume that any small droplet in the path of the large droplet comes into contact and is *collected* (as in the sequence of Fig. 116, the volume of droplets collected per unit time is $\pi(R+r)^2(V-v)$. The liquid water content of the small droplets is $L = q_l\rho$ in kg m^{-3}, giving a mass accumulation rate of

$$\frac{dM}{dt} = L\pi(R+r)^2(V-v) \tag{4.29}$$

We will simplify the equation by assuming $R >> r$ and $V >> v$, and then use (145) which we recall states $\frac{dM}{dt} = 4\pi R^2 \rho_L \frac{dr}{dt}$ to give

$$\frac{dR}{dt} = \frac{LV}{4\rho_L} \tag{4.30}$$

If we take the case of the initial growth of small droplets ($r < 30$ μm) then the terminal velocity was given by $V = X_1 R^2$ giving

$$\frac{dR}{dt} = \frac{LX_1R^2}{4\rho_L} \tag{4.31}$$

Thus the growth rate due to collisions is proportional to the square of the droplet radius in this regime, while we recall that the radius rate change due to the diffusive process was proportional to the inverse of radius. This implies that there is a changing balance between the competition of these two processes, with the dominance of diffusion overcome by the importance of the collection process as the radius increases (see 117)

We can simply integrate (153) to show that for $L = 10^{-3}$ kg m^{-3} a drop can grow from 20 to 30 μm in approximately 10 minutes. We then need to introduce the relationship $V_t = X_2 R$ into (152) and integrate to calculate that the raindrop can attain a radius of around 300 μm in 20 minutes.

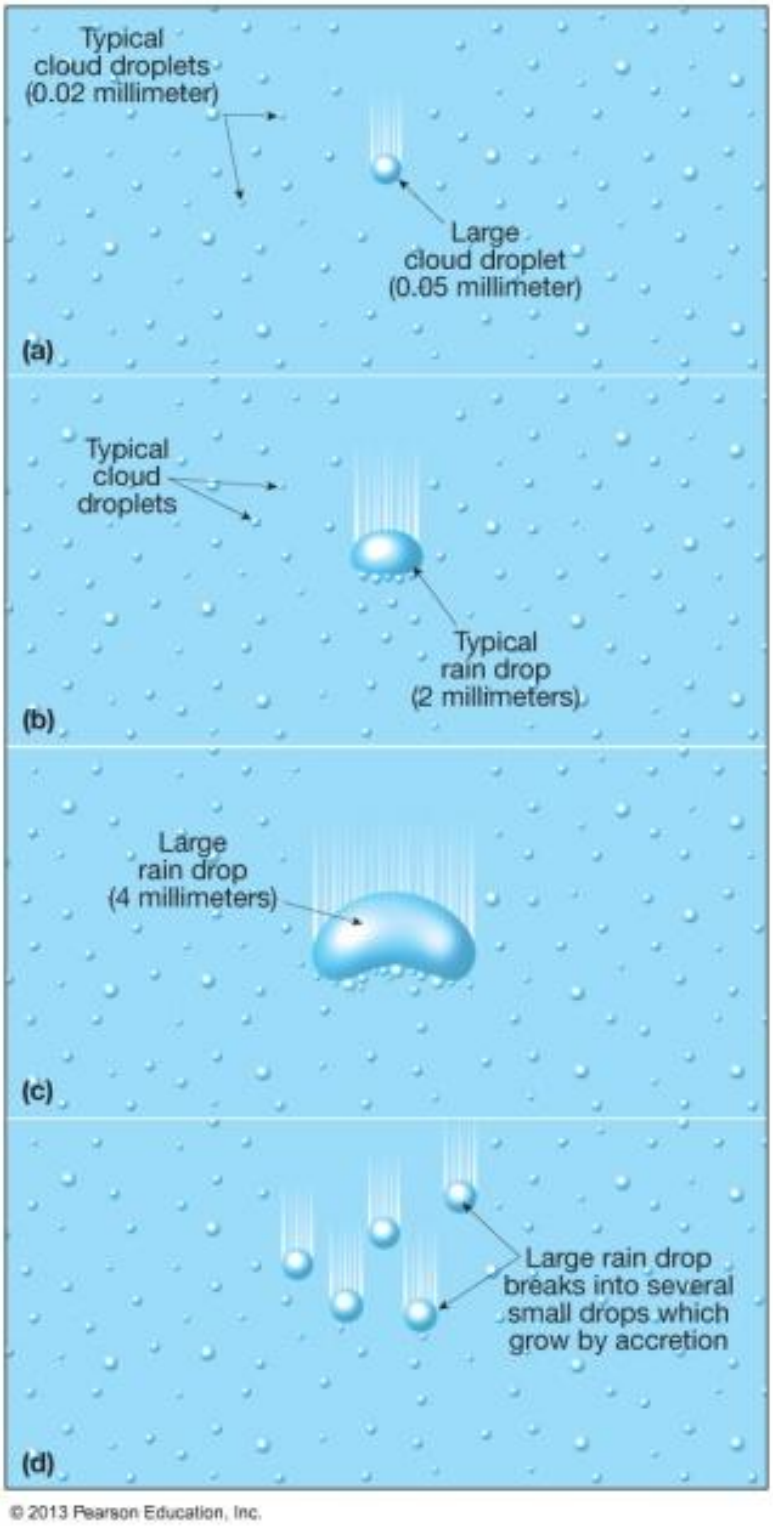

Figure 4.18: Schematic of larger raindrop growth through collisions with smaller drops during descent (a-c) and (d) droplet breakup (source Pearson Education Inc.)).

These times appear to be reasonable compared to cloud lifetimes, but we have ignored two effects in this simple view, *Q: Can you think what they might be?* We assumed simplistically that all droplets with in the large droplet trajectory collided with the large drop and that all collisions led to coalescence. Neither of these two assumptions are very accurate.

Collection efficiency $E(R, r)$

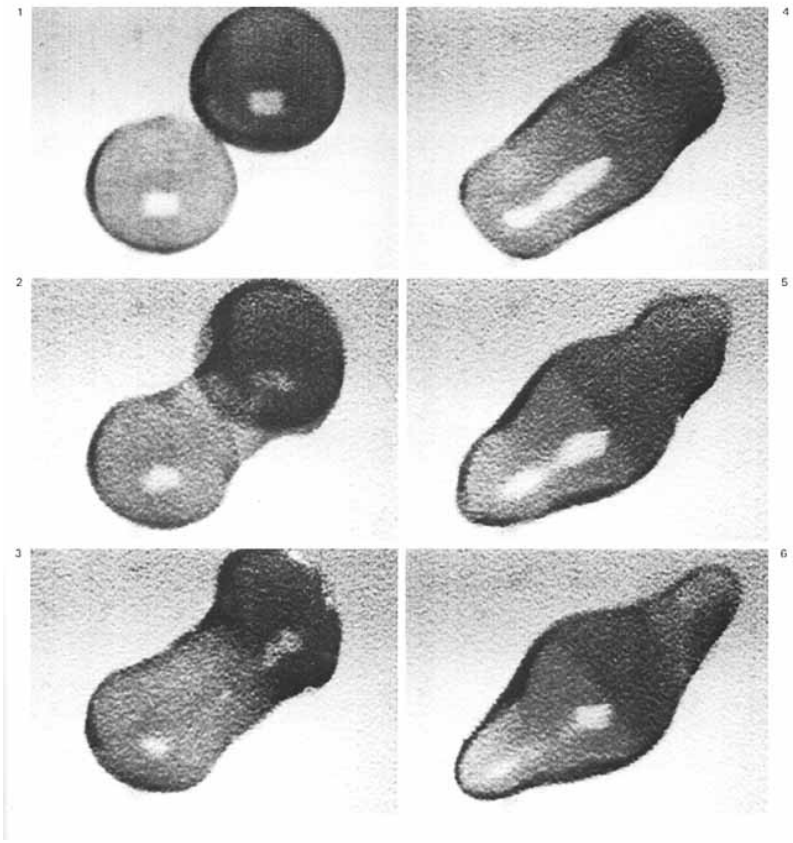

Figure 4.19: Sequence of shots showing droplet collision and subsequent cohesion (source unknown)

We saw earlier in Fig. 113 how the streamlines around various raindrop sizes looked. The lack of inertia of very small droplets implies that they will tend to get swept around the larger droplets if r/R is small (see Fig. 118). To describe this we introduce the *collision efficiency parameter* $E(R, r)$. For small r/R, $E(R, r)$ can be as low as 0.1, while when $R \sim r$ the flow fields can interact in a complex way and result in $E(R, r) > 1$.

Coalescence efficiency, ϵ

The *Coalescence efficiency* ϵ is often assumed to be $\sim$1, but observations show that it can be lower than 0.5.

Figure 119 shows two methodologies for the calculation of $E(R, r)$ from Klett and Davis (1973) which differ greatly for $R < 30$ μm in this case. Taking the *collision efficiency* and *Coalescence efficiency* into account modifies our radius growth rate equation to

$$\frac{dR}{dt} = \frac{LV\epsilon E(R, r)}{4\rho_L} \tag{4.32}$$

and growing a droplet from 20 to 30 μm can now take as much as *100 minutes* instead of 10 minutes, and we no longer grow rain drops in the observed time of cloud development. There are a number of mechanisms that lead to an accelerated growth rate to get us out of this impassé:

- *Statistical models of raindrop growth*: we assumed that droplet growth was a discrete function of time, whereas it consists of a serious of discrete events. If in a time Δt 10% of raindrops collide and coalesce then after time $2\Delta t$ there will be one large drop from 100 initial droplets (see Fig. 120). But this larger droplet will then be favoured for further growth as the growth rate is $\propto r^2$. *A spectrum of drop sizes, often bimodal, is therefore generated* (see Fig. 121).
- It was also assumed that droplets were evenly distributed within the cloud, whereas in reality cloud are *inhomogeneous*, and regions of higher liquid water content will favour droplet growth.

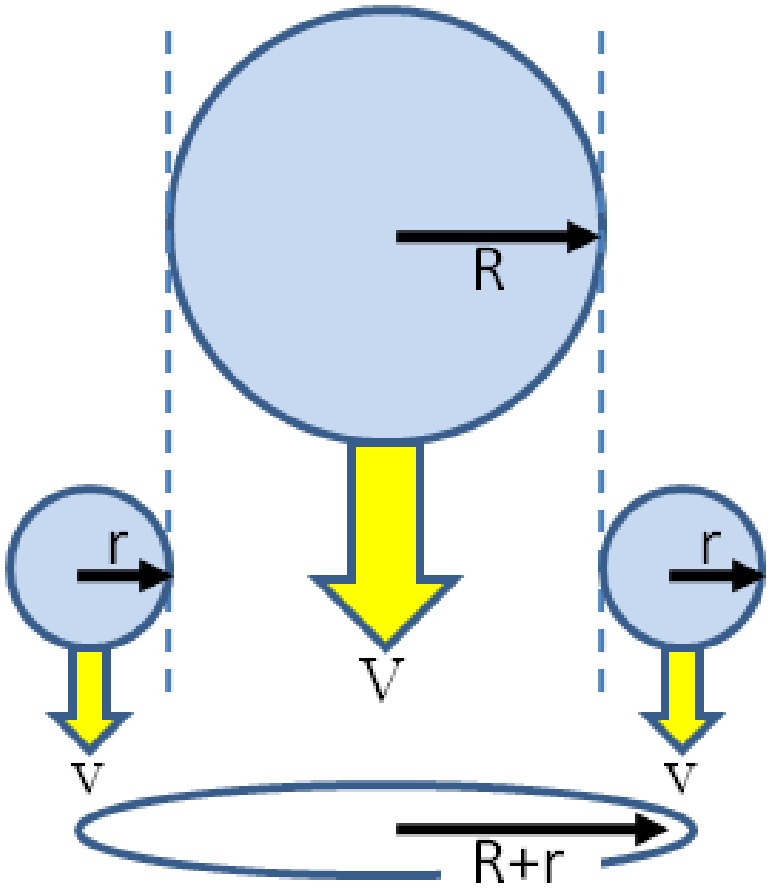

Figure 4.20: Schematic of collision and coalescence. Larger drops of radius R fall at terminal velocity V, collecting all smaller droplets of radius r within a cylinder of radius $R + r$.

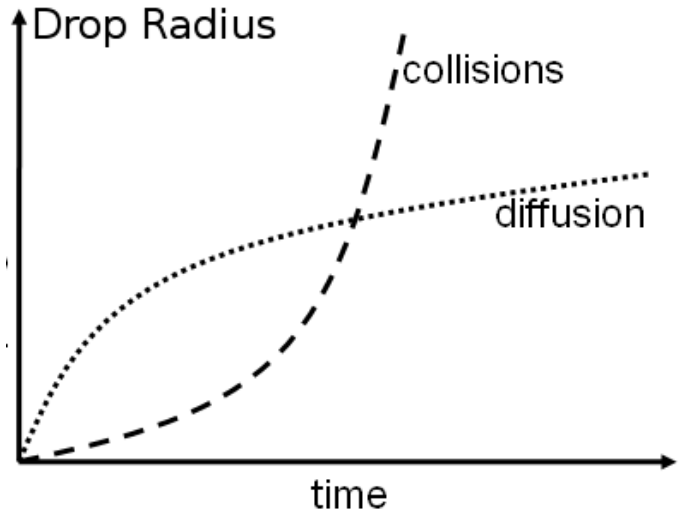

Figure 4.21: Schematic of droplet radius as a function of time resulting from growth by diffusion and collisions processes.

- The process of *entrainment* cause the partial evaporation of droplets broadening the droplet size distribution.

Raindrop size distributions
In many parts of the globe frozen precipitate melt before they reach the surface and thus precip-

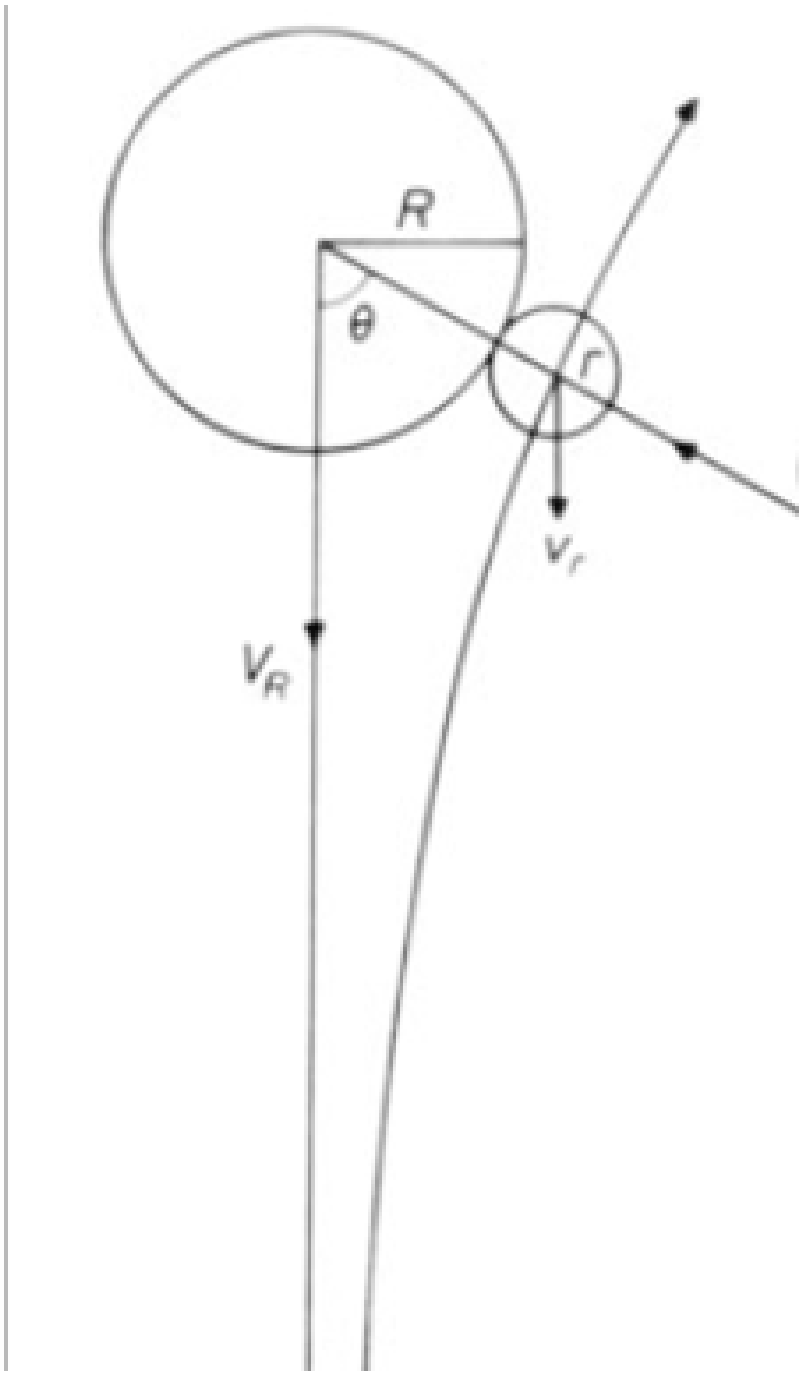

Figure 4.22: Schematic showing more realistic path of small droplet (source Mason, 1978).

itation reaches the surface in the form of rain. There is a natural limit to the raindrop size due to droplet breakup, and it is usually very rare to measure raindrops with radii larger than 3mm - with 2mm a more common limit.

Q: If you stand underneath a tree during a shower, you may get much larger drops fall on you. Why?

The reduction in occurrence with droplet size implies that raindrop radii (or diameters) tend to follow an inverse exponential distribution, known as the Marshall-Palmer distribution (Marshall and Palmer, 1948), after the first authors to suggest the relationship from observations

$$N(D) = N_0 e^{-\Lambda D}, \tag{4.33}$$

where $N(D)dD$ is the number of drops per unit volume with diameters between D and $D + \Delta D$.

The slope factor *Lambda* depends on rainfall rate R and is given by

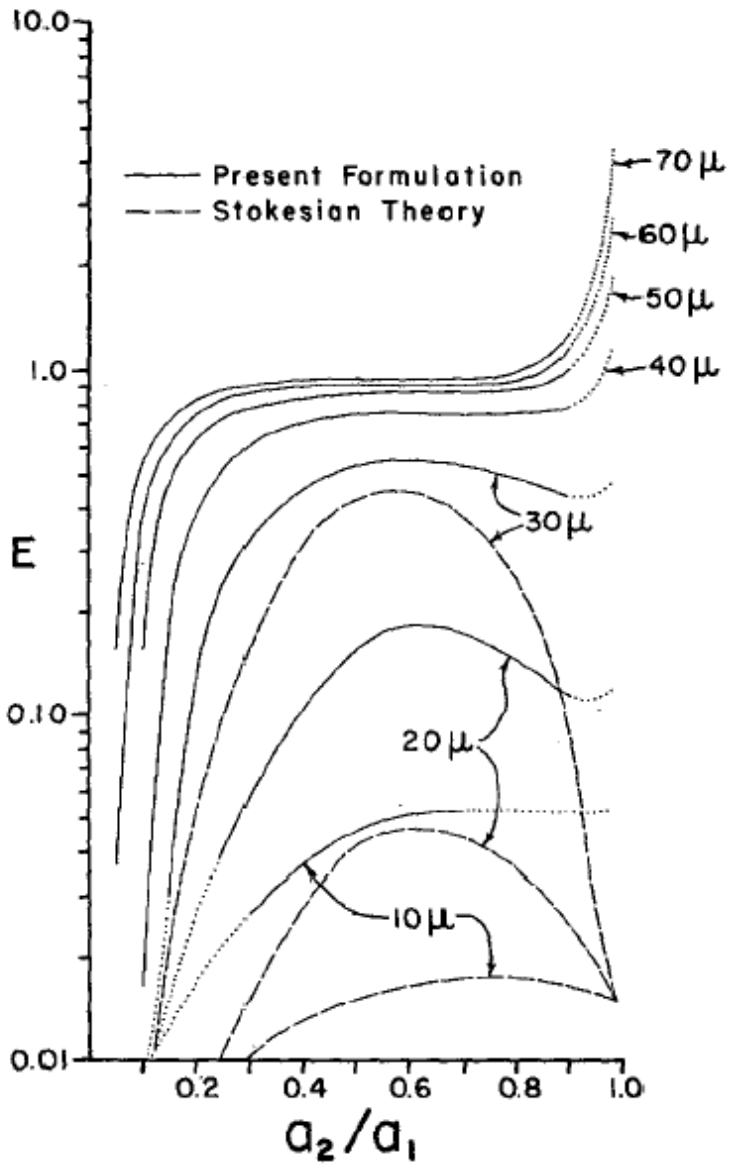

Figure 4.23: Graph of theoretical collection efficiencies $E(R, r)$ for two calculation methodologies with the x-axis showing the radii ratio r/R. Each line is labled with the radius of the larger droplet (source Klett and Davis, 1973).

$$-\Lambda(R) = 41R^{-0.21}, \tag{4.34}$$

where the units of R and *Lambda* are mm hour^{-1} and cm^{-1}, respectively. It was also found that N_0 was independent of rainfall rate, taking a value of $N_0 = 0.08$ cm^{-4}. Fig 122 shows the Marshall-Palmer distribution.

These relationships are empirical and valid over a large-number of observations. Exact relationships will vary with location and time and departures from the MP distribution will always occur (Fig. 123).

4.6 Ice crystal nucleation

Introduction to ice processes

The first thing that should be emphasized when considering the ice phase is that *ice phase processes in clouds are far more complicated (Fig. ??) and consequentially poorly understood* relative to the warm phase cloud processes. This course can only skim the surface of the relevant mechanisms.

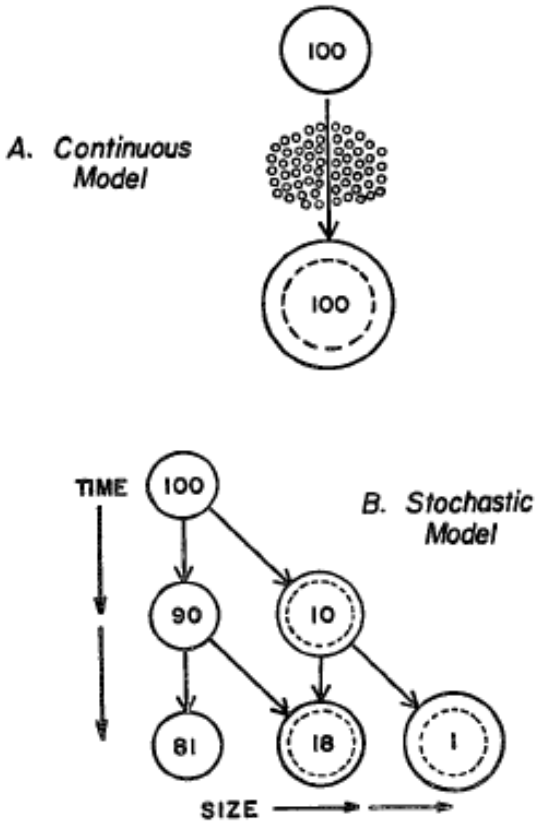

Figure 4.24: stochastic model of sweep out (source Berry, 1967).

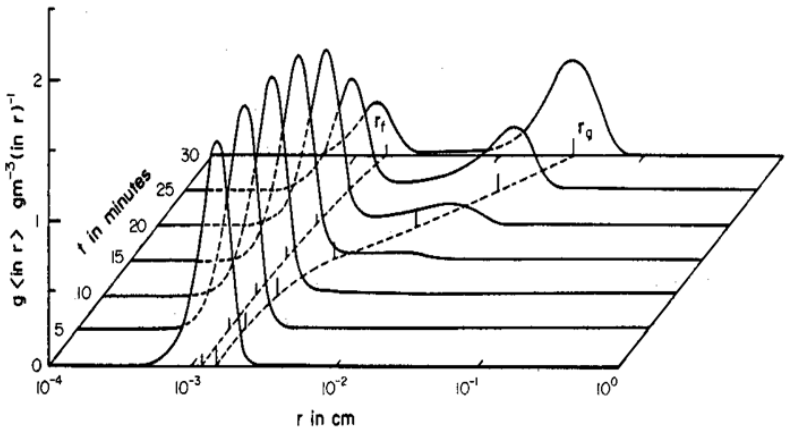

Figure 4.25: Example of the development of a droplet spectrum by stochastic coalescence (source Berry and Reinhardt, 1974).

Liquid water was described as a state where water vapour molecules were jumbled together and weak hydrogen bonds were formed between molecules, which are constantly overcome by thermal agitation. If temperatures become low enough to prevent the disruptive effects of thermal motions, water freezes into ice in which the hydrogen bonds form a rigid and stable network (Fig. 124).

In this well-defined structure of ice each water molecule is surrounded by four neighboring H2Os. Two of these are hydrogen-bonded to the oxygen atom on the central H2O molecule, and each of the two hydrogen atoms is similarly bonded to another neighboring water molecule. This lattice arrangement requires that the molecules be somewhat farther apart than would otherwise be the case in liquid and as a consequence, ice, in which hydrogen bonding is at its maximum, has a more open structure, and thus a lower density than water (Fig. 125).

Q: what properties do you notice from the rainfall size distribution?

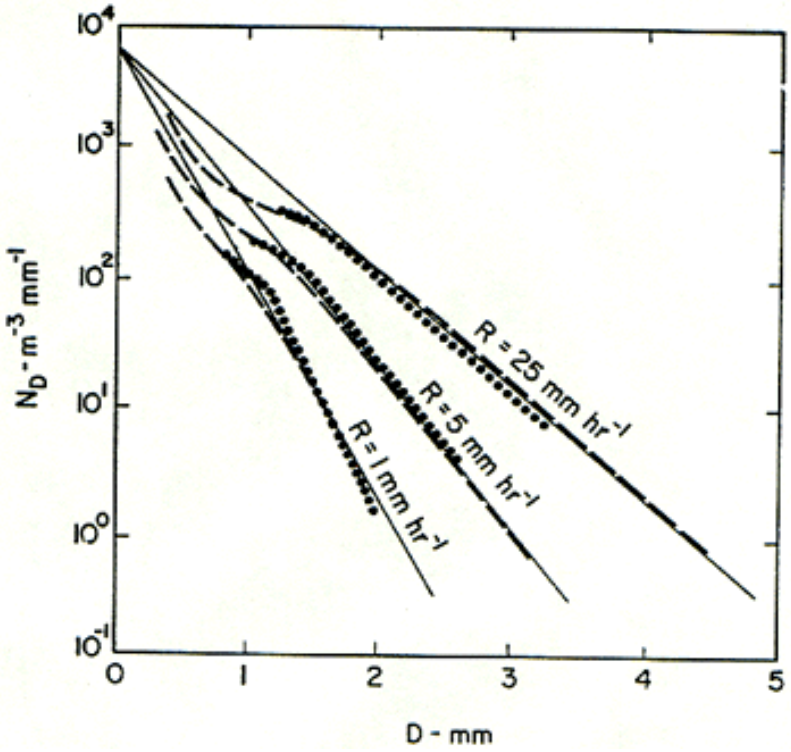

Figure 4.26: Marshall-Palmer distributions (from Marshall and Palmer, 1948)

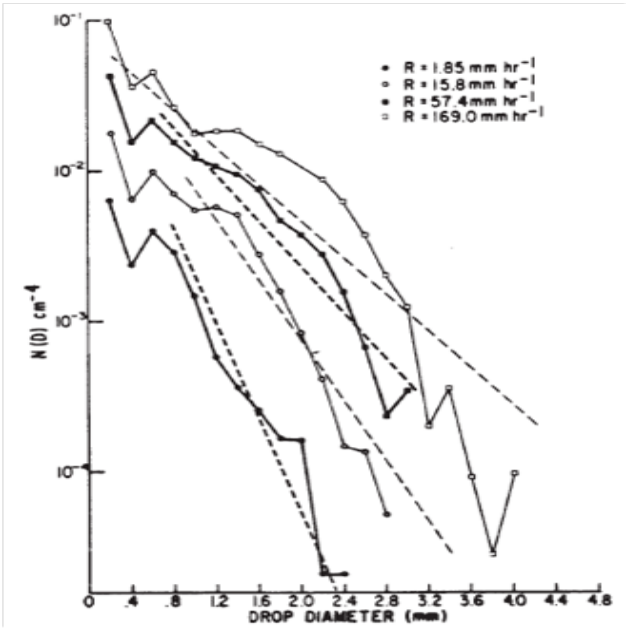

Figure 4.27: An example of raindrop size distributions from Willis (1984)

4.7 Ice saturation

Saturation over a plane surface of pure ice

Before we continue with the discussion of ice we must first consider the concept of saturation over a planar ice surface. Analogous to the liquid water saturation, the air is said to be saturated if the *deposition* (vapour→ice) rate equals the *sublimation* (ice→vapour) rate.

As the intermolecular bonding energy of molecules in ice is greater than that in liquid water,

Figure 4.28: Example of an ice crystal from http://www.its.caltech.edu/)

at a given temperature, the evaporation rate is larger than the sublimation rate. Thus it is clear that $e_{si}(T) < e_{sw}(T)$ (see Fig. 126) where the saturation vapour pressures are

- e_{si} over ice
- e_{sw} over liquid water.

Note that while the *ratio* $\frac{e_{sw}}{e_{si}}$ increases with decreasing temperature, the highly nonlinear saturation curves implies that this is not true of the *absolute difference* between the two $e_{sw} - e_{si}$, which reaches a maximum at a temperature of around -15 to -10^{o}C.

4.8 Ice nucleation mechanisms

There are three potential mechanisms by which ice clouds can form:

1. Homogeneous freezing from the liquid phase
2. Homogeneous nucleation from the vapour phase
3. Heterogeneous nucleation from the vapour phase

Homogeneous nucleation from the vapour phase (mechanism 2) requires very high relative humidities for similar reasons to those given for the warm phase, and thus this is not a viable mechanism for ice crystal formation in the atmosphere. Thus the two key methods by which ice can form is by *freezing of a liquid droplet*, or by direct *vapour deposition on an ice nucleus* (heterogeneous deposition nucleation).

The balance between these two mechanisms depends on the *cloud updraught speed* and the *ambient temperature*.

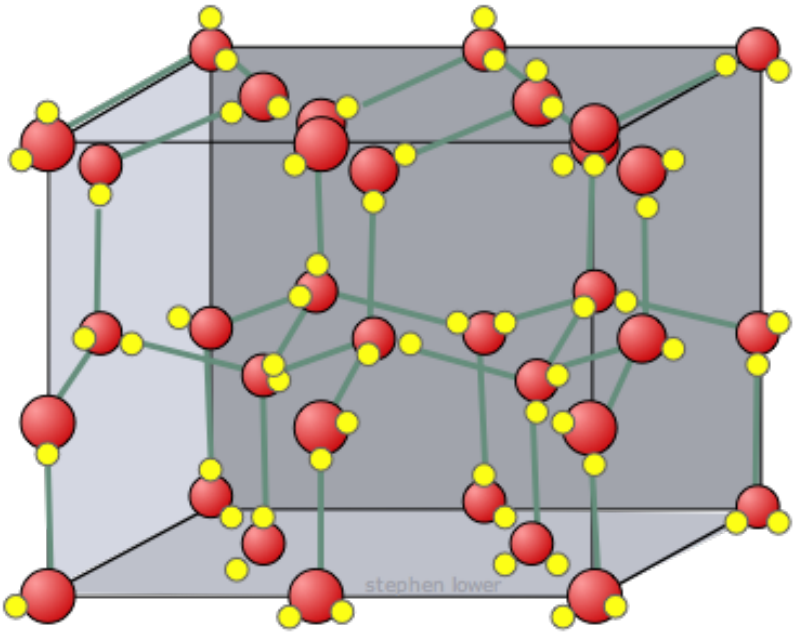

Figure 4.29: The ice latice structure (www.chem1.com)

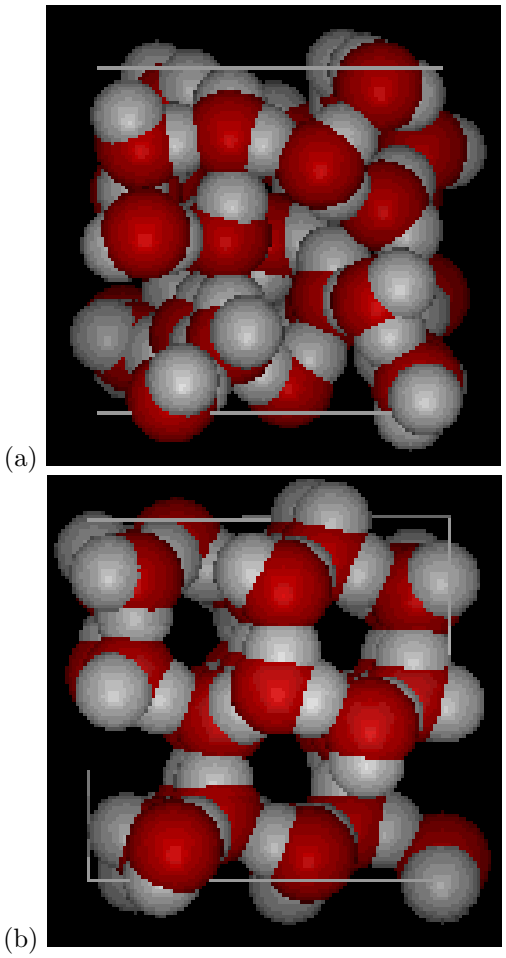

Figure 4.30: Schematic of (a) liquid and (b) ice molecular structures (source edinformatics.com)

- *Homogeneous* nucleation is often the dominant process in clouds forming at temperatures colder than -40C (cirrus) or clouds with fast updraught speeds,

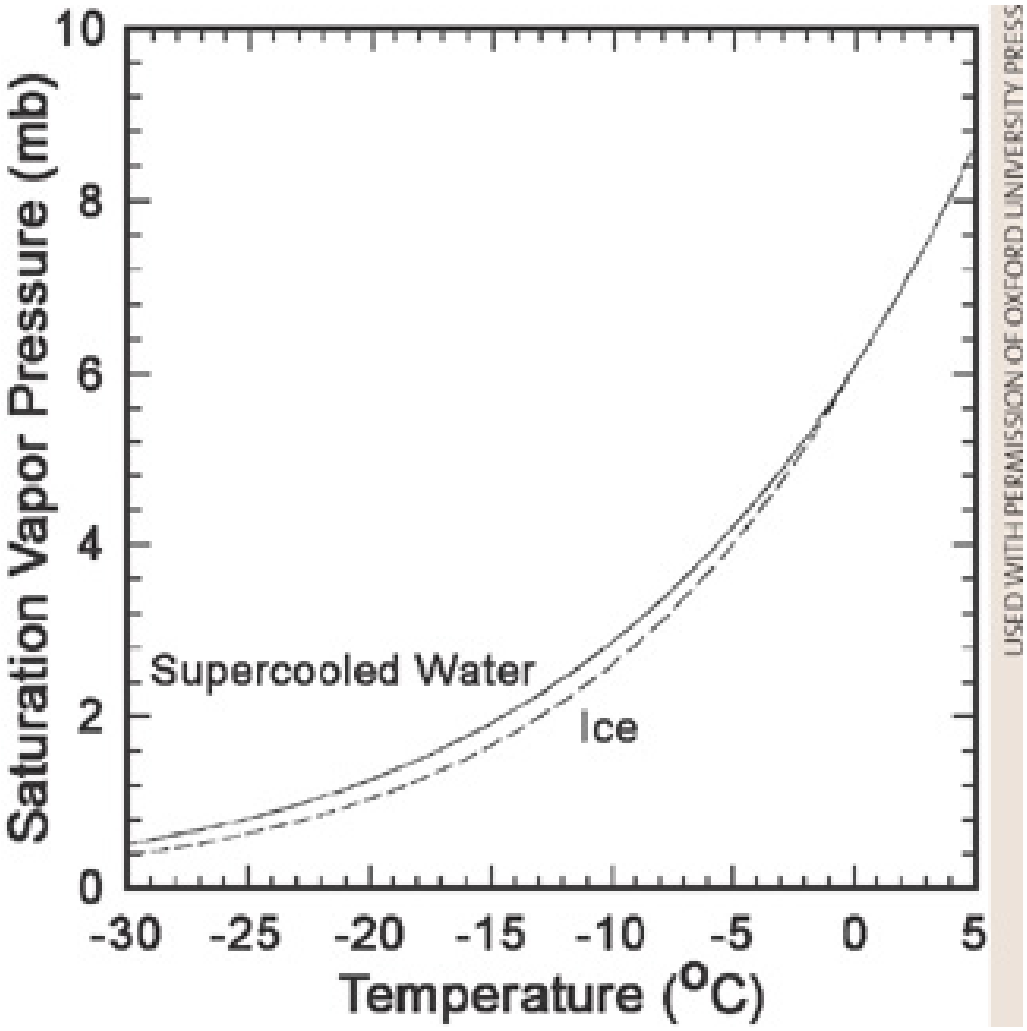

Figure 4.31: The saturation vapour pressure as a function of temperature with respect to ice and liquid (source Atmospheric Thermodynamics by Craig F. Bohren and Bruce A. Albrecht)

- *Heterogenous* nucleation from the vapour phase may dominate crystal formation in mixed phase clouds at temperatures above -40C or also in clouds with slow vertical updraught speeds if sufficient IN are present

ICE2

4.9 Homogenous nucleation from the liquid phase

When the temperature falls below 0°C there is no guarantee that freezing of liquid cloud droplets will immediately occur. Freezing begins when an initial crystal, termed *ice germ*, is formed by statistical fluctuations of the liquid molecular arrangement to form a stable ice-like lattice structure. As in all nucleation processes, energy is required for the formation of the ice germ surface:

$$\Delta G_{i,w} = 4\pi r^2 \sigma_{i,w} - \frac{4\pi r^3 R_v T}{3v_i} ln \frac{e_{s,w}}{e_{s,i}} \tag{4.35}$$

Thus, the lower the temperature, the larger $\frac{e_{s,w}}{e_{s,i}}$ becomes, which lowers the energy barrier to form a critical ice germ. From Fig. 128 it is seen that at colder temperatures the energy barrier is far lower than that for homogenous liquid or ice crystal nucleation from the vapour phase.

- If the germ is over a critical size, then other water molecules will bind to the ice germ rapidly and the water body will freeze rapidly.

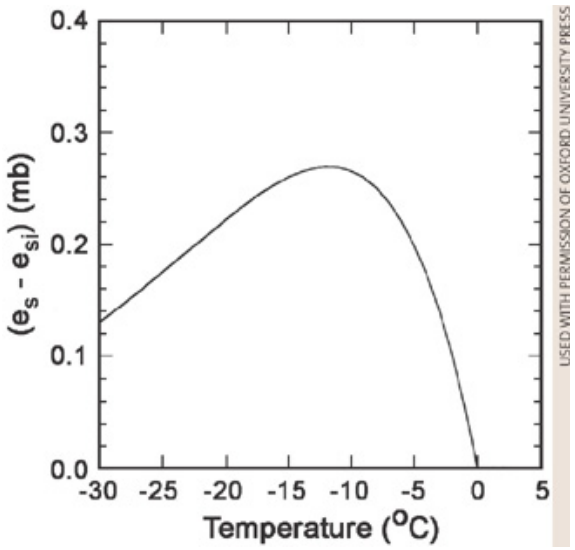

Figure 4.32: The difference in saturation vapour pressure as a function of temperature with respect to ice and liquid (source Atmospheric Thermodynamics by Craig F. Bohren and Bruce A. Albrecht)

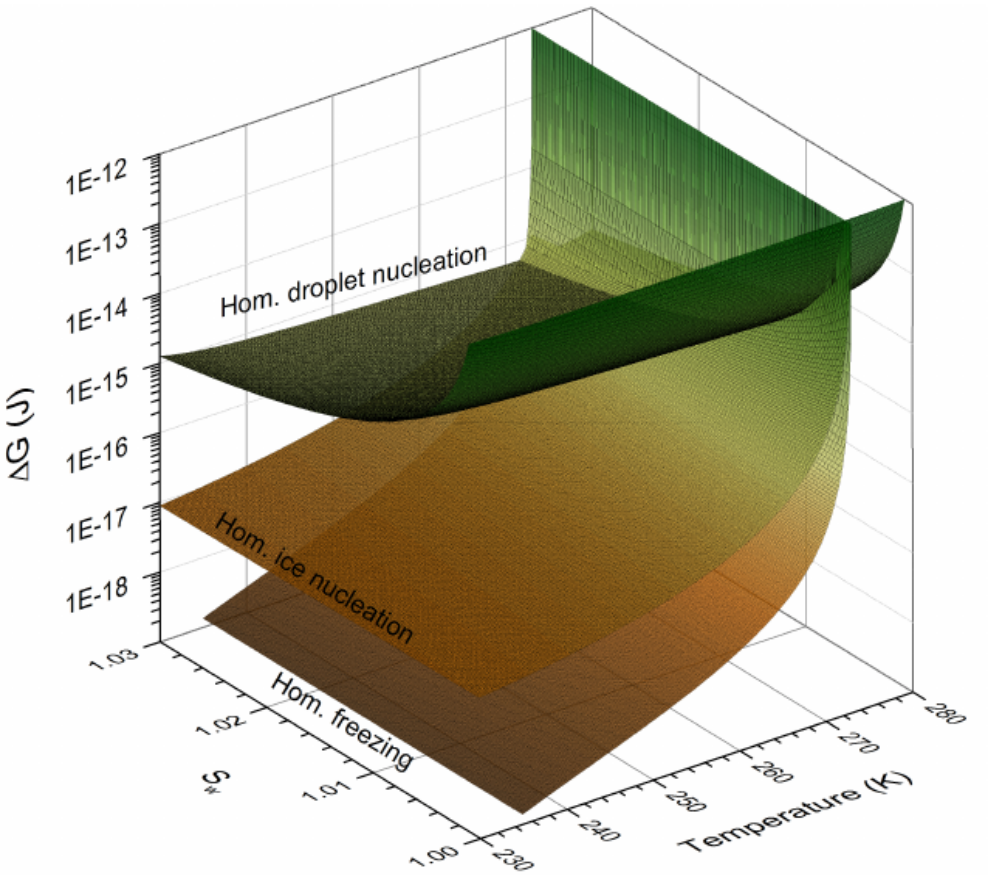

Figure 4.33: Gibbs free energy barrier for homogeous nucleation phase transitions (from Lohmann U.)

- Again, we refer to concepts of statistical mechanics. The larger a body, the more likely it is that random energy fluctuations will occur to create an ice germ of a critical size for spontaneous freezing to occur.

- Large drop are more likely to freeze than small drops.

Theoretical results imply that a liquid drop of 5 μm will spontaneously freeze at temperature of around -40°C, while a 100 μm droplet will freeze at -35°C.

however, these calculations are uncertain as $\sigma_{i,w}$ is poorly known. Empirical measurements inside real clouds show that they contain no liquid drops once temperatures of around -35°C to -40°C are attained (depending on the cloud drop size spectra). Such clouds are said to be completely *glaciated*. It is clear that a pond therefore freezes more readily than a cloud of liquid droplets as the formation of an ice germ of critical size only has to occur once in the pond, while the event needs to occur in each cloud droplet which is far less likely. Thus it is possible and indeed very common to find liquid cloud drops existing at temperatures much below the freezing point; referred to as *supercooled droplets* (see Fig. 129).

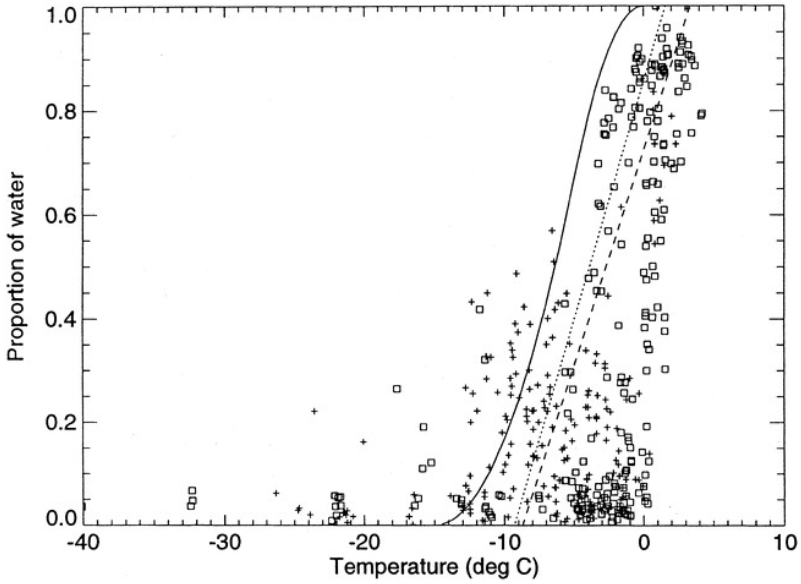

Figure 4.34: Liquid water to ice fraction in aircraft observations, with several diagnostic parameterizations used in models overplotted. (source Rotstayn et al., 2000)

Homogeneous nucleation of ice from vapour

It is also theoretically possible to nucleate ice crystals directly from the vapour phase, however theory shows that very high supersaturations ($> 1000\%$) with respect to ice would be required. At these high supersaturations, air would also be supersaturated with respect to liquid water, forming droplets that would freeze. Thus *homogeneous nucleation of ice directly from the vapour phase is not a relevant mechanism* for creating ice cloud.

Ice supersaturation in the upper troposphere

One consequence of the lack of efficient IN is that cloud-free air can be supersaturated with respect to ice and not form ice cloud. However there is an upper limit to the amount of ice supersaturation set by e_{sw} since at this point liquid droplets form which will homogeneously freeze *if* the temperature is below -40°C. A common sign of the upper troposphere being supersaturated is the presence of *permanent contrail cloud* (Fig. 130).

As temperature get colder, e_{sw} and e_{si} diverge, and larger ice supersaturations are possible. In fact it is more complicated and the limit is below e_{sw} since we recall that aqueous solution droplets (haze) forms at RH with respect to water substantially below 100%.

Koop et al. (2000) investigates this limit in detail and shows an upper limit of 45% ice supersaturation at $T = 235$ K increasing to 67% at $T = 190$K.

In Fig. 131 Spichtinger et al. (2003) shows using retrievals from microwave limb sounder data that ice supersaturated states are quite common in the upper troposphere. We have seen that homogeneous ice nucleation occurs at temperature below -40°C and that supercooled liquid water is very common below 0°C. However it is also true that ice is observed in clouds between 0°C and -40°C. Clouds *Q: How could it get there?*.

Figure 4.35: Photo and satellite picture of permanent contrails over the UK. (source unknown).

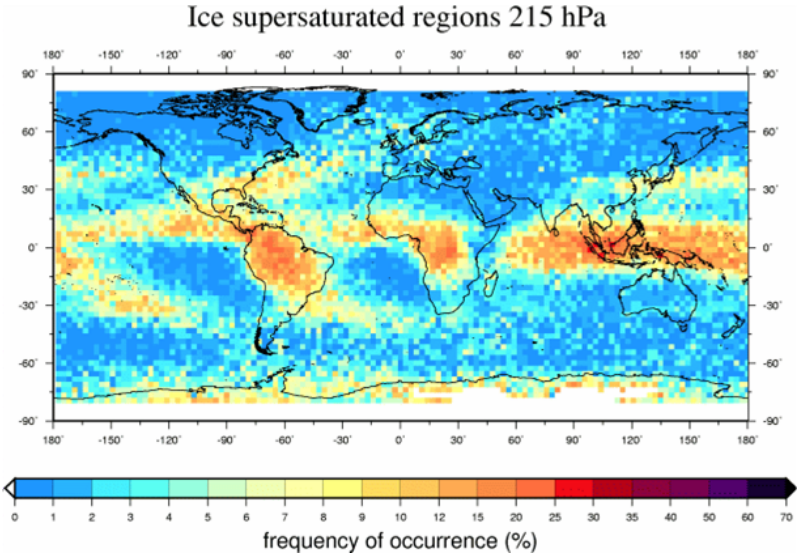

Figure 4.36: Frequency of ice supersaturation at 215hPa (source Spichtinger et al., 2003)

- Air was previously at much colder temperatures: *parcel history*
- Ice has fallen from above: *ice sedimentation*
- Ice has nucleated in situ: *how?*

Ice can form by collision of liquid water droplets with other ice crystals, freezing on contact. Alternatively, ice crystals can form with the aid of aerosols in a heterogeneous nucleation process.
ICE3

Heterogeneous nucleation of ice
Aerosols in the atmosphere can also act as *ice nuclei* (IN) if their molecular structure is close enough to the lattice structure of ice. The first point to emphasize is that it is much less common for aerosols to have this property and therefore ice nuclei are much less common than CCN.

At $T = -20°\text{C}$ a typical number concentration (NC) of ice nuclei might be 10^{-3} cm^{-3} compared to CCN of roughly 10^{2} cm^{-3}.

Whether an aerosol can act as a cloud nuclei depends on the *ice supersaturation* and the *temperature*.

As ice supersaturation increases and temperature reduces more aerosols take on the property of being ice nuclei. Fletcher (1962) found that for each 4°C of cooling the number of ice nuclei increases by a factor of ten (Fig. 132).

Common ice nuclei
Some ice nuclei are given in table 5 along with their maximum nucleation temperature.

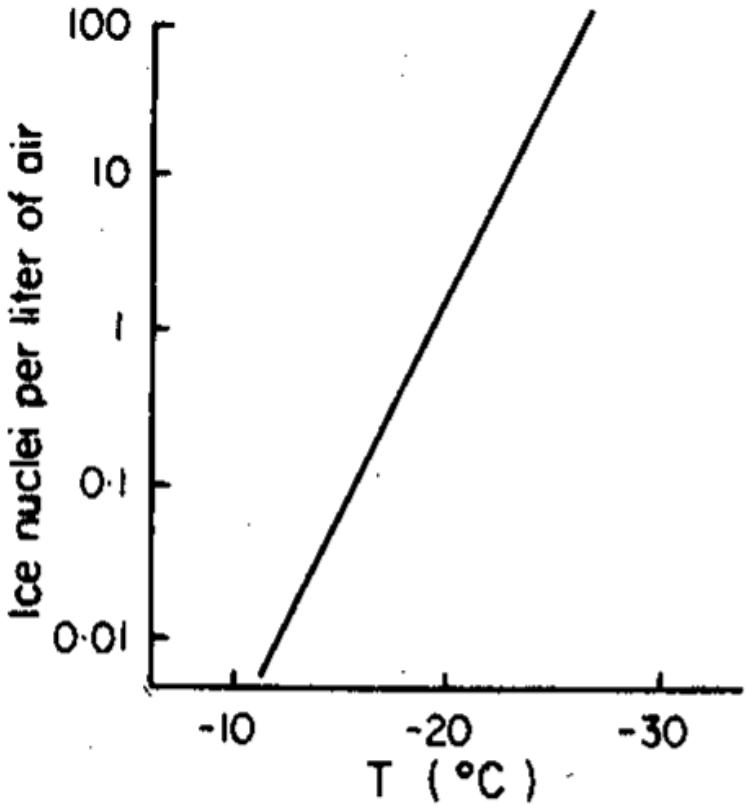

Figure 4.37: Ice nuclei concentration as a function of temperature (source Fletcher, 1962)

Substance	Nucleation T (°C)	Notes
ice	0	
silver iodide	-4	used in cloud seeding
clay	-9	often seen in snow crystals
cholesterol	-2	
bacteria(!)	close to 0	used in snow machines

Table 4.3: ice nuclei and their nucleation temperature maximum

Demott et al. (2003) tested air samples taken from mountain top in mid-Western USA and documented the distribution of IN depicted in Fig. 133. The wide range of supersaturation and temperature thresholds for various classes of IN is shown in Fig. 134 which is taken from Hoose and Möhler (2012).

It should be emphasized that knowledge of which aerosols can act as ice nuclei is uncertain and the subject of current research. Ice nuclei concentrations are highly variable, and although the Fletcher curve may be accepted as typical, concentrations can vary by orders of magnitude. Aerosols may also be carried a long distance in the atmosphere before being involved in ice cloud nucleation events.

Demott et al. (2003) and others have shown that mineral aerosols from Western Africa are a significant source of ice cloud nuclei over the United States for example! In fact many snow or ice particles contain clay mineral aerosols indicating that the desert regions of the world are in general an important source of IN (see Fig. 135). ICE3

General properties of ice nuclei

Observations and laboratory experiments indicate that aerosol particles usually satisfy a list of criteria if they are to serve as IN (Pruppacher and Klett, 1997).

- **Insolubility criterion:** In general, IN must be very insoluble. The disadvantage of a soluble substrate is that it disintegrates under the action of water. Hence the molecular structural

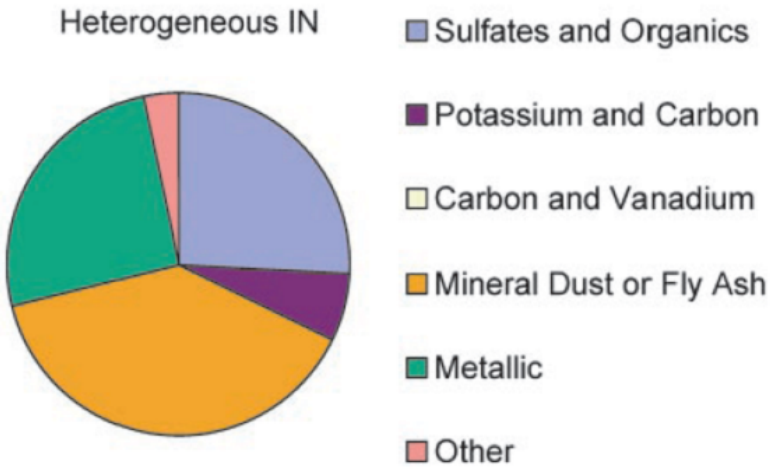

Figure 4.38: From Demott et al. (2003), distribution of IN type from air samples taken over the mid-West USA.

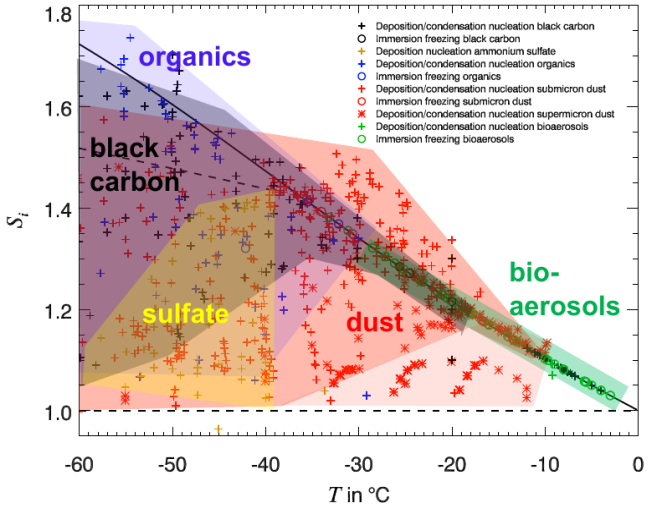

Figure 4.39: The onset temperatures and relative humidities for IN from a compilation of experimental data of sub- and supermi- cron aerosol particles in the literature from Hoose and Möhler (2012). The wide variability in the thresholds is emphasized.

requirement for ice nucleation can not be maintained.

- **Size criterion:** IN must have a size comparable to, or larger than, that of a critical ice embryo. Generally speaking the radius of the IN must be greater than 0.1 μm; i.e. Aitken particles do not tend to be ice nuclei. At sizes less than this critical radius (0.1 μm), the nucleating ability of the particle decreases rapidly (and becomes increasingly more temperature dependent).

- **Chemical Bond criterion:** The chemical nature of an IN, that is the type and strength of the chemical bonding sites at the IN surface, affect nucleation. In view of this bond criterion, certain complex organic molecules (i.e. aerobic bacteria) exhibit good ice nucleation abilities. The hydrogen bonding groups in ice are similar to the hydrogen bonding groups in many organic molecules.

- **Crystallographic criterion:** Since ice nucleation on a substrate is actually an overgrowth of ice on the substrate, it is reasonable to expect the nucleating ability of the substrate to increase when the lattice structure of the substrate is similar to the hexagonal lattice structure of ice. In this way, molecular matching between the molecules of ice and the substrate may

What kind of cloud is this figure showing?

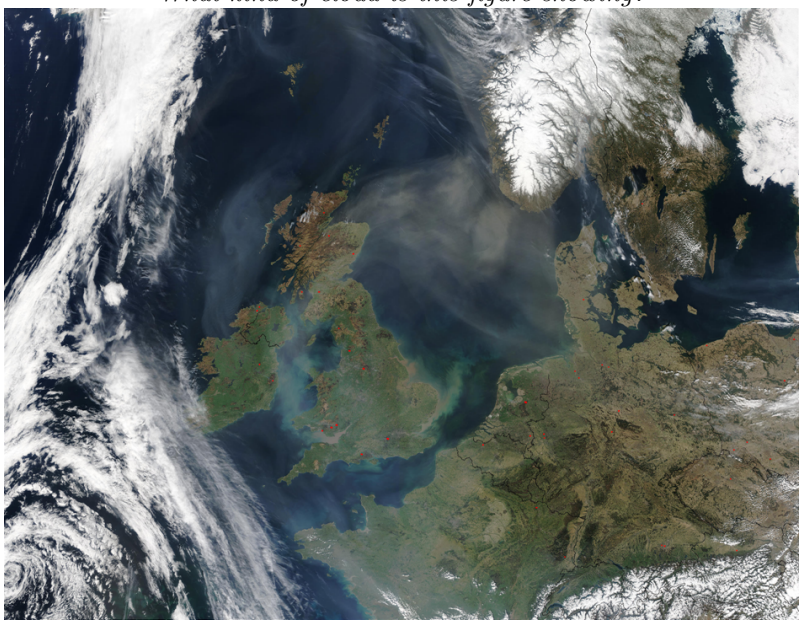

Figure 4.40: Modis image over Europe (source MODIS website)

be achieved (Fig. 136). The crystallographic matching reduces the *"misfit"* and *elastic strain* in the ice.

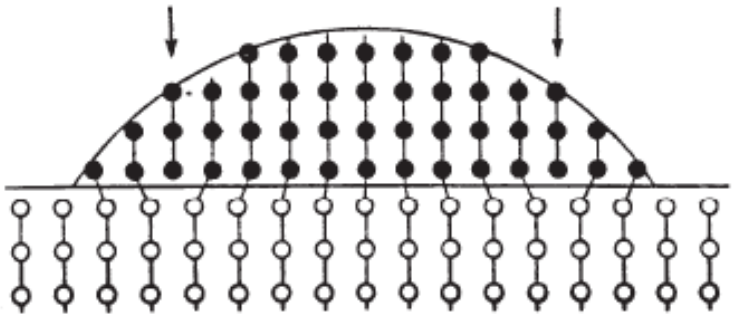

Figure 4.41: An ice-embryo (dark points) growing upon a crystalline substrate with a misfit of 10%. The interface is dislocated, dislocations being indicated by arrows. (from Fletcher, 1969) Fletcher (1969).

Both of the properties of misfit and elastic strain reduce the nucleating ability of the substrate. Kaolinite forms good ice nuclei because it has a *pseudo-hexagonal structure*. AgI (silver iodide) also has a hexagonal form. Other molecules have a non-hexagonal shape (e.g. cubic), but still have crystal structures close enough to ice to aid nucleation. The crystallographic requirement has to do with the arrangement of molecules and is distinct from the chemical bond criterion.

- **Active Site criterion:** Ice nucleation generally occurs at distinct sites on the substrate. Laboratory studies have indicated that ice nucleation is preferred on those substrates which have pits and steps on their surfaces. Those nuclei that have smooth surfaces are less efficient nuclei, that is, nucleation occurs at *lower temperatures*. An example is shown in Fig. **??** where ice crystals preferentially formed on steps etched onto the surface of a cadmium iodide crystal.

Mechanisms for Heterogeneous Nucleation

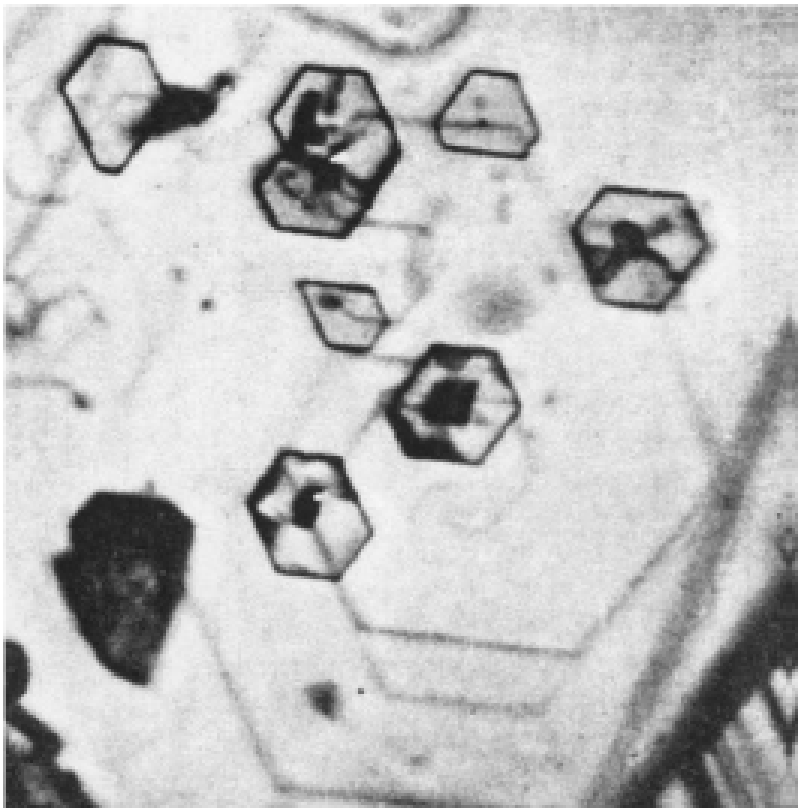

Figure 4.42: An epitaxial deposit of ice crystals growing at the steps of a hexagonal growth spiral on cadmium iodide (source **?**).

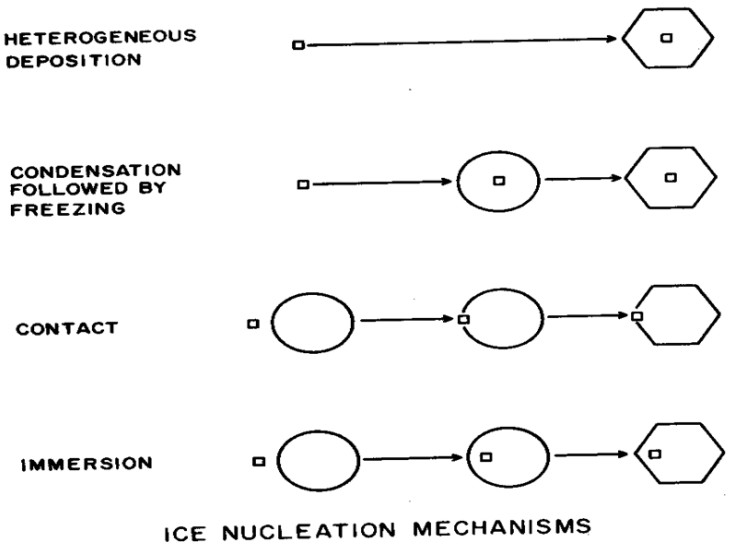

Figure 4.43: Schematic of heterogeneous nucleation pathways (source: Rogers and Yau, 1989).

There are several mechanisms for ice crystal nucleation, schematically illustrated in Fig. 137.

These are

- heterogeneous deposition nucleation: the vapour undergoes deposition directly onto the IN
- condensation nucleation: the IN acts first as a CCN to form a liquid droplet, and then acts as a IN to initiate freezing
- contact nucleation: a supercooled liquid droplet undergoes freezing immediately on contact

with the IN

- immersion nucleation: IN absorbed into a liquid droplet, and later initiates freezing event, possibly after droplet cooling.

ICE4 Contact freezing and immersion freezing occur in mixed phase clouds in which the ambient vapour pressure is equal to the saturation vapour pressure with respect to liquid water. *Why?*

The deposition of water vapour directly onto IN can occur at saturations substantially less than water saturation. Fig. 138 the pathways for ice nucleation are shown, along with the threshold for homogeneous ice nucleation.

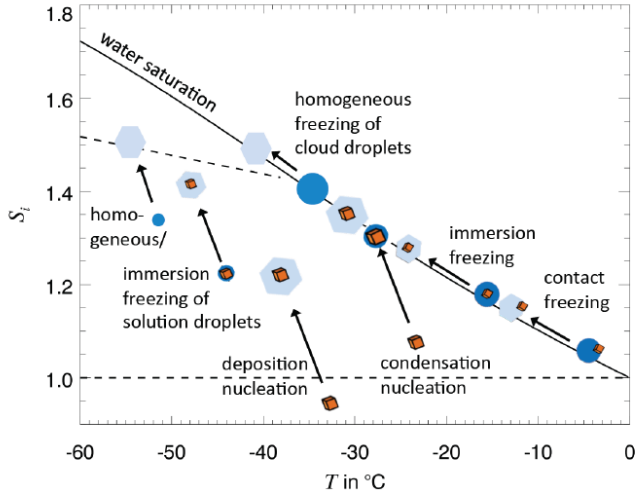

Figure 4.44: Atmospheric trajectories of temperature and ice saturation of a rising air parcel which lead to ice formation in the different nucleation modes (source Hoose and Möhler, 2012)

4.10 Ice crystal growth

We divide the consideration of ice crystal growth by diffusion of water vapour into two regimes: *mixed phase* and *glaciated* clouds. For *mixed phase clouds* we recall that at subfreezing temperatures the ice and water vapour saturation pressures diverge, and thus an air volume at water saturation is supersaturated with respect to a planar ice surface, reiterated in Fig. 139.

Bergeron-Findeisen Effect

The *Bergeron-Findeisen effect* is an important *growth enhancing mechanism* for ice crystals in mixed phase clouds.

If we introduce an ice crystal into a supercooled liquid water cloud, what would be the effect? (Fig. 140):

- The cloud is initially saturated *with respect to liquid water* and thus *ice* supersaturated.
- The ice crystal will thus grow by diffusion of water vapour
- This would reduce the vapour pressure below the liquid water saturation value.
- Liquid droplets thus evaporate on a faster timescale, maintaining the vapour pressure close to liquid water saturation.

The outcome of the Bergeron-Findeisen effect is that the growth rate of the ice crystal is faster than it would be in the absence of liquid cloud droplets. For a water saturated environment the growth rate is fastest when the difference between the saturation limits is largest *in absolute (not relative!) terms*. This occurs around $T = -15°C$.

A laboratory photo shows the result of the BF-effect, with the lack of liquid droplets surrounding the ice crystal on the plate (Fig. 141)

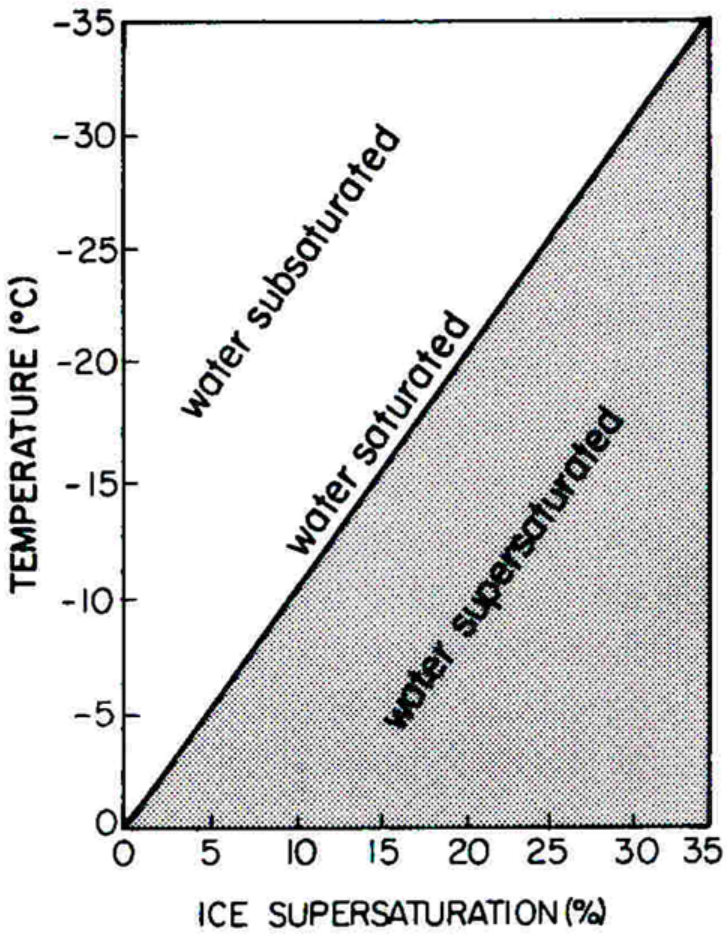

Figure 4.45: Diagram showing relative degrees of ice and liquid water super or sub-saturation as a function of temperature (source: Pruppacher and Klett, 1997))

Ice Habits
Ice habits can be very complex and depend on the temperature and ambient ice supersaturation at which ice nucleation takes place (Fig 142). The crystal shape has a strong impact on radiative properties (Macke et al., 1996) and the fall speeds of the ice particle.

Ice forms crystals having a hexagonal lattice structure, which in their full development would tend to form hexagonal prisms very similar to those sometimes seen in quartz. This does occasionally happen and depends on the ambient temperature and supersaturation. More commonly, crystals form in a flattened fractal-like hexagonal structure. Ice that grows under warmer conditions grow more slowly, resulting in smoother, less intricate shapes. A classification of ice shapes in shown in Figure 143.

4.11 Competition between ice nucleation mechanisms

Competition between ice nucleation mechanisms
At temperatures warmer than -40°C the only nucleation mechanism is heterogeneous. However at temperatures colder than this both heterogeneous and homogeneous nucleation can occur contemporaneously.

As many IN become active at ice supersaturations of 10 to 30%, well below the threshold range for homogeneous nucleation, then *heterogeneous* nucleation has the potential to be the dominant nucleation mechanism, *if and only if* IN are present in sufficient numbers to prevent the RH reaching the homogeneous nucleation threshold in a rising (cooling) parcel of air.

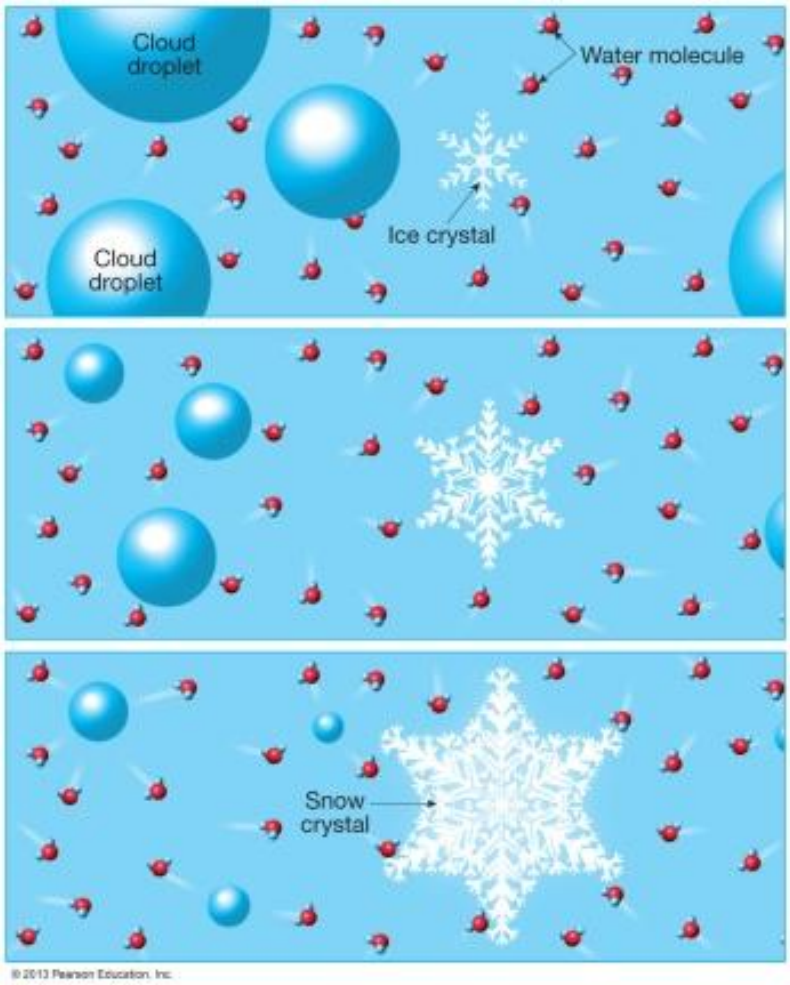

Figure 4.46: Schematic of Bergeron-Findeisen process (source Pearson Education Inc.)

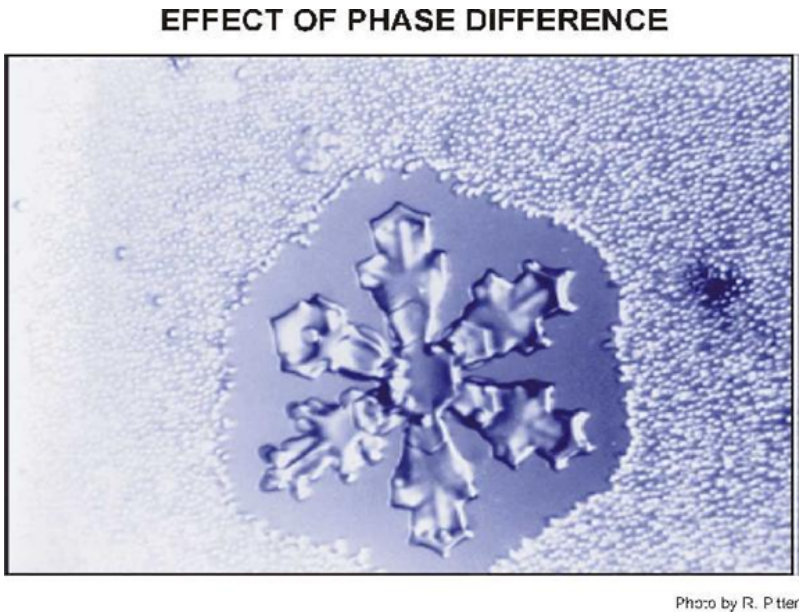

Figure 4.47: Photo of BF-Effect (source R. Potter from ?)

Q: Both mechanism create ice crystals, so why do we care which one dominates? Demott et al. (2003) (Fig. 144) documents the concentration of nucleated ice crystals as a function of

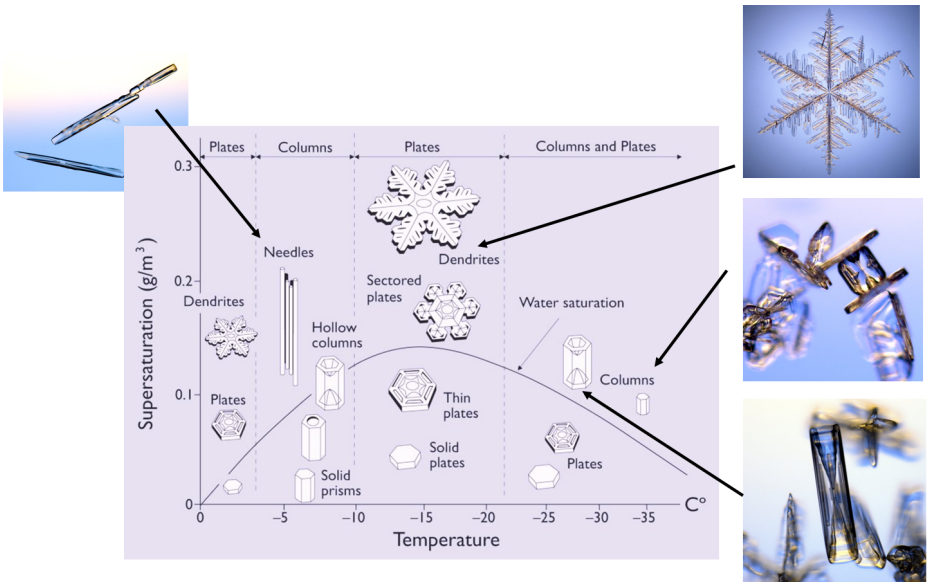

Figure 4.48: Ice crystal types as a function of S_i and T (source caltech.edu)

water saturation for air samples collected over the western United States. For $T > -35°$C the NC increases with supersaturation as more aerosols become active. However at cold temperatures there is a step jump close to water saturation to much higher concentrations due to homogeneous nucleation.. *Homogeneous nucleation thus has the potential to create a much higher concentration of cloud ice crystals - Q: Why?* The homogeneous nucleation process creates more ice particles since it is due to the freezing of aqueous solution droplets and thus related to the number of CCN. The particles nucleated by homogeneous process are much smaller in size therefore.

Whereas in warm clouds the droplet concentration was related directly to the CCN number, in ice clouds the relationship between IN and ice particle number concentration is more complicated and nonlinear, falling into two distinct regimes, illustrated schematically in Fig 145. The figure shows three cases of an lifted hypothetical parcel of air at cold temperature ($T < -40°$C). The left case is for a clean sample of air with no IN. The parcel rises until the RH attains the threshold for homogeneous nucleation, 160% in this example. Many ice particles ensue. These rapidly grow by depositional growth as the air is highly ice supersaturated and the water vapour content returns rapidly (in seconds to minutes) to the ice saturation vapour pressure.

The middle column shows a parcel of air with a low number of IN. These nucleate ice at lower supersaturation thresholds (say 30%) but the number is too small to "use up" (by deposition) much vapour and the homogeneous threshold is still reached. Nevertheless the "overshoot" over this threshold and number of aqueous particle formed will be less due to the take-up of vapour by the IN, and thus the final total number of ice crystals will be less. This also implies that the return of the vapour content to the ice saturation value will be slower.

Finally the right hand column shows air with a high enough content of IN such that the ice particles nucleated are sufficiently numerous to prevent the RH from even reaching the threshold for homogeneous nucleation and the latter mechanism is effectively inhibited. The final number of ice particles is orders of magnitude lower than in the clean air case and the return to ice saturation is much slower and may take on the order of an hour or longer.

After this point further increases of IN will increase the ice particle concentrations as in warm phase clouds, but always at much lower concentrations than produced by homogeneous nucleation.

The final number of ice crystals will be dependent on the both the IN concentration of the air and the updraught velocity of the air parcel. As in warm clouds, parcel models are used to study this, as in this example of Ren and Mackenzie (2005) in Fig.146. *In a weather or climate model, what are the issues involved in representing this relationship?* The following points should be noted about the parcel model results in Fig.146:

- The *overshoot* past S_{cr} for homogeneous nucleation determines the *number* of ice crystal

Figure 4.49: Ice crystal categorization (source caltech.edu)

nucleated.

- The overshoot has a timescale of seconds, and thus is not temporarily resolved by numerical models (parcel models use sub-second timesteps to resolve this),
- The overshoot depends on the updraught velocity and also the number of aerosols present and their own nucleation (S_{cr}) properties.
- A numerical model needs to be able to resolve the updraught velocity of the parcel *on the scale of the cloud*
- A numerical model needs to have accurate information concerning the aerosol quantities present.
- In many cases the diffusional growth timescale is also less than the timestep of a typical global model (O(1 hour)).

Another example of this work is Gierens (2003). To pick up on the point concerning the model vertical velocity, Fig. 147 gives typical PDFs observed and also modelled using a global model. It is seen that the coarse resolution of the model truncates the spectra and does not resolve the

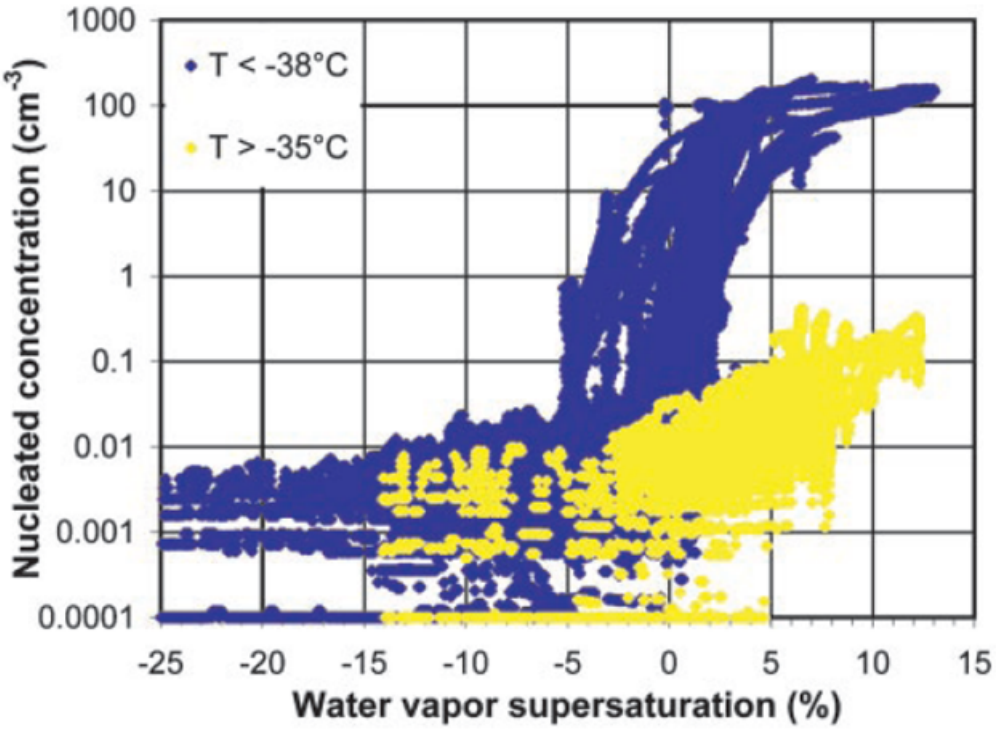

Figure 4.50: Nucleated ice crystal number in air samples as a function of water saturation at two temperatures. (source: Demott et al., 2003).

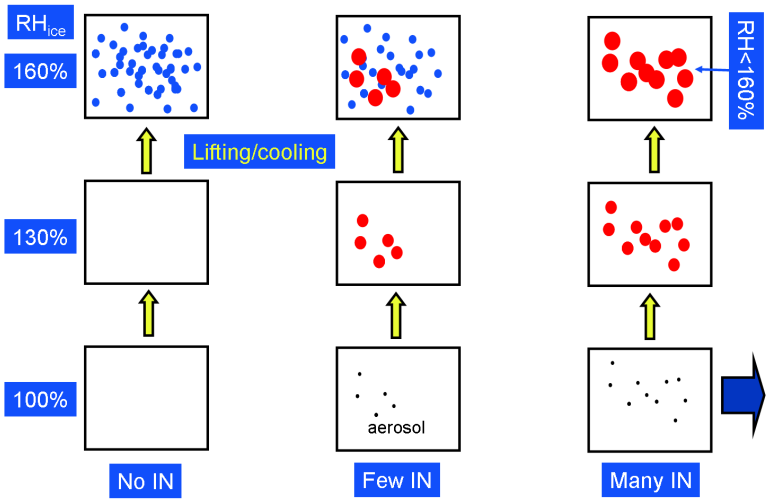

Figure 4.51: Schematic of homogeneous and heterogeneous nucleation competition, see text and lesson for details

highest velocities occurring on small spatial scales. Some success at reproducing the statistics of the vertical velocity spectrum is achieved with a simple parametrization.

In (Tompkins et al., 2007), I attempted to implement a modified cloud scheme into a weather forecast model that takes the zero-order effect of the elevated homogeneous nucleation threshold into account. The schematic in 148 shows the RH evolution of a air parcel undergoing homogeneous nucleation and model assumptions the dotted line add shows the assumptions made in many models (middle panel) and the new scheme (right). The new scheme allows the clear air to be supersaturated, but assumes that once ice crystals are nucleated they grow instantaneously by diffusion to return the vapour to ice saturation within a model timestep. The *zero order* effect of

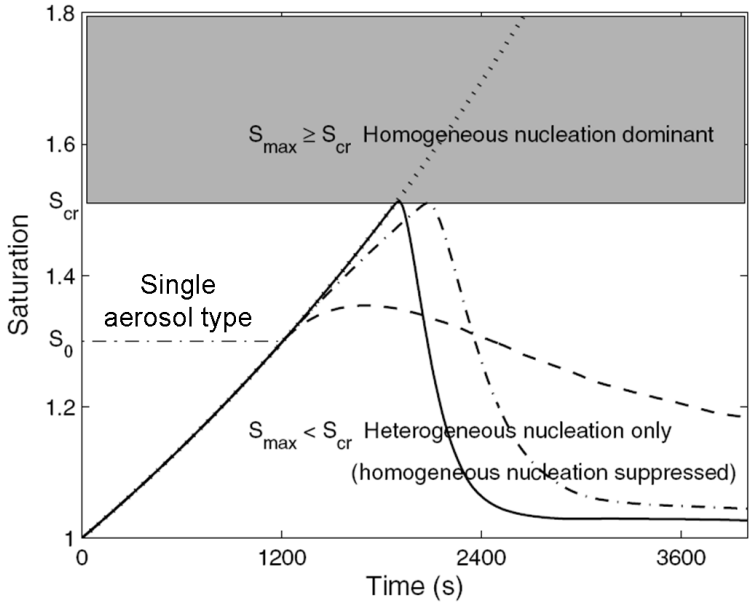

Figure 4.52: Results from parcel model of Ren and Mackenzie (2005) using a single aerosol type with a IN property threshold of $S = 1.3$

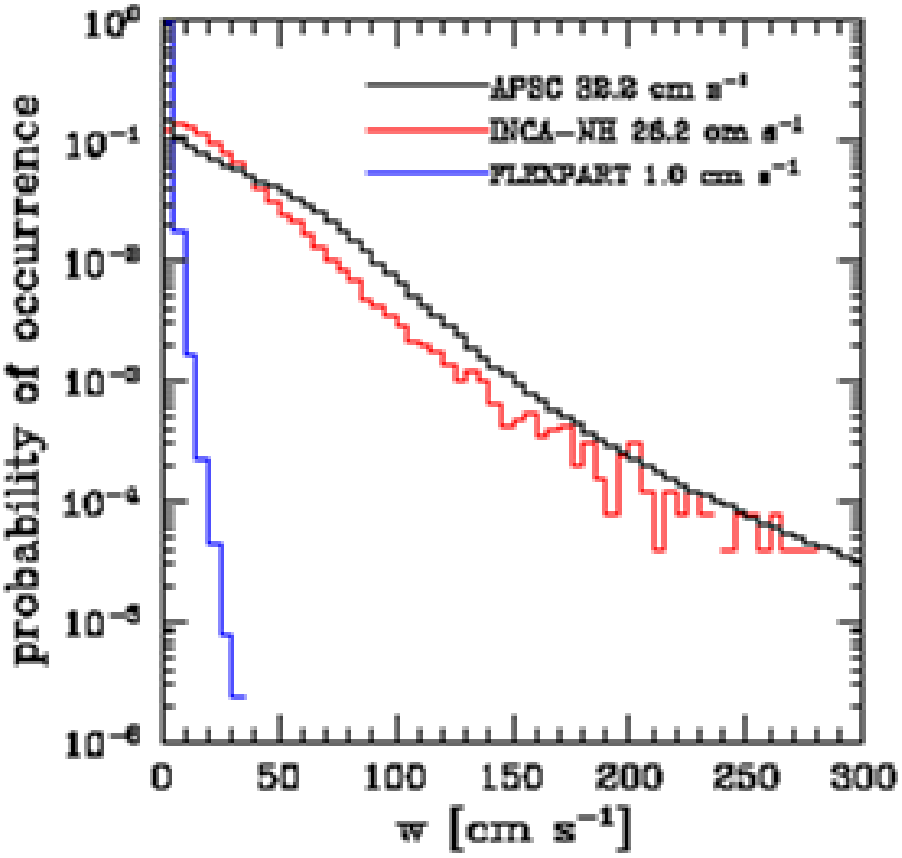

Figure 4.53: Results from Lohmann (citation needed) showing PDF of vertical velocity from (blue) a global model (red) aircraft observations and (black) model results corrected with a simple turbulence based parameterization for use in a ice-cloud model.

the ice nucleation threshold and *hysteresis* behaviour is captured.

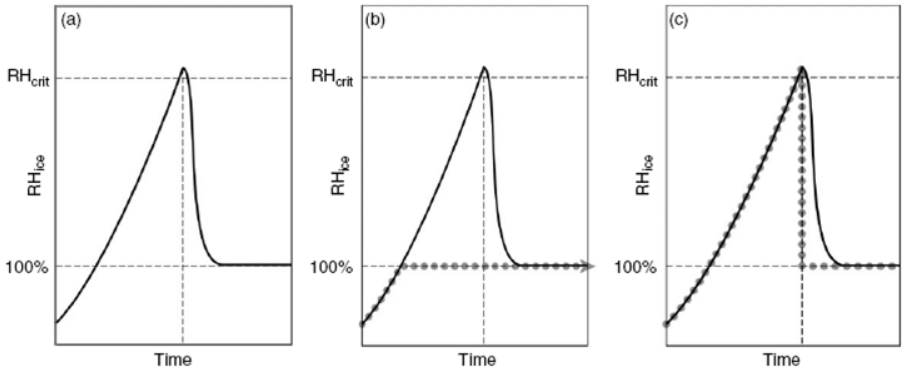

Figure 4.54: Schematic from Tompkins et al. (2007) showing (left) the RH evolution of a air parcel undergoing homogeneous nucleation and model assumptions.

Such a simple scheme is able to reproduce the distribution of frequency of occurrence of supersaturation from satellite retrievals and the PDF of RH from aircraft well (Fig. 149).

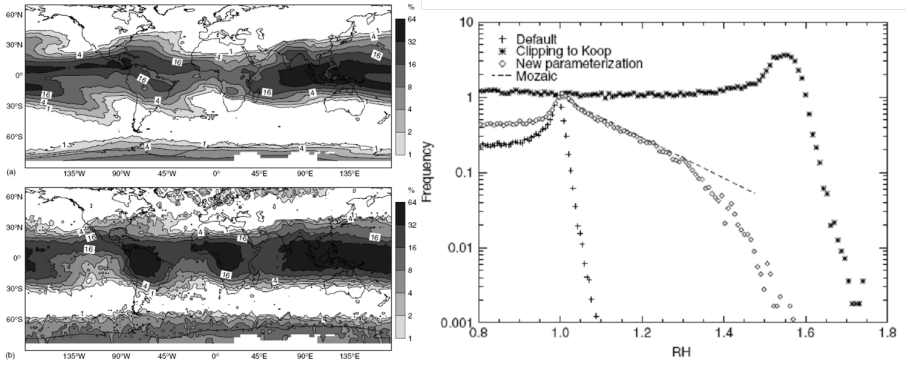

Figure 4.55: Results from Tompkins et al. (2007) showing (left) freq of occurrence of supersaturation compared to retrievals of Spichtinger et al. (2003) and (right) PDF of RH compared to Mozaic data of Gierens et al. (1999)

Some final thoughts

Errors in the map reflect errors in the convection occurrence in this version of the model known from other sources. We note

- that model error sources may be remote and are not easy to track down (cancellation of errors) and
- parametrization complexity does not need to exceed that necessary to represent the zero-order effect of the process, your knowledge of the process, or the complexity of the models' other components!

4.12 Aggregation

Aggregation

The ice particle that form from diffusional growth from an ice crystal are called *pristine*. However pristine ice particles can clump together to form *snowflakes* in a process known as *aggregation*.

At temperatures as low as 200K, the surface of ice is highly disordered and water-like. As the temperature approaches the freezing point, this region of disorder extends farther down from the surface and acts as a lubricant.

Thus the efficiency of the aggregation process increases as the temperature exceeds -5°C, when ice surfaces becomes *sticky*. There is also a secondary peak between -10°C and -16°C when dendrite arms get entangled. Figures 150 and 151 show example aggregates of bullet rosettes and other aggregates.

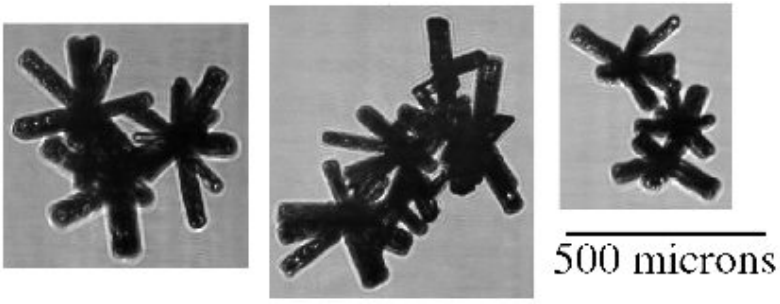

Figure 4.56: Bullet Rosette aggregates aggregates (source Dr. Chris Westbrook, Reading University, UK)

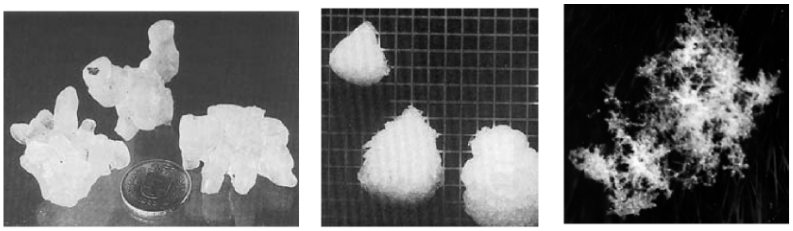

Figure 4.57: Other aggregate example (source Eszter Barthazy).

4.13 Riming

Riming to form graupel
If vapour exceeds the water saturation mixing ratio (in strong updraughts) then water can condense on ice crystals, and then subsequently freeze to form *graupel*, which are round ice crystals of higher densities.

Graupel and Hail are also formed by aggregating liquid drops in mixed phase clouds (see schematic in Fig. 152).

Some examples of lightly and heavily rimed ice are given in Fig. 153. If the latent heat of condensation and fusion keeps temperature close to 273K then high density *hail* particles can form, since the liquid water *"spreads out"* before freezing. Hail is dense and thus has high terminal velocities (up to 40 m/s) implying that it only forms in convection with strong updraught able to support the particle long enough for growth

4.14 Ice particle fall-speeds

The density and size of ice particles determines their respective fallspeeds and its dependence on particle radius (Fig. 154).

There are implications for numerical models that may become clear examining radar animations of cloud systems (see link). *can you think what these might be?*

4.15 Ice multiplication

Ice multiplication

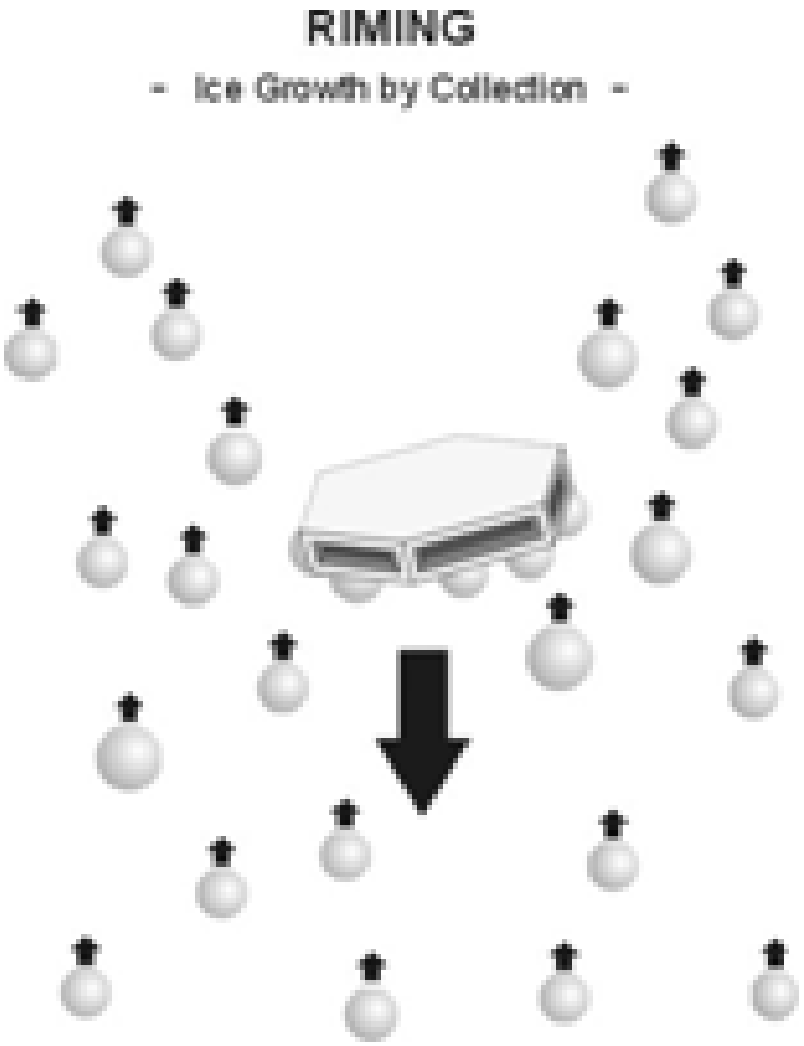

Figure 4.58: Schematic of riming process (source unknown)

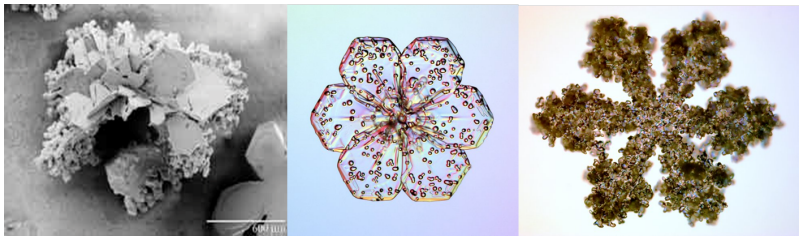

Figure 4.59: Photos of lightly and heavily rimed ice (source caltech.edu)

In recent years it has become increasingly evident that concentrations of ice crystals in "real" clouds are not always represented by the concentrations of IN measured or expected to be activated in such environments. In particular, it has been found that at temperatures warmer than -10°C the concentration of ice crystals can exceed the concentration of IN activated at cloud top temperature by as much as three or four orders of magnitude

There have been a number of hypotheses which have been advocated to explain such discrepancies. In particular, these hypotheses attempt to account for the unexpectedly high concentrations at warm temperatures. Some of the leading hypotheses are:

1. Fragmentation of large drops during freezing.
2. Mechanical fracture of fragile ice crystals (i.e., dendrites and needles) caused by collision of these crystals with graupel and other ice particles.

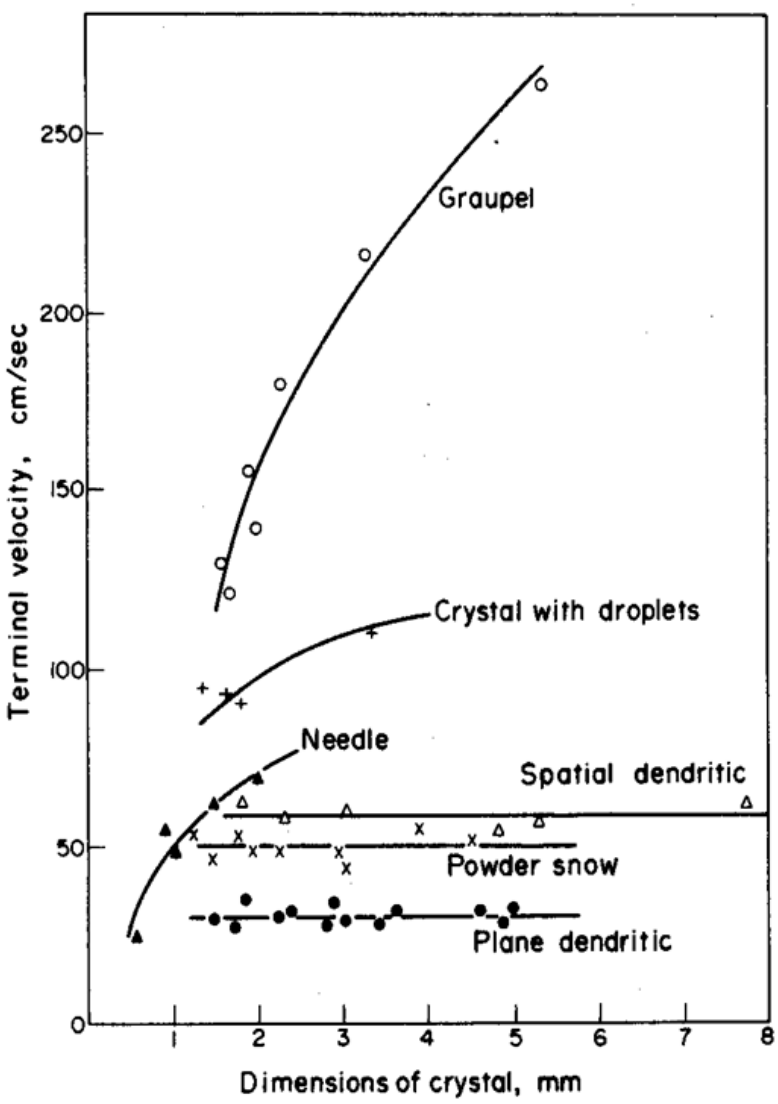

Figure 4.60: Fallspeeds of bulk ice particle categories (source: Rogers and Yau, 1989).

3. Splinter formation during riming of ice crystals.

4. Artificial measurement artifact of ice crystals shattering on impact with aircraft measurement device inlet.

Aircraft observations of ice in mid-level clouds observed in aircraft campaigns by Fleishauer et al. (2002) are shown in Fig. **??**. Although many models make simple assumptions such that ice particle size reduces with temperature, it is seen that this is not necessarily valid in clouds with strong mixing. The small particles may only appear circular due to instrument resolution limitations.

Snowflake size distributions

Most of the ice precipitation that reaches the ground does so as snowflakes and not pristine ice crystals.

Since snowflakes are irregular aggregates of crystals there is no simple way to measure their dimensions, thus they are usually measured in terms of their mass or, equivalently, the diameter of the water drop that would form from their melting.

Gunn and Marshall (1958) found that the exponential approximation still fits the snowflake diameter well with the following parameters:

$$-\Lambda(R) = 25.5R^{-0.48}, \tag{4.36}$$

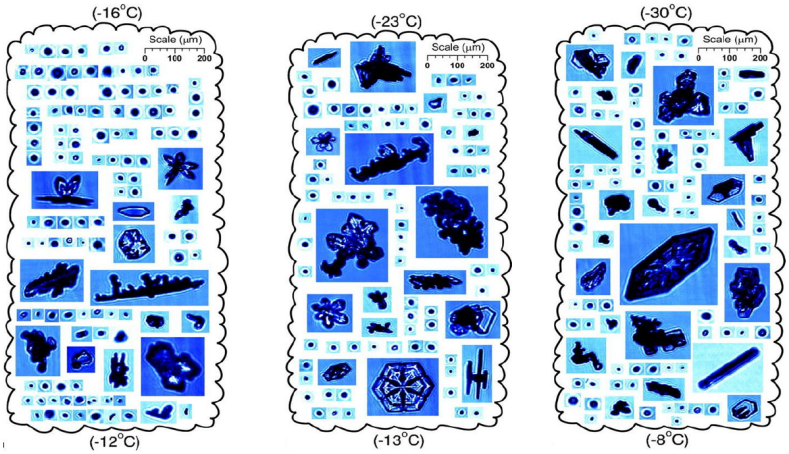

Figure 4.61: Example ice crystals from aircraft observations in mid-level cloud systems by Fleishauer et al. 2002 Fleishauer et al. (2002).

and

$$N_0 = 3.8 \times 10^{-2} R^{-0.87} \tag{4.37}$$

where the units of R and *Lambda* are mm hour^{-1} and cm^{-1} (Fig 155). To summarize, the key

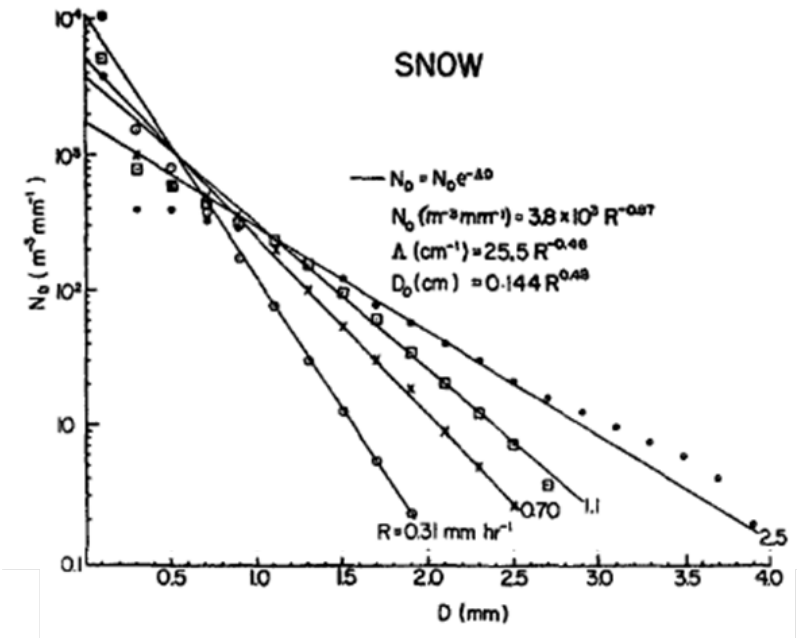

Figure 4.62: Snow flake size distributions (from Gunn and Marshall, 1958)

growth mechanisms are summarized in Fig. 156. and the location of some of these key processes in a typical deep convective cloud are given in Fig. 157.

Reminder Questions

- explain at the board what it means for an aqueous aerosol solution droplet to become "activated".
- What are the main mechanisms of ice nucleation that are relevant for ice cloud formation?
- How is a cloud called that consists only of ice, and one which consists of both liquid and ice? In roughly which temperature regimes does each cloud type exist? In the mixed phase explain what the Bergeron-Findeisen effect is for ice growth

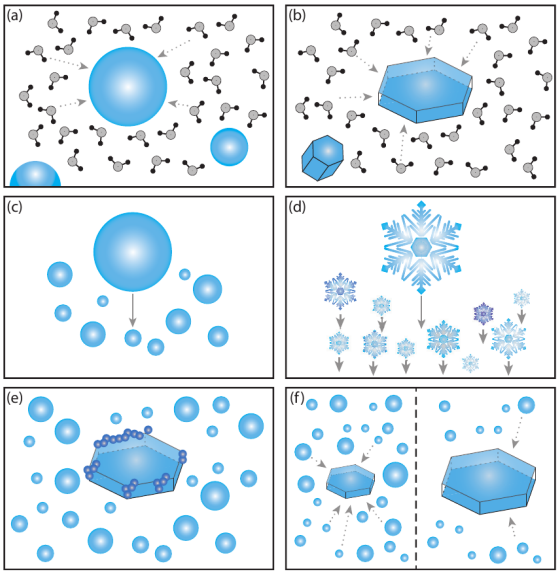

Figure 4.63: Crystal growth processes (a) condensation (b)deposition (c)collision-coalescence, (d) aggregation, (e) riming, (f) Bergeron-Findeisen process. (from Lohmann, U.)

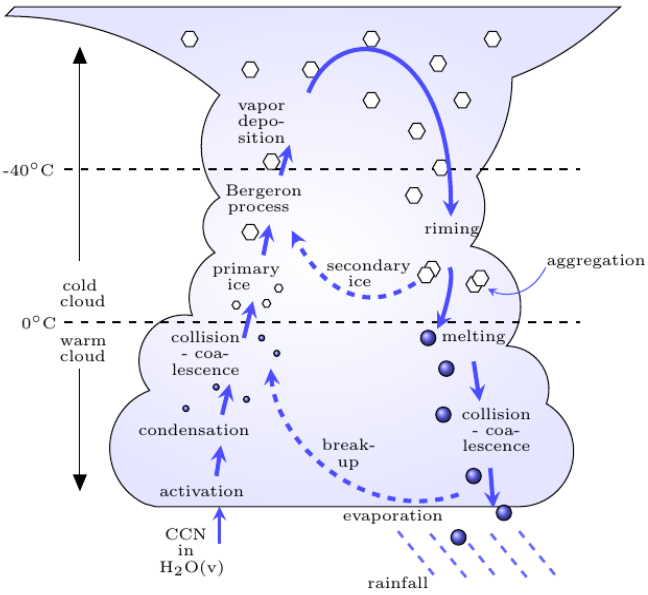

Figure 4.64: microphysical processes in a deep convective cloud (from Lohmann, U.)

- Explain why we can find air that is supersaturated with respect to ice but not with respect to liquid water? What kind of cloud is an indication of supersaturated layers?
- Does the liquid cloud droplet radius increase or decrease with CCN number? Assuming that in a forming cloud, condensing liquid water is equally distributed among CCN, write down the relationship between droplet radius and cloud liquid water density in kgm^{-3}
- Does the ice crystal radius increase or decrease with ice nuclei (IN) number? What is a common source of IN?
- What are the two main mechanisms by which activated aerosols grow into raindrops, and under which droplet size radius do they operate and why? We made a number of approximations in our mathematical descriptions of the two processes, can you name some?

- What factor directly determines the number of ice crystals nucleated by each homogeneous nucleation, and what is this dependent on in turn?

Chapter 5

Radiation

Radiative processes

The sun (Fig. 158) is the fundamental energy source of the planet, and the uneven adsorption of solar radiation leads to the large-scale weather patterns that redistribute heat. Perturbations to radiative processes are responsible for climate variability through the greenhouse effect, volcanic eruptions and solar variability. Understanding radiative processes is also important for remote sensing of the atmosphere.

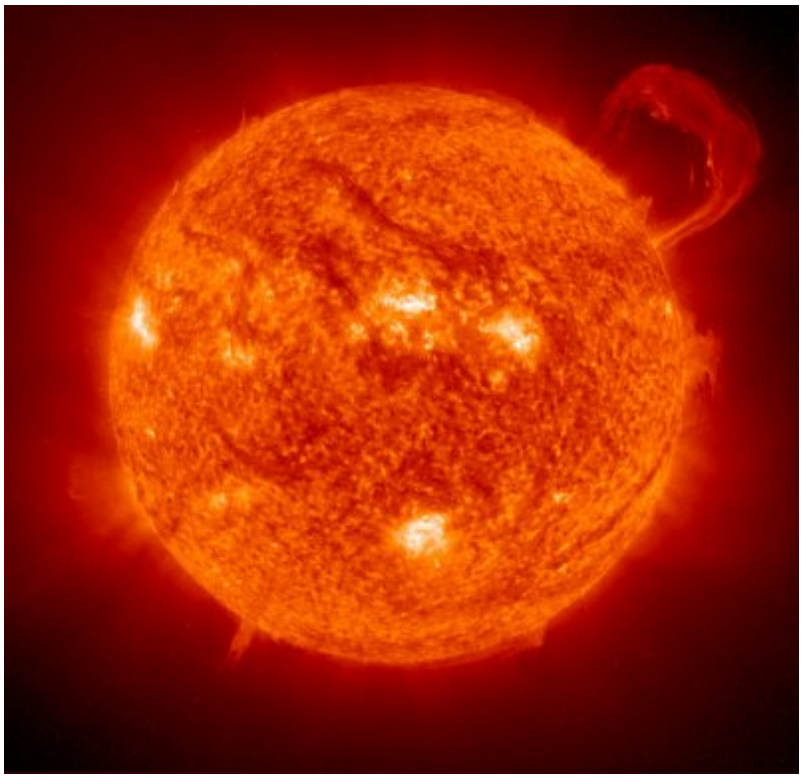

Figure 5.1: The sun! (http://z.about.com)

5.1 Definitions of the radiative field

Electromagnetic radiation

Electromagnetic radiation (EMR) can be considered as an ensemble of waves propagating at the speed of light, but also as photon particles travelling through space. The EMR wave has both electric and magnetic field components and carry energy. EMR is created from other types of energy, and converted to other types of energy when destroyed, usually when interacting with

matter. For example, the vibrational and rotational kinetic energy of molecules can be converted into EMR by the emission of a photon, or can increase by the absorption of a photon.

As with other waves, we describe EMR in terms of its frequency and wavelength.

Electromagnetic spectrum
The electromagnetic (EM) spectrum is the range of all possible electromagnetic radiation frequencies. The "electromagnetic spectrum" of an object is the characteristic distribution of electromagnetic radiation from that particular object.

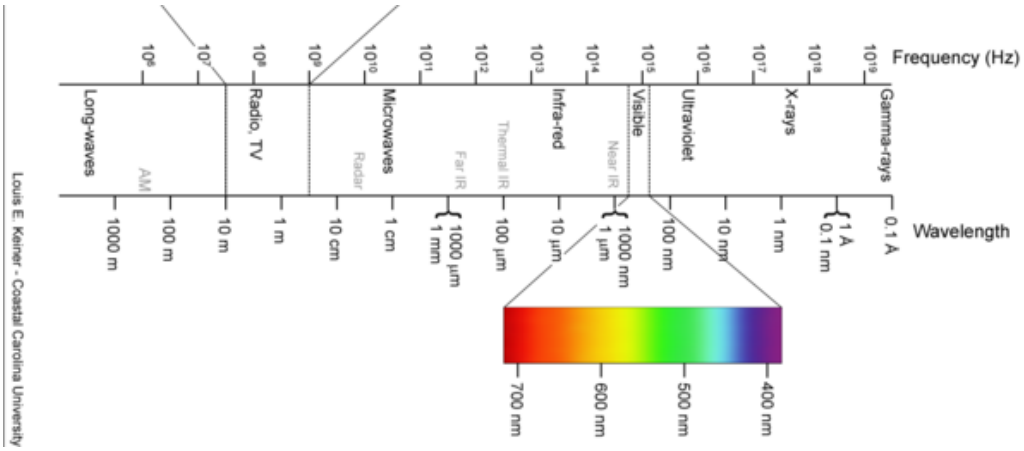

Figure 5.2: Electromagnetic spectrum with visible bands highlighted (source see caption).

Bands that are important for atmospheric radiative processes are the ultraviolet, visible (400 to 700nm), near/thermal infra-red (Fig. 159).

Electro-magnetic wave
Electro-magnetic waves have a speed of $c = 3 \times 10^8$ m/s, (Fig. 160) with speed, frequency ν and wavelength λ related by

$$c = \nu\lambda \tag{5.1}$$

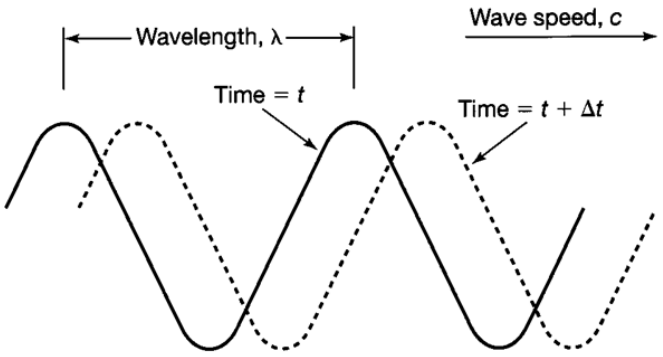

Figure 5.3: Propagating electromagnetic wave.

The Earth with radius[1] r_e orbits the sun (r_s) at a radius of r_d and intercepts a tiny fraction of the emitted energy (see sketch in Fig. 161). We assume that the sun emits as a *black body*.

Black Body
A black body is an object that completely absorbs all incident electromagnetic radiation. No electromagnetic radiation passes through it and none is reflected. It is also a perfect emitter of radiation.

[1]In the radiation section r is used for radius, not to be confused with mixing ratio! Other duplications of notation will also occur.

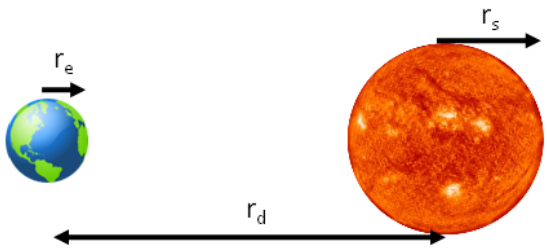

Figure 5.4: Schematic of sun earth system.

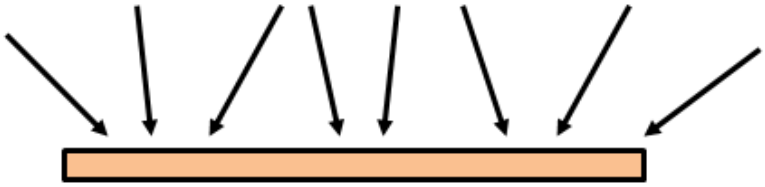

Figure 5.5: Sketch of radiation incident on a flat flat.

Irradiance and Radiant Emittance E

Irradiance and *radiant emittance* are radiometry terms for the power of electromagnetic radiation arriving or leaving a flat-plate surface, per unit area, integrated over the *hemisphere* above the plate (Fig. 162). *Irradiance* is used when the electromagnetic radiation is incident on the surface while *radiant emittance* is used when the radiation is emerging from the surface.

The total energy per unit time is called the *radiant flux* and has units of J s^{-1} or W. As the irradiance and radiant emittance are measured per unit area they have units W m^{-2}. Note that *there is nothing in the definition of irradiance that tells us from which direction the radiation arrives or is emitted* (Fig. 163), so we therefore introduce the *solid angle*.

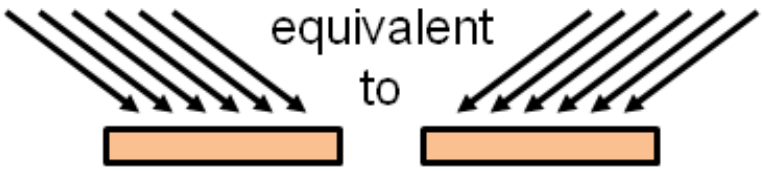

Figure 5.6: Sketch showing how the irradiance can be equivalent with the radiation arriving from two different directions.

Solid Angle Ω

The solid angle, Ω is the angle in three-dimensional space that an object subtends at a point. It is a measure of how big that object appears to an observer looking from that point. The solid angle is proportional to the surface area, A, of a projection of that object onto a sphere centered at that point, and inversely proportional to the square of the sphere's radius, r (Fig. 164).

We define the solid angle

$$\Omega = \frac{A}{r^2} \tag{5.2}$$

and it has units of *steradians* or *ster*. An important special case for radiation is the integration over a hemisphere of unit radius in spherical coordinates (Fig. 165).

$$\int_{\text{hemisphere}} d\Omega = \int_0^{2\pi} \int_0^{\frac{\pi}{2}} \sin\theta d\theta d\phi = 2\pi \quad \text{ster} \tag{5.3}$$

The angle to the zenith is defined by θ, with $\theta = 0$ marking the vertical axis normal to the surface. The

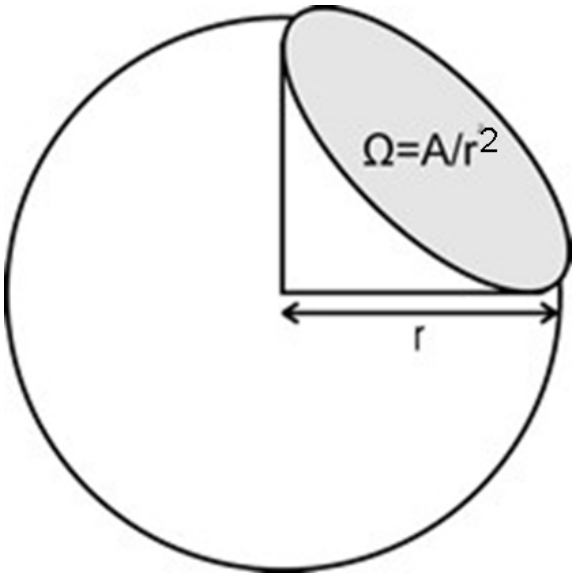

Figure 5.7: Definition of the solid angle.

azimuth angle is defined by ϕ. We integrate elements of solid angle $d\Omega$ over concentric circles starting in the horizontal direction. The radius of the circle element of width $d\theta$ from the vertical axis is $r\sin\theta = \sin\theta$. Thus the azimuth dimension of the solid angle element $d\Omega$ is $\sin\theta d\phi$. The vertical dimension of $d\Omega$ is $d\theta$.

Radiance

The *radiance* tells us the radiant flux density per unit *solid angle* coming from a direction (θ, ϕ). For a surface area of ΔA_{norm} *normal* to the direction (θ, ϕ), the radiant flux received from the solid angle $\Delta\Omega$ will be $L(\theta, \phi)\Delta\Omega\Delta A_{\text{norm}}$ (Fig. 166).

$L(\theta, \phi)$ is the *radiance* with units W m^{-2} ster^{-1}

However, in general the receiving surface *will not be normal to* θ, ϕ. If we take the special case where the receiving surface of dimension ΔA is *horizontal*, then the projection of this area on to the surface normal to direction (θ, ϕ) is given by $\Delta A_{\text{norm}} = \Delta A\cos\theta$ (Fig. 167).

Thus in general the contribution to the radiant flux incident on a horizontal surface is given by: $L(\theta, \phi)\Delta\Omega\Delta A\cos\theta$. If we take $\Delta A = 1$ for a unit area, then the radiant flux per unit area from solid angle (i.e. the contribution to the *irradiance* from that solid angle) is $L(\theta, \phi)\cos\theta\Delta\Omega$ with units W m^{-2}. From now on we will assume the (θ, ϕ) angle dependence and simply write L for radiance. With remote sensing we need a device capable of measuring radiation from different directions with very small solid angles to achieve the best resolution possible (Fig. 168).

Irradiance E Definition

We are now able to return to the concept of *irradiance*, which is the total radiance integrated over all solid angles over a hemisphere.

Thus

$$E = \int_{\text{hemisphere}} L\cos\theta d\Omega = \int_0^{2\pi}\int_0^{\frac{\pi}{2}} L\cos\theta\sin\theta d\theta d\phi \tag{5.4}$$

Isotropic radiation

An important special case is *isotropic radiation*, namely that the radiative flux has the same intensity regardless of the direction, and thus L is independent of direction. *Q: can you think of some examples?* Examples include:

- Emission from a black body.
- Solar radiation beneath a cloud of moderate thickness due to multiple scattering of photons.
- Background microwave radiation from big bang.

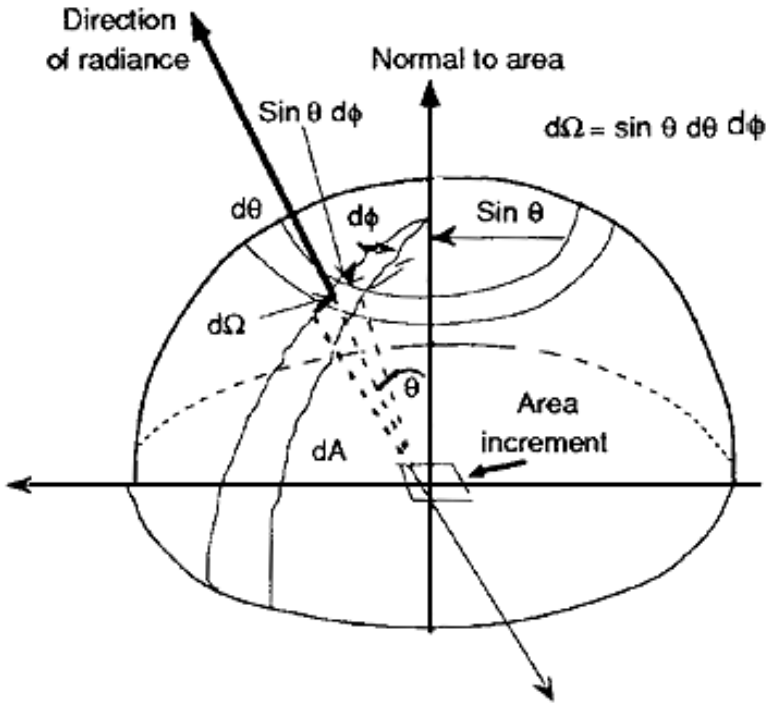

Figure 5.8: Integration of solid angle over a hemisphere

In this case we may write

$$E = L \int_0^{2\pi} \int_0^{\frac{\pi}{2}} \cos\theta \sin\theta d\theta d\phi = \pi L \tag{5.5}$$

Exercise: show! Q: What are the units of π in (164)? The units of π are steradians.

Planck Function

Experiments lead to the derivation of Planck's law, which describes the spectral radiance of electromagnetic radiation at all wavelengths from a black body at temperature T. The *Planck Function* giving the radiance for wavelength λ as a function of T is:

$$L_\lambda(T) = \frac{2hc^2}{\lambda^5(e^{\frac{ch}{k\lambda T}} - 1)} \tag{5.6}$$

where h=6.63e^{-34} J s is the Planck constant and k=1.38e^{-23} J K^{-1} is the Boltzmann constant. The emitted power per unit area of emitting surface, per unit solid angle, and per unit wavelength.

We can derive the frequency form of the Planck function. The change in the Planck function for a finite change in wavelength $d\lambda$ is equal to the change for an equivalent change in frequency $d\nu$:

$$L_\lambda(T)d\lambda = -L_\nu(T)d\nu, \tag{5.7}$$

with the minus sign indicating that an increase in wavelength corresponds to a decrease in frequency. Using the chainlaw on eqn. 160 we find that $\frac{d\lambda}{d\nu} = \frac{-c}{\nu^2}$, substituted into eqn. 165 and using again eqn. 160 gives:

$$L_\nu(T) = \frac{2h\nu^3}{c^2(e^{\frac{h\nu}{kT}} - 1)} \tag{5.8}$$

At room temperature, black bodies emit mostly infrared light ($\lambda > 4\mu$m), but as the temperature increases past a few hundred degrees Celsius, black bodies start to emit visible wavelengths, from red, through orange, yellow, and white before ending up at blue, beyond which the emission includes increasing amounts of ultraviolet (e.g. Fig. 169). Examples of the Planck function for temperatures between 200 to 300 K are given in Fig. 170.

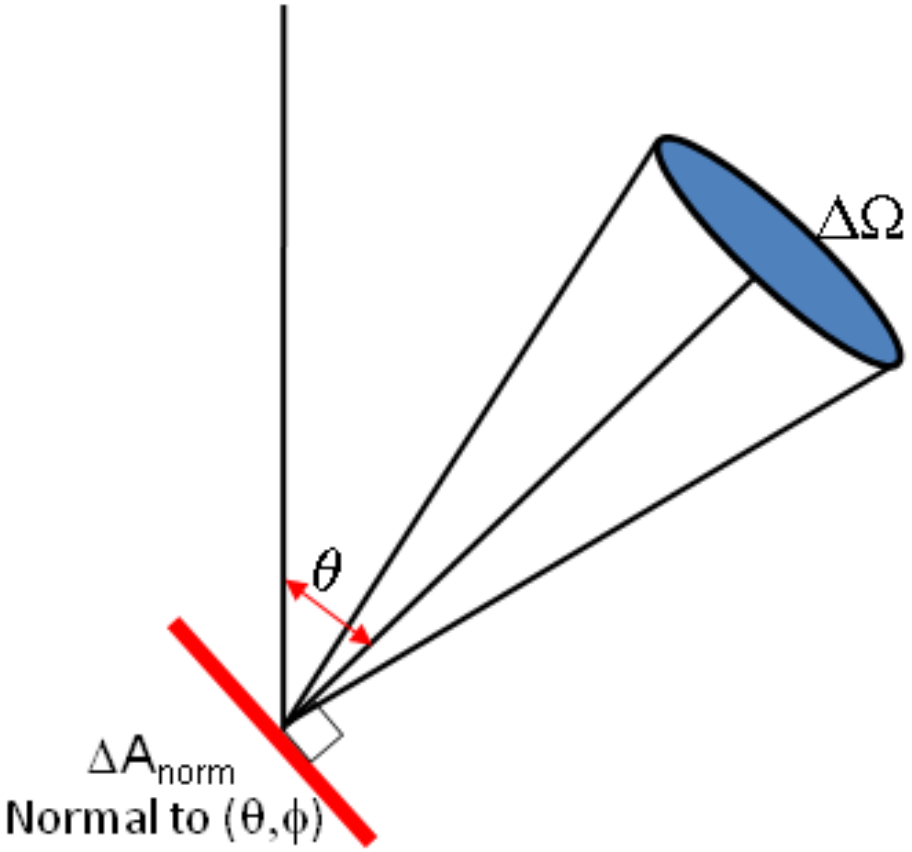

Figure 5.9: Definition of radiance sketch.

Note how the peak in Fig. 170 moves to shorter wavelengths as the temperature increases. The position of the peak as a function of wavelength can be found solving $dL_\lambda/d\lambda = 0$. From eqn. 165 we see

$$dL_\lambda/d\lambda = \frac{-hc^2\left(\lambda^5 e^{\frac{hc}{k\lambda T}}\frac{-hckT}{(k\lambda T)^2} + (e^{\frac{hc}{k\lambda T}}-1)5\lambda^4\right)}{\lambda^{10}(e^{\frac{hc}{k\lambda T}}-1)^2} = 0 \tag{5.9}$$

and with some cancellation and simplification we get

$$-e^{\frac{hc}{k\lambda T}}\frac{hc}{k\lambda T} + (e^{\frac{hc}{k\lambda T}}-1)5 = 0 \tag{5.10}$$

We now substitute $x = \frac{hc}{k\lambda T}$ to get:

$$5(e^x - 1) - xe^x = 0. \tag{5.11}$$

This has to be solved numerically, which results in the solution x=4.965, and thus $\lambda_{max} = \frac{hc}{kxT}$. Inserting the values of h,c,k and x we get

Wien's Displacement Law

The relationship describing the wavelength at which emission is at a maximum is

$$\lambda_{\max} = \frac{2897\mu\mathrm{K}}{T} \tag{5.12}$$

Integrating eqn.(165) across all wavelengths gives the total emitted energy per unit area *per unit solid angle*, in other words the radiance L. Thus

$$L \equiv \int_0^\infty L_\lambda d\lambda = \int_0^\infty \frac{2hc^2}{\lambda^5(e^{\frac{ch}{k\lambda T}}-1)}d\lambda. \tag{5.13}$$

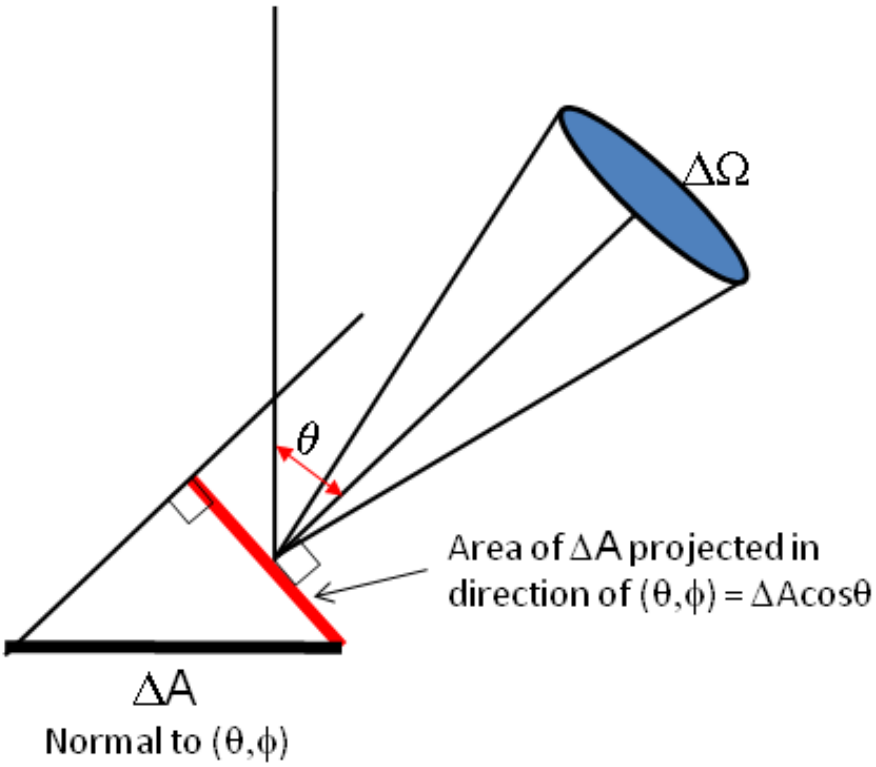

Figure 5.10: Definition of radiance sketch.

We again make the substitution of $x = \frac{hc}{k\lambda T}$, implying $dx = \frac{-hc}{k\lambda^2 T} d\lambda$, to get

$$L = \frac{-2hc^2 kT}{hc} \left(\frac{kT}{hc}\right)^3 \int_{\infty}^{0} \frac{x^3}{(e^x - 1)} dx, \tag{5.14}$$

which simplifies to (dropping minus as we reverse the integration limits)

$$L = \frac{2(kT)^4}{h^3 c^2} \int_0^{\infty} \frac{x^3}{(e^x - 1)} dx \tag{5.15}$$

Using the solution $\int_0^{\infty} \frac{x^3}{(e^x - 1)} dx = \frac{\pi^4}{15}$ we get

$$L = \frac{2\pi^4 (kT)^4}{15 h^3 c^2} \tag{5.16}$$

We now want to integrate L over the hemisphere to give us the total radiant emittance E from a unit area flat plate over all wavelengths. We calculated this in the derivation of eqn.164 which tells us in the case of isotropic blackbody radiation $E = \pi L$. Thus we derive the

Stephan-Boltzmann Law

$$E = \frac{2\pi^5 k^4}{15 h^3 c^2} T^4 = \sigma T^4 \tag{5.17}$$

where σ is the Stefan Boltzmann constant:

$$\sigma = \frac{2\pi^5 k^4}{15 h^3 c^2} = 5.67 \times 10^{-8} W m^{-2} K^{-4} \tag{5.18}$$

Grey Bodies and Kirchoff's Law

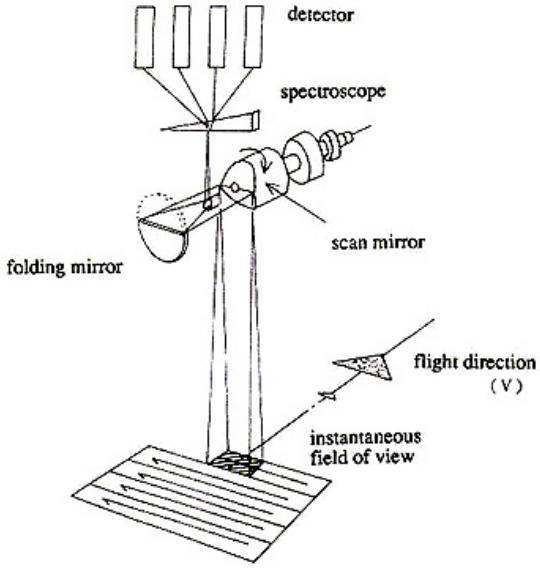

Figure 5.11: Schematic of why small solid angles measurements are required for remote sensing (source NASA website).

Figure 5.12: The colours indicate the temperature of the emitting body

A grey body emittance is one which emits radiation according to

$$E_{\text{grey}} = \epsilon \sigma T^4, \tag{5.19}$$

where ϵ is the fractional emittance ($\epsilon \leq 1$).

Kirchoff's Law states that, if *at a given wavelength* we know how good an emitter a body is, then we also know how good an absorber it is. Kirchoff's Law specifies:

- Absorptance $a = \epsilon$
- Transmittance $\tau = 1 - \epsilon$

5.2 Energy balance models of the atmosphere

Energy balance models of the atmosphere

We are now in a position to construct a simple energy balance model of the earth-atmosphere system. If the sun is considered to be a black body (a good approximation) then its emittance is given by σT_{sun}^4 where T_{sun} is the surface temperature of the sun. This is emitted over a surface area of $4\pi r_s^2$ giving a total energy of $4\pi r_s^2 \sigma T_{\text{sun}}^4$.

The energy of the sun is spread over the surface of a sphere of area $4\pi r_d^2$ at a distance of r_d, known as the inverse square law (Fig. 171). The *irradiance* E (W m^{-2}) at a distance r_d is thus

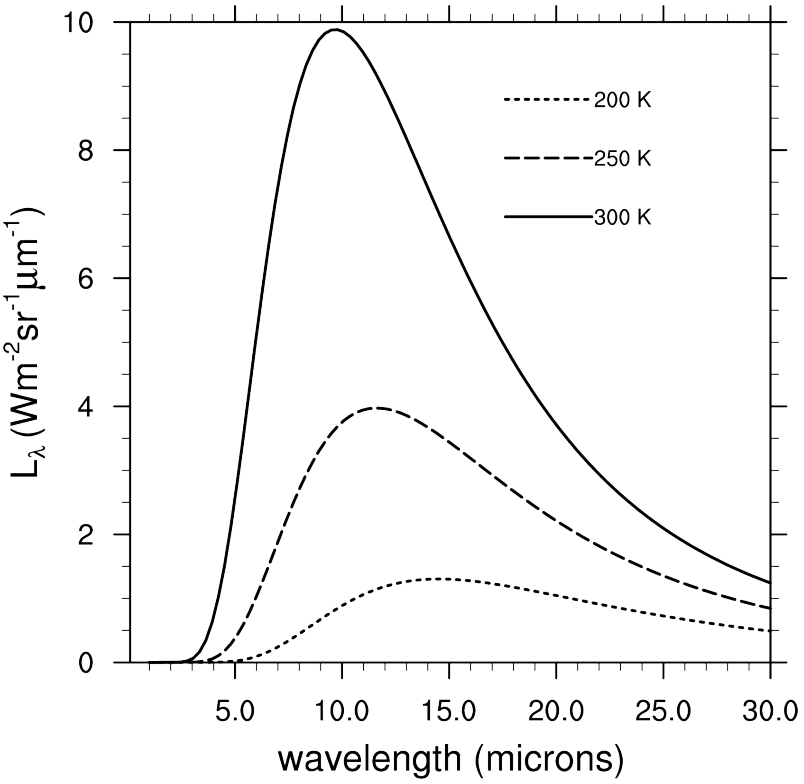

Figure 5.13: Black body emission at three tropospheric temperatures.

$$E = \sigma T_{\text{sun}}^4 \left(\frac{r_s}{r_d}\right)^2. \tag{5.20}$$

If r_d corresponds to the distance of separation between the earth and the sun, then we define $S_0 \equiv E$, called the *solar constant*.

Solar Constant S_0

S_0, the average irradiance at the top of the earth's atmosphere, is known as the *Solar Constant*. Measurements from satellites show that $S_0 \simeq 1370$ W m^{-2}. The value varies by ≈ 1 W m^{-2} over a solar cycle that has an average length of 11 years.

Knowing the solar constant we can invert (179) to get the surface temperature of the sun:

$$T_{\text{sun}} = \sqrt[4]{\left(\frac{r_d}{r_s}\right)^2 \frac{S_0}{\sigma}} \tag{5.21}$$

giving T_{sun} as 5800K. The energy intercepted by the earth is (Fig.172) $S_0 \pi r_e^2$, so that E_e, the average incident solar radiation on the earth's surface, which has a surface area of $4\pi r_e^2$, is

$$E_e = \frac{S_0 \pi r_e^2}{4\pi r_e^2} = \frac{S_0}{4} \tag{5.22}$$

which has a value of 340 W m^{-2}.

Planetary Albedo

A proportion of this radiation is scattered back to space by clouds, atmospheric gases and the planet's surface. We thus introduce the parameter α_p as the *planetary albedo*. Which is defined as

$$\alpha_p = \frac{\text{Reflected solar irradiance (at top of atmosphere)}}{\text{Incident solar irradiance}} \tag{5.23}$$

Observations from Satellites put the earth albedo at $\alpha_p \simeq 0.3$. Thus the average irradiance absorbed is $\frac{S_0}{4}(1 - \alpha_p)$ which is 240 W m^{-2}.

Effective Emitting temperature of the Earth

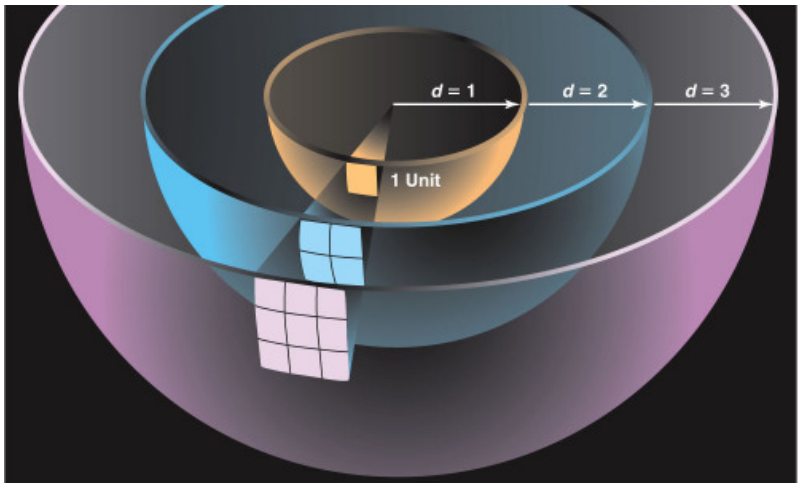

Figure 5.14: Inverse square law. source: http://jersey.uoregon.edu/ imamura/122/lecture-1/lecture-1.html

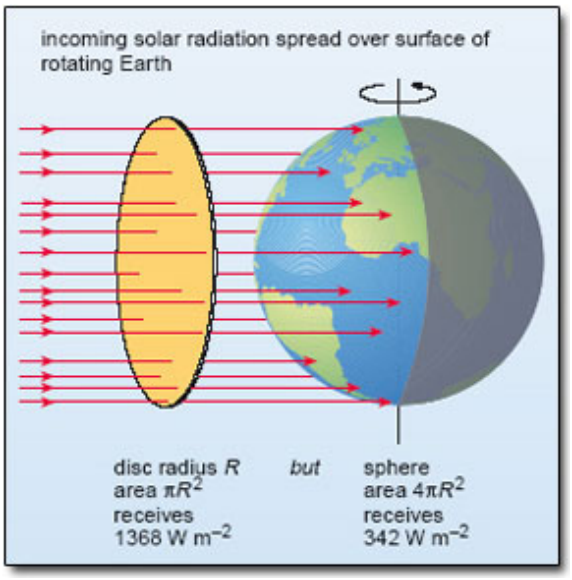

Figure 5.15: Shadow area of earth

The Earth/atmosphere system is assumed to emit to space as a black body at some effective temperature T_e. Thus the rate of emission is $4\pi r_e^2 \sigma T_e^4$. We will assume that there is a *long term balance* (i.e. an equilibrium) between absorbed solar and emitted infrared radiation on an earth:

$$S_0 \pi r_e^2 (1 - \alpha_p) = 4\pi r_e^2 \sigma T_e^4 \tag{5.24}$$

Thus

$$T_e = \sqrt[4]{\frac{S_0}{4\sigma}(1 - \alpha_p)} = 255\text{K} \tag{5.25}$$

Neglecting this albedo issue, we have two contrasting temperature of the sun (5800K) and the earth (255K). This is important since the peak wavelengths (λ) at which energy is emitted is a function of temperature. The Planck function L_λ is shown graphically for the sun and earth effective emitting temperatures in Fig. 173. It should be pointed out the solar radiation energy is *not* restricted to the visible (0.4 to 0.7 μm), rather 35% of the solar energy received at the earth is in this band, with 50% in the *near-infrared* and 15% in the *ultra-violet*.

Comparing the normalized curves for L_λ, depicted in Fig. 174, it is also clear that the result of the different emitting temperatures is that the radiation from the sun and earth are in *distinct wavelength regions* with little overlap. We found that $T_e = 255$ K and yet surface measurements

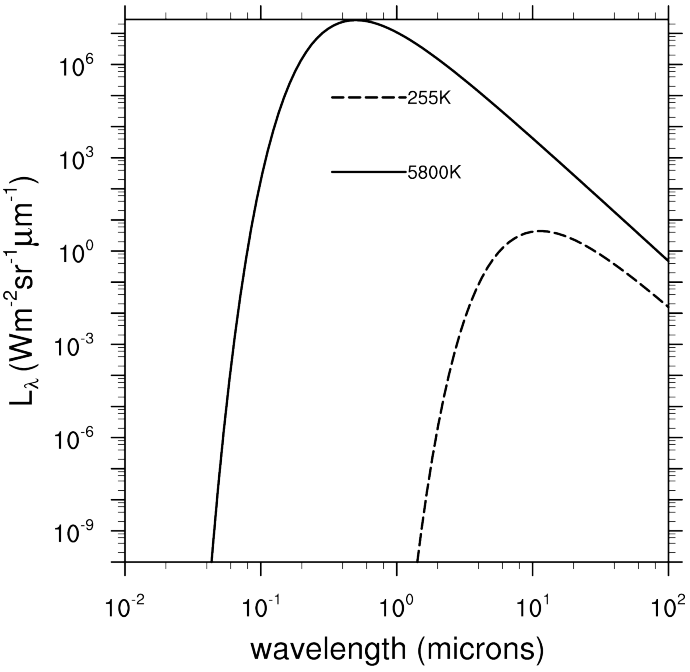

Figure 5.16: Planck function for sun and earth's effective emitted temperatures of 5800K and 255K, respectively.

indicate an average global temperature of roughly 288K. *Q: Why are these so different?* These are different because T_e is the effective emitting temperature of the *whole earth-atmosphere system*, this is *not* the same as the surface temperature. Some gases in the atmosphere are not transparent to infrared radiation emitted by earth, thus warming the surface relative to T_e in a process known as the *greenhouse effect*.

5.3 Sun and Earth Geometry

In the previous section we constructed a simple slab-atmosphere radiative balance model. We now briefly discuss the sun-earth geometry in more detail as this determines the insolation of the earth by the sun and the sun position in the sky needed for radiative transfer calculations.

Sun-Earth Geometry
The sun-earth geometry is shown in Fig.175. Note the

1. Declination angle of the earth ϑ
2. Eccentricity of the earth's orbit

Declination Angle ϑ

- $\vartheta = +23.5°$: at the summer solstice June 21st
- $\vartheta =$ -23.5° : at the winter solstice December 21st
- $\vartheta = 0°$: at the spring and Autumn Equinoxes

Eccentricity of orbit
The Earth's orbit is slightly elliptical with an *eccentricity factor* of $e = 0.0167$. Since the average sun-earth separation is $r_d = 149.6 \times 10^6$km, we can calculate:

- The *Perihelion* (distance of closest approach) is $r_d(1-e) = 147.1 \times 10^6$km.
- Thus the *Aphelion* (distance of furthest approach) is $r_d(1+e) = 152.1 \times 10^6$km.

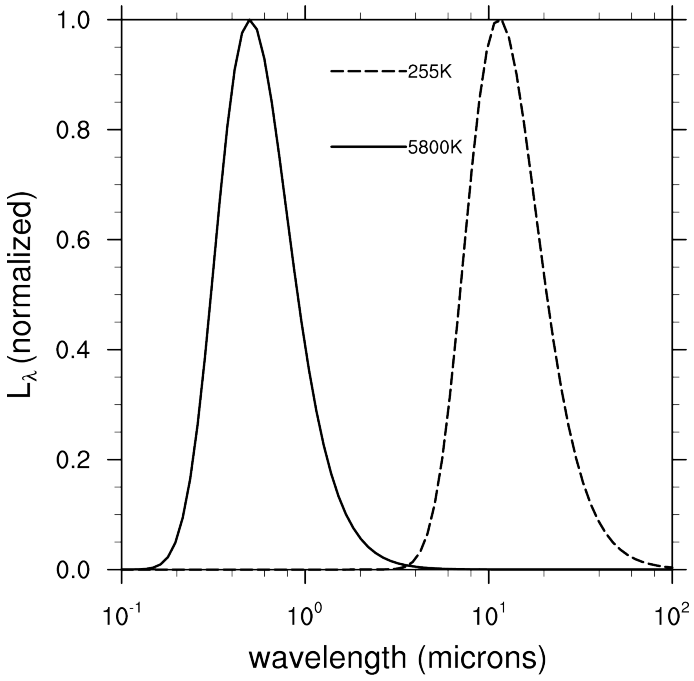

Figure 5.17: As Fig. 173 but normalised and plotted with a linear y-scale.

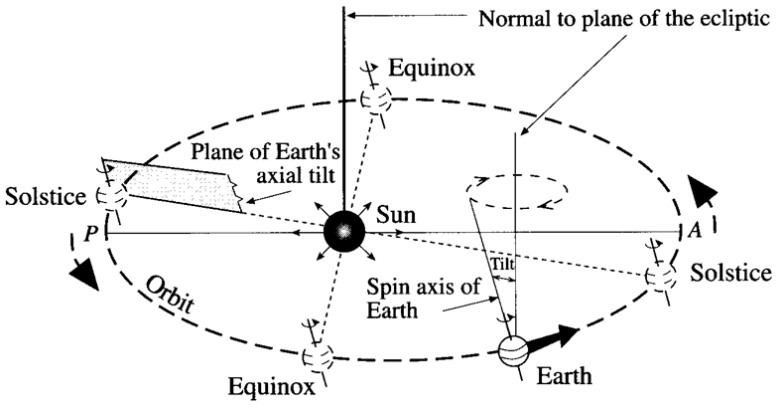

Figure 5.18: B

Presently, the Perihelion occurs on January 3rd while the Aphelion July 4th, but the closeness of these dates to the solstices is a present-day coincidence.

Solar Zenith Angle

The solar zenith angle (θ) is a function of latitude, time of year and time of day. The *daily averaged* insolation is given in Fig. 176. *Q: At midsummer, at which latitude do you think Q_{av} is greatest: Tropics, subtropics, midlatitudes or at the north pole?*

In midsummer Q_{av} is maximum at the north pole. θ ranges from 0° at a latitude of 23.5°N to 66.5° at the north pole. *Q: If the sun is overhead at 23.5°N, why is Q_{av} is maximum at the north pole?* It is due to the day length which more than offsets the lower value of $S_0 \cos\theta$.

5.4 Radiation interactions with a slab

Radiation interaction with a slab

We now consider the interaction of radiation with a layer of the atmosphere in more detail, considering the processes depicted in the schematic. We imagine a layer that is homogeneous in the infinite horizontal direction, and has a finite vertical depth of Δz (Fig. 177).

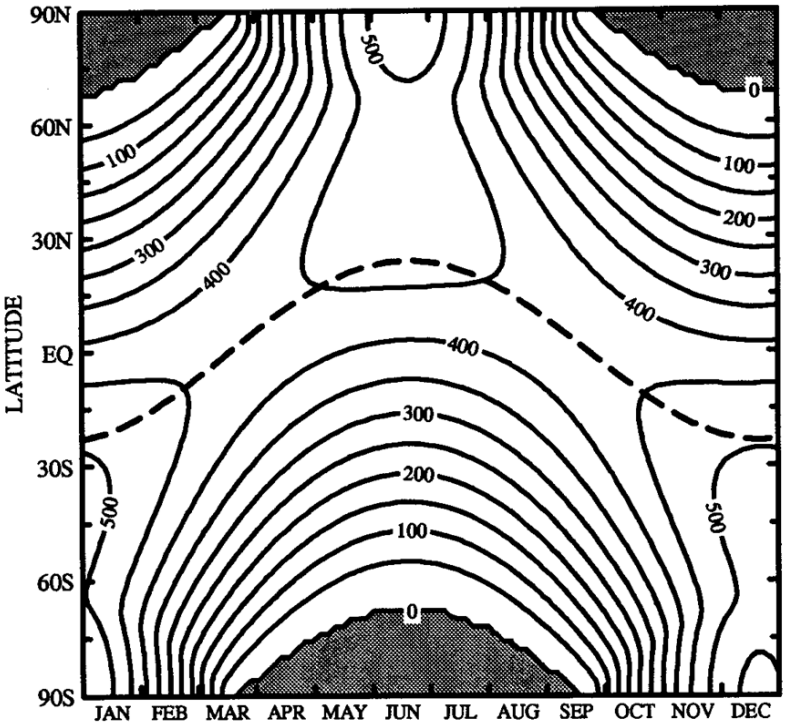

Figure 5.19: Day averaged insolation Q_{av} (W m^{-2}) at the TOA as function of season and latitude. The heavy dashed line marks the latitude of the subsolar point at noon Berger (1988).

The radiance L_λ which we recall is a function of (θ, ϕ), can be divided into three distinct components.

1. *The direct solar component*: radiative flux that passes unimpeded through the slab direction (θ, ϕ).
2. *The scattered component*: radiative flux originating from a different solid angle, but undergoes scattering within the slab to emerge in direction (θ, ϕ).
3. *Emission*: Radiation emitted from the slab in direction (θ, ϕ).

5.4.1 Direct Radiation

Direct Radiation - Beer's Law
Beer's Law The law states that there is a logarithmic dependence between the transmission τ of the a radiative flux through a substance and the product of the absorption coefficient of the substance, a, and the thickness of the material (i.e. the path length).

To derive this, we note that the finite reduction in the direct component by the slab dL_λ will be directly proportional to (Fig. 178):

- L_λ: The original intensity of the radiative beam
- $sec\theta dz$: The path length through the slab of the radiation.
- ρ: The density of radiatively active material in the layer (e.g. cloud drops, gases).
- k^e_λ: The mass extinction coefficient at wavelength λ

Thus

$$dL_\lambda = -L_\lambda k^e_\lambda \rho sec\theta dz, \tag{5.26}$$

where ρ is the density of the material (kg m^{-3}).

Mass extinction, absorption and scatter coefficients

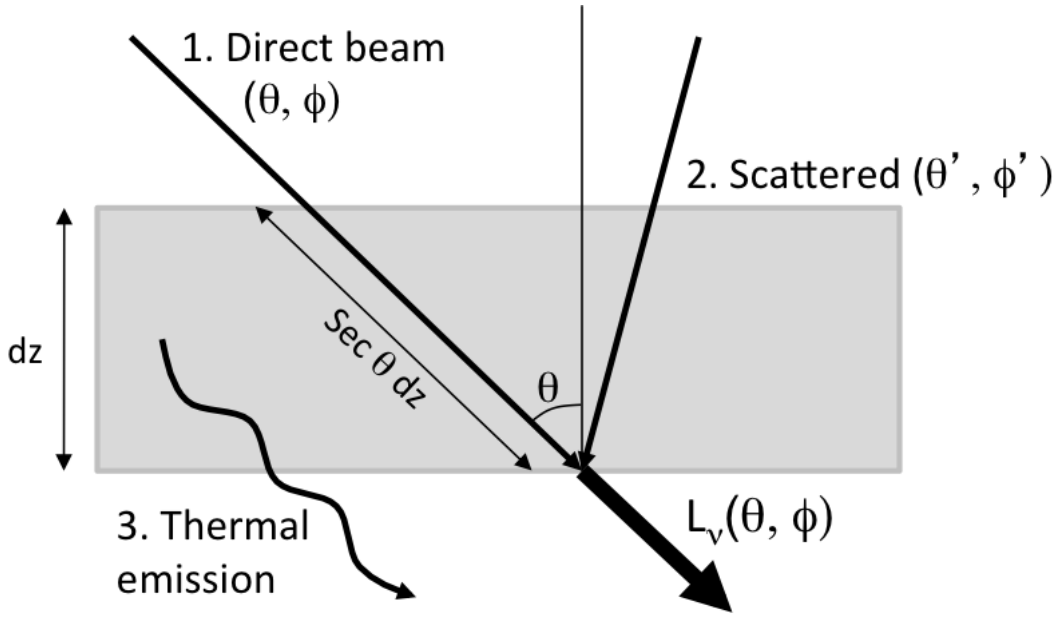

Figure 5.20: Schematic of radiation interaction with a medium of thickness dz.

For a specific material, it is useful to define the mass extinction k^e_λ. This specifies how strongly a unit mass of a medium depletes a direct beam of radiation of a given wavelength λ (or equivalently frequency ν) and has units $\mathrm{m}^2\ \mathrm{kg}^{-1}$.

The mass extinction coefficient is the sum of the absorption k^a_λ and scattering k^s_λcoefficients.

$$k^e_\lambda = k^a_\lambda + k^s_\lambda \tag{5.27}$$

Single scattering albedo
The *single scattering albedo* is defined as the ratio

$$\omega = \frac{k^s_\lambda}{k^e_\lambda} \tag{5.28}$$

The two extreme regimes are

- $\omega = 1$: Pure scatter (conservative scatter)
- $\omega = 0$: Pure absorption

We now integrate (185) over a finite depth slab (Fig. 179) to get the direct component of radiation as

$$L^{z_1}_\lambda = L^{z_2}_\lambda exp\left(-\int_{z_1}^{z_2} k^e_\lambda \rho sec\theta dz\right). \tag{5.29}$$

Optical Thickness/Depth
If from (188) we set

$$\delta_\lambda = \int_{z_1}^{z_2} k^e_\lambda \rho dz. \tag{5.30}$$

Then δ_λ is known as the *optical thickness* or *optical depth* of a *v*ertical path through the layer between z_1 and z_2; the integrated extinction coefficient.

Beer's (or Lambert's Law) then can be written

$$L^{z_1}_\lambda = L^{z_2}_\lambda e^{-\frac{\delta_\lambda}{cos\theta}} \tag{5.31}$$

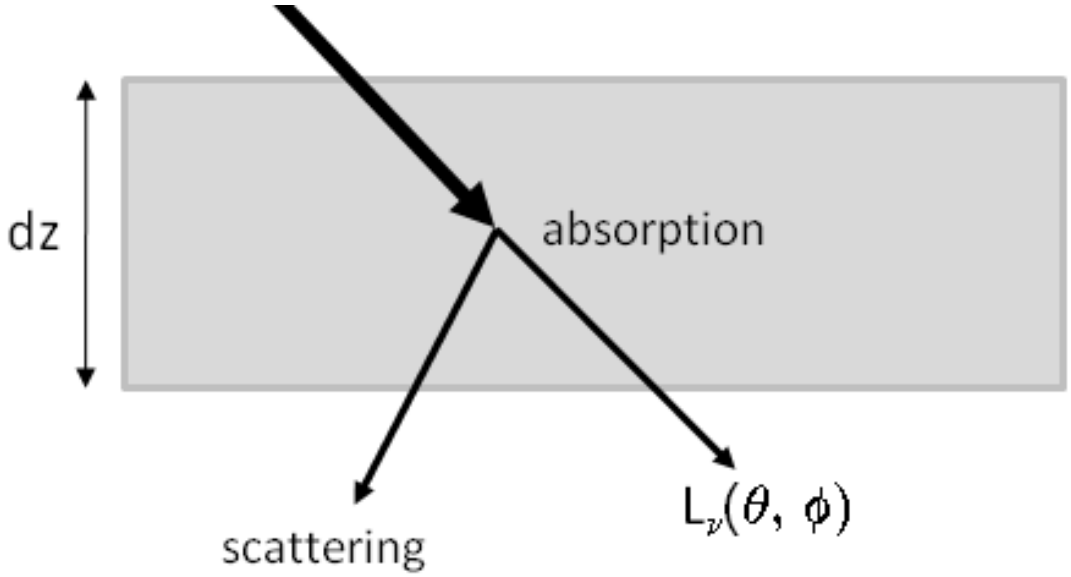

Figure 5.21: Schematic of radiation interaction with a medium of thickness dz.

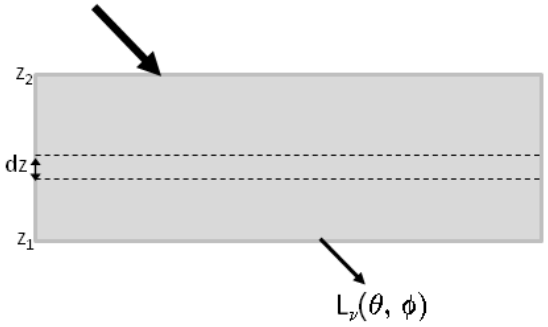

Figure 5.22: Schematic of integral over slab depth dz.

showing us that the transmittance τ is related to optical depth by

$$\tau_\lambda = e^{-\delta_\lambda} \tag{5.32}$$

We lastly emphasize that the transmittance, absorptance, extinction and optical depth are *functions of wavelength* or equivalently frequency.

If an absorber a has a constant mass mixing ratio with height, then the density ρ_a in an isothermal atmosphere in hydrostatic balance is related to the surface value ρ_{as}:

$$\rho_a = \rho_{as} e^{\frac{-z}{H}} \tag{5.33}$$

The value of H is the pressure scale height in hydrostatic balance: RT/g, which is approximately 7km.

Note that the scale height for water vapour is much smaller (approximately 2km) as water vapour mass mixing ratio reduces strongly with height for reasons discussed in the thermodynamic section of the course, and the vast majority of water vapour, the key greenhouse gas is found in the lower 3 or 4 km of the troposphere.

If we substitute this into Eqn. 189, then we get

$$\tau = \frac{p_s}{g} \frac{rho_a}{\rho} k_\lambda^a e^{\frac{z}{H}} \tag{5.34}$$

(

and thus it is clear that

$$\frac{d\tau}{dz} = -\frac{\tau}{H} \tag{5.35}$$

!!!!!!!!!!! TEXT HERE !!!!!!!!!!!!!

5.4.2 Scattering from other directions

Scattering from other directions
The scattering from other directions (θ', ϕ') is defined as

$$L_\lambda^{\text{scatter}} = \frac{\omega_\lambda}{4\pi} \int_0^{2\pi} \int_0^{\pi} L_\lambda(\theta', \phi') P(\theta', \phi', \theta, \phi) \sin\theta d\theta d\phi \tag{5.36}$$

We note

- The two integrals are to integrate over the sphere.
- 4π is a normalization factor, the solid angle integrated over a sphere, while we recall that ω_λ is the single scattering albedo.
- Recall $\sin\theta d\theta d\phi$ is the element of solid angle.

Phase Function
$P(\theta', \phi', \theta, \phi)$ is called the *Phase Function* and gives the probability that a photon will be scattered from direction (θ', ϕ') into direction (θ, ϕ)

We note that for *solar radiation* ($\lambda < 4\mu$m) *thermal emission is unimportant* as L_λ is very small at typical earth temperatures (recall Fig. 174). For *thermal infrared* ($\lambda > 4\mu$m) *scattering can generally be neglected*, thus only the extinction and emission are important. We now examine these in turn.

5.5 Absorption by atmospheric gases

Gases are not like black bodies that absorb equally and completely at all wavelengths. Rather, they absorb only at specific, often narrow ranges of wavelengths.

Absorption by atmospheric gases
In general molecules posses three kinds of quantized energy

- Electronic Energy (Visible and UV)
- Vibrational Energy (Near IR, Thermal IR 0.7-20 μm)
- Rotational Energy (Thermal IR)

To absorb or emit radiation the molecule must possess a permanent dipole, as it vibrates or rotates the electric field varies, allowing the interaction with the incoming/outgoing radiation.

N_2 and O_2
The major species of N_2 and O_2 are simple molecules that possess no permanent dipole (Fig. 180), and thus possess almost no vibrational or rotational absorption.

CO_2
Carbon dioxide CO_2 is a linear molecule, and thus from its symmetry possesses no dipole and thus no rotational spectrum. However, there are certain vibrational modes shown in (Fig. 181).

H_2O and O_3
H_2O and O_3 do possess a permanent dipole as the molecular structure is "bent" and hence asymmetric[2]. They therefore also have a rotational spectrum. (Fig. 182),

A more complete diagram of modes is given in Fig. 183

[2] see the atmospheric thermodynamics lecture notes from term 1, specifically Fig. 33

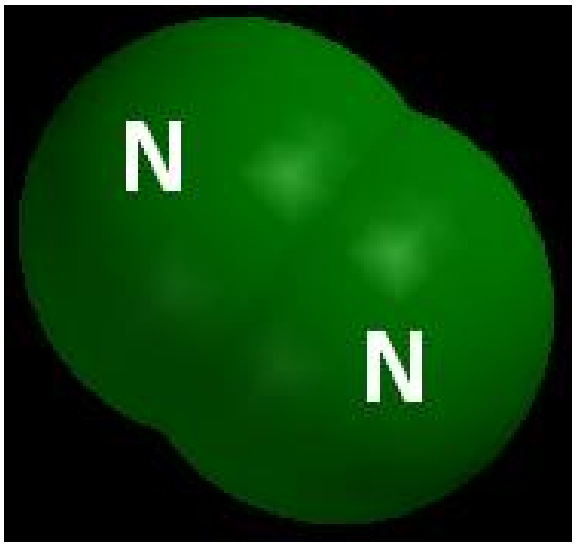

Figure 5.23: N_2 molecule

Around the turn of the century Max Planck theorized that radiation energy is quantized in order to address the shortcomings of the classical theory. As radiation is quantized, it implies that for a given frequency of radiation, there can be only one value of quantum energy for the photons of that radiation. Planck suggested the relation

$$E = h\nu \tag{5.37}$$

The energy levels of atoms and molecules can have only certain quantized values and transitions between these quantized states occur by absorption and emission.

The photon energy given by the Planck relationship is equal to the energy separation of the participating pair of quantum energy states (Fig. 184)

Different rotational and vibrational states can be combined to give a variety of possible energy transitions. The excited states do not persist: after some random amount of time, the molecules revert back to their original, lower energy state. The vibrational or rotational mode decays, emitting a photon. The energy associated with with a transition between two states is

$$\Delta E = h\nu \tag{5.38}$$

where h is the Planck Constant

Due to the existence of various rotational and vibrational discrete levels, molecules can absorb or emit at many different wavelengths or wavenumbers, with the strength of the absorption related to the probability of the transition between the relevant energy levels. This leads to the unique *Absorption Spectrum* of gases

Line broadening

Due to the discretised nature of the molecular energy levels one might expect absorption and emission to occur at distinct set *delta function* wavelengths as in Fig. 186a. In reality the energy levels are slightly "fuzzy" due to *line broadening mechanisms* so that absorption is spread over a finite width of wavelengths (Fig. 186b).

Three mechanisms for line broadening are

- *Natural Broadening*: a fundamental limit to the narrowness of the spectral lines due to Heisenberg's uncertainty principle, which relates the uncertainty of the time spent in excited states to the energy of the state transition
- *Pressure Broadening*: The energy levels are perturbed by the presence of other particles nearby the emitting one, for example, collisions of other particles with the emitting particle interrupts the emission process.
- *Doppler Broadening*: the emitting particles will have a variety of motions towards and away from the observer leading to a Doppler shift in the radiation.

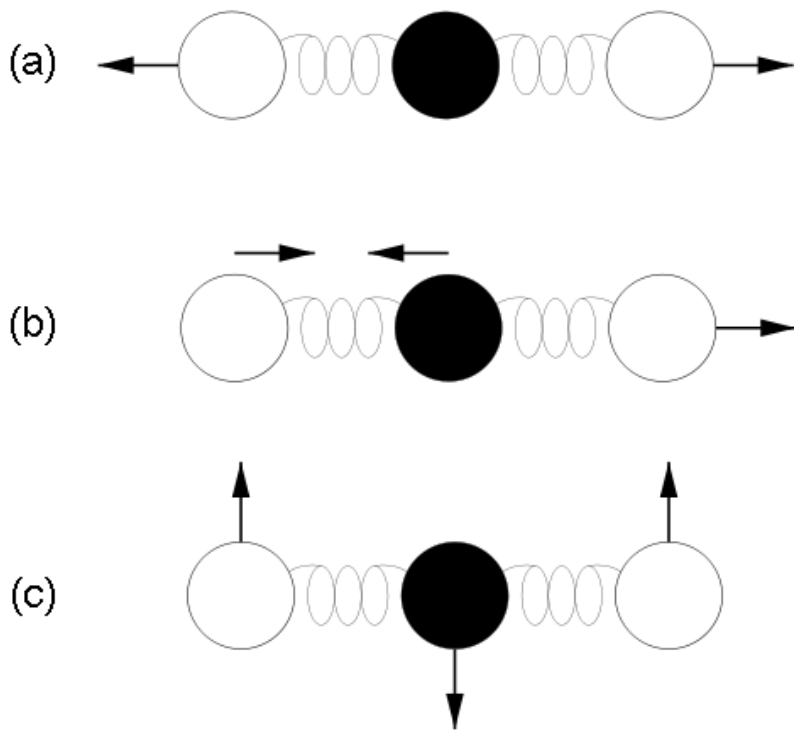

Figure 5.24: CO_2 molecule with its main vibrational modes

Natural Broadening is overwhelmed by the other two processes. *Q: Where in the atmosphere will pressure broadening dominate?* Pressure broadening dominates in the troposphere where p is relatively high and Doppler broadening is important in the upper stratosphere ($z > 30$km). We recall from earlier (191) that the transmittance is related to optical depth as $\tau_\lambda = e^{-\delta_\lambda} = \exp(-\int_{z_1}^{z_2} k_\lambda^e \rho sec\theta dz)$. If we assume a *homogeneous material* (k_λ^e is constant) and a solar zenith angle of zero, then this simplifies to

$$\tau_\lambda = \exp(-k_\lambda^e \rho(z_2 - z_1)) \tag{5.39}$$

The absorption in a band depends on the product $k_\lambda^e \rho(z_2 - z_1)$. If a particular gas is an efficient absorber (high k_λ^e) and/or is present is high amounts (large $\rho(z_2 - z_1)$) then the incoming/outgoing radiation of a band of wavelengths around the line centre may be completely absorbed. We thus find that we can have two regimes of *absorption lines* (Fig. 187):

- *Weak Limit*: Absorption is linear with absorber amount
- *Strong Limit*: Radiation is totally absorbed at line centre, adding more absorber only increases absorption at band edges. Absorption increases proportionally to the *square root/log* of the absorber amount with the constant of proportionally depending on pressure.

This is important when considering the greenhouse effect of gases. *Carbon dioxide* CO_2 for example is present in substantial amounts and *is in the strong limit*. Doubling CO_2 does *not* double its greenhouse affect. On the other hand CFCs are not present naturally and absorb in a part of the spectrum where other atmospheric gases are not active (referred to as an *absorption window*), and therefore their greenhouse effect increases linearly with concentration.

The major absorption bands are shown in Fig. 189 with the contribution by the main active gases. It is seen that nearly all of the outgoing infra-red radiation from the earth's surface is absorbed by water vapour except for the window between 8 and approximately 15 μm. However, CO_2 is strongly active in this window with an absorption band between 14 and 16μm.

We saw in Fig. 189 the existence of the water vapour window in the IR. *Q: In remote sensing what would this be useful for?* The window region of 8-13 μm is useful for remote sensing of the surface (e.g. SST).

In contrast to the earth's IR radiation, the majority of the solar radiation at the top of atmosphere reaches the earth's surface, with the atmosphere on average absorbing around 17% of solar

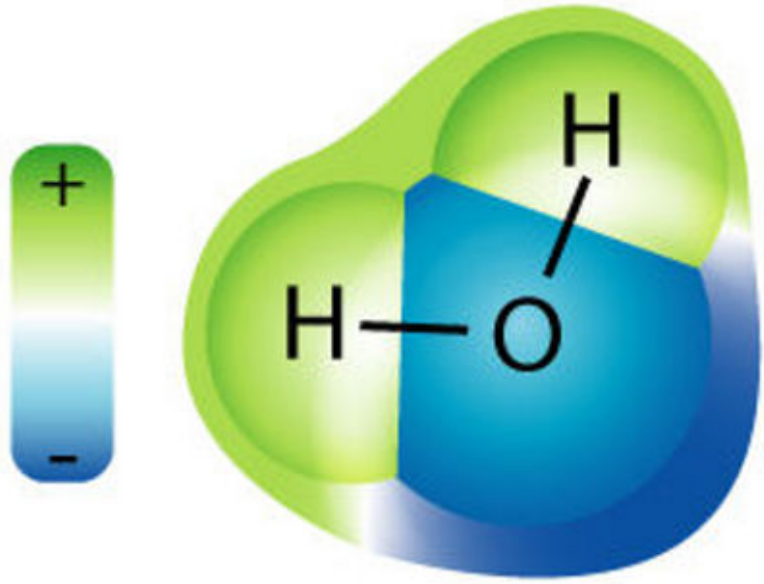

Figure 5.25: H_2O molecule and its charge structure

radiation. Fig. 190 shows the measured incoming solar radiation spectra and marks the specific gas absorption bands marked in addition to a reference blackbody curve.

5.6 Scattering

The *scattering* of radiation by a particle, depends strongly on the ratio of the wavelength of the radiation to the radius of the particle. The theory that governs this is called Mie theory, involving the internal and external refraction of the radiation by the particle and the full description is beyond the scope of this course. (Fig.191)

The scattering regime has a large impact on the phase function $P(\theta', \phi', \theta, \phi)$ (Fig. 192, see also Maxwell animations online). The relevant parameter to determine the scattering regime is the ratio of the particle radius r to the radiation wavelength $2\pi r/\lambda$.

One can see that in the regime $2\pi r/\lambda << 1$ the scattering is more regular in direction, with the phase function loosing its directional dependence in the limit $2\pi r/\lambda \to 0$.

Rayleigh Scattering
If we assume in the regime $2\pi r/\lambda << 1$ (the limit is about 5×10^{-3}) that the phase function P is independent of direction and thus the scattering is a function of λ only, then this *approximation* is called *Rayleigh Scattering*. The scattering extinction coefficient is proportional to the inverse fourth power of the wavelength, $k^s_\lambda \propto \frac{1}{\lambda^4}$. In the Rayleigh regime the scatterer can be treated as a single dipole.

The regimes where Rayleigh scattering approximation is valid are shown in Fig 193.

In general the radiatively "active" species are the trace gases such as CO_2, H_2O, O_3. Rayleigh Scattering is one of the few examples where the major species such as N_2 and O_2 are "active". *Q: why is the sky blue?*
We recall that the scattering coefficient in the Rayleigh regime is proportional to the inverse fourth power of the wavelength. Red light has $\lambda = 0.7\mu$m while blue light has $\lambda = 0.4\mu$m, indicating an order of magnitude increase in scattering at blue wavelengths.In addition, our eyes are less sensitive to violet, and the number of photos in this band is less (cf. Planck).

Contribution of Rayleigh scatter to planetary albedo
Rayleigh scattering's contribution to albedo depends on the solar zenith angle. *Q: why?*. The solar zenith angle determines the *pathlength* of the radiation and the likelihood of a scattering event. When the sun is overhead Rayleigh scattering contributes 0.037 to the albedo, while the figure is 0.13 for a solar zenith angle of 80°. The global average value is about 0.06, thus 0.06/0.30= 20% of the planetary albedo is due to Rayleigh scatter.

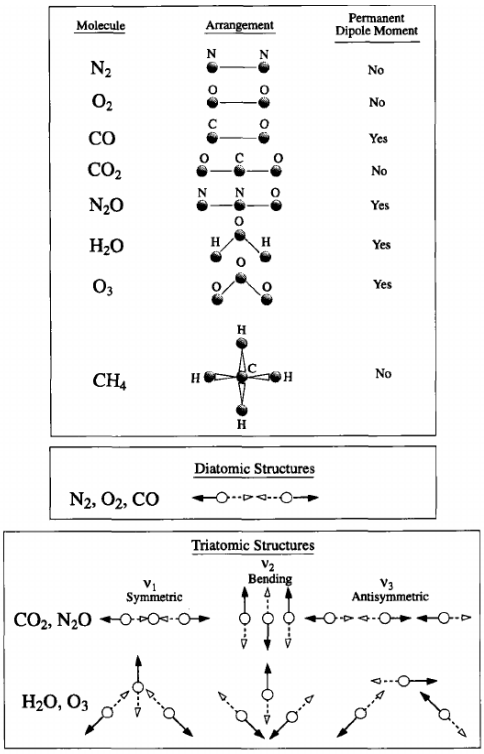

Figure 5.26: Schematic diagrams of vibrational modes of diatomic and triatomic molecules (source McCartney, 1983; Hartmann, 1994)

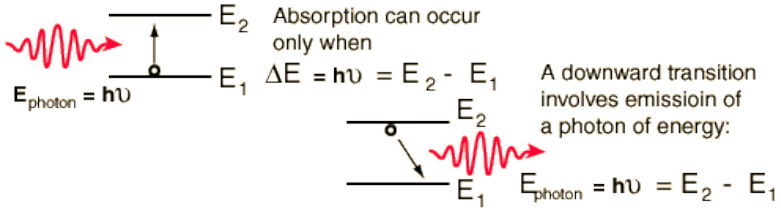

Figure 5.27: Schematic of state transitions (source: http://hyperphysics.phy-astr.gsu.edu)

Q: How does a greenhouse work?

A simple model for the greenhouse effect

To illustrate the *Greenhouse Effect* we will now construct a simple radiative balance model for the earth surface with an overlying atmosphere which will be considered a single radiatively active *homogeneous slab*.

We make the following simplifying assumptions:

- The earth surface is a black body.
- The atmosphere does not absorb solar radiation.
- Atmosphere can be represented as a *grey body*.

We can now write down the radiative energy balance of each component (according to the sketch in Fig. 194), assuming a state of *radiative equilibrium*.

Q: Derive these components.

Top of atmosphere

$$\frac{S_0}{4}(1-\alpha_p) = \sigma T_s^4(1-\epsilon) + \epsilon\sigma T_a^4 \tag{5.40}$$

Atmosphere

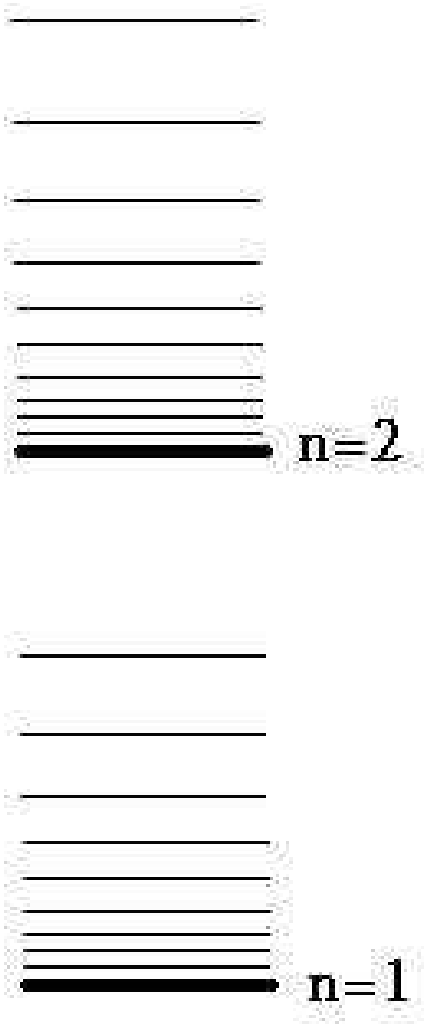

Figure 5.28: Quantized vibrational energy levels.

$$\epsilon\sigma T_s^4 = 2\epsilon\sigma T_a^4 \tag{5.41}$$

Q: Why is there a factor 2 on the RHS?

Surface

$$\epsilon\sigma T_a^4 + \frac{S_0}{4}(1-\alpha_p) = \sigma T_s^4 \tag{5.42}$$

Q: Why isn't there an ϵ factor in the solar term?

We thus have 3 equations with 2 unknowns T_s and T_a, and can use any two to calculate these unknowns. For example, from (200) we have

$$T_a = \frac{T_s}{\sqrt[4]{2}}, \tag{5.43}$$

which if we substitute into (199) gives

$$T_s = \sqrt[4]{\frac{S_0(1-\alpha_p)}{2\sigma(2-\epsilon)}} \tag{5.44}$$

Exercise: Check this derivation and also try other equation combinations using (201)

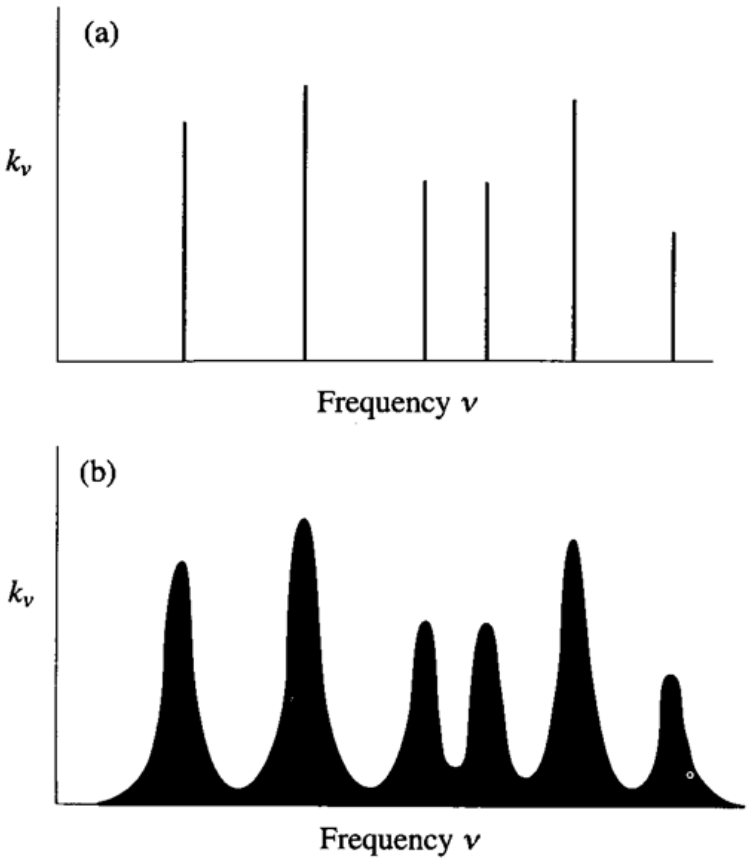

Fig. 3.5 Hypothetical line spectrum (a) before broadening, (b) after broadening.

Figure 5.29: (a) Hypothetical discrete absorption lines (b) actual absorption due to line broadening mechanisms (source Hartmann, 1994)

If we assume that $\epsilon = 0$ then we get the same result we achieved earlier, namely $T_s = 255$K, *Q: Why?*. A more reasonable value is $\epsilon = 0.6$, which results in $T_s = 278$K and $T_a = 235$K. Thus we can see that introducing an atmosphere that can absorb in the thermal IR *causes a surface warming*. This is known as the *greenhouse effect*. We will later consider what determines ϵ and its variation in a continuous media.

What happens to T_a as ϵ increases? From eqn. 202 we see that T_a increases. In fact the warming is a function of height [3], but in contrast temperatures in the stratosphere will reduce since they receive less IR radiation from below.

We could take this approach further and divide the atmosphere up into many vertical slabs, each with its own emittance according to the absorbing gases present in the layer. This would provide a *vertical atmospheric temperature profile* of the earth-atmosphere system in a state of *radiative equilibrium*. However this would *not* be a good model of the atmosphere temperature structure, *Q: Can you think why this would be the case?*

As an example, we extend the slab model to two layers (T_1 upper layer temperature, T_2 lower), but for simplicity we will assume that the layers are *black bodies*, and calculate the energy balance at the layer interfaces

The top of atmosphere energy balance in this case is given by

$$\frac{S_0}{4}(1 - \alpha_p) = \sigma T_e^4 = \sigma T_1^4 \tag{5.45}$$

As for the slab model, but considering the black body assumption, the balance for layer 1 is

$$\sigma T_2^4 = 2\sigma T_1^4 \tag{5.46}$$

[3] in the tropics due to the role of convection we expect a slightly larger increase in the upper troposphere

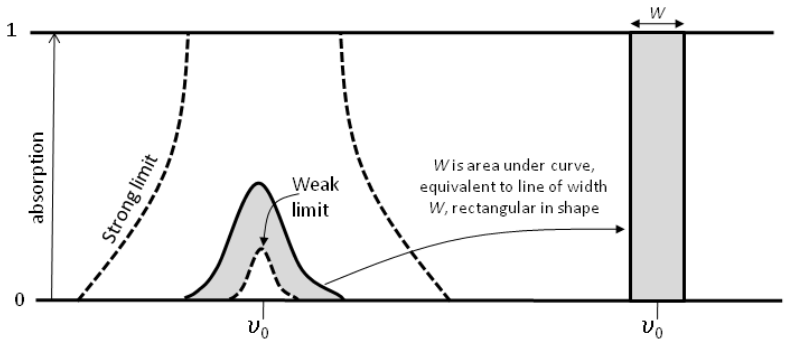

Figure 5.30: Schematic of integral over slab depth dz.

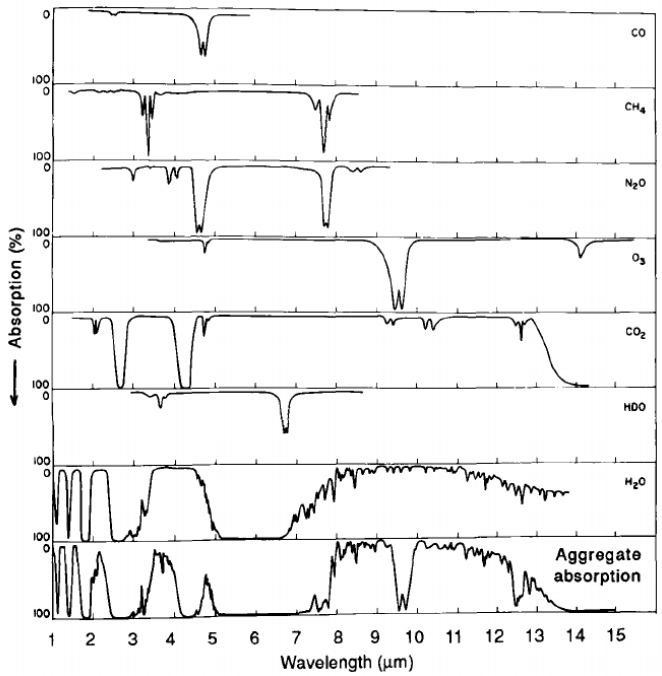

Figure 5.31: Transmission in 1-15 micro bands (source ?Hartmann, 1994).

and for layer 2:

$$\sigma T_1^4 + \sigma T_s^4 = 2\sigma T_2^4 \tag{5.47}$$

and at the surface:

$$\frac{S_0}{4}(1-\alpha_p) + \sigma T_2^4 = \sigma T_s^4 \tag{5.48}$$

So the energy of the sun is supplemented by the downward longwave from layer 2, and the surface temperature will be warmer than it would be without an atmosphere We can combine the above four equations to substitute T_2 in eqn. 207:

$$T_s^4 = \frac{3}{\sigma}\frac{S_0}{4}(1-\alpha_p) = 3T_e^4 \tag{5.49}$$

If we were to solve the same set of equations for an n-layer system, the general solution would be:

$$T_s = \sqrt[4]{n+1}T_e \tag{5.50}$$

Substituting values for S_0 and σ and α into eqn. 208, one gets a surface temperature of T_s =335.6K,

This is of course much hotter than the present day surface temperature, showing that radiative equilibrium is a poor approximation of processes on the planet. If one calculates the vertical temperature structure that would arise from radiative equilibrium in an n-layer system it turns

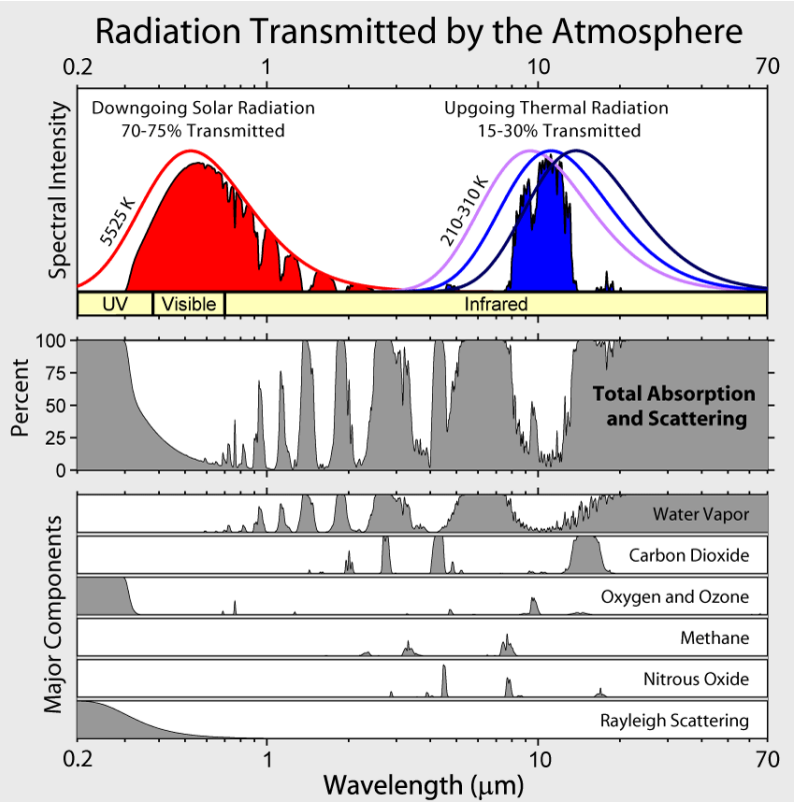

Figure 5.32: Upper panel shows the transmitted radiation in comparison to theoretical blackbody curves. Lower panels show the percentage absorptance due to the atmosphere and the contribution to this by the main active gases (source Wikipedia).

out that it is *absolutely unstable* to both dry and moist deep convection. Thus convection will transport heat from near the earth's surface to higher in the atmosphere. Rather than being in radiative balance, the earth's atmosphere is thus in a state of radiative-convective equilibrium , where radiative flux divergence balances convective heat transport. One of the earliest studies to examine this using a column model of the atmosphere was conducted by Manabe and Strickler (1964) (Fig. 196).

Q: in a state of radiative equilibrium, what would be the net radiative heating everywhere in the atmosphere? In a radiative equilibrium the net heating rate would be zero everywhere by definition. Instead in the *troposphere* there is a net cooling rate of O(1 K day^{-1}) which is balanced by convective heating processes.

5.7 Radiation budget of clouds

Scattering and absorption by clouds
In clouds Rayleigh scattering approximation no longer holds and $2\pi r/\lambda \approx 100$, and the full (complicated) Mie theory is required.

We saw in Fig. 192 that in this case there was a strong "forward lobe" where the forward scatter was much stronger than the backwards scatter. For liquid water droplets the forward scattering lobe can be many orders of magnitudes greater than the back-scattered radiation. This leads to an apparent paradox as clouds reflect up to 90% of the incident solar radiation back to space. *Q: how can this occur?* The solution is that we have so far considered only *single* scattering events. In optically thin clouds photons may undergo only a single scattering events and thus the vast majority pass through unimpeded. In optically thick clouds though multiple scattering may occur (Fig. 197). Thus the possibility of light reemerging at the cloud top is much higher. *This is why thick clouds appear dark when viewed from the surface.* Cloud albedo asymptotes to around 0.8 for thick clouds. We recall that ω tells us according to (187) what proportion of the direct

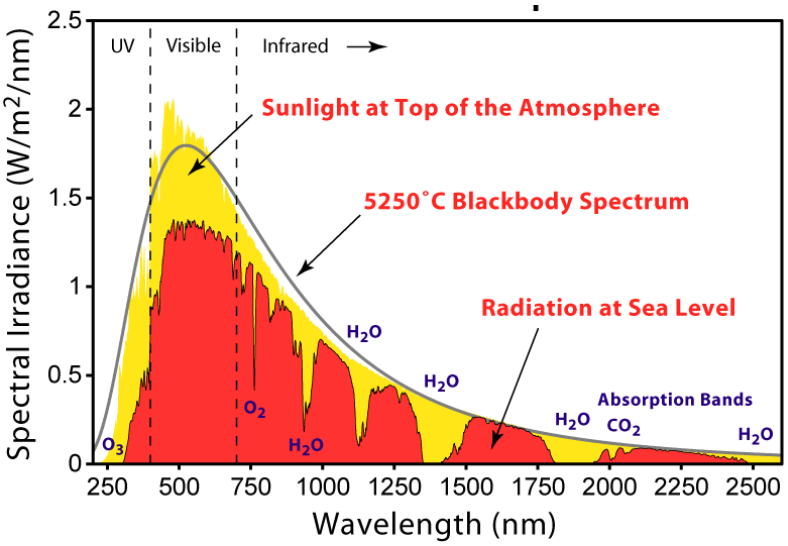

Figure 5.33: Solar incoming TOA and surface radiation spectra with the gases responsible for the major bands marked.

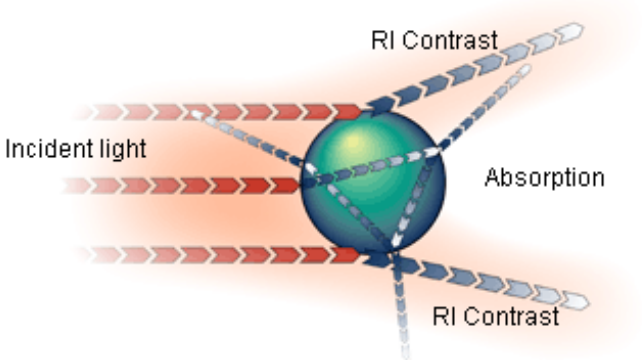

Figure 5.34: Schematic of mie scattering (source www.malvern.co.uk)

beam extinction is due to scatter or absorption. For solar radiation $\omega > 0.9$ meaning most of the radiation is scattered and indeed for visible wavelengths $\omega > 0.999$; the *conservative scattering* regime. Assuming a plane parallel cloud, actual albedo of the cloud will depend on the assumed droplet effective radius (often a fixed constant in climate model's radiation calculations), the solar zenith angle, and the cloud liquid water path, which is the vertically integrated mass of liquid water in the cloud with units of kg m^{-2}. Calculations made using a typical effective radius are shown in Fig. 198. *How does albedo change with SZA and why?.* These calculations show that the albedo increases rapidly with liquid water path at low values, but asymptopes to 80% for thick clouds. The albedo increases with solar zenith angle due to the fact that the forward scattering lobe is far stronger than the other scattering modes. Thus albedo is higher when the sun angle is low. The albedo of cloud is dominated by variations in the cloud liquid water path, but the droplet size of the liquid also impacts albedo. Results from Slingo and Schrecker (1982) show how albedo decreases as the droplet effective radius increases in cloud with fewer larger drops. Ice crystal scattering is more complex due to the various habits, but similar qualitative relationships exist between cloud albedo and ice crystal effective mean diameter.

If a photon undergoes n interactions with drops, the chance of *not* being absorbed is ω^n. In the thermal infra-red, generally $\omega < 0.5$, thus implying that there is little chance of a photon at these wavelength undergoing multiple scattering events and escaping from the cloud for $n > 5$. Thus *clouds are essentially black bodies in the infra-red* if their water content exceeds about 10 to 20 g m^{-2} (Fig. 200).

We can see from the above that clouds will have large effect on the earth's radiation budget depending on their height and optical depth.

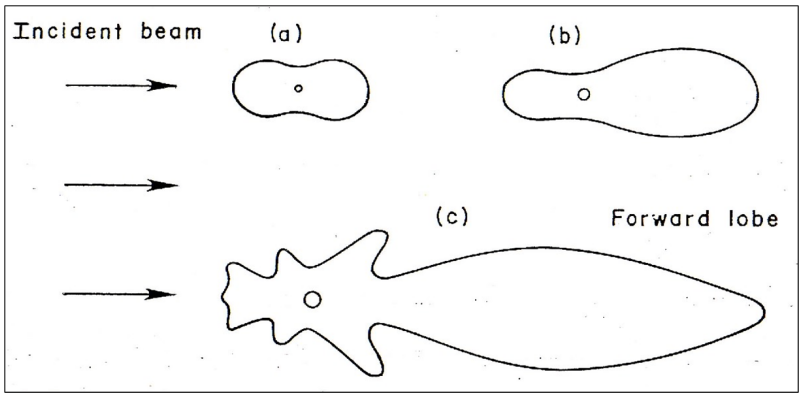

Figure 5.35: Scatter regimes as a function of $2\pi r/\lambda$ (a) $2\pi r/\lambda << 1$, (b)$2\pi r/\lambda \sim 1$ (c) $2\pi r/\lambda > 1$

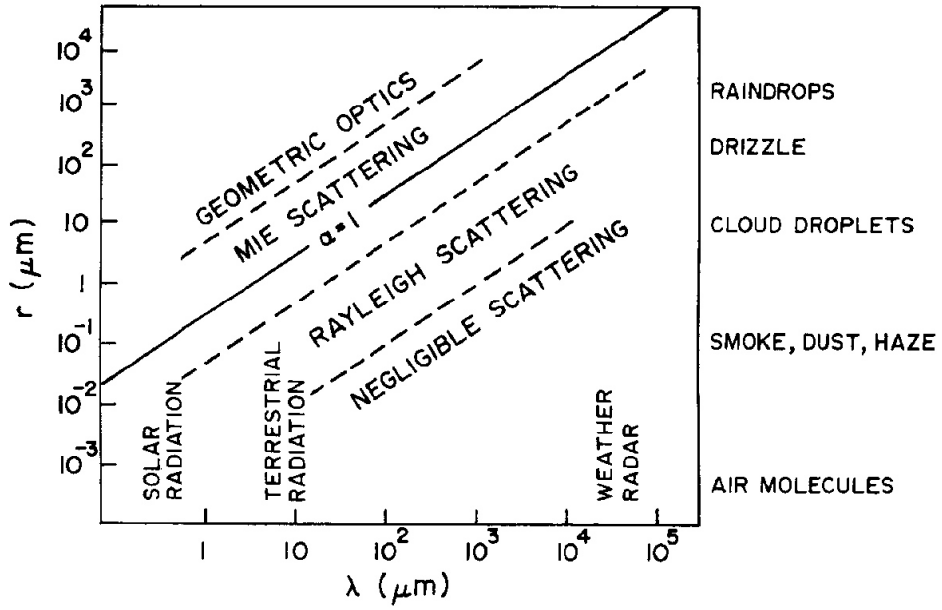

Figure 5.36: Scattering regimes as a function of wavelength and particle radius.

We consider the impact of clouds on the top of the atmosphere radiation budget, considering that the imbalance of radiation is the difference between the solar and OLR F_{olr}.

$$R_{TOA} = \frac{S_0}{4}(1-\alpha_p) - F^{\uparrow}_{OLR} = F^{\downarrow}_{sol} - F^{\uparrow}_{olr} \tag{5.51}$$

Thus the impact of clouds can be summarized in terms of its impact on the long and short wave

$$R_{TOA} = R_{cloudy} - R_{clear} = \Delta F^{\downarrow}_{sol} - \Delta F^{\uparrow}_{olr} \tag{5.52}$$

The impact on the solar flux is predominantly via the impact on the cloud albedo

$$\Delta F^{\downarrow}_{sol} = \frac{S_0}{4}(1-\alpha_{cloudy}) - \frac{S_0}{4}(1-\alpha_{clear}) = -\frac{S_0}{4}\Delta\alpha_p \tag{5.53}$$

Instead the impact on the OLR will depend on the cloud top temperature (and therefore height). We assume the clouds are black bodies in the infra-red and that their temperature is the same as the air temperature at the same height. We then derive (sketch on board):

$$\Delta F^{\uparrow}_{olr} = \sigma T^4_{z_{cld}}(1-\epsilon_{z_{cld},\infty}) - (\sigma T^4_s(1-\epsilon_{z_s,\infty}) + \epsilon_{z,\infty}\sigma T^4_{a,clr}) \tag{5.54}$$

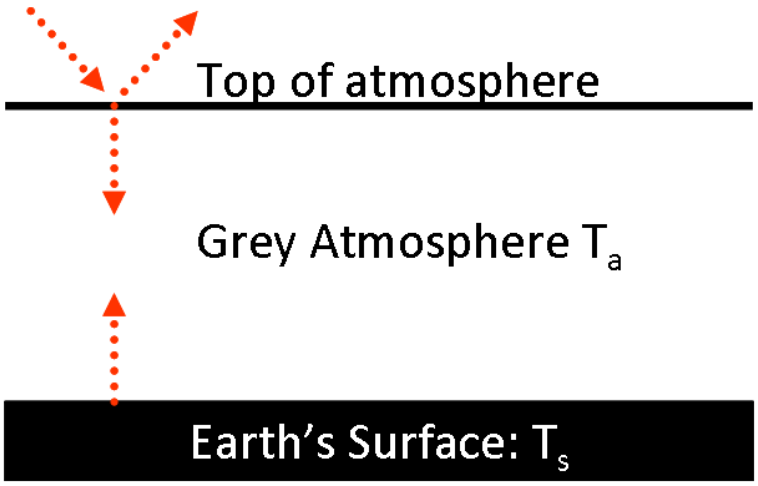

Figure 5.37: Sketch of the greenhouse slab model (source: me!)

where the subscript *clr* refers to the clear sky and T_a to the temperature at the mean emitting temperature of the clear sky column.

We can make a simplifying approximation to this by assuming the cloud top is above most of the column water vapor (roughly 4 to 5 km), so that we can assume that $\epsilon_{z_{cld},\text{inf}} \approx 0$,

In this case we can write

$$\Delta F^{\uparrow}_{olr} \approx \sigma T^4_{z_{cld}} - F^{\uparrow}_{clr} \tag{5.55}$$

Thus the net flux imbalance due to clouds is

$$R_{TOA} = -\frac{S_0}{4}\Delta\alpha_p - \sigma T^4_{z_{cld}} + F^{\uparrow}_{clr} \tag{5.56}$$

Clouds will thus have opposing impacts on SW and OLR TOA budgets. The SW impact on albedo is a strong function of the cloud optical depth for clouds thinner than 20 g m^{-2} ice/liquid water path, which the infra-red impact is a strong function of cloud top temperature (height).

Depending on the balance of the impact of SW and LW radiative forcing, there is a range of combinations of cloud top temperature and optical depth at which the cloud impact in the SW and LW cancel. We can estimate this by setting eqn. 215 to zero:

$$T_{z_{cld}} = \left(\frac{-\frac{S_0}{4}\Delta\alpha_p + F^{\uparrow}_{clr}}{\sigma}\right)^{0.25} \tag{5.57}$$

which corresponds approximately to the zero line in Fig. 201.

If we now assume that temperature decreases at a typical approximately moist lapse rate Γ=6.5 K km^{-1}, then we can write $T_{z_{cld}} = T_s - \Gamma z_{cld}$. If we insert this into eqn. 216, we can calculate the albedo effect. Assuming $T_s = 288K$ and a typical clear sky OLR of 265 Wm^{-2} we get Fig. 201.

Low clouds

- SW: Low clouds will sufficient optical depth will reflect sunlight back to space efficiently, thereby reducing the amount of solar radiation absorbed at the surface.
- LW: In the long wave infra red, cloud absorb the surface emitted radiation efficiently as they are effectively black bodies. They emit infrared radiation back to earth at the approximate temperature of the cloud lower surface, and to space the cloud top temperature. *Q: Do low clouds have a strong impact in the IR therefore?*

The answer depends on the level you are concerned with! The TOA budget is not impacted since the cloud top temperature will be similar to the surface. But low cloud will change the surface budget witnessed by the fact that winter nights are warmer with low cloud cover.

High clouds

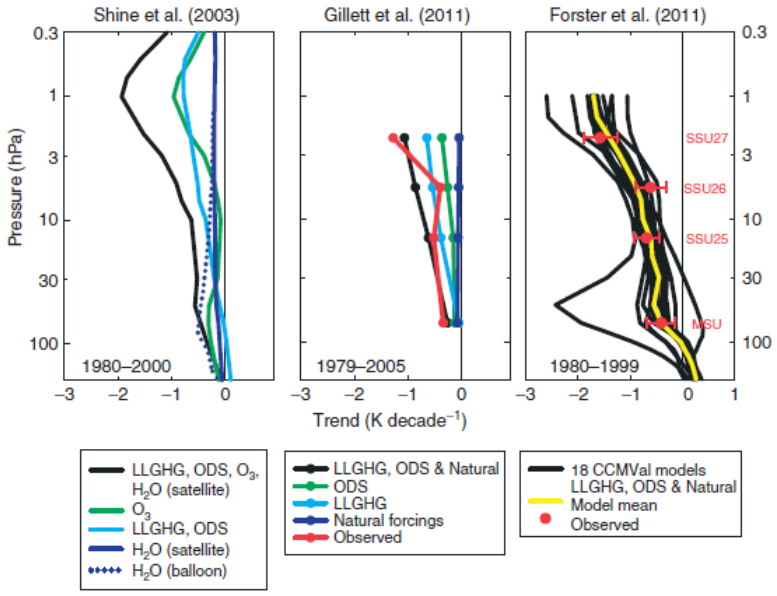

Figure 5.38: Observed and modelled temperature trends from Seidel et al. (2011) (Seidel et al., 2011)

High clouds of both reflect light back to space, but they can also have a strong IR signature since they are very cold (temperatures close to that of the tropopause). The balance can be in favour of warming or cooling depending on the crystal type[4] and the optical depth.

An intriguing result in the tropics is that on the average it appears that *high cloud radiative forcing is almost exactly zero*, i.e. the solar and the infra-red effects balance each other. This may be a coincidence of the present climate and not hold in past or future climates, but some authors have suggested that this result is no accident, and have put forward mechanisms involved negative feedbacks between radiation and convection that maintain this balance (see Hartmann et al., 2001).

5.8 Summary of Earth's radiation budget

We now examine the radiative budget of Earth (Fig. 202). This emphasizes the fact that once clouds are accounted for, very little of the surface emitted radiation escapes directly to space. Fig. 203 shows the net TOA shortwave radiation budget.

- Up to 300 Wm^{-2} in the tropics and below 100 Wm^{-2} in polar regions (why?)
- the highest values are over the oceans (why?)
- the lowest vaues are over the deserts (why?)

Fig. 203 shows the net TOA longwave radiation budget.

- Strong gradient from equator to poles (why?),
- But with low values in some tropical regions (why?)
- highest values over the deserts (why?)

If the net (SW+IR) effect is shown (Fig. 205) we see

- Surplus of incoming energy in tropics, deficit at poles.
- There is also a deficit over some desert regions

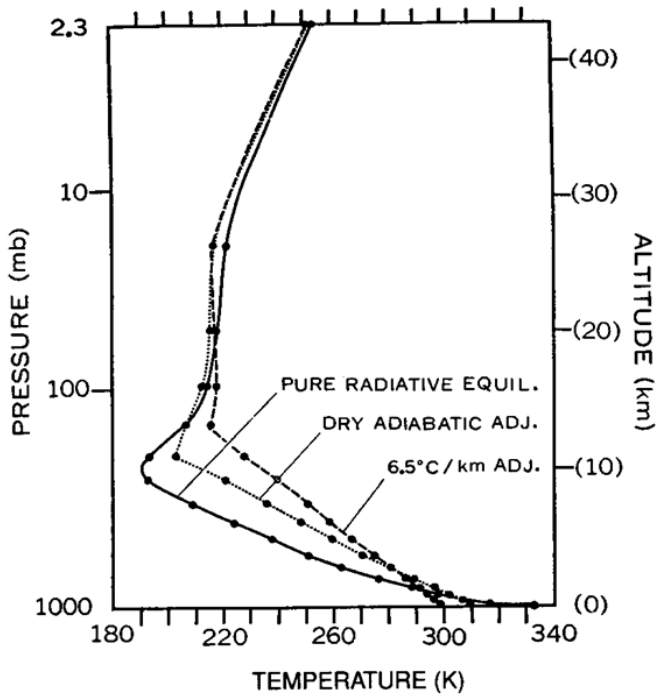

Figure 5.39: Temperature profiles resulting from a pure radiative equilibrium, or a radiative-convective equilibrium assuming a simple parametrization of convection that adjust the profile to a dry (9.8 C km^{-1}) or mean moist (6.5 C km^{-1}) temperature lapse rate. From Manabe and Strickler (1964).

The effects of clouds can be isolated by calculating the cloud radiative forcing in the SW, IR and net (SW+IR) (Fig. 206). These are calculated at each location by comparing the mean TOA outgoing radiative flux *at all times* with the mean averaged for only those times *when clouds are present*. The difference between these two values gives a measure of the cloud radiative forcing.

The TOA radiative forcing of clouds is shown in Fig. 206, and it should be possible to identify which panel is for SW and which for LW.

Calculating heating rates

To calculate the atmospheric heating rate a range of models are used that divide the spectrum up into a number of bands, with the spectrum resolution depending on available computing time.

- *Line by Line*: The most complicated models will divide the spectrum of 0-2500cm^{-1} into well over 100,000 spectral intervals. These models are very expensive to run but provide the benchmarks by which to test the cheaper models below.
- *Narrow Band*: These models will divide the infra-red spectrum into $\sim$ 250 spectral intervals, but these models are still too expensive to use in weather prediction or climate models.
- *Broad Band*: These may employ 5 to 20 spectral intervals, although numerical tricks can be used to improve representation of gas absorption bands.

The courses in the second term will aim to go into to more details concerns the components of earth system models for NWP and climate and highlight so of the reasons for the uncertainty in the modelling of these important processes.

[4]Remember that these are ice clouds with complex crystal geometries affecting scattering properties. See Macke et al. (1996) for a seminal analysis of ice crystal scattering.

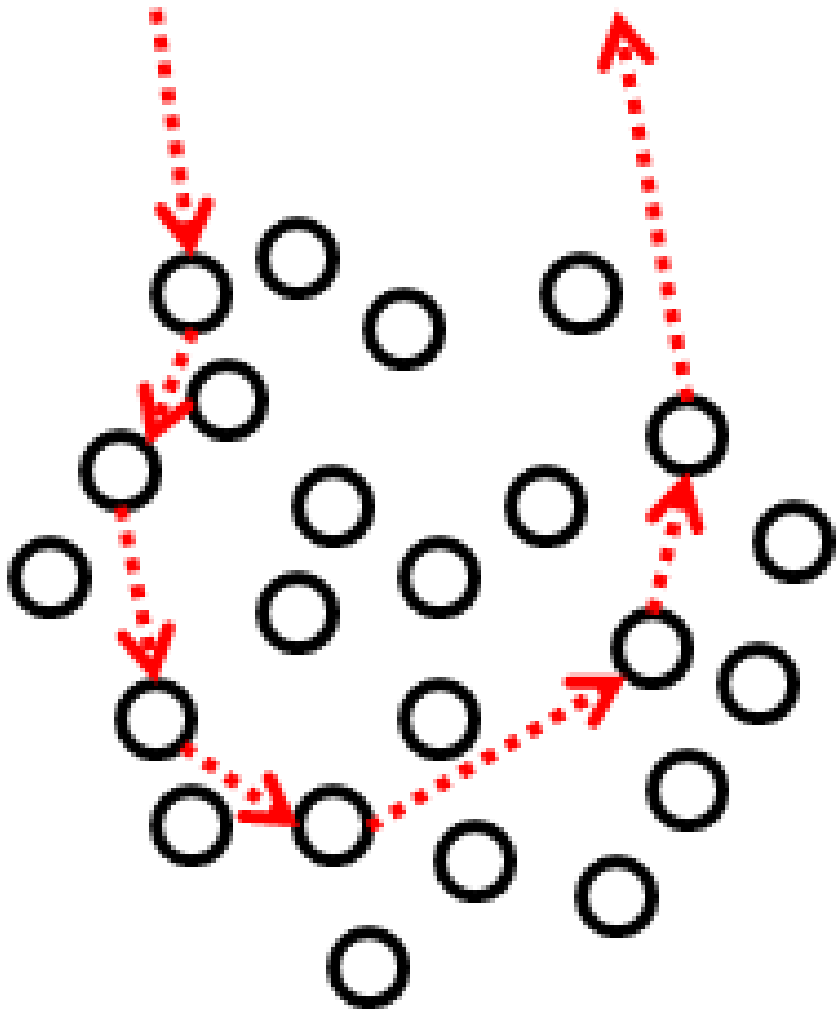

Figure 5.40: Schematic of multiple scattering with a cloud.

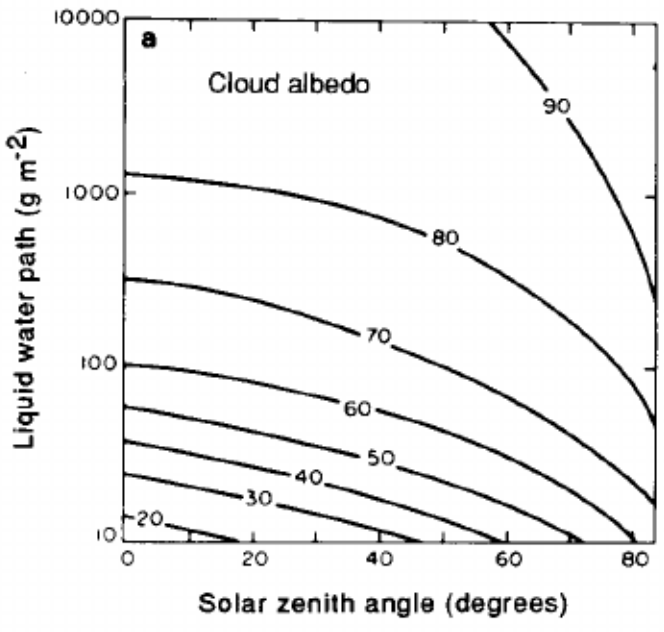

Figure 5.41: Cloud albedo as a function of cloud liquid water path and zenith angle (source Stephens, 1978a,b; Stephens et al., 1978).

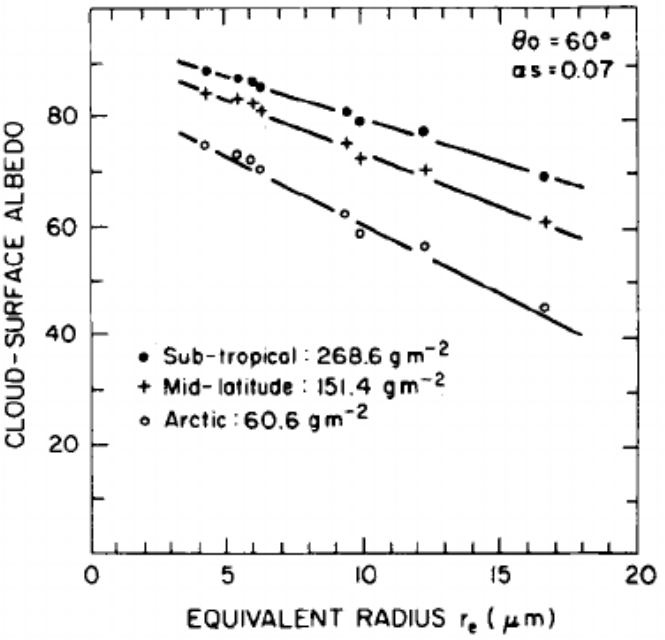

Figure 5.42: Cloud albedo as a function of dropless effective radius (source Slingo and Schrecker, 1982).

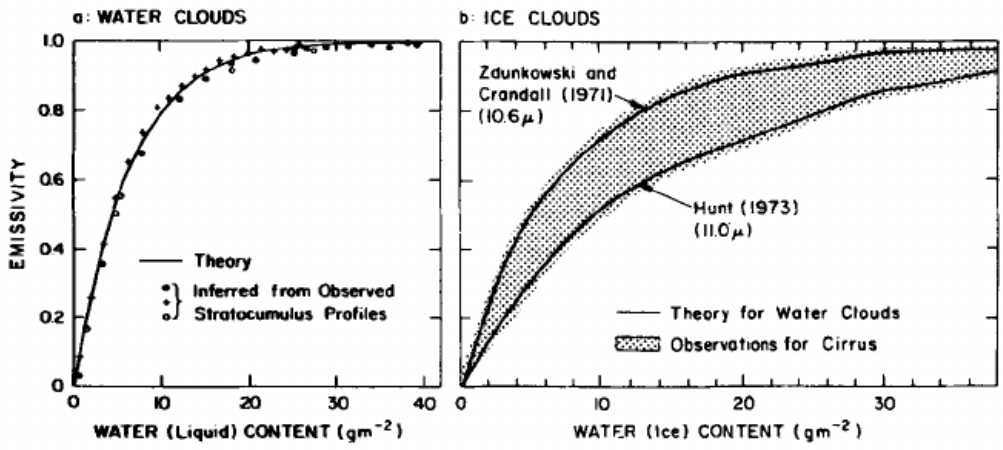

Figure 5.43: Cloud emissivity as a function of liquid/ice vertically integrated water content in g m^{-2} (source Griffith et al., 1980).

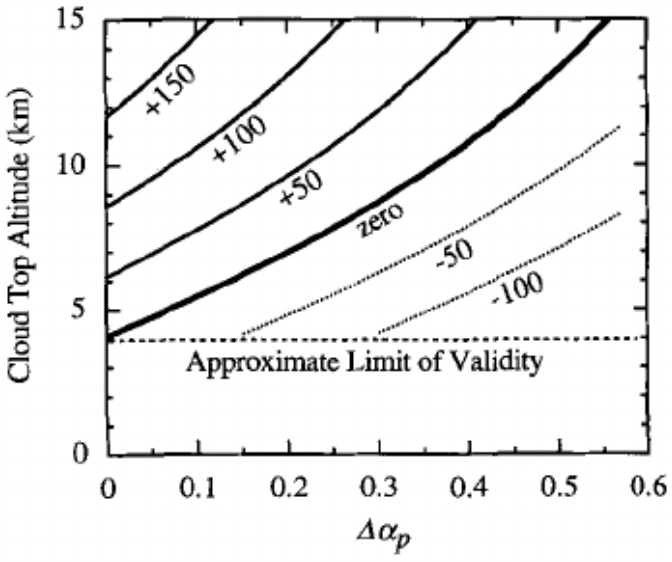

Figure 5.44: Contours of the change in TOA radiative balance as a function of cloud albedo impact and Cloud top altitude (source Hartmann, 1994).

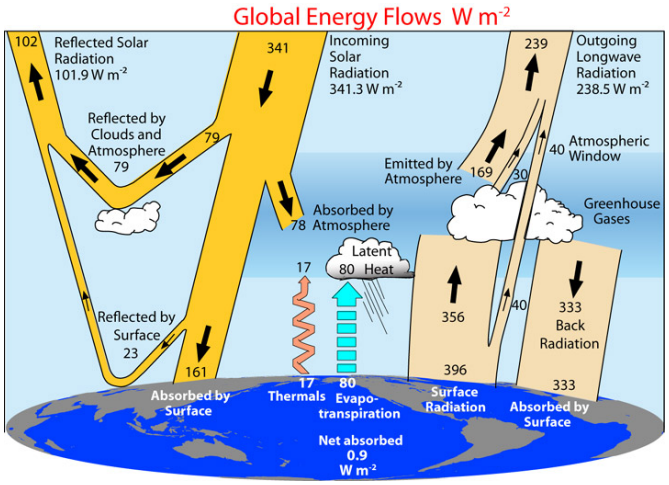

Figure 5.45: Radiative budget from Kiehl and Trenberth(2008)

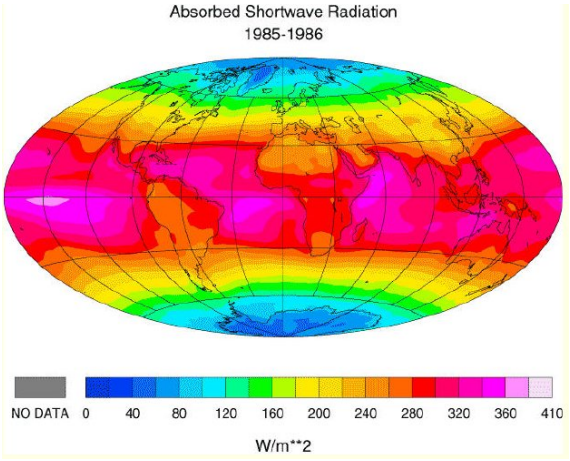

Figure 5.46: top of atmosphere (TOA) SW radiation budget

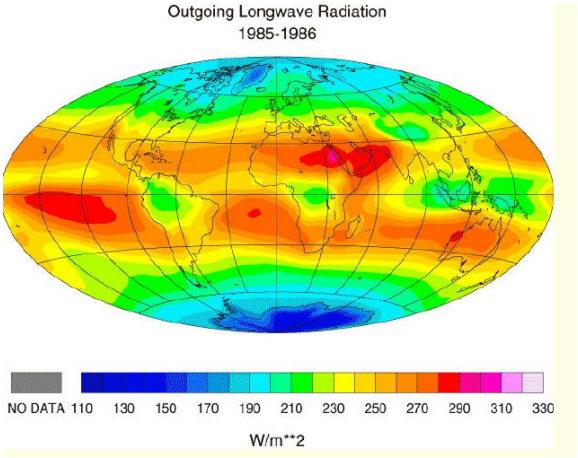

Figure 5.47: TOA OLR budget from ERBE

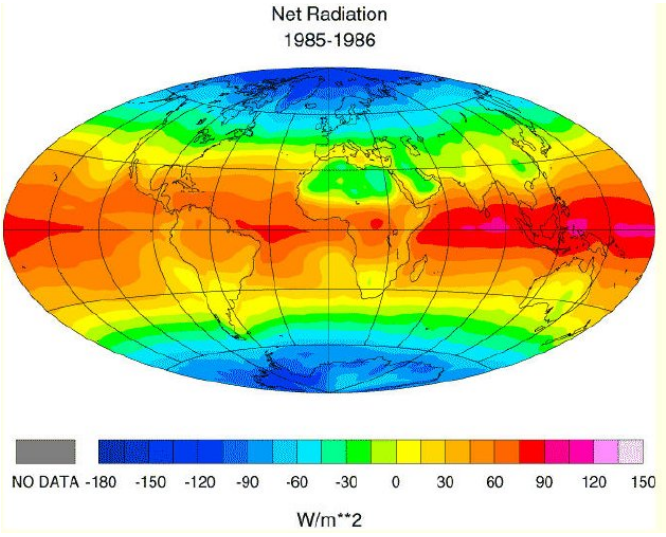

Figure 5.48: Net TOA radiation budget

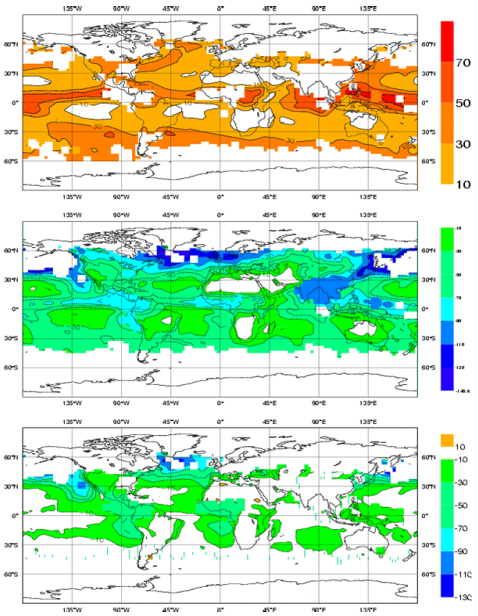

Figure 5.49: Cloud radiative forcing calculated from ERBE in the (top) LW (middle) SW and lower net (LW+SW)

Appendix A

Exercises

A.1 Thermodynamics Exercises

Exercise 1

1. A parcel of air at 800 hPa has a temperature of 280K is surrounded by air with a temperature of 278K and is lifted to a pressure of 700 hPa where the air temperature is 272K. Is the parcel warmer or cooler than its environmental when arriving at 700 hPa? What have you assumed to make this calculation?
2. If the atmosphere warms by 5^o, does the pressure at 5km increase or decrease? What is the rough magnitude of the change, assuming an average temperature of 280K and a surface pressure of 1013 hPa?
3. Use the equation of state for dry air to calculate the air density at the summit of Mt Everest on an occasion where the pressure and temperature were 313 hPa and -38.5^{o}C there, respectively. If the height of the summit is 8800m, make some suitable assumptions to estimate what fraction of the mass of the atmosphere is below you.
4. A parcel of dry air is at a temperature of 15^{o}C and a pressure of 1013 hPa. Heat is added to the parcel to cause it to expand. It expands at constant pressure to 1.5 times its original volume.
   a) What is the new temperature of the parcel?
   b) What is the amount of heat per unit mass that was added to the parcel?
   c) How much work per unit mass was done by the parcel during this expansion?
   d) What was the change in specific internal energy of the air parcel?
5. An parcel of dry air is at a temperature of 15^{o}C and a pressure of 1013 hPa. Heat is added to the parcel to cause it to expand. It expands at constant temperature to 1.5 times its original volume. (a) what is the final pressure? (b) what is the change in internal energy in this process?
6. In the subtropical free (above the boundary layer) troposphere there is an approximate balance between radiative cooling and dry adiabatic motion of the air. Assuming a constant net radiative diabatic cooling of Q_{rad}=1.5 K day^{-1}, what is the velocity w of the air to maintain temperature equilibrium? Is the motion upwards or downwards? How long would it take an air parcel to move through the depth of the troposphere (assume a depth of 10km) In general, let's assume that we can neglect the impact of radiation if the heating/cooling associated with vertical motion of an air parcel is at least two orders of magnitude (hundred times) greater. What would be the minimum vertical velocity of an air parcel for this to be the case? Do you know how this compares to typical rates of ascent in cumulus clouds?
7. Starting from eqn. 36, derive eqn. 46 for the definition of entropy.
8. Find the density of water vapour and dry air at STP (1000hPa and 0C). Which density is lower? At a given pressure, will a moist parcel of air with unit volume therefore have a lower or higher density than a unit volume of dry air?
9. A parcel of air at p=900hPa, has a temperature of 10^{o}C, a mass mixing ratio of 5 g kg^{-1}. It is vertically lifted to reach it's lifting condensation level (i.e. saturated). (a) What is the

temperature at which the parcel becomes saturated? (b) What is this temperature called? (c) What is the pressure at which condensation is reached? (check your answers with a tephigram)

10. Find the density of moist air with a specific humidity of 15 g kg^{-1}, temperature 15^{o}C and pressure 1010 hPa, and compare it with the density of dry air at the same temperature and pressure. Find the temperature at which dry air would have the same density as the moist air at the same total pressure. This temperature was introduced as the virtual temperature T_v
11. Name of all the following quantities that are conserved in *pseudoadiabatic moist saturated* ascent: mixing ratio r_v, pressure p, wet bulb potential temperature θ_w, dry bulb temperature T, potential temperature θ, dew point temperature T_d, vapour pressure e, wet bulb temperature T_w, adiabatic equivalent temperature T_e, equivalent potential temperature θ_e?
12. An air parcel of moist (but non-cloudy) air has a temperature of 24.9^{o}C. It is neutrally buoyant sitting in an environment that has a temperature of 25.0 ^{o}C and a mixing ratio of 10 g kg^{-1}. What is the mixing ratio in the air parcel?
13. The environmental air with temperature of 25.0 ^{o}C and a mixing ratio of 10 g kg^{-1} is located near the surface at a pressure of 1000hPa.
    a) What is the relative humidity (assume $RH = \frac{r_v}{r_s}$.) ?
    b) The airstarts to cool isobarically at nightnight until eventually a fog forms. Assuming the pressure is 1000hPa. Which is the temperature at which the fog occurs? (Use the tephigram to answer this)
    c) What is the common name given to this temperature?
14. Name of all the following quantities that are conserved in *pseudoadiabatic moist saturated* ascent: mixing ratio r_v, pressure p, wet bulb potential temperature θ_w, (dry bulb) temperature T, potential temperature θ, dew point temperature T_d, vapour pressure e, wet bulb temperature T_w, adiabatic equivalent temperature T_e, equivalent potential temperature θ_e?
15. Explain in words why you can sometimes see your breath in winter when there are cold, damp conditions?
16. A layer of air has a potential temperature of 303K and a mixing ratio of 5 g/kg at its LOWER boundary at p=700 hPa, and a potential temperature of 305K, a mixing ratio of 1 g/kg at its UPPER boundary. If the whole layer is lifted will it eventually undergo convection or not ?

Answers

1. You need eqn. 35 to give you the parcel's final temperature. It is not necessary to calculate θ, simply take the reference level at the parcel origin of 800 hPa, and then $T = T_0 \left(\frac{p}{p_0}\right)^{\frac{R_d}{c_p}}$, which is 269.5 K. Thus the parcel is cooler than its surroundings on arrival.
2. ans: 0.465 kg m^{-3}
3. ANSWER
4. ANSWER
5. The rate of change of temperature due to vertical motion of an air parcel is $w\frac{dT}{dz}$, where the lapse rate is that of the parcel and is given by the adiabatic lapse rate (eqn. 32). Thus, if the vertical motion balances radiative cooling rate given $-w\frac{g}{c_p} = Q_{rad}$, this gives $w = 1.7 \times 10^{-3} ms^{-1}$. The motion is downwards (watch the signs!) and to move through 10000 metres would take 68 days, around 2 months! In order to neglect radiation the vertical velocity would have a velocity of 0.14 ms^{-1}, which is less that observed in shallow convection ($1ms^{-1}$) or deep convection thunderstorms ($10ms^{-1}$).
6. To start, we take the log of eqn. 46

   $ln\theta = ln(T\frac{p_0}{p}^{\frac{R_d}{c_p}})$

   $ln\theta = lnT + \frac{R_d}{c_p}(lnp_0 - lnp)$

   then differentiate

$dln\theta = dlnT - \frac{R_d}{c_p} dlnp = \frac{dT}{T} - \frac{R_d dp}{c_p p}$

thus using $pv = R_d T$ we get

$c_p dln\theta = \frac{c_p dT - v dp}{T} = \frac{dq}{T} = d\phi$

7. Using the different gas constants for water vapour and dry air and the gas law, ρ_v=0.79 kg m^{-3} and ρ_d=1.28 kg m^{-3}. Thus a moist parcel will be less dense than the equivalent unit volume of dry air at STP!

8. T_v=290.7K cf T=288.2K

9. We write the momentum equation in terms of the parcel displacement dz about the LNB: $\frac{D^2 z}{Dt^2} = g\frac{\theta - \theta_{env}}{\theta_{env}}$. As θ is conserved (dry adiabatic) then $\theta = \theta_{env}$ at the LNB. We can write $\theta_{env}(\delta z) = \theta_{env}(0) + \frac{d\theta}{dz})\delta z$. Thus $\theta - \theta_{env} = \theta_{env}(0) - \theta_{env} = -\frac{d\theta}{dz}\delta z$.

   This gives $\frac{D^2}{Dt^2} = -\frac{g}{\theta_{env}(0)}\frac{d\theta}{dz} dz = -N^2 dz$

   where $N = \frac{g}{\theta_{env}(0)}\frac{d\theta}{dz}$ is usually referred to as the *buoyancy frequency*. We look for solutions of the form $dz = Aexp(iNt)$, which gives a period of $2\pi/N$. Thus the period is 531 seconds.

10. The virtual temperature has to be the same $T_{v-parcel} = T_{v-env} = T_{env}(1 + Kr_{env})$ where $K = \frac{1-\epsilon}{\epsilon} = 0.608$ Thus $r_{parcel} = \frac{(T_{env}/T_{parcel})(1+Kr_{env})-1}{/}K$ plugging in the numbers we find r_v=0.01056 or 10.56 g kg^{-1}

11. You need to insert p and T into Teton's formula to get r_s=19.8 g/kg. thus r_v/r_s=50.4% or 0.54.

    The fog forms at approximately 14C and it is known as the wet bulb temperature.

12. θ_w and θ_e

13. Due to the nonlinearity of the saturation vapour pressure curve and the linearity of temperature and mixing ratio mixing (recall diagram).

A.2 Convection Exercises

Exercise 2

1. Diurnal Cycle: Assume the ocean has a upper mixed layer of 10 metres deep. The daily flux imbalance (SW, IR, LH and SH) is assumed to be a sinewave with an amplitude of 300 Wm^{-2} (i.e. $F = Msin(2\pi t/\theta)$, where M=300 Wm^{-2} and θ=86400s). What is the magnitude of the diurnal cycle variation in temperature of the ocean? If at 30N the seasonal cycle of F is such that M=60Wm^{-2}, what is the seasonal cycle of temperature?
2. At what time of day (local time) do you expect to see the most stable boundary layer (assume no large-scale weather pat- terns are passing through, i.e. situation of stable high pressure)? Explain why in one or two sentences? (a) 9am (b) 3pm (c) 9pm (d) 3am

A.3 Exercises: Tephigram Exercises

Tephigram Exercise I

Using the correct tephigram shown in Fig. (42) plot the sounding data given in table A.1.

1. How deep is the planetary boundary layer (PBL) in hPa?
2. Is the PBL neutral, stable or unstable ?
3. What is the RH at 1000 hPa and 900 hPa?
4. What is T_d at 1000 hPa?
5. Is the PBL "well mixed" in humidity?

$p(hPa)$	T (°C)	r (g kg^{-1})
1000	10.0	5.0
950	6.5	5.0
900	3.1	5.0
850	2.5	3.2
800	0.0	2.8
700	-5.1	1.4
600	-12.0	1.3
500	-17.6	0.9

Table A.1: An arbitrary atmospheric sounding

6. What is the potential temperature θ of an air parcel at p=800hPa?

7. If this air parcel undergoes adiabatic ascent until it reaches a pressures of p=700hPa. What is its new T and θ?

Tephigram Exercise II
Return to the sounding you plotted using the data in Table A.1.

1. For a parcel of air at 1000 hPa, what is the condensation temperature T_c and pressure ?

2. For a parcel of air at 1000 hPa, what is the dry bulb or dew point temperature T_d?

3. If rainfall is evaporated into this parcel, at what temperature will it become saturated and what is this temperature called?

4. What will be the parcel's mixing ratio at this point?

5. What is the parcel's equivalent potential temperature θ_e?

6. What is θ_e for a parcel at 900 and 700 hPa?

7. Is θ_e increasing or decreasing with height?

Tephigram Exercises III
Return to the sounding you plotted using the data in Table Tab:sounding1.

1. What is the LCL of a surface parcel of air?

2. What is the LFC?

3. What is the convective trigger temperature?

4. Do you think deep moist convection is likely to occur here?

Tephigram Exercises IV
A 50hPa thick layer of air residing between has the values $T = 0°\text{C}$ and $r_v = 4.8$ g kg^{-1} at its lower boundary at 700 hPa, and $T = -2.5°\text{C}$ and $r_v = 3.0$ g kg^{-1} at the upper boundary at 650 hPa.

1. Is the layer absolutely stable/unstable, or conditionally unstable?

2. The layer is lifted by 100 hPa such that the lower boundary is at 600 hPa, what are the new temperatures at its boundaries?

3. Will the lifted layer be unstable to overturning?

4. Can you think of a criterion for this layer instability ?

A parcel lifted from the boundary layer forms deep convection since it has negligibly small CIN, and between the LCL at 900 hPa and LNB at 200 the cloudy has an average temperature excess of 1K. Assuming that the temperature excess does not vary much throughout the depth of the cloud, estimate the $CAPE$.

(Hint, recall that CAPE is given by

$$CAPE_i = g \int_i^{LNB} \left(\frac{T_u - T_{env}}{T_{env}} \right) dz, \tag{A.1}$$

but you may find it useful to assume the atmosphere is in hydrostatic balance and rewrite the definition in terms of pressure). (b) Apart from the constant temperature excess, what are the approximations made in this calculation (c) Estimate the CAPE from the GATE atmospheric sounding profile you plotted earlier in the course.

Tephigram Exercises VI
Plot this (slightly doctored) GATE profile on the tephigram.

GATE Sounding

P (hPa)	T (C)	T_d (C)
1010	24.5	21.6
950	20.2	19.2
900	17.5	16.1
800	13.2	11.0
700	7.2	5.1
600	0.0	-1.6
500	-7.6	-11.0
400	-17.5	-21.8
300	-34.3	-38.9
250	-43.4	-49.3
200	-50.6	-71.2

1. Determine the Lifting condensation level (LCL) for the surface parcel

2. Determine the Trigger temperature for the surface parcel

3. Draw the temperature profile for a moist adiabatically (no mixing) ascending parcel

4. Determine the level of neutral buoyancy (LNB)

An updraught air parcel mixes with the cloud environment in a single entrainment event at $p = 700hPa$, such that the mixture is composed of equal amounts of cloudy and environmental air. Precipitation then passes through the parcel and evaporates, bringing the mixed parcel to saturation.

1. What is the final temperature of the mixed parcel?

2. Can the parcel form a convective downdraught?

3. Recalculate this for a mixing event between updraught at 600 hPa.

4. If a downdraught can form, we assume it is keep at saturation during its descent by further precipitation evaporation. What temperature does it have at the surface?

5. Finally compute the CAPE of the surface parcel (you will probably find it easier to use pressure coordinates for this, assume hydrostatic balance)

6. Explain with a sketch diagram what the LCL, LFC and LNB are, and graphically what CAPE and CIN are. Explain with a diagram how one graphically determines the wet-bulb temperature and with which process is it associated? How is the wet bulb temperature related to the equivalent potential temperature?

7. Explain what the criteria are for absolute convective stability and instability, and also conditional instability.

A.4 Radiation Exercises

1. Rederive the energy balance equations with a slight modification to the assumptions. In the IR part of the spectrum, the atmosphere is still a grey body with emissivity of ϵ^{IR}, but now we assume that the atmosphere is also a grey body in solar part of the spectrum with $\epsilon^{SW} = 0.1$. In order to derive the equilibrium temperature T_s and T_a we need one further simplifying assumption concerning the fraction β of the total emitted energy by the atmosphere that lies in the short-wave part of the spectrum. What would be a good assumption for β do you think?

2. Extinction in the atmosphere

   i A parallel beam radiation of wavelength λ is passing vertically through a layer of 1 km in thickness, containing a homogeneous gas with a density of 0.01 kg m^{-3} with an absorption coefficient k^e_λ=0.1 m^2 kg^{-1} and a zero scattering coefficient.
   What is the optical thickness of the layer?

   ii What is the transmissivity τ of the layer?

   iii How thick would the layer have to be to absorb half of the incidence radiation beam?

   Answer:

   i optical thickness $\delta_\lambda = \int_{z_1}^{z_2} k^e_\lambda \rho sec\theta dz$ thus 1000 x 0.01 x 0.1 = 1 (no units)

   ii transmission = exp(-d) = 0.367

   iii exp(-k.rho.dz)=0.5 thus dz=693 m

3. What is special characteristic of the scattering phase function in the Rayleigh scattering approximation?

4. Can the scattering of solar radiation by clouds be described by the Rayleigh scattering approximation and why (or why not)?

A.5 Cloud Physics Exercises

1. (a) Calculate the time taken for a cloud droplet of radius 5μm to avaporate completely in an environment of ambient relative humidity of 90% and when the temperature of the droplet and environment is 11^{o}C. You may use Bolton's empirical formula given in (75) or the saturation vapour pressure as a function of T in ^{o}C: $e_s(T) = 611.2exp\left(\frac{17.67T}{T+243.5}\right)$ (b) What are the approximations/assumptions that are made with this calculation? (c) Repeat for a temperature of -15^{o}C

2. (a) Calculate the time taken for a droplet to grow from 20μm to 500 μm by the collision and coallescence in a cloud with mean liquid water density of $L = 1.2 \times 10^{-3}$ g m^{-3}. (b) How much longer is required to grow the 500 μm to 1000 μm?

3. In two clouds $5 \times 10^{-4} kgm^{-3}$ water condenses. In the first cloud the CCN concentration is 100 cm^{-3} and in the second the concentration is 1000 cm^{-3}. (a) Assuming the liquid water is equally distributed among the CCN, what is the droplet size in each cloud? (b) What might the different concentrations of CCN indicate about the locations of the clouds? (c) What are the consequences for the subsequent development of the clouds?

4. Explain why we never observe significant (more than 1%) supersaturations with respect to liquid water, but supersaturations with respect to ice are common

5. What is the Bergeron-Findeison Effect, and explain how it leads to accelerated ice crystals growth rates than might otherwise be expected.

6. Which ice nucleation mechanism leads to the highest ice crystal number concentrations, homogeneous or heterogeneous, and why?

Answers:

1. (a) Use 150, setting S=0.9 to get 0.56 s (b) The approximations are numerous: neglect of latent heat diffusion away from droplet, that the ambient relative humidity is fixed and unaffected by droplet evaporation, the curvature and solute effects when radius falls below 1 micron.

2. (a) Use 152 and substitute the relevant forms for the terminal fall speeds to find that 462s are required to grow the drop to 30 microns (where $V_t = X_1 r^2$), and then a further 1170s are required to grow this 30μm droplet to 500 μm (where $V_t = X_2 r$). (b) 289 seconds

3. The mass of N droplets is $N\rho_L \frac{4}{3}\pi r^3$. This is equal to the liquid water water content of the cloud in kg m^{-3}, thus (a) r=12.8 μm and (b) 5.96 μm (c) in the first case the distribution is likely to have drops greater than 20 μm for coalescence to take place, so the cloud may produce rainfall.

Appendix B

Tables

Table B.1: Table of thermodynamical constants

Avogadro's constant	N_A	6.02×10^{23}	mol $^{-1}$
Specific heat capacity at constant pressure for dry air	c_p	1005	J kg^{-1} K^{-1}
Specific heat capacity at constant volume for dry air	c_v	718	J kg^{-1} K^{-1}
Specific heat capacity of water	c_p	4185	J kg^{-1} K^{-1}
Specific heat capacity of sea water	c_p	≈ 3985	J kg^{-1} K^{-1}
Ratio of gas constants	$\epsilon = \frac{R_d}{R_v}$	0.622	
Latent heat of vaporization	L_v	2.5×10^6	J kg^{-1}
Latent heat of sublimation	L_s	2.83×10^6	J kg^{-1}
Latent heat of sublimation	L_s	2.83×10^6	J kg^{-1}
Gas constant for dry air	R_d	287.06	J kg^{-1} K^{-1}
Gas constant for vapour	R_v	461.5	J kg^{-1} K^{-1}
Density of liquid water	ρ_l	1000	kg m^{-3}
Molar mass of water	m_v	18.02	g mol^{-1}
Universal Gas Constant	R	8.314	J K^{-1} mol^{-1}
Saturation vapour pressure at $T_0 = 0^o$C	e_{s0}	611.2	Pa
Vapour diffusion coefficient	D	$\approx 2.2 \times 10^{-5}$	m$^2 s^{-1}$
Surface tension of liquid water	$\sigma_{l,v}$	7.5×10^{-2}	Nm^{-1}

Table B.2: Table of radiation constants

Planetary albedo of Earth	α_p	0.3	
Planetary albedo of Mercury	α_p	0.07	
Speed of light	c	3×10^8	m s^{-1}
Planck Constant	h	6.625×10^{-34}	J s
Boltzmann constant	k	1.3806×10^{-23}	J K^{-1}
Stefan Boltzmann constant	σ	5.67×10^{-8}	Wm^{-2} K^{-4}
radius of the earth	r_e	6340	km
radius of the sun	r_s	0.7×10^6	km
distance between Earth and the Sun	r_d	149.6×10^6	km
distance between Mercury and the Sun	r_d	58×10^6	km
Solar Constant	S_0	1370	W m^{-2}

Index

Bibliography

Banta, R. M., and C. Barker Schaaf, 1987: Thunderstorm genesis zones in the Colorado Rocky Mountains as determined by traceback of geosynchronous satellite images. *Mon. Wea. Rev.*, **115 (2)**, 463–476.

Berger, A., 1988: Milankovitch theory and climate. *Reviews of geophysics*, **26 (4)**, 624–657.

Berry, E. X., 1967: Cloud droplet growth by collection. *J. Atmos. Sci.*, **24**, 688–701.

Berry, E. X., and R. L. Reinhardt, 1974: An analysis of cloud drop growth by collection Part II. Single initial distributions. *J. Atmos. Sci.*, **31**, 1825–1831.

Byers, H. R., and R. R. Braham Jr., 1948: Thunderstorm structure and circulation. *J. Meteorology*, **5**, 71–86.

Demott, P. J., D. J. Cziczo, A. J. Prenni, D. M. Murphy, S. M. Kreidenweis, and D. S. Thomson, 2003: Measurements of the concentrations and composition of nuclei for cirrus formation. *Proc. Nat. Acad. Sci.*, **100**, 14 655–14 660.

Emanuel, K. A., 1994: *Atmospheric Convection*. Oxford University Press, 580 pp.

Fischer, E. M., S. I. Seneviratne, P. L. Vidale, D. Lüthi, and C. Schär, 2007: Soil Moisture–Atmosphere Interactions during the 2003 European Summer Heat Wave. *J. Climate*, **20**, 5081–5099.

Fleishauer, R. P., V. E. Larson, and T. H. Vonder Haar, 2002: Observed microphysical structure of midlevel, mixed-phase clouds. *J. Atmos. Sci.*, **59**, 1779–1804.

Fletcher, N., 1969: Active sites and ice crystal nucleation. *J. Atmos. Sci.*, **26 (6)**, 1266–1271.

Fletcher, N. H., 1962: *The Physics of Rainclouds*. Cambridge Univ. Press, New York, 386pp.

Gierens, K., 2003: On the transition between heterogeneous and homogeneous freezing. *Atmos. Chem. Phys.*, **3**, 437–446.

Gierens, K., U. Schumann, M. Helten, H. Smit, and A. Marenco, 1999: A distribution law for relative humidity in the upper troposphere and lower stratosphere derived from three years of MOZAIC measurements. *Ann. Geophysicae*, **17**, 1218–1226.

Griffith, K. T., S. K. Cox, and R. G. Knollenberg, 1980: Infrared radiative properties of tropical cirrus clouds inferred from aircraft measurements. *J. Atmos. Sci.*, **37 (5)**, 1077–1087.

Gunn, K. L. S., and J. S. Marshall, 1958: The distribution with size of aggregate snowflakes. *J. Atmos. Sci.*, **15**, 452–461.

Hartmann, D., L. Moy, and Q. Fu, 2001: Tropical Convection and the Energy Balance at the Top of the Atmosphere. *J. Climate*, **14**, 4495–4511.

Hartmann, D. L., 1994: *Global Physical Climatology*. Accademic Press, pp. 411.

Hoose, C., and O. Möhler, 2012: Heterogeneous ice nucleation on atmospheric aerosols: a review of results from laboratory experiments. *Atmospheric Chemistry and Physics*, **12 (20)**, 9817–9854.

Johnson, R. H., T. M. Rickenbach, S. A. Rutledge, P. E. Ciesielski, and W. H. Shubert, 1999: Trimodal characteristics of tropical convection. *J. Climate*, **12**, 2397–2418.

Kashchiev, D., 2000: *Nucleation*. Butterworth-Heinemann.

Kikuchi, K., G. N. Kiladis, J. Dias, and T. Nasuno, 2018: Convectively coupled equatorial waves within the mjo during cindy/dynamo: Slow kelvin waves as building blocks. *Climate Dynamics*, 1–20.

Klett, J. D., and M. H. Davis, 1973: Theoretical collision efficiencies of cloud droplets at small reynolds numbers. *J. Atmos. Sci.*, **30**, 107–117.

Koop, T., B. P. Luo, A. Tsias, and T. Peter, 2000: Water activity as the determinant for homogeneous ice nucleation in aqueous solutions. *Nature*, **406**, 611–614.

Macke, A., J. Mueller, and E. Raschke, 1996: Single scattering properties of atmospheric ice crystals. *J. Atmos. Sci.*, **53**, 2813–2825.

Manabe, S., and R. F. Strickler, 1964: Thermal equilibrium of the atmosphere with a convective adjustment. *J. Atmos. Sci.*, **21**, 361–385.

Marshall, J. S., and W. M. K. Palmer, 1948: The distribution of raindrops with size. *J. Atmos. Sci.*, **5**, 165–166.

Mason, B. J., 1978: Physics of a raindrop. *Physics Education*, **13**, 414–419.

McCartney, E. J., 1983: Absorption and emission by atmospheric gases-the physical processes. *New York, John Wiley and Sons, 1983, 331 p.*

McDonald, J. E., 1958: The physics of cloud modification. *Advances in Geophysics*, **5**, 223–303.

McIlveen, R., 1991: *Fundamentals of weather and climate*. Psychology Press.

Noilhan, J., and S. Planton, 1989: A simple parametrization of land surface processes for meteorological models. *Mon. Wea. Rev.*, **117 (3)**, 536–549.

Paluch, I. R., 1979: The Entrainment Mechanism in Colorado Cumuli. *J. Atmos. Sci.*, **36**, 2467–2478.

Pruppacher, H. R., and J. D. Klett, 1997: *The Microphysics of Clouds and Precipitation*. Kluwer Academic Publishers, pp. 954.

Quante, M., 2004: The role of clouds in the climate system. *Journal de Physique IV (Proceedings)*, EDP sciences, Vol. 121, 61–86.

Ren, C., and A. R. Mackenzie, 2005: Cirrus parametrization and the role of ice nuclei. *Q. J. R. Meteorol. Soc.*, **131**, 1585–1605.

Rogers, R. R., and M. K. Yau, 1989: *A short course in cloud physics*. Pergamon Press, 290pp pp.

Rotstayn, L., B. Ryan, and J. Katzfey, 2000: A scheme for calculation of the liquid fraction in mixed-phase stratiform clouds in large-scale models. *Mon. Wea. Rev.*, **128**, 1070–1088.

Rotunno, R., J. B. Klemp, and M. L. Weisman, 1988: A theory for long-lived squall lines. *J. Atmos. Sci.*, **45**, 463–485.

Sabin, T., C. Babu, and P. Joseph, 2013: Sst–convection relation over tropical oceans. *Int. J. Climatol.*, **33 (6)**, 1424–1435.

Seidel, D. J., N. P. Gillett, J. R. Lanzante, K. P. Shine, and P. W. Thorne, 2011: Stratospheric temperature trends: Our evolving understanding. *Climatic Change*, **2 (4)**, 592–616.

Seigel, R. B., and S. C. van den Heever, 2012: Dust lofting and ingestion by supercell storms. *J. Atmos. Sci.*, **69 (5)**, 1453–1473.

Slingo, A., and H. Schrecker, 1982: On the shortwave radiative properties of stratiform water clouds. *Q. J. R. Meteorol. Soc.*, **108 (456)**, 407–426.

Spichtinger, P., K. Gierens, and W. Read, 2003: The global distribution of ice-supersaturated regions as seen by the Microwave Limb Sounder. *Q. J. R. Meteorol. Soc.*, **129**, 3391–3410.

Stephens, G. L., 1978a: Radiative properties of extended water clouds: Part I. *J. Atmos. Sci.*, **35**, 2111–2122.

Stephens, G. L., 1978b: Radiative properties of extended water clouds: Part II. *J. Atmos. Sci.*, **35**, 2123–2132.

Stephens, G. L., G. Paltridge, and C. Platt, 1978: Radiation profiles in extended water clouds. iii: Observations. *J. Atmos. Sci.*, **35 (11)**, 2133–2141.

Taylor, C. M., F. Said, and T. Lebel, 1997: Interactions between the land surface and mesoscale rainfall variability during HAPEX-Sahel. *Mon. Wea. Rev.*, **125**, 2211–2227.

Telford, J. W., and J. Warner, 1962: On the measurement from an aircraft of buoyancy and vertical air velocity in cloud. *J. Atmos. Sci.*, **19**, 415–423.

Tompkins, A. M., 2001: Organization of tropical convection in low vertical wind shears: The role of coldpools. *J. Atmos. Sci.*, **58**, 1650–1672, URL http://journals.ametsoc.org/doi/abs/10.1175/1520-0469%282001%29058%3C1650:OOTCIL%3E2.0.CO;2.

Tompkins, A. M., K. Gierens, and G. Rädel, 2007: Ice supersaturation in the ECMWF integrated forcast system. *Q. J. R. Meteorol. Soc.*, **133**, 53–63.

Turner, J., 1963: The motion of buoyant elements in turbulent surroundings. *Journal of Fluid Mechanics*, **16 (01)**, 1–16.

Waliser, D. E., and N. E. Graham, 1993: Convective cloud systems and warm-pool sea-surface temperatures - coupled interactions and self-regulation. *J. Geophys. Res.*, **98**, 12 881–12 893.

Warner, J., 1955: The water content of cumuliform cloud. *Tellus*, **7**, 449–457.

Warner, J., and T. D. Newnham, 1952: new method of measurement of cloud water content. *Q. J. R. Meteorol. Soc.*, **78**, 46–52.

Willis, P. T., 1984: Functional fits to some observed drop size distributions and parameterization of rain. *J. Atmos. Sci.*, **41**, 1648–1661.